

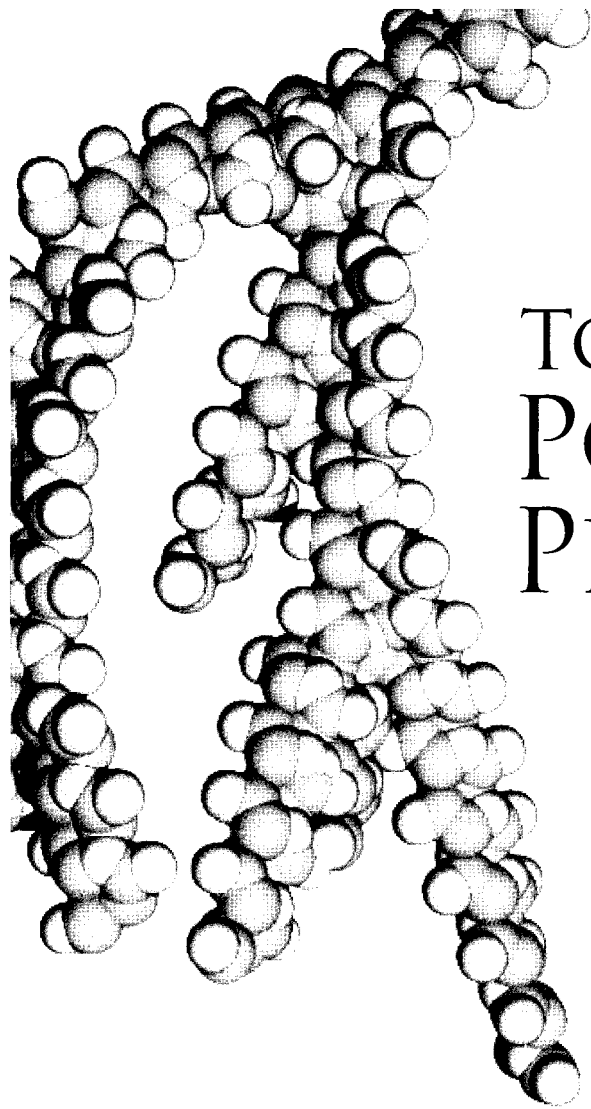
TOPICS IN
POLYMER
PHYSICS

RICHARD S STEIN
JOSEPH POWERS

Imperial College Press

TOPICS IN
POLYMER
PHYSICS

This page is intentionally left blank



TOPICS IN POLYMER PHYSICS

RICHARD S STEIN

Goessmann Professor of Chemistry, Emeritus
University of Massachusetts, Amherst

JOSEPH POWERS

United Technologies Corporation, retired



Imperial College Press

Published by

Imperial College Press
57 Shelton Street
Covent Garden
London WC2H 9HE

Distributed by

World Scientific Publishing Co. Pte. Ltd.
5 Toh Tuck Link, Singapore 596224
USA office: 27 Warren Street, Suite 401-402, Hackensack, NJ 07601
UK office: 57 Shelton Street, Covent Garden, London WC2H 9HE

British Library Cataloguing-in-Publication Data

A catalogue record for this book is available from the British Library.

TOPICS IN POLYMER PHYSICS

Copyright © 2006 by Imperial College Press

All rights reserved. This book, or parts thereof, may not be reproduced in any form or by any means, electronic or mechanical, including photocopying, recording or any information storage and retrieval system now known or to be invented, without written permission from the Publisher.

For photocopying of material in this volume, please pay a copying fee through the Copyright Clearance Center, Inc., 222 Rosewood Drive, Danvers, MA 01923, USA. In this case permission to photocopy is not required from the publisher.

ISBN 1-86094-411-6

ISBN 1-86094-412-4 (pbk)

TO OUR WIVES

JUDY BALISE STEIN

MARY GRIFFIN POWERS

This page is intentionally left blank

Preface

This book can serve as an introduction to students interested in learning the techniques used in developing mathematical models of physical phenomenon; or it can furnish the background information to the experienced professional desiring to broaden his/her knowledge of polymers.

The senior author presented material in this book to students interested in learning the fundamental mathematics underlying many areas of polymer physics and in lectures to audiences with varying backgrounds in polymer physics.

The material in this book should prove helpful to readers who have knowledge of introductory mathematics, chemistry and physics.

The text emphasizes the derivation of many equations used in Polymer Physics. The assumptions used in modeling, and in making the mathematical apparatus solvable in closed form, are presented in detail. Too many times, the basic equations are presented in final form in journal articles and books from either lack of space or the assumption that the derivation is widely disseminated and does not require repetition.

The fundamentals of any discipline have to be constantly tested against new findings. This book presents the assumptions and simplifications of the fundamentals of many areas of Polymer Physics so that the testing process can be expedited.

The authors have discussed this material with many colleagues and in return received many pertinent suggestions for improvement. These include Philip Wilson, Mohan Srinivasaro, Hiromichi Kawai, Shigeharu Onogi, Garth Wilkes, Takeji Hashimoto and Marion Rhodes, James J. Burke and many others who attended courses or collaborated with Professor Stein in research projects.

The improvements belong to our colleagues. The residual factual errors, typos and other problems belong to the authors.

For supplementary material, corrections and communications with us, please visit <http://web.mac.com/rsstein1/iWeb>

This page is intentionally left blank

Contents

Dedication	v
Preface	vii
Chapter 1	1
INTRODUCTION	1
1.1. Background.....	1
1.2. Linear Chain Molecules	4
1.2.1. Structure.....	4
1.2.2. Synthesis	8
1.2.3. Molecular Weight.....	10
1.3. Network Molecules	15
1.3.1. Structure.....	15
1.3.2. Synthesis	16
1.3.3. Molecular Weight.....	16
1.4. Rubber	17
1.4.1. Structure.....	17
1.4.2. Synthesis	21
1.4.3. Molecular Weight.....	21
1.5. Multicomponent Systems	21
1.5.1. Copolymers	21
1.5.2. Polyblends.....	25
1.5.3. Composites.....	25
1.5.4. Ceramers	26
References	27
Appendix 1A - Derivation of the Most Probable Distribution	28
Reference.....	30
Chapter 2	31
STATISTICS OF CHAIN CONFORMATIONS.....	31
2.1. Introduction.....	31
2.2. Small Molecules.....	31
2.3. Larger Molecules, Statistical Variation of Molecular Conformations	40
2.4. Statistical Segment Model	41
2.5. Generalization to High Polymers	44
2.6. Polymer Chains Containing Two Kinds of Atoms	45

2.7. Model Chains with Restricted Rotation and No Interaction Among the ϕ 's	47
2.8. Rotational Isomeric State (RIS) Approximation.....	49
2.9. Chains with Interactions between ϕ Values of Neighboring Monomers.....	51
2.10. Asymmetric Barriers	53
2.11. Comparison with Experiment	56
2.12. Chain End-to-End Distribution Functions	58
2.12.1 One Dimensional Case.....	58
2.12.2. Extension to a Three Dimensional Chain	61
2.12.3. Extension to Non-Gaussian Case	64
References	71
Appendix 2A - Statistical Mechanics.....	73
References	80
Statistical Thermodynamics of an Ideal Monatomic Gas	81
Appendix 2B - Vector Analysis.....	83
2B.1. Vector Addition	83
2.B.2 Scalar Product.....	84
Reference.....	85
Appendix 2C - Radius of Gyration.....	86
Appendix 2D. Evaluation of $(\mathbf{a}_{m+n} \cdot \mathbf{a}_m)$	92
Appendix 2E. Restricted Rotation with Symmetrical Barrier	99
Appendix 2F. Rotational Isomeric State (RIS) Approximation	103
2F.1. Introduction.....	103
2F.2. The Conformational Partition Function.....	104
2E.3. Mean Square Distance.....	106
References	107
Appendix 2G. Random Walk of Gaussian Chains	109
References	113
Appendix 2H. Radius of Gyration, Size and Shape.....	114
Definition of $\langle \mathbf{r}_q^2 \rangle$	114
$\langle \mathbf{r}_q^2 \rangle$ for a Rigid Rod.....	115
$\langle \mathbf{r}_q^2 \rangle$ for a Sphere of Radius R.....	116

CONTENTS

Determination of $\langle r_q^2 \rangle$ from Scattering.....	117
Chapter 3	121
THERMODYNAMICS.....	121
3.1. Introduction.....	121
3.2 Thermodynamics of Elasticity	121
3.3. Force on a Chain in the Presence of Energy Contributions to Elasticity	129
3.4. Solution Thermodynamics.....	134
3.4.1. Flory-Huggins Theory	134
3.4.2. Calculation of P_2	138
3.3.3. Entropy of Mixing	140
3.5. Polymer Miscibility	145
3.6. Spinodal Decomposition.....	147
3.7. Heat Capacity	153
3.8. Thermodynamics of Crystallization	154
3.8.1 Polymer Structure – Melting Point.....	155
3.8.2. Effect of Diluent and Impurities.....	157
3.8.3. Crystallization Induced by Stretching	164
References	167
Appendix 3A Classical Thermodynamics.....	169
References	175
Appendix 3B. Heat of Mixing	176
Appendix 3C Osmotic Pressure.....	181
Chapter 4	185
OPTICS	185
4.1. Introduction.....	185
4.2. Nature of Electromagnetic Waves	186
4.3. Refraction	187
4.4. Scattering	191
4.4.1. Intensity of Light Scattering for an Isolated Atom or Molecule	194
4.4.2. Effect of the Polarization of Light.....	195
4.4.3. The Scattering Intensity for a Collection of Scattering Objects	196
4.5. Diffraction.....	205

4.5.1. The Reciprocal Lattice.....	205
4.5.2. Interpretation of the Vector Bragg Equation.....	208
4.5.3. The Distance Between Crystal Planes	209
4.5.4. The Diffraction Phenomenon in One Dimension..	211
4.6. Absorption	215
4.7. Fluorescence	216
4.8. Birefringence.....	218
4.9. Scattering from Inhomogeneous Media	222
4.10. Quasi-elastic Light Scattering.....	228
4.11. Variation of Scattering with Electric Fields	229
4.12. Non-Linear Optics.....	230
4.13. Piezo-Electric Materials	232
4.14. Kerr Effect	233
References	234
Appendix 4A Depolarization of Scattering.....	236
Appendix 4B Scattering from a Collection of Molecules	239
Appendix 4D The Magnitude of the Reciprocal Vector H ...	244
Appendix 4E Orientation Fluctuations.....	246
Appendix 4F Scattering from Concentration Fluctuations ...	249
Evaluation of $(\partial\alpha/\partial c)$	252
Evaluation of $[-(\partial\mu_1/\partial c)]$	252
Molecular Weight from Light Scattering	253
Dealing with Large Molecules.....	255
Extensions to Other Kinds of Radiation.....	256
Extensions to Concentrated Solution and Bulk Polymers	257
Effect of Anisotropy and Orientation.....	257
Appendix 4G Why Concentration Fluctuations Relate to Molecular Weight.....	257
How to Measure the Size of an Elephant	258
ANOTHER WAY OF LOOKING AT IT -	260
Chapter 5	263
ELECTRICAL PROPERTIES	263
5.1 Introduction.....	263
5.2. Dielectrics	264

CONTENTS

5.2.1. Dielectric Constant	264
5.2.2. Orientation of permanent dipoles	269
5.2.3. Dielectric Loss.....	269
5.3. Piezo- and Pyroelectric Effects	272
5.4. Piezo-Electric Coefficient.....	274
References	276
Appendix 5A. Lines of Flux	278
5A.1. Electrical Field Strength	278
5A.2. Electric displacement and Flux Density	278
5A.4. The Electrostatic Potential (Voltage).....	280
5A.5. The Field between Parallel Plates.....	280
Appendix 5B. Lorentz Calculation, Internal Field Correction	282
Chapter 6	285
SPECTROSCOPY	285
6.1. Introduction.....	285
6.2. General Background.....	286
6.3. Infrared	288
6.4. Raman.....	295
6.5. Ultraviolet and Visible	299
6.6. Nuclear Magnetic Resonance	300
6.7. Neutron Inelastic Scattering (NIS).....	301
References	303
Appendix 6A Fourier Transform Infrared (FTIR).....	305
References	307
Appendix 6B. Normal Coordinate Analysis.....	308
References	312
Appendix 6C. Spectrographic Notation	313
Chapter 7	314
THE RUBBERY STATE.....	314
7.1. Introduction.....	314
7.2. Force - Extension Relation for Rubbers	316
7.2.1. Simple Case.....	316
7.2.2. Consideration of Network Crosslinks.....	318
7.3. Affine Transformation.....	322
7.4. Uniaxial Stretching at Constant Volume.....	329

7.5. Biaxial Stretching at Constant Volume	331
7.6. Application to the Inflation of a Balloon.....	333
7.7. Network Defects -The Relationship between N_c and ν .	334
7.8. Effect of Swelling on an Isotropic Network	336
7.9. Elastic Properties of Swollen Rubber.....	339
7.10. Elasticity of a Sample That is Swollen When Crosslinked.	341
7.11. Elasticity of Rubbers at Small Extensions.....	343
7.12. Guth-Smallwood Equations	347
References	348
Appendix 7A – Evaluation of Equation 7.30	350
CHAPTER 8.....	352
THE CRYSTALLINE STATE.....	352
8.1. Introduction.....	352
8.2. Evidence for Crystallinity.....	354
8.2.1. X-Ray Diffraction.....	354
8.2.2. Electron Microscopical Observations.....	358
8.2.3. Optical Microscopy	359
8.2.4. Thermodynamic Transitions	360
8.3. Determination of Degree of Crystalline	361
8.3.1. Density Measurements.....	361
8.3.2. X-Ray Diffraction.....	364
8.3.3. Infrared (IR) and Raman.....	365
8.3.4. Wide Line Nuclear Magnetic Resonance	366
8.3.5. Thermal Measurements.....	368
8.4. Morphology	369
8.4.1. Electron Microscope.....	369
i) The observed pyramidal structure.....	369
ii) Moiré Patterns.....	370
i.) Density.....	370
ii) nmr	371
iii) X-ray diffraction	371
iv) Kinetics.....	371
8.4.2. Optical Microscopy	372
8.4.3. Liquid Crystals	373
8.5 Mechanisms of Crystallization	375

CONTENTS

8.5.1. Nucleation and Growth.....	375
8.6. Kinetics of Crystallization	376
8.6.1. Temperature Dependence of the Nucleation Rate.....	376
8.6.2. Nucleation and Growth.....	379
8.6.3. Experimental Determination of n and k	384
i. Slope-Intercept Method	384
ii. Half-life Method.....	385
8.6.4. Temperature Dependence of the Rate of Homogeneous Crystallization.....	386
References	387
Glossary of Symbols Arranged by Chapters	389
Chapter 1.....	389
Chapter 2.....	389
Chapter 3.....	392
Chapter 4.....	396
Chapter 5.....	398
Chapter 7.....	402
Chapter 8.....	403
Index	407

Chapter 1

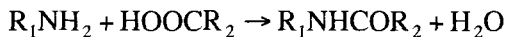
INTRODUCTION

1.1. Background

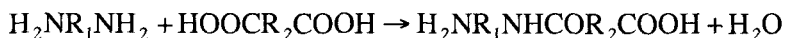
The concept of long chain molecules in which the atoms forming the backbone are bonded by strong primary valence forces, usually covalent in nature, is the foundation of polymer science. Until relatively recently, chemistry, which is the study of molecules in all their ramifications, emphasized the study of small molecules. These could be readily purified to yield materials with constant composition and well characterized properties. Naturally occurring polymers, such as natural rubber or cellulose, did not fit into this framework of small well-characterized molecules [1]. Many investigators considered that the naturally occurring polymers constituted a fourth state of matter, essentially colloidal in nature, because these materials did not seem to obey the laws derived for gases, liquids, or solids as these laws were then understood. The assertion that, since rubber and cellulose were the products of living organisms, a vital principle, not amenable to physico-chemical laws, was involved reinforced this viewpoint.

Based on chemical evidence, Staudinger [2], in the early 1920s, was the first investigator to strongly advocate long, linear chain structures for polystyrene, polyoxymethylene, and natural rubber. During this time span, x-ray diffraction developed as a tool for determining the structure of molecules. The diffraction photographs of natural rubber and cellulose taken by Meyer and Mark were interpreted as showing that these polymers did have long chain structures [3]. Carothers furnished a key argument, based on purely chemical reasoning, in favor of the view that polymers, in the main, were composed of long linear chains. By the late

1920s, organic chemists had accumulated a large store of knowledge on the reaction conditions, products, yields and structures of many small monomeric molecules involved in organic chemical reactions. For example, the reaction between an amine and an organic acid was known to produce an amide with the elimination of a molecule of water:



(R_1 , R_2 being typically methyl, ethyl or other aliphatic radicals). Carothers reasoned that, if both molecules were difunctional (i.e., two amine groups on R_1 and two organic acid groups on R_2), sites would be available for further reactions:



The reaction would continue until the starting materials (difunctional amines and organic acids) were exhausted. Thus, a long chain polymer structure could be synthesized using a well known and well understood organic chemical reaction. In a classic series of investigations [4], Carothers and a small group of co-workers were able to demonstrate that this and similar chemical reactions produced long linear chain molecules. As a point of interest, Carothers produced nylon 66 by using C_6H_{12} (hexamethylene) for R_1 and C_4H_8 for R_2 . Carothers [4] coined the term condensation polymers for the long chain molecules produced by these reactions because the elimination of small molecules such as water condensed the length of the polymer repeat unit compared to that of the starting molecules. Conversely, Carothers called polymers such as polystyrene and polyoxymethylene addition polymers because the monomer units add through the opening of double bonds. Thus, these latter polymers added monomers during formation with no elimination of small molecules.

Many of these linear chain polymers have the advantage for characterization that they are soluble in organic solvents. This has aided greatly, as will be shown later, in the analysis of chain structures and reaction mechanisms and the determination of molecular weight. Most linear polymers, both condensation and addition, also reversibly soften and flow on heating and conversely harden and become rigid on cooling. These materials are sometimes called thermoplastics because they flow

INTRODUCTION

at sufficiently high temperatures. This thermal characteristic is used to advantage in reprocessing these polymers. The thermoplastics did not become commercially available, with a few exceptions such as cellulose acetate, polystyrene, poly(methyl methacrylate), until after World War II. A second class of polymeric materials (thermosets) had been introduced earlier (ca. 1910) starting with the phenol-formaldehyde polymers developed by Leo Baekeland [5]. Thermosets are composed of non-linear polymer chains (based on a functionality of 3 or more) that combine chemically to form three dimensional network polymers. They are soluble and fusible only up through the intermediate stages of polymerization. Once polymerization is complete, the thermosets form hard infusible insoluble structures that soften on heating over a temperature range. The average temperature for the range is called the glass temperature. On heating to higher temperatures, thermosets decompose because of their network structure. The lack of solubility and general intractability rendered thermosets difficult to study from a fundamental standpoint.

Elastomers or rubbers represent an intermediate stage in terms of functionality between thermoplastics and thermosets. Elastomeric behavior in polymers originates from a special type of chain structure. This point is discussed more fully in Chapter 7. Elastomers to be useful articles of commerce require a controlled number of crosslinks (chemical bonds between neighboring chains). Natural rubber (and its progeny, the synthetic rubbers, spawned during and after World War II) elongates readily to several times its original length on the application of a small force and readily retracts with release of the applied force. But, unless it is crosslinked, rubber will tend to flow on being held at high elongations and gradually lose its ability to retract. Goodyear [6] found in the 1830s that, upon adding sulfur to natural rubber latex and heating, the coagulated latex changed from a flowable gum to a retractive elastic material. He also observed that the hardness of natural rubber ranged from a soft crepe rubber (essentially thermoplastic) on small sulfur additions to hard infusible rubber (or thermoset) with large sulfur additions.

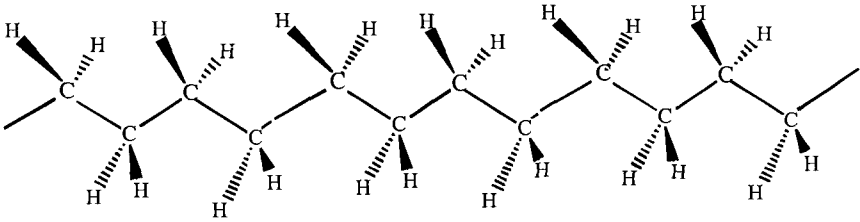


Figure 1.1a. Linear Polyethylene.

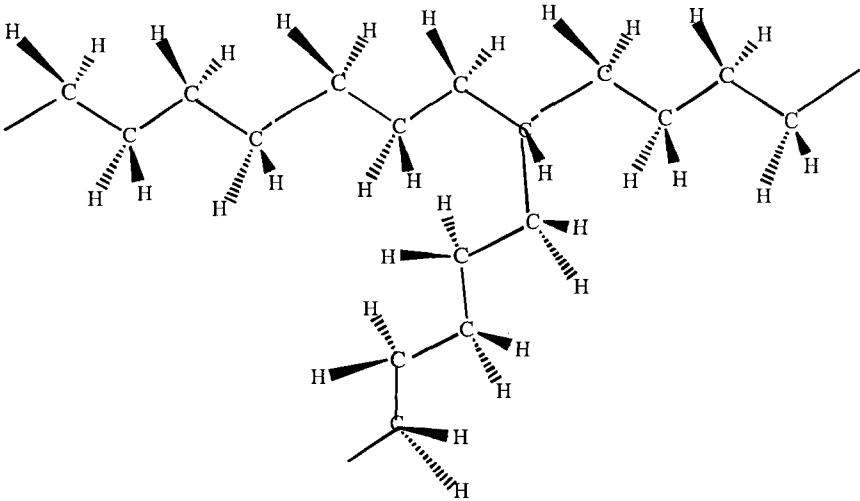


Figure 1.1b. Branched Polyethylene.

1.2. Linear Chain Molecules

1.2.1. Structure

Polyethylene, the prototype or model chain for linear addition polymers, is composed of ethylene monomer units linked by covalent bonds to form long chains (Figure 1.1a.) But, this linear chain was only produced in the mid 50's by the Ziegler–Natta catalysts. Before this, the Fawcett process that required high pressure and temperature produced a polyethylene chain that contained many small side chains or branches attached by covalent bonds to the main chain (Figure 1.1b). Nuclear

INTRODUCTION

magnetic resonance (NMR) work [7] elucidated the type and number of branch chains in high pressure polyethylene. These results support a mechanism for branch chain formation proposed earlier by Roedel [8]. The extent of branching and the branch length alter polymer properties. Linear polyethylene has a higher density, greater degree of crystallinity (Chapter 8) and higher melting point than branched polyethylene.

As a trivial example, the higher melting point of high-density polyethylene allows it to be used in the manufacture of sterilizable baby bottles. At the temperature required for steam sterilization, branched or low density polyethylene bottles soften, flow and collapse into a hollow blob. Linear or high density polyethylene bottles on the other hand maintain their shape. Substitution of a hydrogen atom in the ethylene monomer by a different atom (say chlorine to form poly (vinyl chloride)) or a molecular group (by a methyl group to form polypropylene) imparts a directional character or orientation to monomer addition during polymerization. Three types of monomer additions are possible: head-to-tail, head-to-head, or tail-to-tail (Figure 1.2) with the carbon atom having the substituent group termed the head. The sequence of monomer orientation during polymerization determines the polymer chain configuration. Synthesis sets the chain configuration. It cannot be altered without breaking chemical bonds. Most commercial vinyl polymers have configurations based predominantly on head to tail monomer orientation [9,10]. Until the mid 1950s, catalysts based on free radicals (see Section 1.2) were the customary agents used to produce linear addition polymers. Chain branching and monomer orientation were the main areas investigated in the structure determinations of substituted linear addition polymers. The advent of the Ziegler–Natta or coordination catalysts opened up new vistas in polymer structure work [11]. Using these catalysts, it became possible to produce stereoregular polymers by controlling the placement of a substituent group with respect to the axis of the main chain. As a result, monomers such as propylene, that had previously only yielded low molecular weight waxy oils, could now be polymerized as high melting, highly crystalline solids.

G. Natta [12] first synthesized many of these stereoregular polymers using coordination catalysts and defined many terms used to describe these polymers. Using polypropylene as an example, its monomer

orientation is predominantly head to tail, but polymers with different stereoregularity (or tacticity) and different configurations can be produced by varying the polymerization conditions. Natta initially considered three possible placements with respect to the chain axis. [For simplicity, the chain backbone is assumed to lie in a plane with the subst-

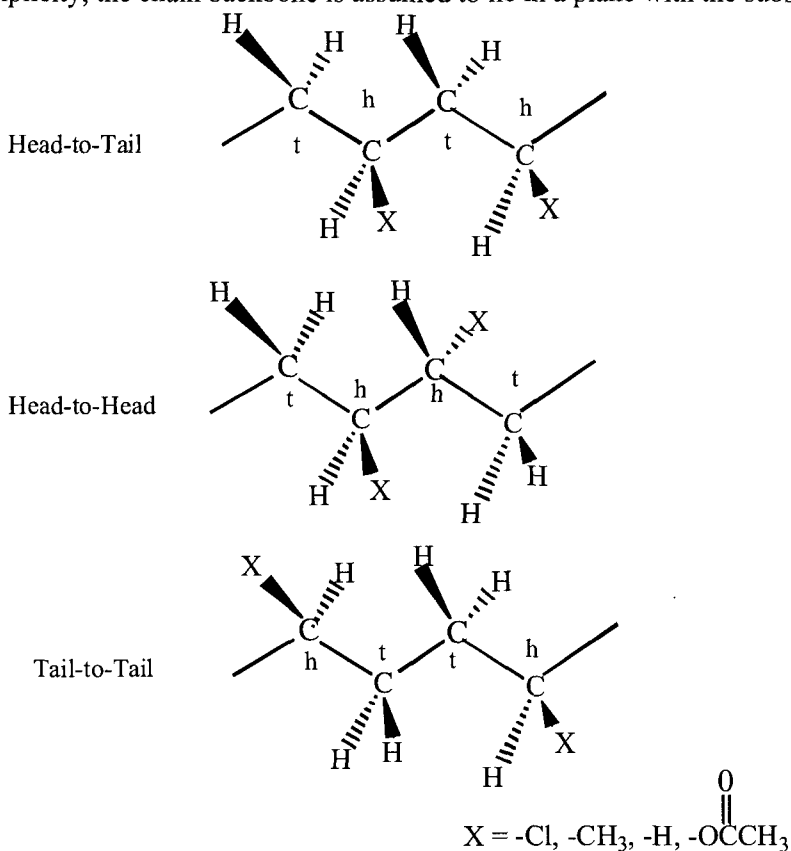


Figure 1.2. Possible Monomer orientations.

tuent groups lying either above or below the plane (Figure 1.3).]

Isotactic - the R substituents are all on the same side of the plane defined perpendicular to the chain backbone axis.

Syndiotactic - the R substituents alternate above and below this plane.

INTRODUCTION

Atactic - the R substituents vary randomly in placement along the chain backbone.

Bovey and others [7] refined tacticity concepts by using NMR techniques to specify the placement of three consecutive main chain substituents or triads. In addition to isotactic or syndiotactic triads, another type, the heterotactic, was defined in which pairs of isotactic placements alternate with pairs of syndiotactic placements in regular fashion (Figure 1.3) More recently, polymer chain tacticity has been described in terms of tetrads or the placement of four consecutive chain substituents.

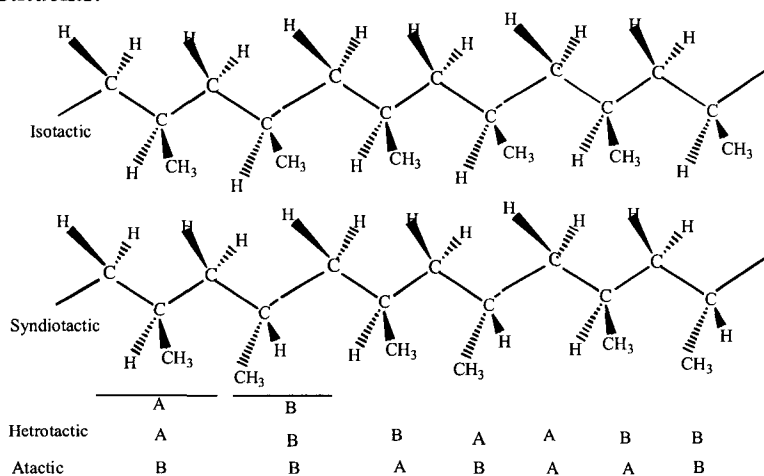


Figure 1.3. Types of Polymer Chain Tacticity.

The nomenclature described above has been elaborated to include diene polymers and optically active chains among others [13]. As mentioned above, tacticity or stereoregularity of chain substituents modifies polymer properties. For example, isotactic polypropylene forms a helical chain structure because of severe over-crowding between neighboring methyl groups and has a crystalline melting point of ca. 165°C. Syndiotactic polypropylene has a linear chain structure similar to that of polyethylene and has a melting point of ca. 131°C. Atactic polypropylene, polymerized by free radical catalysts forms low molecular weight, non-crystalline waxes or oils. Rubbers, based on new

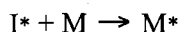
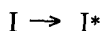
monomer compositions, have been produced using Ziegler–Natta catalysts. One of these, for example, is produced from ethylene and propylene monomers in which neither homopolymer is an elastomer since they crystallize. But, when their monomers are combined to form a copolymer, crystallization is prevented and the product is an elastomer that has found many applications.

Many tactic polymers have asymmetric backbone carbons – the condition for a compound to show optical activity. Tactic polymers usually are not optically active. This lack results from several factors. One is that the asymmetric groups attached to a given carbon are so long in length that a difference of a few carbons does not have a significant effect on the optical activity. Second, one optically active form does not predominate so that right and left hand forms compensate. This topic is discussed in more detail in the references cited [14].

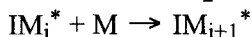
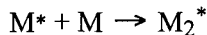
1.2.2. Synthesis

Chain growth during addition polymerization has the three steps of classical chain reactions (other examples are combustion processes or nuclear explosions):

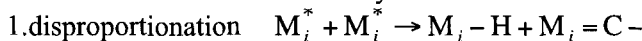
- a. Initiation* – formation of a reactive free radical (I^*), ion or monomer unit usually generated by catalyst or heat.



- b. Propagation* – formation of a long polymer chain by reaction between a monomer unit (M) and a reactive chain end, transfer of the reactive site to the new end, etc.



- c. Termination* – loss of the reactive site by



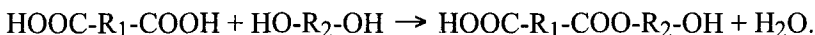
- d. Chain transfer* $M_i^* + M_j \rightarrow M_i - H + M_j^*$

Chain transfer is not a true termination in that the active radical is not terminated but is transferred. This transfer results in modifying the final molecular weight distribution of the polymerizing polymer. The

INTRODUCTION

polymerizing mixture during chain growth, if examined instantaneously, consists of monomer, high molecular weight chains and a few actively growing chains. Initiation is the slow step in this mechanism. Once initiated, the polymer chain grows rapidly to form long, high molecular weight polymers.

Step growth, on the other hand, follows the classical reactions of organic chemistry, but uses, as mentioned earlier, difunctional monomers to link molecules together. For example, on reaction of



The product contains end groups that are available for further reaction. In contrast to chain growth, the polymerizing mixture in step growth at any given instant consists mainly of low molecular weight polymer chains with little of either monomer or high molecular weight polymer present. The polymerization must be carried to high monomer conversion rates to attain high molecular weight polymer by a step growth mechanism [15]. The presence of impurities or of side reactions that reduce monomer conversion to polymer must therefore be avoided.

The above classifications are based on polymerization mechanism or on polymer molecular weight. The physical process however by which a polymer is synthesized is sometimes used for classification. The four main processes are bulk, solution, suspension and emulsion. Bulk polymerization, as the name implies, is carried out by adding catalyst (initiator) to the undiluted monomer. This process has the advantage of simplicity. Methacrylate monomer is cast directly into thin sheets by this process. But, because most polymerizations are exothermic, heat build-up leading to a runaway reaction can be a problem. Solution and suspensions are variants of the bulk process designed to minimize heat build-up. In solution polymerization, the monomer is diluted with an inert liquid that may act as a chain transfer agent thereby reducing the molecular weight of the final product. Because of environmental concerns in use of organic solvents and because of solvent recovery, solution polymerization is becoming less popular. In suspension polymerization, the monomer droplets are dispersed or suspended in a liquid phase, usually water. Thickening agents such as gelatin are added to improve dispersion. Each droplet serves as a site for bulk

polymerization and the liquid medium dissipates the heat generated. Removal of the last traces of liquid in order to obtain pure polymer is a problem in both the solution and suspension processes. Emulsion polymerization is carried out by dispersing monomer droplets in an inert liquid, usually water. Surface active agents or detergents stabilize a portion of the droplets. The water-soluble initiator migrates into the monomer droplet. As polymerization proceeds, fresh monomer from the bulk phase migrates into and adds to the growing chain within the stabilized droplet.

1.2.3. Molecular Weight

As indicated previously, polymeric materials can be prepared over a wide gamut of chain lengths, or alternatively, molecular weights. Oligomers are short chains, containing roughly three to eight monomer units. Telomers are chains composed of an intermediate number of monomer units. Above 15-20 units, the chains are high polymers. Properties improve with increasing chain length up to the high polymer range. Properties tend to approach a constant value with increasing size within the high polymer range.

The ability to measure the size and shape of polymer molecules has been a key factor in the transformation of polymer technology into a science. The techniques used to measure molecular weight share the common characteristic, with few exceptions, that the polymer must be soluble. The polymer molecular weight is calculated by multiplying the molecular weight of the monomer unit by the number of monomer units or alternatively by the degree of polymerization (DP).

The last statement is deceptively simple. Polymers have a distribution of molecular weights in contrast to the set structure and hence constant molecular weight assigned to small molecules such as ethylene or styrene. Differing molecular weights can be obtained from the same sample because different techniques measure different averages over the molecular weight distribution.

Osmotic pressure, equilibrium centrifugation, end group analysis, freezing point depression (cryoscopy), boiling point elevation (ebulliometry) and vapor pressure lowering measure the colligative

properties (the number and not the kind of molecule). The equilibrium centrifugation technique is the only one capable of measuring the number average molecule weight of high molecular weight samples. These measurements, except for equilibrium centrifugation, are analogous to those used in the perfect gas law. Thus, these techniques measure the number average molecular weight ($\langle M_n \rangle$)

$$\langle M_n \rangle = \frac{\sum W_n}{\sum N_n} = \frac{\sum N_n M_n}{\sum N_n} \quad (1.1)$$

where W_n is the weight of material with degree of polymerization n and N_n is the number of molecules with degree of polymerization n whose weight is M_n .

Light scattering and centrifugation techniques (sedimentation and equilibrium) measure the weight contribution of each polymer molecule. Molecular weight data obtained by these techniques yield a weight average molecular weight ($\langle M_w \rangle$):

$$\langle M_w \rangle = \frac{\sum W_n M_n}{\sum W_n} = \frac{\sum N_n M_n^2}{\sum N_n M_n} \quad (1.2)$$

Viscosity is a commonly used technique for determining polymer molecular weights because it is rapid and requires only simple equipment. However, the equipment requires calibration based on samples with molecular weights previously determined by other techniques. The molecular weight average ($\langle M_m \rangle$) determined from viscosity measurements lies between M_n and M_w . The sedimentation centrifugation technique can also be employed to measure a Z average molecular weight ($\langle M_z \rangle$)

$$\langle M_z \rangle = \frac{\sum N_n M_n^3}{\sum N_n M_n^2} \quad (1.3)$$

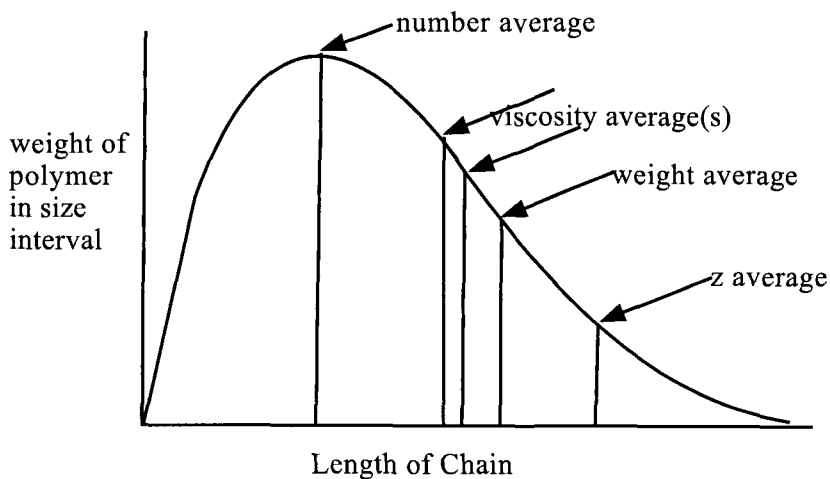


Figure 1.4 Relation between different molecular weight distributions.

Data of this type are useful in evaluating theories of molecular weight distributions. Figure 1.4 illustrates the different types of molecular weight distribution. If the polymer distribution is monodisperse (i.e., all chains have the same length), then it naturally follows that $\langle M_n \rangle = \langle M_w \rangle = \langle M_\eta \rangle = \langle M_z \rangle$ and different characterization techniques will give the same molecular weight. But, polymer distributions are usually polydisperse and the broadness of the polymer distribution can be estimated by taking the ratio of

$$P = \frac{\langle M_w \rangle}{\langle M_n \rangle} \quad (1.4)$$

where P is the polydispersity index. Narrow molecular distributions can be obtained by 'living' anionic polymerizations. In other cases, narrow molecular weight distributions are obtained by fractionation of polymers with a broad distribution. Commercial polymers commonly fall in the range of $P = 2-5$ or greater. The most probable distribution (Appendix 1A) is a special case in molecular weight distributions. It occurs in condensation polymerizations and in random chain cleavage during high temperature degradation [15,16]. The weight average molecular weight is

INTRODUCTION

twice the number average molecular weight in this distribution; therefore, its polydispersity ratio has a value of two. On the other hand, heterogeneous catalysts produce broad dispersities because initiation starts from many sites.

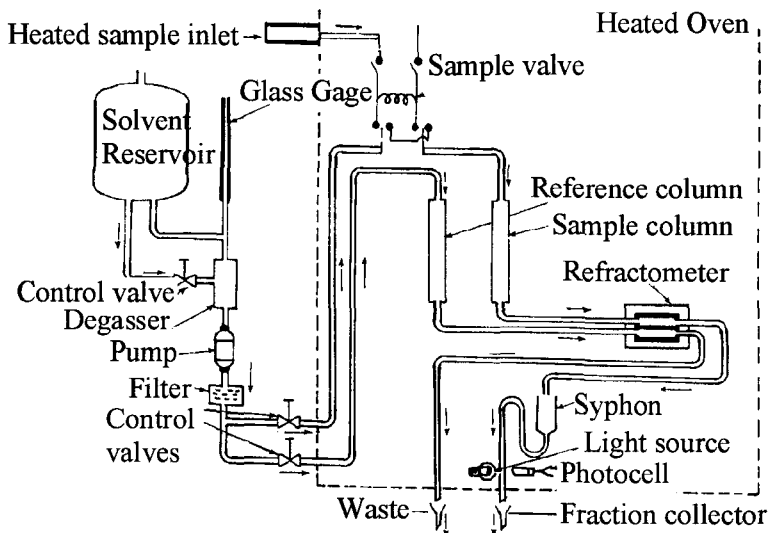


Figure 1.5 Diagram of a Gel Permeation Chromatograph.

Molecular weight distributions were originally measured by fractional precipitation [17]. In this technique, the polymer sample is dissolved in a suitable solvent, a small amount of a nonsolvent added and the mixture allowed to reach equilibrium. The largest molecular chains precipitate, while the smaller chains remain in solution. The process is repeated to obtain fractions of lower and lower molecular weight. The amount of added nonsolvent can be adjusted to obtain distributions of any desired size differences. The availability of gel permeation chromatographic (GPC) (or size exclusion chromatography) equipment has transformed determination of molecular weight distributions from a tedious, time consuming procedure into a routine operation. Dissolved polymer is placed at the top of a column containing porous polymer particles (commonly polystyrene beads crosslinked with divinyl benzene). Washing or eluting the sample down the chromatographic column with

solvent (Figure 1.5) segregates the polymer chains. In gel permeation chromatography (GPC), the largest polymer molecules travel through the column by the shortest path because they cannot fit into the porous beads and therefore are the first to exit. The shortest chains conversely travel a long tortuous path in and out of pores so that they are the last to emerge from the column. Alternatively, in high performance liquid chromatography (HPLC), differences in solubility between components are used to separate polymer and additive fractions. The HPLC technique usually detects eluent stream composition by ultraviolet measurements in the 190 to 600 micron range. Until recently, all commercial GPC instruments required calibration with polymer (usually polystyrene) of a known molecular weight distribution. For calibration, the polymer is eluted through the column and a plot is constructed of molecular weight fraction against the aggregate volume of solution collected to that point. Any subsequent fraction from a polymer with an unknown distribution collected at that particular aggregate volume has the same molecular size because it travels the same path through the column as the calibration fraction. In one commercial instrument, a refractometer measures the amount of polymer in the exit stream. A siphon collects the sample stream into 5 ml sequential fractions. The fractions are counted as they flow between a light source and a photocell detector into a collector. The molecular weight for a particular fraction number or aggregate volume is then read off the calibration plot [18]. There is a caveat however to the use of the GPC technique. GPC measures the polymer hydrodynamic radius of a chain that is a measure of chain stiffness. Therefore, a sample needs chain stiffness similar to that of polystyrene for accurate measurement. Light scattering calibration, which measures the polymer chain radius directly, avoids this problem. Benoit et al. [18] have developed an "absolute" calibration technique.

Two developments in instrumental technique eliminate the need for preliminary calibration: one is based on chromatography and the other on mass spectroscopy.

The chromatographic technique eliminates the need for preliminary calibration by using a laser light source and measuring the stream turbidity or light scattering as the sample flows to the collector. The molecular weight can thus be determined directly on stream. In another

variant, the sample absorption is measured as the sample flows between an ultraviolet or an infrared source and a suitable detector. Thus, copolymer composition can be determined by locating a wavelength at which absorption is sensitive to composition and then observing the changes in absorption as the sample is eluted from the column. By setting up suitable calibration curves, molecular weight distribution and copolymer composition can thus be measured simultaneously by gel permeation chromatographic techniques. A second instrument developed by Yau [19] measures the solution viscosity at a constant flow rate for the eluent on exiting from the GPC unit to measure the molecular weight.

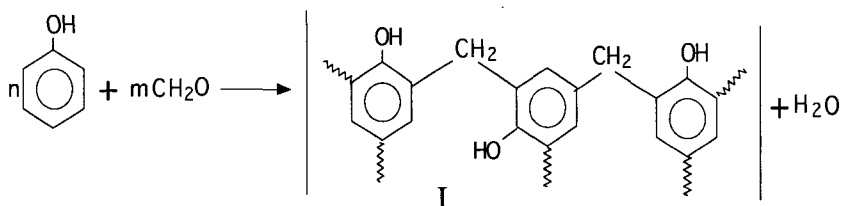
In the mass spectrometric technique, MALDI (matrix assisted laser desorption/ionization), the polymer sample is dissolved, the solutions atomized so that a single polymer chain is contained in a droplet. The droplets are then ionized and pumped into a mass spectrometer where they are accelerated and separated based on their mass. The resulting spectrum is based directly on the molecular weight of the polymer chain

1.3. Network Molecules

1.3.1. Structure

Carothers based his work in condensation polymers on the concept of functionality (i.e., sites available for chemical reaction). As mentioned earlier, molecules with two reactive sites form linear or two-dimensional chains. Molecules with three or more reactive sites form network or three-dimensional polymers. Although the mechanism was not elucidated until much later, Baekeland [5] used multifunctional monomers in 1909 to produce the first completely synthetic polymer by reacting phenol with formaldehyde:

The structure (I) on the right is an idealization because many possible permutations for linking phenol and formaldehyde are possible. Also, the three dimensional nature of this polymer is difficult to depict properly on this two dimensional page. As might be expected, the product of these reactions is a hard, infusible, insoluble polymer because essentially it is one molecule, albeit gigantic, with many bonds between segments.



1.3.2. Synthesis

The properties and processing characteristics of thermoset polymers can be varied by adjusting the ratio of monomeric reactants. Baekeland developed different products by varying the ratio of phenol to formaldehyde and the nomenclature he used to describe his results is still used today.

In the one-stage process, phenol reacts with excess formaldehyde, so that the phenol to formaldehyde ratio is less than one. Bases such as sodium hydroxide or ammonium hydroxide catalyze the reaction. At short times, A- or B- stage resins form. The A-stage resin (or Resol) is a low molecular weight linear polymer that readily dissolves in basic media. The B-stage resin (or Resitol) has a higher molecular weight and a small amount of crosslinking between chains. Resitol is insoluble in bases, but completely soluble in organic solvents and is thermoplastic. Heating B-stage resin at higher temperatures produces C-stage resin (the thermoset).

In the two-stage process, the phenol to formaldehyde ratio is greater than one. The mixture is reacted using heat and an acid catalyst until no further reaction occurs. The reaction product, novalac, is readily soluble in organic solvents. In the second stage, novalac resin is ground to a fine powder and a compound ("hexa" or hexamethyl tetramine) that generates formaldehyde on heating is added. Subsequent heating produces a thermoset resin through network formation.

1.3.3. Molecular Weight

A completely crosslinked polymer consists of one molecular chain. Therefore, no molecular weight distribution, as discussed above, can be

defined. An incompletely crosslinked thermoset contains both crosslinked fractions (gel) and soluble fractions (sol). As the degree of crosslinking increases, the gel to sol ratio rises until finally the sol fraction effectively disappears. The extent of crosslinking can be followed by measuring the amount of sol phase compared to insoluble gel phase. The gel point concept as developed by Flory [20] can be used to determine the point at which a network forms. This concept is also discussed in Chapter 7, Section 8.

The molecular weight between crosslinks affects polymer properties. At high strains, differences in molecular weight between crosslinks lead to different failure modes.

1.4. Rubber

1.4.1. Structure

The elastic character of natural rubber (and the synthetic rubbers) originates because it is a polymeric liquid, albeit one with a very long relaxation time. Most polymers show rubber-like behavior over some temperature range, but only a comparative few are rubbery near room temperature. Figure 1.6 that diagrams the modulus change with temperature for an idealized polymer illustrates the rubbery state in polymers. Many polymer properties (viscosity, density, and heat capacity) show similar changes with temperature, but modulus was selected because it changes by several orders of magnitude with temperature. At low temperatures, a polymer exists as a hard, brittle glass. A tennis ball, cooled to liquid nitrogen temperature, will shatter on impact when dropped from a height of four to five feet. On heating to a temperature that varies with the polymer, the polymer chains soften with a concomitant decrease in modulus and become rubbery. The glass temperature is the midpoint of this transition from the glassy to the rubbery state. [The word transition is not used in the thermodynamic sense, see 8.2.4]. For thermoplastics such as polystyrene or poly(methyl methacrylate), the glass temperature lies near 100°C. Therefore, these polymers are hard, brittle solids at room temperature. On raising the

temperature further, a polymer changes from a rubber to a fluid liquid with a further reduction in modulus.

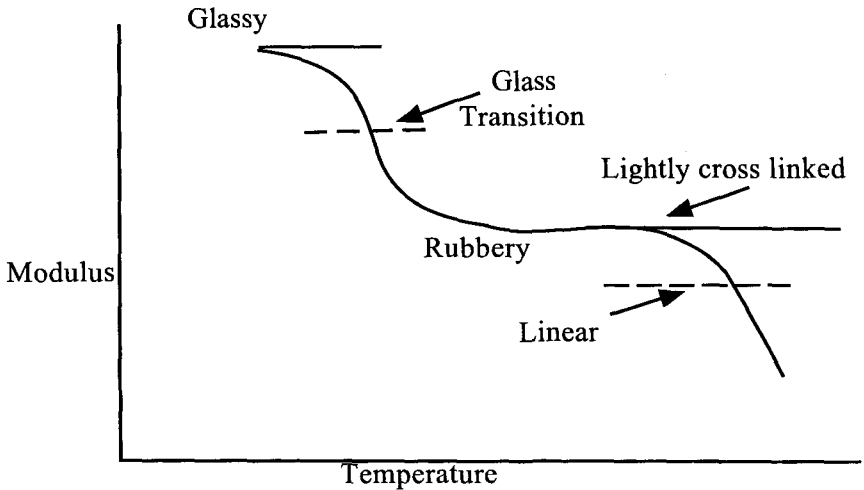


Figure 1.6 Modulus temperature plot depicting the different states of an idealized polymer.

Crosslinking the polymer chains will inhibit this fluidity and, with sufficient crosslinks, a polymer will decompose at high temperatures rather than pass through a fluid state. Thus, heating cannot render rubber fluid for reprocessing because of crosslinks. Semi-crystalline polymers such as polyethylene can be made into rubbers by crosslinking the polymer chains and then heating them above their crystalline melting point to form a rubbery liquid. Polyethylene crosslinked at room temperature by irradiation with a Co beam is a commercial product used in low cost gaskets and sealants in applications where intermediate thermal stability is satisfactory.

Structurally, most polymers that are rubbers near room temperature are composed of long linear chains with: a) freely rotating links and b) weak interactions between chains. This combination results in flexible chains that can readily extend in response to an applied stress. Crosslinks introduced in the rubber during processing generate retractive forces required for elasticity. As shown in Chapter 2, Section 7, the length of the polymer chain limits the total extension. The molecular weight of

INTRODUCTION

natural rubber is commonly reduced by mechanical means such as the use of a Banbury mixer to produce material suitable for processing into finished articles. Because of the superiority in applications such as truck tires where heat buildup is a concern, natural rubber is still processed in large quantities. As a point of interest, the superiority of natural rubber compared to man made natural rubber lies in the higher degree of stereoisomerism of the natural product (99.9% stereoisomeric for natural rubber compared to 99.0% for the man made product).

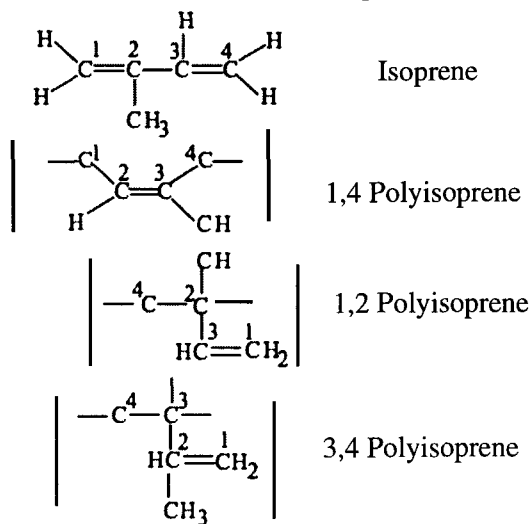


Figure 1.7. Polyisoprene configurations.

As mentioned previously, Mark and Meyer [21] determined the chain structure of natural rubber (poly-1,4 isoprene) in the late 1920s. This molecule has two double bonds which means that the monomer can polymerize in one of three ways to form three possible isomeric chains. Figure 1.7 shows the possible arrangements. The presence of double bonds in the 1,4 polyisoprene chain restricts bond rotation so that two chain isomers are possible. Using terminology borrowed from classical organic chemistry, if the carbon atoms lie on the same side of the double bond (Figure 1.8), the polymer is termed *cis*-1,4 polyisoprene. In *trans*-1,4 polyisoprene, the carbon atoms lie on opposite sides of the double bond (Figure 1.8) is called *gutta percha*.

The importance of the isomeric form can be illustrated by comparison of the properties of two natural products. Natural rubber is almost exclusively composed of *cis*-1,4 polyisoprene, an arrangement that allows freely rotating links. At high extensions, however, natural rubber crystallizes thereby limiting flow. Again, at low temperatures, this material crystallizes and embrittles. Gutta percha, the *trans*-1,4 polyisoprene isomer of natural rubber, is also a natural product. But, synthetic polymers have displaced gutta percha, a poorly elastic rubber, from its main application as the cover material in golf balls. The *trans* isomer that crystallizes above room temperature (35°C) does not have sufficient liquid like character near room temperature to constitute an acceptable elastomer.

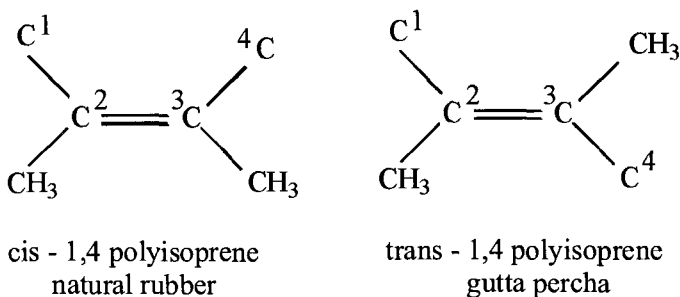


Figure 1.8. Cis-trans isomers in dienes.

Vulcanization or cross-linking chains by reacting the double bond in natural rubber with sulfur and other crosslinking agents is used to limit stress induced flow in natural rubber. Various means were tried to crosslink the synthetic elastomer ethylene propylene rubber (EPR). The technique commonly used is based on experience with natural rubber. A small amount of a diene [a monomer with two double bonds] is incorporated into the EPR chain to furnish sites for vulcanization reactions.

A crosslinking technique, based on the use of thermoplastic/block copolymers discussed in Section 1.5, has recently been developed for limiting flow at high extensions.

1.4.2. Synthesis

Synthetic rubbers first developed in the 1930s were based on butadiene and its copolymers with styrene and acrylonitrile. Emulsion polymerization of these monomers using free radical initiators yielded high molecular weight polymers at high polymerization rates. During the Second World War, production in the United States was concentrated on producing butadiene-styrene (SBR). This rubber is still one of the leaders among all rubbers used in commercial applications.

The synthesis of *cis*-polyisoprene that approximated the molecular weight and structural regularity of natural rubber was first achieved by the use of Ziegler–Natta catalysts in the 1950s.

1.4.3. Molecular Weight

The molecular weight of uncrosslinked rubbers is measured by the same techniques applied to other addition polymers. The concept of a molecular weight for individual chains is not applicable to bulk rubber crosslinked to a degree exceeding the gel point; rather, the concept of chain length between tie points is substituted. The use of swelling liquids to elucidate this quantity is described in Chapter 7, Section 8.

At one time, it was expected that a narrow molecular weight distribution would improve polymer properties. Samples of narrow molecular distribution were tested. Properties of these samples changed over a narrow range. For many applications then, a sample with a broad molecular weight yields better properties because properties change over a broad range.

1.5. Multicomponent Systems

These systems have proven highly successful in tailoring or modifying the properties of two or more polymers to fit a particular application or end use requirement. Multicomponent systems encompass several different types:

1.5.1. Copolymers

When two or more monomers react chemically to form a polymer chain, the result is a copolymer. One example of a copolymer, styrene

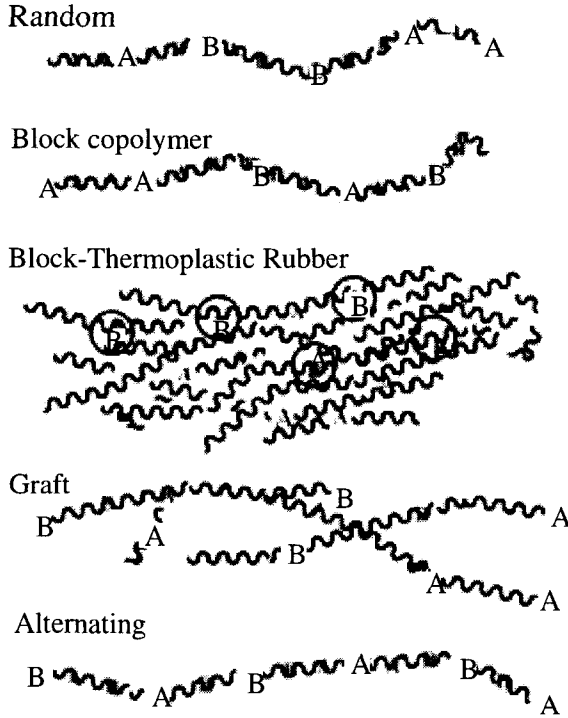


Figure 1.9. Copolymer arrangements.

butadiene rubber, has already been mentioned. Several types of copolymer structures can be distinguished. These are diagrammed in Figure 1.9. The same pair of monomers may be fabricated into different copolymer types by proper selection of reaction conditions. For example, styrene/butadiene copolymers have random placement (Figure 1.9) along the chain backbone if emulsion polymerized by a free radical initiator. Alternatively, batch reaction of these two monomers using an ionic initiator such as butyl lithium produces a block copolymer. Under these conditions, the butadiene monomer polymerizes almost completely

INTRODUCTION

before the styrene monomer starts to polymerize (Figure 1.9). The size of the blocks can be regulated by the amount of each monomer added to the batch reactor. Block copolymers have been applied in recent years to the production of thermoplastic rubbers. As pointed out previously, rubbers require crosslinks or interchain bonds to have adequate strength. This requirement has usually been met by forming chemical bonds through treatment with crosslinking agents based on sulfur compounds or peroxides. However, the presence of chemical crosslinks renders the processing of rubbers difficult and their reclamation almost impossible.

Thermoplastic rubbers avoid these drawbacks. In a typical system, polystyrene blocks attached to each end of a polybutadiene block provide reinforcement to the rubbery polybutadiene at or near room temperature through microphase separation of glassy polystyrene domains. The reinforcing effect is lost on heating the block copolymer to temperatures at which the polystyrene chain segments soften and flow. The block copolymer can thus be processed at temperatures and on equipment suitable for homopolymer polystyrene. On cooling, the polystyrene blocks harden to provide linking points for the polybutadiene rubber domains (Figure 1.9). Both the relative domain sizes and the overall chain lengths are critical factors in determining the desired degree of elasticity.

Graft copolymers are a third copolymer type in which the polymerization of a comonomer initiates at reactive sites present on a preformed chain backbone. This technique improves the mixing of two incompatible polymers. As an example, grafting butadiene monomer units onto the polystyrene chain backbone (Figure 1.9) increases the impact resistance of polystyrene.

Alternating copolymers alternate comonomers in a regular sequence along the chain backbone (Figure 1.9). 1,2 disubstituted ethylenes are usually difficult to polymerize as homopolymers. But, when present in excess, they readily form alternating copolymers with more tractable monomers. Thus, reacting iso-2-butene with ethylene using a Ziegler-Natta catalyst produces an alternating copolymer. The resulting copolymer chain is a head-to-tail polypropylene [22].

Living polymerization was a phrase coined by Michael Szwarc [23] to describe a polymerization process that stops because it runs out of

monomer and has no termination step. He was awarded the Kyoto Prize for his work in this area. When additional monomer is added, polymerization resumes. A block polymer such as polystyrene and polyisoprene, for example, can be formed if the second monomer is isoprene when the polymerization continues. This principle of limited monomer supply with no termination step has been combined with stereoregular catalysts [11] to design new polymer chain structures with narrow molecular weight distributions, controlled structures and functional groups. For example, this combination has produced a syndiotactic polypropylene [24].

Living polymerization and stereo-specific catalysts led to novel polymer structures such as: dendrimers, star and comb (Figure 1.10). Living polymerization techniques are used to produce. These polymers are finding applications as catalysis and light amplifiers.

Dendrimers (Figure 1.10) are three dimensional spherical structures composed of chains arranged similar to tree branches, Hence their name derived from the Greek word for tree, dendros. Dendrimers can be synthesized with a dense array of functional groups and are finding applications in catalysis and light amplification.

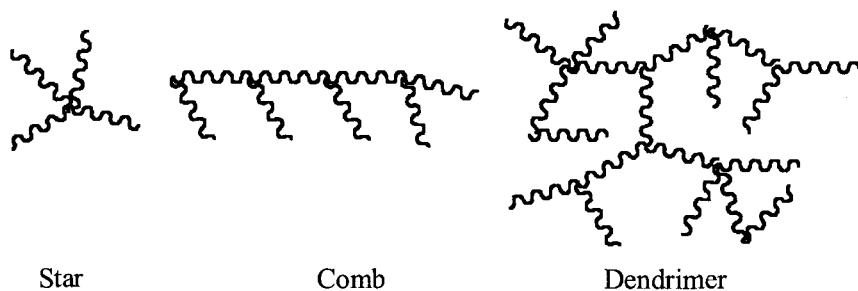


Figure 1.10. Newer polymeric structure diagrams.

Comb polymers (Figure 1.10) alter a polymer structure and can be used to modify the functionality of polymer surface.

Mediated radical polymerization is a derivative of living polymerization in which the chain ends are capped with a protective chemical group in order to better control the polymerization process [25].

Several acronyms are used to describe these polymerizations: Reversible Addition-Fragmentation Transfer (RAFT), Group transfer polymerization, Ring Opening Metathesis Polymerization (ROMP), Group Transfer polymerization.

1.5.2. Polyblends

Polyblends are physical mixtures of two miscible polymers that are thermodynamically stable. By contrast, compatible polymers are mixed systems that are not thermodynamically stable, but phase separate over very slow time scales. Polymers are less miscible than low molecular weight compounds because the high molecular weight of polymers results in a low entropy of mixing (Chapter 3.6). One commercial polyblend is the polystyrene/polyphenylene oxide mixture. Polyphenylene oxide, by itself, softens and flows above 300°C – the temperature at which this polymer starts to show oxidative and thermal degradation. Addition of polystyrene allows the mixture to be processed well below 300°C. Other polymers investigated for blending because of their wide compatibility range are poly(butylene terephthalate), polycaprolactone, and poly(vinyl chloride). Interpenetrating polymer networks (IPN) represent polymer blends that use crosslinking in an attempt to circumvent miscibility limitations [26]. True IPNs consist of crosslinked chains mixed on a molecular level. This ideal is rarely, if ever, realized. Interpenetrating phases have been formed, but not interpenetrating networks. Several methods have been devised for forming IPNs. One scheme involves forming a crosslinked network and then subsequently polymerizing and crosslinking a second independent network in situ. Polystyrene/polybutadiene IPN's formed in this manner show improved dimensional stability at higher temperatures than do polystyrene/polybutadiene mixtures.

1.5.3. Composites

Incorporating fillers or reinforcing agents is another means of improving polymer properties. High particulate loadings improve the dimensional stability of electronic circuit boards so that the thermal expansion is greatly reduced. Particulate fillers (talc, mica, silica, clay, etc.) are used

to modify polymer properties in other ways. Carbon black in small amounts increases the oxidative resistance of polyethylene film many fold. Reinforcing agents, usually in fiber form, are used to increase polymer strength. Silica is distributed uniformly throughout a rubber by mixing a silane into the mixing step and subsequently reacting the silane to form silica. Glass fiber or glass fiber mats combined with thermoset polyester produce the strong, rugged structures that are required in boat hulls. Thermoset epoxy and polyimide resins are being combined with carbon, glass, and Kevlar™ fibers to build structures for aerospace applications. These materials offer lightweight, high stiffness and good temperature stability. Thermoplastic composites such as polyetheretherketone (PEEK™) and carbon fiber are being developed. Polyetherimide (PEI™), polyethersulfone (PES™), RYTON™, and polysulfone are other thermoplastic resins being used in composites. These resins have the advantage of short processing time and reusable scrap – both factors in reducing cost while maintaining part quality. Torlon™ has a long processing time (several days), but offers excellent thermal stability at high temperatures. Torlon™ has been used to fabricate the engine blocks in racing cars.

1.5.4. Ceramers

Combining polymers with inorganic glass formers has recently been used to form ceramers [27]. These hybrid materials show many desirable properties for example, the optical properties of polymers, and the hardness/wear of glass.

References

1. H.F. Mark, *Polymer Chemistry: the past 100 years*; Chem. Eng. News **1976**, 176-189
2. H.A. Staudinger, BER **1920**, 53, 1073
3. H. Morawetz, *Polymers, The Origin and Growth of a Science*;
Wiley-Interscience: New York, **1985**
4. W.H. Carothers *J. Am. Chem. Soc.* **1929**, 51, 2548
5. L.H. Baekeland, *The Synthesis, Constitution and Use of Baekelite*;
Ind. Eng. Chem. **1909**, 1(3), 149 reproduced CHEMTECH **1976**, 6, 49
6. Charles Goodyear, U. S. Patent 1,090, February 28, 1836
7. F.A. Bovey, *Polymer Conformation and Configuration*; Academic: New York, **1969**
8. M.J. Roedel, *J. Am. Chem. Soc.* **1953** 75, 6110
9. C.S. Marvel, J.H. Sample, M.F. Roy, *J. Am. Chem. Soc.* **1939**, 61, 3241
10. C. W. Bunn, *J. Polymer Sci.* **1962**, 56, s16; *ibid.* **1963**, A1, 1395
11. G. Natta, *J. Am. Chem. Soc.* **1955**, 77, 1708
K. Ziegler et al., *Angew. Chem.* **1955**, 67, 541
12. G. Natta et al., *Nuovo Cimento Suppl.* **1960**, 15, 10
13. P. L. Luigi, *Intern. J. Polymeric Materials* **1975**, 4, 33
14. M. Farina, *Topics in Stereochemistry*, **1987**, 17, 1; G. Wulff,
Angew. Chem. Int. Ed. Engl. **1989**, 28, 21
15. R.W. Lenz, *Organic Chemistry of Synthetic High Polymers*;
Interscience: New York, **1967**
16. D.C. Blackley, in *Addition Polymers: Formation and Characterization*,
Derek A. Smith, Ed; Plenum: New York, **1966**
17. M.L. Miller, *The Structure of Polymers*; Reinhold: New York, **1966**
18. H. Benoit, P. Remp and Z. Grubisic, *J. Poly. Soc.* **1967**, B5, 753
19. W. Yau, *Chemtracts-Macromolecular Chemistry* **1990**, 1(1), 1
20. P. J. Flory, *Principles of Polymer Chemistry*; Cornell: Ithaca, New York, **1953**
21. K. H. Meyer and H. Mark, BER **1928**, 61, 1939
22. G. Natta, et al., *J. Am. Chem. Soc.* **1961**, 83, 3343
23. M. Szwarc, M. Levy, R. Milkovitch, *J. Am. Chem. Soc.* **1956**, 78, 2656
24. H. Hagihara, T. Shiono, T. Ikeda, *Macromolecules* **1998**, 31, 3184
25. B.A. Howell, ACS Division of Polymeric Materials,
Science and Engineering (PMSE) **2000**, 83, 578
26. J.A. Manson and L.H. Sperling, *Polymer Blends and Composites*;
Plenum: New York, **1976**
27. H. Huang, B. Orler and G.L. Wilkes, *Macromolecules* **1987**, 20(6), 13

Appendix 1A - Derivation of the Most Probable Distribution

For condensation polymerization, the repeat unit reactivity is independent of chain length. This means that probability arguments can be used to derive the number average or the weight average molecular weight [1]. Thus, the probability (P_n) of forming a chain containing n number of monomers is

$$P_n = p^{n-1}(1-p) \quad (1A.1)$$

where p is the probability of propagation. The total number of molecules is given by

$$N = C \sum P_n = C \sum p^{n-1}(1-p) = C \quad (1A.2)$$

where C = a proportionality constant.
since

$$\sum_{n=1}^{\infty} p^{n-1} = \frac{1}{1-p} \quad (1A.3)$$

based on the series expansion

$$S_0 = 1 + p + p^2 + p^3 + \dots + p^i = \frac{1}{1-p} \quad (1A.4)$$

The weight (W_n) of the n -bonded chain is

$$W_n = M_n P_n = n M_0 P_n \quad (1A.5)$$

where M_0 = the molecular weight of a monomer unit.

M_n = the molecular weight of the chain of degree of polymerization, n .

Substituting equation 1A.2 into equation 1A.5

$$W = C M_0 \sum n P_n = C M_0 \sum n p^{n-1}(1-p) \quad (1A.6)$$

$$= \frac{C M_0}{1-p} \quad (1A.7)$$

since

INTRODUCTION

$$\sum np^{n-1} = \frac{1}{(1-p)^2} \quad (1A.8)$$

based on the series expansion

$$S_1 = \frac{\partial S_0}{\partial p} = 1 + 2p + 3p^2 + \dots + ip^{i-1} = \frac{\partial(1-p)^{-1}}{\partial p} = \frac{1}{(1-p)^2} \quad (1A.9)$$

substituting equations 1A.7 and 1A.2 into 1A.1, the number average molecular weight ($\langle M_n \rangle$) is given by

$$\langle M_n \rangle = \frac{W}{N} = \frac{\frac{CM_0}{1-p}}{C} = \frac{M_0}{1-p} \quad (1A.10)$$

A similar procedure is used to derive an analogous expression for the weight average molecular weight, $\langle M_w \rangle$. Using the definition of $\langle M_w \rangle$ given in equation 1.2,

$$\langle M_w \rangle = \frac{\sum N_n M_n^2}{\sum N_n M_n}$$

and modifying equation 1A.6 for the square term in equation 1.2,

$$\begin{aligned} \sum N_n M_n^2 &= CM_0^2 \sum n^2 p^{n-1} (1-p) \\ &= CM_0^2 \frac{1+p}{(1-p)^3} (1-p) = CM_0^2 \frac{1+p}{(1-p)^2} \end{aligned} \quad (1A.11)$$

based on the series

$$S_2 = pS_1 = p + 2p^2 + 3p^3 + \dots + ip^i \quad (1A.12)$$

$$\frac{\partial(pS_1)}{\partial p} = 1 + 4p + 6p^2 + \dots + i^2 p^{i-1} = \frac{\partial \left[\frac{p}{(1-p)^2} \right]}{\partial p} \quad (1A.13)$$

$$\begin{aligned}
 &= \frac{(1-p)^2 - p[2(1-p)(-1)]}{(1-p)^4} \\
 &= \frac{1-p^2}{(1-p)^4} = \frac{(1-p)(1+p)}{(1-p)^4} = \frac{1+p}{(1-p)^3}
 \end{aligned} \tag{1A.14}$$

Substituting equation 1A.11 and 1A.7 into equation 1.2

$$\langle M_w \rangle = \frac{CM_0^2(1-p) \frac{(1+p)}{(1-p)^3}}{\frac{CM_0}{(1-p)}} = \frac{M_0(1+p)}{(1-p)} \tag{1A.15}$$

Taking molecular weight ratios using 1A.7 and 1A.15

$$\frac{\langle M_w \rangle}{\langle M_n \rangle} = \frac{M_0 \frac{(1+p)}{(1-p)}}{\frac{M_0}{(1-p)}} = 1+p \tag{1A.16}$$

As p approaches 1, as will be the case for a high molecular weight polymer where the probability for propagation is high,

$$\frac{\langle M_w \rangle}{\langle M_n \rangle} = 2 \tag{1A.17}$$

It should be recalled that condensation polymerizations must go to high degrees of conversion to attain high molecular weight polymer chains. For example for a p value of 0.22, the ratio has value of 1.22. Thus, these polymers show the most probable distribution.

Reference

1. P.J. Flory, *J. Am. Chem. Soc.* **1936**, *58*, 1877; *Chem. Revs.* **1946**, *39*, 137

Chapter 2

STATISTICS OF CHAIN CONFORMATIONS

2.1. Introduction

The experimental data and mathematical models derived for the isolated polymer chain and for the size distribution of polymer chains in the aggregate have been the basis for describing many polymer properties in rubbers and thermoplastics. Early work in this area concentrated on simplified models that were amenable to the calculation devices then available. With the advent of high-speed computers and the consequent reduction in computational labor, the more exact rotational isomeric model has been developed and fruitfully applied to many polymer problems.

This chapter lays the groundwork for the various topics discussed in subsequent chapters. The mathematics associated with the statistics of the isolated chain are developed starting with the bonding and structure found in small molecules. Several models of chain structure are presented. Finally, the size distribution of polymer chains is introduced and their description in terms of mathematical equations derived, origin of rubber elasticity, the nature of polymer crystalline and polymeric heat capacities and the miscibility of polyblends.

2.2. Small Molecules

Most polymers of technological importance are based on the carbon atom and the covalent bonding typical of organic compounds. In this sense, organic polymers represent only one branch, albeit a substantial one, of classical organic chemistry. The structural concepts elucidated for small

molecules can be applied to the much larger chain molecules or polymers. Small molecules whose atoms are linked by covalent bonds such as H_2O , CO_2 , and CH_4 have fixed geometry (Figure 2.1). The arrangement of atoms is determined once the bond lengths and angles have been established, for example, by electron diffraction [1]. (There is vibrational motion, of course, but at a given temperature, the average positions are fixed). Configurational isomers are set during synthesis and cannot be interconverted except by chemical reaction.

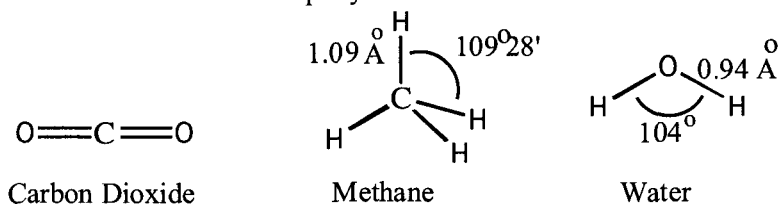


Figure 2.1. Examples of fixed geometries in small molecules.

In methane, each pair of hydrogen atoms forms a tetrahedral angle ($109^{\circ} 28'$) with the central carbon atom and the carbon-hydrogen distance is 1.09 \AA . The tetrahedral geometry changes slightly when a methyl group replaces a hydrogen atom, with a small increase in the tetrahedral angle. In addition, the carbon-carbon bond distance increases to 1.54 \AA . However, in contrast to the double bond case, rotation of substituent groups about the axis of a carbon-carbon single bond is possible. Substituents interact as they rotate about a single bond and go through minima in their interaction energy at certain rotational angles.

Substituents interact as they rotate about a single bond and go through minima in their interaction energy, $V(\phi)$, at certain rotational angles, ϕ . The probability of finding a system with rotation angle, ϕ , at a temperature, T , is described by the Boltzmann equation (Appendix 2A),

$$P(\phi) = C \exp[-V(\phi)/kT]$$

where k is Boltzmann's constant. This means that it is most probable to find systems in states of lowest energy. Thus, if there are energy minima, one is most likely to find systems with values of ϕ corresponding to these minima. These states are referred to as rotational isomers. It is a

good approximation to consider only these rotational isomeric states, although it should be realized that other values of ϕ occur, albeit with lower probability. It should be that at sufficiently high temperatures, this weighing of probabilities becomes less significant, and ultimately, all values of ϕ become equally probable, a state of free rotation.

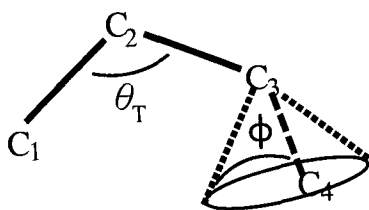


Figure 2.2. The tetrahedral angle θ_T and the rotational bond angle ϕ .

The rotational angle (ϕ) or the angle between non-bonded atoms (Figure 2.2) is thus required to describe these structures completely [2]. The result for a symmetrical molecule is shown in Figure 2.3. Conformations can be described by using 1,2 dichloroethane as an example. One conformation is the same as in the double bond case: trans represents the conformation in which the two chlorine atoms are furthest apart and have the least steric hindrance the second conformation, because of the threefold symmetry of the carbon atom substituents, is the gauche (right or left). The energetics for internal rotation about the single covalent bond axis in 1,2 dichloroethane can be summarized by a plot of potential energy against rotational angle ϕ (Figure 2.4). The trans conformation has the lowest potential energy the gauche conformer represents intermediate states of potential energy for this molecule. While most probable, small deviations from the trans and gauche angles can lead to appreciable differences in the overall chain conformation.

Evidence for such internal rotation comes from infrared spectra [3] or from dipole moments of substituted hydrocarbons [4]. For example, if the average value of $\phi = 0$, then the dipole moment of 1,2 dichloroethane would be zero. At finite values of ϕ , the dipole moment is finite and can be calculated from the non-vanishing components given by

$$\mu_x = \mu \sin \theta (1 - \cos \phi) \quad (2.1)$$

and

$$\mu_y = \mu \sin \theta \sin \phi \quad (2.2)$$

where

- μ = the dipole moment for the C-Cl bond in units of Debyes
- x = the direction along the chain axis
- y = the direction perpendicular to the chain axis

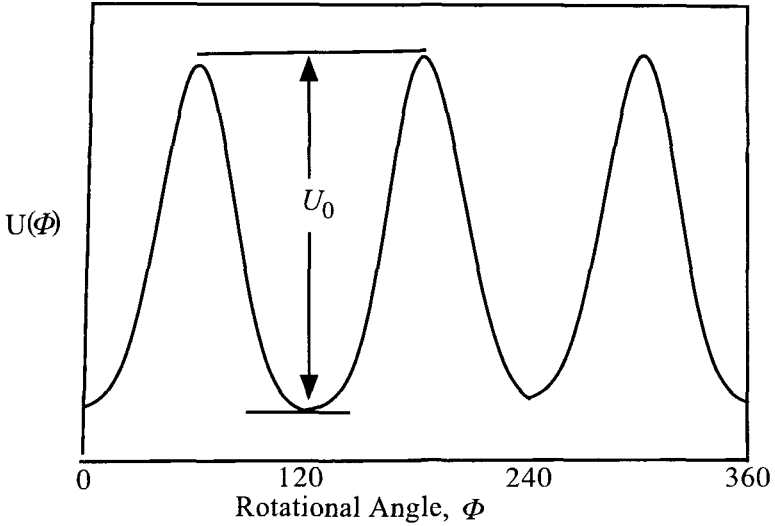


Figure 2.3. Potential Energy Diagram for symmetrical barriers.

For free rotation, in which all values of ϕ are equally probable, so that

$$\langle \mu_x \rangle = \mu \sin \theta (1 - \langle \cos \phi \rangle) = \mu \sin \theta \quad (2.3)$$

and

$$\langle \mu_y \rangle = \mu \sin \theta \langle \sin \phi \rangle = 0 \quad (2.4)$$

since

$$\langle \cos \phi \rangle = \langle \sin \phi \rangle = 0 \quad (2.5)$$

Because the trans conformation has the lowest energy, it is preferred. Therefore, the dipole moment is not zero, which is what is found experimentally.

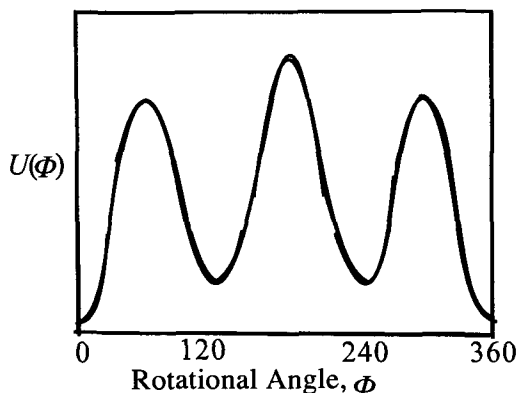


Figure 2.4. Potential Energy Diagram for a molecule with symmetrical barriers and with trans the lowest energy state.

Rotation, then, is not completely free. The probability of a given value is specified by $P(\phi)$, which can be obtained from a theoretical analysis of bonding and interaction potentials, giving rise to a calculated potential energy function $U(\phi)$ and using a Boltzmann expression (Appendix 2A),

$$P(\phi) = \left\{ e^{-U(\phi)/kT} \right\} / \left\{ \int_{\phi=0}^{2\pi} e^{-U(\phi)/kT} d\phi \right\} \quad (2.6)$$

Because of the difficulty in carrying out direct calculations, an approach sums over the pair potential between atoms

$$U(\phi) = \sum_i \sum_j U_{ij}(r_{ij}) \quad (2.7)$$

where r_{ij} is the interaction potential between the i^{th} and the j^{th} atoms separated by the distance r (which is a function of ϕ). Typical potential functions that have been used include the Lennard-Jones [5] potential,

$$U_{ij}(r_{ij}) = \frac{A_{ij}}{r_{ij}^{12}} - \frac{B_{ij}}{r_{ij}^6} \quad (2.8)$$

or exponential forms [6,7] such as

$$U_{ij}(r_{ij}) = K_{ij}e^{-a_{ij}r_{ij}} - \frac{K'_{ij}}{r_{ij}^6} \quad (2.9)$$

or more complex functions. Summaries of the results of such approaches have been given [8,9].

For substituted ethanes such as 1,2 dichloroethane, one-parameter equations such as 2.8 are not adequate, and a better approximation is

$$U(\phi) = \frac{U_0}{2} [x(1 - \cos \phi) + (1 - x)(1 - \cos 3\phi)] \quad (2.10)$$

giving rise to the variation shown in Figure 2.5 [6,10]. In equation 2.12 below, x is the fraction of conformers with a $\cos \phi$ type potential. Taylor [8] gives values of $\cos \phi$

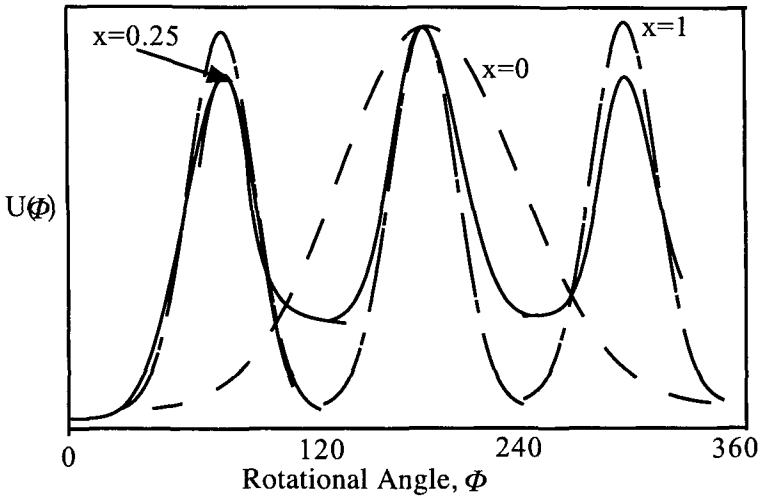


Figure 2.5. Potential Energy Diagram for a two parameter equation 2.11.

obtained by using the potential of equation 2.12 in equation 2.6 and numerically evaluating the integral of equation 2.5. It is possible, for

example, by substituting this value and the corresponding value of $\sin \phi$ into equations 2.3 and 2.4 to predict the variation of the dipole moment of 1,2 dichloroethylene with temperature. Since the value of $P(\phi)$ depends exponentially upon $U(\phi)$, it will be much greater for $\phi = 0^\circ$, 120° and 240° corresponding to potential energy minima than for other values.

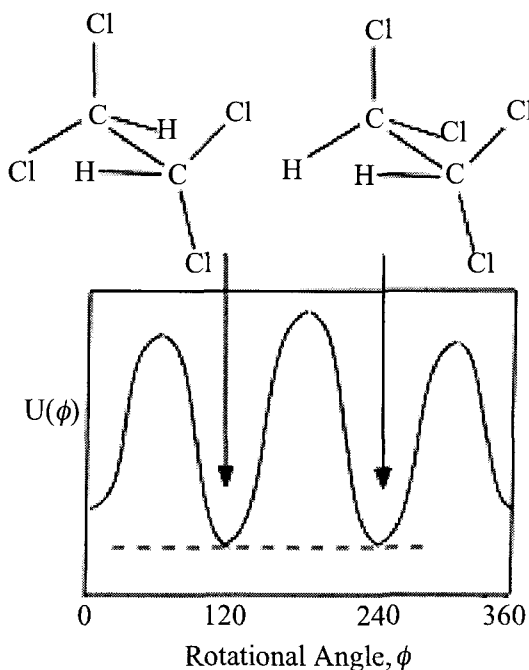


Figure 2.6. Potential Energy Diagrams for $\text{Cl}_2\text{H-CHCl}_2$ in which the gauche forms have the minimum potentials.

This is the basis of the rotational isomeric approximation of Volkenstein [9] and others. The lowest energy conformation at $\phi = 0^\circ$ is the trans conformation, while the two minima at $\phi = 120^\circ$ and 240° are the gauche plus (g^+) and gauche minus (g^-) conformations (Figure 2.6). It is a good approximation in the calculation of molecular properties to assume that the molecule is an equilibrium mixture of these conformers, so that

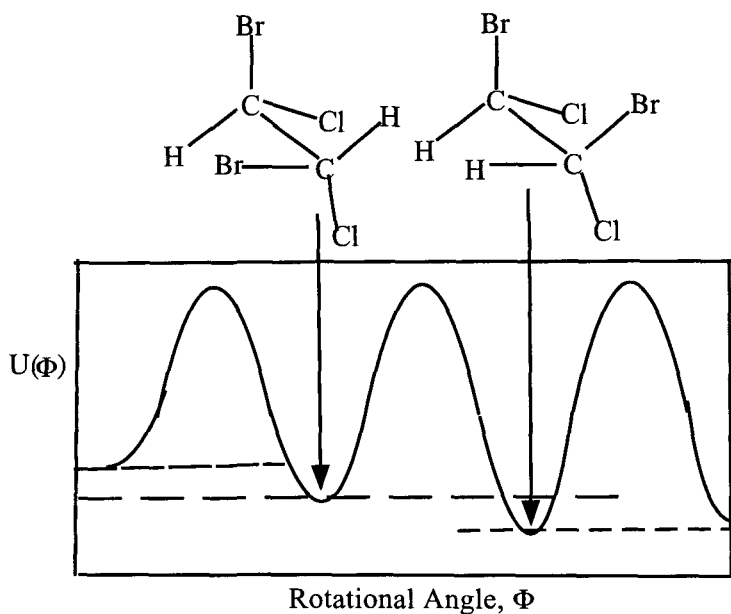


Figure 2.7. Potential energy diagram for BrCLHC-CHClBr in which the gauche forms are the minimum energy conformers.

$$P(t) = \frac{e^{-U(t)/RT}}{e^{-U(t)/RT} + 2e^{-U(g)/RT}} = P(\phi = 0^\circ) \quad (2.11)$$

and

$$P(g) = \frac{e^{-U(g)/RT}}{e^{-U(t)/RT} + 2e^{-U(g)/RT}} = P(\phi = 120^\circ) = P(\phi = 240^\circ) \quad (2.12)$$

Now, from equation 2.10

$$U(t) = U(0^\circ) = 0$$

and

$$U(g) = U(120^\circ) = (U_0/2)(1 - \cos 120^\circ) = (3/4)U_0 \quad (2.13)$$

so that

$$P(t) = \frac{1}{(1+2\sigma)} \quad (2.14)$$

and

$$P(g) = P(g+) = P(g-) = \frac{2\sigma}{(1+2\sigma)} \quad (2.15)$$

where

$$\sigma = \exp[-U(g)/RT] = \exp[-3U_0(g)/RT] \quad (2.16)$$

Then

$$\langle \cos \phi \rangle = (\cos 0^\circ)P(t) + (\cos 120^\circ)P(g+) + (\cos 240^\circ)P(g-) = \frac{1-\sigma}{1+2\sigma} \quad (2.17)$$

and

$$\sin \phi = (\sin 0^\circ)P(t) + (\sin 120^\circ)P(g+) + (\sin 240^\circ)P(g-) = 0 \quad (2.18)$$

Thus, the average dipole moment of 1,2 dichloroethylene with its hindered rotation (equation 2.1) is

$$\langle \mu \rangle = \mu_{\text{C-Cl}} \sin \left[\frac{3\sigma}{1+2\sigma} \right] \quad (2.19)$$

For other arrangements of substituents, the potential energy barrier has a different shape. For example, for $[\text{Cl}_2\text{HC}-\text{CHCl}_2]$, the gauche conformation has the lowest energy and the potential energy varies as in Figure 2.6. For an asymmetric potential as in Figure 2.6, $P(g-) \neq P(g+)$. Whether $g(-)$ or $g(+)$ is lowest energy state in an asymmetrically substituted molecule such as $\text{BrH}_2\text{C}-\text{CClBr}_2$ (Figure 2.7), the barrier height depends upon which optical isomer (about the asymmetric carbon) is present. In this case, $\sin \phi \neq 0$ (cf. equations 2.4 and 2.18). The presence of asymmetric carbons can be detected by rotation of plane polarized light on passage through an organic compound. The polarization direction of the light can rotate clockwise or counterclockwise depending on the type of asymmetry about the asymmetric carbon.

2.3. Larger Molecules, Statistical Variation of Molecular Conformations

For larger molecules, the dimensions of the molecule depend upon the internal rotation. If the first three carbon atoms lie in the plane of the paper, then the dimensions of the molecule depends upon the internal rotation angle (ϕ) defining the position of the fourth atom.

To calculate the dimensions of the molecule, one defines a vector (\mathbf{R}) connecting the first to the fourth atom (Figure 2.8). This may be described in terms of the unit vectors \mathbf{a}_1 , \mathbf{a}_2 and \mathbf{a}_3 that give the direction of each of these bonds. The bond length is ℓ . Then

$$\langle \mathbf{R} \rangle = \ell (\langle \mathbf{a}_1 \rangle + \langle \mathbf{a}_2 \rangle + \langle \mathbf{a}_3 \rangle) \quad (2.20)$$

The mean-square length of the molecule is then, using the scalar product of two vectors (Appendix 2B)

$$\langle R^2 \rangle = \langle \mathbf{R} \cdot \mathbf{R} \rangle = \ell^2 \left[\langle \mathbf{a}_1 \rangle^2 + \langle \mathbf{a}_2 \rangle^2 + \langle \mathbf{a}_3 \rangle^2 + 2 \langle \mathbf{a}_1 \cdot \mathbf{a}_2 \rangle + 2 \langle \mathbf{a}_2 \cdot \mathbf{a}_3 \rangle + 2 \langle \mathbf{a}_1 \cdot \mathbf{a}_3 \rangle \right] \quad (2.21)$$

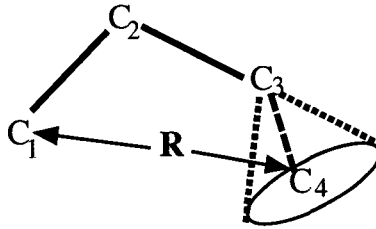


Figure 2.8. Vector distance between the end atoms in the n-butane molecule.

$\langle R^2 \rangle^{1/2}$ is the root mean square distance between the ends of the molecule and should not be confused with the molecular contour length or the distance along the molecule's backbone. The contour length has a constant value set by the molecular bond angles and lengths in contrast to $\langle \mathbf{R} \rangle$ which varies depending on the rotation angle.

As will be discussed later, $\langle R^2 \rangle^{1/2}$ is only one measure for characterizing molecular dimensions. Another measure is the radius of

gyration (Appendix 2C). The bond vectors in equation 2.21 are transformed in terms of molecular parameters as shown in Appendix 2D

$$\begin{aligned}\langle a_1 \rangle^2 &= \langle a_2 \rangle^2 = \langle a_3 \rangle^2 = 1 \\ \langle \mathbf{a}_1 \cdot \mathbf{a}_2 \rangle &= \langle \mathbf{a}_3 \cdot \mathbf{a}_4 \rangle = \cos \theta\end{aligned}\quad (2C.22)$$

and

$$\langle \mathbf{a}_1 \cdot \mathbf{a}_2 \rangle = \cos^2 \theta + \sin^2 \theta \cos \phi \quad (2C.24)$$

Therefore, by substituting into equation 2.21, one obtains

$$\langle R^2 \rangle = l^2 \left[3 + 4 \cos \theta + 2 \left(\cos^2 \theta + \sin^2 \theta \langle \cos \phi \rangle \right) \right] \quad (2.22)$$

For free rotation, $\langle \cos \phi \rangle = 0$ and

$$\langle R^2 \rangle = l^2 \left[3 + 4 \cos \theta + 2 \cos^2 \theta \right] \quad (2.23)$$

2.4. Statistical Segment Model

Several theories dealing with polymer topics embody the use of the statistical segment model first proposed by Kuhn [10]. This model, though admittedly not realistic in terms of chain structure or geometry, has the great virtues of simplicity and ease in calculation [see for example Section 4 in this chapter]. For this model, a fictitious chain composed of Z stiff segments of length, L , joined by freely rotatable ball and socket joints replaces the real chain with its bond lengths and angles. Then, if \mathbf{a}_i is a unit vector along a Kuhn segment, $\langle \mathbf{a}_i \cdot \mathbf{a}_i \rangle = 1$. If $i \neq j$ since Kuhn segments orient randomly with respect to each other, $\langle \mathbf{a}_i \cdot \mathbf{a}_j \rangle = 0$. Two equations relate the model chain to the real chain:

$$\langle \mathbf{R}^2 \rangle = Nl^2 \left[\frac{1 + \cos \theta (1 + \eta)}{1 - \cos \theta (1 - \eta)} \right] = ZL^2 \quad (2.24)$$

and

$$R = Nl \sin \alpha = ZL \quad (2.25)$$

where α = the dihedral angle as shown in Figure 2.8. The statistical segment length (L) is expressed in terms of the bond length (ℓ) and bond angle (θ) by the following transformations. From Figure 2.9, the relation.

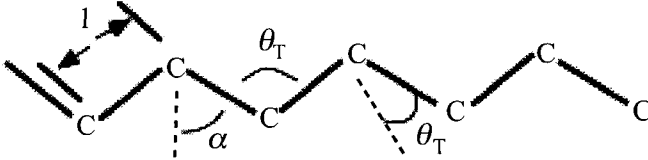


Figure 2.9. Relationship between quantities used in the statistical segment derivation.

$$\begin{aligned}\theta + 2\alpha &= \pi \\ \alpha &= \frac{\pi - \theta}{2}\end{aligned}\quad (2.26)$$

is seen.

Using the trigonometric identity

$$\sin(90^\circ - \theta) = \cos \theta$$

The angle α can be expressed in terms of θ by

$$\sin \alpha = \sin\left(\frac{\pi - \theta}{2}\right) = \sin\left(\frac{\pi}{2} - \frac{\theta}{2}\right) = \cos \frac{\theta}{2}\quad (2.27)$$

From equations 2.25 and 2.27

$$Z = \left(\frac{N\ell}{L}\right) \sin \alpha = \left(\frac{N\ell}{L}\right) \cos\left(\frac{\theta}{2}\right)\quad (2.28)$$

Substituting equation 2.28 in equation 2.24 yields

$$L = \ell \left[\frac{1 + \cos \theta}{1 - \cos \theta} \frac{1 + \eta}{1 - \eta} \right]\quad (2.29)$$

This equation states that the statistical segment length L increases with increasing values of η . Thus a stiffer chain has a larger η , a larger L and a smaller Z . The Kuhn segment length is thus adjusted to account for chain stiffness. On the other hand, L depends on temperature since freedom of rotation, and hence, chain stiffness, is temperature dependent.

The following example illustrates the simplicity of calculation afforded by the statistical segment model. From equation 2.25, the chain contour length is $R = ZL$ and from equation 2.24, the mean square end-to-end distance is

$$\langle \mathbf{R}^2 \rangle = ZL^2$$

or

$$\sqrt{\langle \mathbf{R}^2 \rangle} = \sqrt{ZL^2}$$

Taking the ratio (α_∞) of the contour length to the mean square length

$$\alpha_\infty = \frac{ZL}{\sqrt{ZL^2}} = \sqrt{Z} \quad (2.30)$$

Thus in a few steps, equation 2.30 demonstrates mathematically the intuitively reasonable idea that a stiff chain contains fewer segments for a given chain length. Because the extension increases as the square root, this equation also shows why rubbers are composed of high polymer chains.

This is one of the most important results in polymer physics. Since Z is proportional to the molecular weight, it predicts that the root mean square dimension of a polymer molecule, $\langle \mathbf{R}^2 \rangle^{1/2}$ is proportional to its molecular weight, M , an important consequence in understanding solution viscosity and differing from the Staudinger stiff rod which predicts dimensions proportional to M . This formalism was used in the "problem of the Random Walk" prior to its polymer application and has been basic to the understanding of Brownian motion and diffusion, error calculations, and the critical mass for nuclear chain reactions.

One should point out that the statistical segment is a mathematical fiction, used to make calculations easier, and differs from the true monomer unit. It may contain more than one monomer unit and L depends on chain stiffness, with stiffer chains being represented by larger L values. Since the freedom of rotation is temperature dependent, the statistical length, L , may vary with temperature.

2.5. Generalization to High Polymers

The procedure given above for n-butane may now be generalized to a chain containing N identical bonds of length l in which

$$\langle \mathbf{R} \rangle = l \sum_{i=1}^N \mathbf{a}_i \quad (2.31)$$

replaces the three bonds considered in the n-butane example. On expanding equation 2.24

$$\langle R^2 \rangle = \langle (\mathbf{R} \cdot \mathbf{R}) \rangle = l^2 \left[\sum_{i=1}^N a_i^2 + 2 \sum_{i=1}^{N-1} (\mathbf{a}_i \cdot \mathbf{a}_{i+1} + 1) + 2 \sum_{i=1}^{N-2} (\mathbf{a}_i \cdot \mathbf{a}_{i+2} + 2) + 2 \sum_{i=1}^{N-3} (\mathbf{a}_i \cdot \mathbf{a}_{i+3} + 3) + \dots \right] \quad (2.32)$$

By analogy with n-butane (equation 2.20) and, as before, using equation 2C-22

$$\langle a_i \rangle^2 = 1$$

and

$$\langle \mathbf{a}_i \cdot \mathbf{a}_{i+1} \rangle = \cos \theta$$

for all values of i . Similarly, as in the n-butane case (equation 2C-24)

$$\langle \mathbf{a}_i \cdot \mathbf{a}_{i+2} \rangle = \cos^2 \theta + \sin^2 \theta \langle \cos \phi_{i+2} \rangle \quad (2.33)$$

where ϕ_{i+2} is the ϕ coordinate of \mathbf{a}_{i+2} in the coordinate system defined by \mathbf{a}_i and \mathbf{a}_{i+1} . If we make the assumption that the ϕ 's are independent because of no interaction between chain segments, then $\langle \cos \phi_{i+2} \rangle$ will be independent of ϕ and we shall define, as does Eyring [11] and also Volkenstein [9], an average $\cos \phi$ value

$$\eta = \langle \cos \phi \rangle \quad (2.34)$$

Then, substituting equations 2C.29, 2C.31, 2.33 and 2.34 into equation 2.31 and collecting terms

$$\langle R^2 \rangle = l^2 \left[N + 2(N-1) \cos \theta + 2(N-2) (\cos^2 \theta + \sin^2 \theta) \eta + \dots \right] \quad (2.35)$$

In the special case of free rotation for which $\eta = 0$, equation 2.35 becomes (see Appendix 2D for treatment of higher terms)

$$\begin{aligned} \langle R^2 \rangle &= l^2 \left\{ N + 2 \left[(N-1) \cos \theta + (N-2) \cos^2 \theta + (N-3) \cos^3 \theta + \dots + \cos^{N-1} \theta \right] \right\} \\ &= l^2 \left\{ N \left[1 + 2 \left(\cos \theta + \cos^2 \theta + \cos^3 \theta + \dots + \cos^{N-1} \theta \right) \right] \right. \\ &\quad \left. - 2l \left[\cos \theta + 2 \cos^2 \theta + 3 \cos^3 \theta + \dots + (N-1) \cos^{N-1} \theta \right] \right\} \end{aligned} \quad (2.36)$$

Using the trigonometric relations

$$\cos \theta + 2 \cos^2 \theta + 3 \cos^3 \theta + \dots + (N-1) \cos^{N-1} \theta = \frac{\cos \theta - \cos^N \theta}{1 - \cos \theta} \quad (2.37)$$

and

$$\begin{aligned} &\cos \theta + 2 \cos^2 \theta + 3 \cos^3 \theta + \dots + (N-1) \cos^{N-1} \theta \\ &= \frac{\cos \theta - N \cos^N \theta + N \cos^{N-1} \theta - \cos^{N+1} \theta}{(1 - \cos \theta)^2} \end{aligned} \quad (2.38)$$

Substituting equations 2.37 and 2.38 into equation 2.36 yields

$$\langle R^2 \rangle = l^2 \left[\frac{N - N \cos^2 \theta - 2 \cos \theta + 2 \cos^{N+1} \theta}{(1 - \cos \theta)^2} \right] \quad (2.39)$$

For the case in which $N = 3$, this equation reduces to the special case of equation 2.23. For very large N , $\cos^{N+1} \theta$ is negligible for angles other than 0° , and terms multiplied by N are much larger than the other terms, so that equation 2.39 reduces to

$$\langle R^2 \rangle = N \ell^2 \left[\frac{1 + \cos \theta}{1 - \cos \theta} \right] \quad (2.40)$$

2.6. Polymer Chains Containing Two Kinds of Atoms

The same procedures apply to chains containing two different atoms such as the backbone chains of a silicone polymer or polyoxymethylene (Figure 2.10). In this case, while all bonds have the same length, ℓ , there are two different bond angles, θ_1 and θ_2 . Thus, instead of equation 2.32, we have

$$\begin{aligned} \langle \mathbf{R}^2 \rangle = & \ell^2 \left(\sum_{i=1}^N \mathbf{a}_i^2 + 2[\langle \mathbf{a}_1 \cdot \mathbf{a}_2 \rangle + \langle \mathbf{a}_2 \cdot \mathbf{a}_3 \rangle + \langle \mathbf{a}_3 \cdot \mathbf{a}_4 \rangle + \dots + \langle \mathbf{a}_{N-1} \cdot \mathbf{a}_N \rangle] + \right. \\ & + 2[\langle \mathbf{a}_1 \cdot \mathbf{a}_3 \rangle + \langle \mathbf{a}_2 \cdot \mathbf{a}_4 \rangle + \langle \mathbf{a}_3 \cdot \mathbf{a}_5 \rangle + \dots + \langle \mathbf{a}_{N-1} \cdot \mathbf{a}_N \rangle] \\ & \left. + 2[\langle \mathbf{a}_1 \cdot \mathbf{a}_4 \rangle + \langle \mathbf{a}_2 \cdot \mathbf{a}_5 \rangle + \langle \mathbf{a}_3 \cdot \mathbf{a}_6 \rangle + \dots + \langle \mathbf{a}_{N-3} \cdot \mathbf{a}_N \rangle] + \dots \right) \end{aligned} \quad (2.41)$$

As before, $\sum_{i=1}^N \mathbf{a}_i^2 = 1$. However, two groups of dot products must now be distinguished.

$$\mathbf{a}_1 \cdot \mathbf{a}_2 = \mathbf{a}_3 \cdot \mathbf{a}_4 = \mathbf{a}_5 \cdot \mathbf{a}_6 = \dots = \cos \theta_1 = x \quad (2.42)$$

and

$$\mathbf{a}_2 \cdot \mathbf{a}_3 = \mathbf{a}_4 \cdot \mathbf{a}_5 = \mathbf{a}_6 \cdot \mathbf{a}_7 = \dots = \cos \theta_2 = y \quad (2.43)$$

Also, for the case of free rotation

$$\mathbf{a}_1 \cdot \mathbf{a}_3 = \mathbf{a}_2 \cdot \mathbf{a}_4 = \mathbf{a}_3 \cdot \mathbf{a}_5 = \dots = \cos \theta_1 \cos \theta_2 = xy \quad (2.44)$$

But

$$\mathbf{a}_1 \cdot \mathbf{a}_4 = \mathbf{a}_3 \cdot \mathbf{a}_6 = \mathbf{a}_5 \cdot \mathbf{a}_8 = \dots = \cos^2 \theta_1 \cos \theta_2 = x^2 y \quad (2.45)$$

and

$$\langle \mathbf{a}_1 \cdot \mathbf{a}_4 \rangle = \langle \mathbf{a}_2 \cdot \mathbf{a}_5 \rangle = \langle \mathbf{a}_4 \cdot \mathbf{a}_7 \rangle = \dots = \cos \theta_1 \cos^2 \theta_2 = xy^2 \quad (2.46)$$

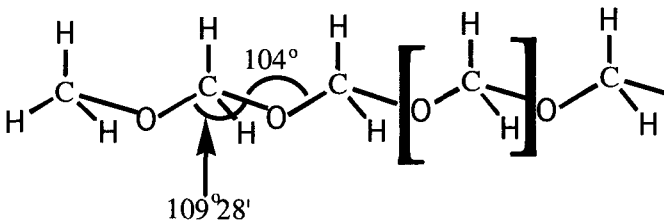


Figure 2.10. Polyoxymethylene chain showing the two backbone angles. Brackets enclose the chain repeat unit.

Then, for the infinite chain with free rotation, equation 2.41 becomes

$$\begin{aligned}\langle \mathbf{R}^2 \rangle &= Nl^2 \left[1 + x + y + 2xy + x^2y + xy^2 + 2x^2y^2 + x^3y^2 + x^2y^2 \dots \right] \\ &= Nl^2 \left[1 + x + y + (2 + x + y)(xy + x^2y^2 + x^3y^2 + \dots) \right]\end{aligned}\quad (2.47)$$

Now, for an infinite series [8]

$$xy + x^2y^2 + x^3y^3 + \dots = \frac{xy}{(1 - xy)} \quad (2.48)$$

So that substituting equation 2.48 into equation 2.47 and rearranging terms gives

$$\langle \mathbf{R}^2 \rangle = Nl^2 \left[\frac{(1+x)(1+y)}{(1-xy)} \right] = Nl^2 \left[\frac{(1+\cos\theta_1)(1+\cos\theta_2)}{(1-\cos\theta_1\cos\theta_2)} \right] \quad (2.49)$$

For the case in which $\theta_1 = \theta_2$, this equation reduces to equation 2.40.

2.7. Model Chains with Restricted Rotation and No Interaction Among the ϕ 's

In this case, terms such as the one containing η of equation 2.32 must be retained. The calculation is best accomplished using matrix multiplication [10, 11, 13-16] and leads to the result [see Appendix 2F for details].

$$\langle \mathbf{R}^2 \rangle = Nl^2 \left[\frac{1+\cos\theta}{1-\cos\theta} \right] \left[\frac{1+\eta}{1-\eta} \right] \quad (2.50)$$

for an infinitely long chain with a symmetrical potential energy barrier ($\langle \sin\phi \rangle = 0$) similar to those depicted in Figures 2.4, 2.5 and 2.6. These would be expected for polymer chains like polyethylene or, more generally, those with the repeat unit $[-CX_2-CY_2-]$, but not for the case of chains with asymmetrical barriers $[-CX_2-CYZ-]$. While this approach can be extended to describe this more complex case of asymmetrical barriers, it is better to use newer methods such as the rotational isomerism approach. In the case for which $N = 0$, equation 2.50 reduces to equation 2.40. By using a potential function of the form of equation 2.12, Taylor [12] has calculated the variation of $\langle R^2 \rangle$ for polyethylene with temperature giving the result shown in Figure 2.11 where $\langle R^2 \rangle_0$ is the

value for free rotation. The chain contracts and approaches the free rotation case with increasing temperature.

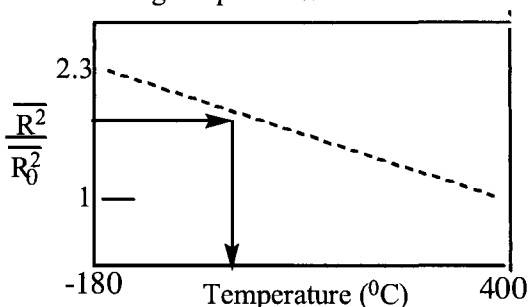


Figure 2.11. The temperature dependence of R for Polyethylene based on the Taylor equation.

It should be noted that the dimensions of this molecule decrease with increasing temperature because the trans conformation, which is the extended chain conformation and the one of lowest energy for polyethylene, has a potential energy curve like that of Figure 2.3. If the polymer chain has a different sort of potential energy barrier such as the one shown in Figure 2.5 in which the gauche conformations have the lowest energy, then η is negative and the chain would extend with increasing temperature. This type of response has been observed in silicone polymer chains [15].

These types of calculations may be generalized to describe more complex types of chains. For example, for cis 1,4 polybutadiene, the dimensions are given approximately by [16]

$$\langle R^2 \rangle = \frac{1}{2} Nl^2 \left[\frac{(1 + \cos \theta)(1 + \eta)}{(1 - \cos \theta)(1 - \eta)} \right] \quad (2.51)$$

while for trans 1,4 polybutadiene

$$\langle R^2 \rangle = \frac{3}{2} Nl^2 \left[\frac{(1 + \cos \theta)(1 + \eta)}{(1 - \cos \theta)(1 - \eta)} \right] \quad (2.52)$$

where l is the length of the monomer unit. Differences in lengths and valence angles for single and double bonds have been neglected in these equations, but have been considered in a more complete analysis [17].

2.8. Rotational Isomeric State (RIS) Approximation

The RIS model [18] is based on known chain structure and geometry in contrast to the statistical segment model described in Section 2.4. The RIS model assumes that the energetics of a chain conformation, in many cases, can be expressed in terms of a few discrete rotational angles between neighboring bonds [Appendix 2E]. In polyethylene, for example, the bond lengths and the bond angles are well characterized and fixed, so that only the rotational angles remain to be specified in order to characterize the conformational energies involved in the interaction of a given rotational angle θ_n with its two nearest neighboring angles θ_{n-1} and θ_{n+1} . These interactions can be summarized by potential energy contour plots in which one rotational angle is taken as the abscissa and a neighboring angle as the ordinate (see for example Figure 2.6). The potential energy of a chain having a given conformation is thus dependent upon the pair interaction between adjacent bond rotational angles. Certain conformations however are energetically unfavorable due to steric hindrances. One variety of those is the so-called pentane interaction that is more fully described in Section 2.11. Rotational isomers have been discussed previously (Section 2.2). The statistical weight assigned to each rotational isomer can be written as

$$\varepsilon_n = e^{-(U_n - U_1)/RT} \quad (2.53)$$

where, as before U_1 , the potential energy of the trans state, is the state with the lowest potential energy and is assigned a value of one. Thus,

$$\varepsilon_n = e^{-U_n/RT} e^{U_1/RT} \quad (2.54)$$

For a threefold rotational barrier, with one trans and two gauche isomers, the partition function, Q , (Appendix 2A) is given by

$$Q^{-1} = 1 + 2\sigma \quad (2.55)$$

Further, the average value of the $\cos\phi$ in the RIS approximation is given by

$$\langle \cos\phi \rangle = Q^{-1} \sum_{i=1}^N U_n \cos\phi_n \quad (2.56)$$

For the special case of a threefold rotational barrier, equation 2.56 becomes

$$\langle \cos\phi \rangle = \left[\frac{(\cos 0^\circ)(1) + 2(\cos 120^\circ)\theta}{1 + 2\sigma} \right] = \frac{1 - \sigma}{1 + 2\sigma} \quad (2.57)$$

This equation was derived previously for the case of 1,2 dichloroethylene (equation 2.17). The possible permutations for neighboring bonds with a threefold potential barrier can be represented by a statistical weight matrix composed of elements based on individual statistical weights. The matrix methods involved are described in Appendix 2E. The reference bond angle Ω_i is placed in a right-handed coordinate system. Transformation matrices $|A|$ (see for example equation 2C.25) are then used to transform the coordinates of the Q_i^h bond into that of the Q_{i-1}^h one. The process is repeated until the coordinates of all the bonds in a given conformation are generated.

As mentioned above, values of conformation dependent properties such as those for the root mean square chain distance ($\langle R^2 \rangle$), the dipole moment or the strain optical coefficient can be derived by the RIS approximation. For example, the values of $\langle R^2 \rangle$ for a given chain are calculated (assuming no interaction between rotational angles on adjacent bonds) from (see equation 2F.23, Appendix 2F).

$$0 = \frac{\langle R^2 \rangle}{n\ell^2} = 1 + \frac{2}{n\ell^2} \sum l^T |A|^{j-i} l \quad (2.58)$$

where ℓ = the bond vector or column vector

$$= \text{col} \begin{vmatrix} \ell_i & 0 & 0 \end{vmatrix} = \begin{vmatrix} \ell_i \\ 0 \\ 0 \end{vmatrix} = \ell_i \begin{vmatrix} 1 \\ 0 \\ 0 \end{vmatrix}$$

l^T = the transpose of ℓ Or row vector = $|\ell_i \ 0 \ 0| = \ell_i |1 \ 0 \ 0|$

$|\mathbf{A}|$ = the transformation matrix which for the case of restricted bond rotation

$$= \begin{vmatrix} \cos \theta & -\eta \sin \theta & \varepsilon \sin \theta \\ \sin \theta & \eta \cos \theta & -\varepsilon \cos \theta \\ 0 & \varepsilon & \eta \end{vmatrix} \quad (2.58A)$$

where

$$\eta = \langle \cos \phi \rangle_i$$

$$\varepsilon = \langle \sin \phi \rangle_i$$

Equation 2.58 can be shown to be equivalent to equation 2.50

$$\frac{\langle R^2 \rangle}{n\ell^2} = \left[\frac{1 + \cos \theta}{1 - \cos \theta} \frac{1 + \eta}{1 - \eta} \right]$$

which was derived from vector analytic considerations. Although the form of equation 2.43 makes it easier to visualize the change in chain dimensions from structural parameter variation, equation 2.58 is better suited for computer computation of chain dimensions.

2.9. Chains with Interactions between ϕ Values of Neighboring Monomers

A realistic chain structure has to take into account the occurrence of combinations of bond rotational angles that would bring the chain atoms into sterically prohibited arrangements. Simply put, atoms would be required to occupy the same space. One example is the pentene configuration in polyethylene. For four consecutive bonds, a sequence $g(+)$, $g(-)$ and $g(+)$ (or more gauche pairs of opposite sign) would place the first and the fifth carbon atoms in the same location. As discussed previously for n-butane, the distance between two carbon atoms separated by three consecutive bonds is specified by one rotational bond angle. This can be termed either a three-bond interaction or a first order interaction. In analogous fashion, the distance between carbon atoms

separated by four bond angles involves the specification of two successive rotational bond angles. These are termed either four bond interactions or a second order interaction. The possibility of generating gauche pairs of opposite sign and hence "pentane type" interaction is encountered in second orders as can be seen by inspection of Figure 2.12.

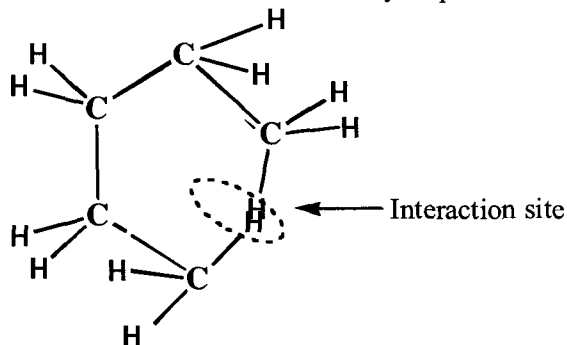


Figure 2.12. Pentane type interaction.

For linear polyethylene, the first order interaction can be given by a diagonal statistical weight matrix

$$|D| = \begin{vmatrix} 1 & 0 & 0 \\ 0 & \sigma & 0 \\ 0 & 0 & \sigma \end{vmatrix} = \text{diag}(1, \sigma, \sigma) \quad (2.59)$$

where, as previously (equation 2.54)

$\sigma = \exp(\sigma/RT)$ = the statistical weight of the gauche conformer

Second order interactions for a symmetrical chain such as linear polyethylene may be given in matrix form, assuming a three minima RIS, by

$$|V| = \begin{matrix} & t & g+ & g- \\ \begin{matrix} t \\ g+ \\ g- \end{matrix} & \begin{vmatrix} 1 & 1 & 1 \\ 0 & \psi & \omega \\ 1 & \omega & \psi \end{vmatrix} \end{matrix} \quad (2.60)$$

where ω = the statistical weight for the steric overlap of $g+g-$ pairs

ψ = the statistical weight of for $g-g-$ or $g+g+$ pairs
 Multiplying the matrices in equations 2.59 and 2.60

$$|\mathbf{U}| = |\mathbf{VD}| = \begin{vmatrix} 1 & 1 & 1 \\ 1 & \psi & \omega \\ 1 & \omega & \psi \end{vmatrix} \begin{vmatrix} 1 & 0 & 0 \\ 0 & \sigma & 0 \\ 0 & 0 & \sigma \end{vmatrix} = \begin{vmatrix} 1 & \sigma & \sigma \\ 1 & \sigma\psi & \sigma\omega \\ 1 & \sigma\omega & \sigma\psi \end{vmatrix} \quad (2.61)$$

yields the statistical weight matrix for the combined four-bond matrix. $\sigma\psi$ denotes the combined statistical weight for a $g+g-$ (or $g-g+$) pair, $\sigma\omega$, for a $g+g+$ (or $g-g-$) pair neighboring bonds. For linear polyethylene, it has been found [19] that the value of $\sigma\omega$ is small enough that it can be set equal to zero. The $\sigma\omega$ pair bonds occupy the same position so that steric hindrance exists. Equation 2.61 for a second order interaction may be accordingly modified

$$|\mathbf{U}| = \begin{vmatrix} 1 & \sigma & \sigma \\ 1 & \sigma\psi & 0 \\ 1 & 0 & \sigma\psi \end{vmatrix} \quad (2.62)$$

By this device, equation 2.64 eliminates $g+g-$ pairs in computation of chain dimensions. Second order interaction matrices have been expanded to include intermediate rotational states. Heatley [20] has used a 21×21 matrix for polymethylene. In analogous fashion, Boyd and Breiting [21] set up a 3×3 matrix.

Interactions of third (or higher) order can be extended in a straightforward manner. The order of equation 2.61 has a dimensionality of $n=3$. A third order interaction (involving five bonds or three bond rotational angles) has a dimensionality of $n^2 = 9$ because the rotational states of two bonds have to be considered. Thus, the state of bond $i-2$ has to be included with that of bond $i-1$. Similarly, the state of bond $i+1$ has to be included in that of bond i . This calculation thus involves the transition between bonds $i-2, i-1$ to bonds $i, i+1$.

2.10. Asymmetric Barriers

The results of the previous section assumed that the potential function is symmetrical

$$U(\phi_1) = U(-\phi_1) \quad (2.63)$$

so that barriers such as those depicted in Figure 2.13 are prohibited. This assumption is not valid, for example, for tactic vinyl polymers ($-\text{CH}_2-\text{CHX}-$), the most common type. R^2 can be calculated by taking the more general case for which the potential function is unsymmetrical.

Two matrices that describe conformations that alternate in sequence are used to specify conformation in tactic vinyl polymers. Tacticity introduces asymmetric elements into the chain. One convention used in specifying chain asymmetry consists of distinguishing between right handed chains termed *d* and left handed or *l* chains. This convention, admittedly arbitrary, is borrowed from the field of optical activity. For a tactic polymer with a threefold potential (Figure 2.13), the statistical weight matrix for a *d* placement between neighboring bonds is

$$|U_d| = \begin{vmatrix} \tau & 1 & \tau \\ 1 & 1 & \tau\omega \\ 1 & \omega & \tau \end{vmatrix} \quad (2.64)$$

where τ = the statistical weight for a *gauche* conformation.

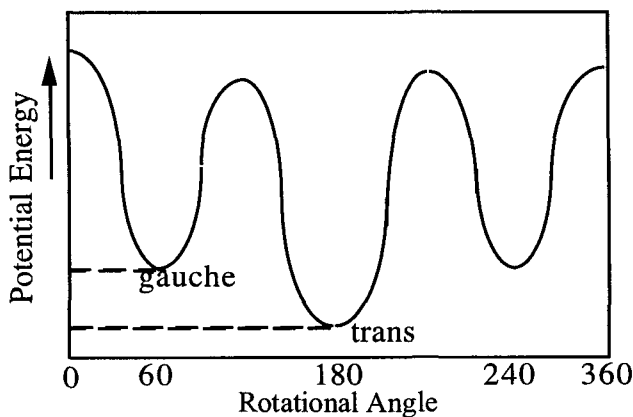


Figure 2.13. Potential energy diagram showing the minimum in potential energy for the *trans* form for a tactic polymer chain.

Incorporating a third bond with the same asymmetric *d* element yields,

$$|U_{dd}| = \begin{vmatrix} \omega & \tau\omega & 1 \\ 1 & \tau\omega & \omega \\ \omega & 0 & \omega \end{vmatrix} \quad (2.65)$$

Analogous matrices can be constructed for l type placements or for ld types [22].

The conformational partition function for tactic vinyl polymers using two statistical weight matrices is given by

$$Z = \mathbf{J}^T \left[\prod_1^{n/2} U_i U''_{i+1} \right] \mathbf{J} \quad (2.66)$$

where as in equation E-8, \mathbf{J}^T represents the transform of the column matrix \mathbf{J}

$$\mathbf{J}^T = \begin{vmatrix} 1 \\ 1 \\ 1 \end{vmatrix} \quad \text{and} \quad \mathbf{J} = \begin{vmatrix} 1 & 1 & 1 \end{vmatrix}$$

The equation, analogous to equation 2.58, for the characteristic ratio for asymmetric barriers is modified to the form

$$\frac{R^2}{n\ell^2} = 1 + \frac{2}{Zn\ell^2} [\mathbf{J}^T \mathbf{0} \dots \mathbf{0}] \zeta_1 \prod_1^{n/2} \zeta'_i \zeta''_{i+1} \begin{vmatrix} 0 \\ \vdots \\ \mathbf{J} \times \mathbf{1} \\ \mathbf{J} \end{vmatrix} \quad (2.67)$$

where $\mathbf{J} \times \mathbf{1}$ = the direct product of \mathbf{J} with the column vector $|\mathbf{1} \ 0 \ 0|$

$$|\zeta'| = \begin{vmatrix} \mathbf{U}'(\mathbf{E}_s \times \mathbf{1}^T) & (\mathbf{U}' \times \mathbf{E}_3) \|\mathbf{T}\| & 0 \\ 0 & (\mathbf{U}' \times \mathbf{E}_3) \|\mathbf{T}\| & (\mathbf{E} \times \mathbf{1}) \mathbf{U}' \\ 0 & 0 & \mathbf{U}' \end{vmatrix} \quad (2.68)$$

$$|\zeta''| = \begin{vmatrix} \mathbf{U}''(\mathbf{E}_s \times \mathbf{1}^T) \|\mathbf{T}\| & (\mathbf{U}'' \times \mathbf{E}_3) \|\mathbf{T}\| & 0 \\ 0 & (\mathbf{U}'' \times \mathbf{E}_3) \|\mathbf{T}\| & (\mathbf{E}_s \times \mathbf{1}) \mathbf{U}'' \\ 0 & 0 & \mathbf{U}'' \end{vmatrix} \quad (2.69)$$

$$\|T\| = \begin{vmatrix} T^1 & & & \\ & T^2 & & \\ & & \dots & \\ & & & T^3 \end{vmatrix} \quad (2.70)$$

= the pseudo-diagonal matrix formed from the transformation matrices T_1, \dots, T_s for the different rotational states.

References 23 and 24 give techniques for evaluating equation 2.70.

2.11. Comparison with Experiment

Polymer chain dimensions are usually determined experimentally on dissolved polymers using either intrinsic viscosity (η) (Chapter 3), light scattering angular dependence (Chapter 4) or neutron scattering measurements. These measurements are carried out in very dilute solutions to minimize interactions between chains. In addition, theta (θ) conditions are commonly used in order to balance long range interactions between non-adjacent segments of the same chain and solvent interactions. A theta solvent refers to experimental conditions of temperature and solvent selected such that the polymer is just on the verge of precipitation. Under such conditions, the chain expansion arising from excluded volume is balanced by the repulsive forces of the solvent, so the system is "pseudo-ideal" and chain dimensions assume the values for the unperturbed state. This means that a given polymer chain segment is indifferent as to whether it has a solvent molecule or another chain segment as a neighbor.

Light scattering can only be used for stiffer chains or higher molecular weight chains; molecules whose dimensions are greater than about 50 to 100 nm. The shorter wavelength neutrons can be used for smaller molecules. In addition, with deuterium labeling, neutron scattering can be extended to concentrated or bulk polymer studies.

The chain dimensions obtained from the theoretical treatments described previously in this chapter may be compared by use of the characteristic ratio (C_n) expressed as either

$$C_n \equiv \frac{R^2}{n\ell^2} \quad (2.71)$$

for a chain of finite length with n monomers, or

$$C_{\infty} \equiv \lim_{n \rightarrow \infty} \frac{R^2}{nl^2} \quad (2.72)$$

for infinitely long chains. This characteristic ratio may serve as a measure of the chain stiffness.

For the statistical segment model (equation 2.25)

$$C_{\infty} = 1 \quad (2.73)$$

For the case of tetrahedral bonding with free rotation (equation 2.40)

$$C_{\infty} = \frac{1 + \langle \cos \theta_T \rangle}{1 - \langle \cos \theta_T \rangle} = 2 \quad (2.74)$$

where $\langle \cos \theta_T \rangle = 1/3$. This equation states that the imposition of tetrahedral bonding increases the end-to-end vector length by a factor of $\sqrt{2}$ compared to the statistical segment model.

Table 2.1 lists values of C_{∞} derived from experimental measurements. These data show that the unperturbed polymer chain is more flexible and more coiled up than is implied by chain model calculations based only on fixed bond angles and restricted bond rotation. The RIS approach [24] has had better success in matching measured C_{∞} values because it includes longer range interactions and excluded pentane type interactions in the calculations. The chain parameters thus determined, in most cases, correspond well to values determined by structural techniques. The change in chain dimensions with temperature offers an important means for estimating the energetics of chain conformations. Two approaches have been followed for obtaining the temperature dependence. One approach uses the straightforward procedure of calculating chain dimensions at several temperatures from light scattering or viscosity measurements. However, to attain theta conditions over a range of temperatures, several solvents are usually required. The resulting solvent/polymer interaction effect tends to obscure the quantity of interest – the change in chain dimension with temperature – because of the small magnitude of the change.

The second approach is indirect and involves the measurement of the stress-temperature coefficient of a solid polymer. For the measurement, the polymer must be in the rubbery state. Crosslinking a thermoplastic polymer at room temperature and then heating it above its melting point accomplishes this. Chapter 3 describes the mathematics involved in calculating stress-temperature coefficients. Other approaches use the birefringence dependence on temperature or the Kerr Effect to measure the stress-temperature coefficient.

As seen in Table 2.1, the change in C_{∞} with temperature is small. Polyethylene chains contract on heating since the shorter gauche conformations become more numerous at higher temperatures because of energetic considerations. This chain contraction with increasing temperature was previously discussed in this chapter (Section 2.7).

Table 2.1 Characteristic Ratio Values for Typical Polymers ^{a.)}

Polymer	Solvent	Temperature ($^{\circ}\text{C}$)	C_{∞}
Polyethylene	α -chloronaphthalene	140	6.6
	diphenylmethane	142	6.8
	dodecanol-1	138	6.7
Polypropylene, isotactic	diphenyl ether	145	5.7
Polyisobutylene	benzene	24	6.6
Polystyrene	cyclohexane	34.8	10.2
Poly-dimethyl silicone	butanone	20	6.2

a.) P.J. Flory, "Statistical Mechanics of Chain Molecules", Hansa Publishers New York 1989

2.12. Chain End-to-End Distribution Functions

2.12.1 One Dimensional Case

The probability of an end-to-end vector distance can be derived. For this derivation, the statistical segment model (Section 2.4) is used in which the chain is approximated by Z statistical segments [25]. Each segment is assumed to be comprised of several monomer units. The statistics of the random walk are applied to this model.

For one dimension, the chain axis is constrained to lie parallel to one axis of a Cartesian coordinate system, say the x -axis. N_1 segments lie in the $+X$ direction and N_2 segments in the $-X$ direction with equal a priori probability (Figure 2.14). The probability of obtaining a given value of $P(R_x)$ [see Appendix 2G] is given by

$$P(R_x) = \exp\left(-\frac{R_x^2}{2ZL^2}\right) \quad (2.75)$$

This equation is substituted into equation 2.21 to derive the entropy of a single chain (equation 2.22) and the force required to restore a chain to its equilibrium dimensions (equation 2.21).

Equation 2.75 is the probability that $P(R_x)$ can be found in the interval $P(R_x)$ to $P(R_x) + P(R_x)dR$. Thus

$$P(R_x)dR = C \exp\left(-\frac{R_x^2}{2ZL^2}\right) \quad (2.76)$$

where C is a normalization constant determined from

$$\int_{-\infty}^{\infty} P(R_x)dR_x = C \int_{-\infty}^{\infty} \exp\left(-\frac{R_x^2}{2ZL^2}\right)dR_x = 1 \quad (2.77)$$

leading to

$$C = \frac{1}{\sqrt{2\pi ZL^2}} \quad (2.78)$$

Substituting equation 2.78 into equation 2.76

$$P(R_x) = \frac{1}{\sqrt{2\pi ZL^2}} \exp\left(-\frac{R_x^2}{2ZL^2}\right) \quad (2.79)$$

This is a Gaussian function, plotted in Figure 2.14 which has a most probable value of $R_x = 0$. It should be noted that $P(<R_x>)$ asymptotically

approaches zero as $\langle R_x \rangle$ (or $\langle -R_x \rangle$) approaches infinity. This must be in error at large $\langle R_x \rangle$ values because $P(\langle R_x \rangle)$ must discretely become zero for the completely stretched out chain for which $\langle R_x \rangle = R_\infty$ and

$$R_\infty = ZL \tag{2.80}$$

This error due to the neglect of higher terms of the expansion will be considered later in the discussion of “non-Gaussian” behavior [Section 2.12.3]. Another source of error is the use of Stirling’s approximation for factorials that is valid only for large numbers. This is not the case at high chain extensions when the number of possible chain conformations becomes small. Neglect of expansion terms is a Gaussian function that has a most probable value of $R_x = 0$. It should be noted that $P(\langle R_x \rangle)$, asymptotically approaches zero as R_x (or $-R_x$) approaches infinity. This must be in error at large $|R_x|$ values because $P(\langle R_x \rangle)$ must discretely become zero for the completely stretched out chain for which $R_x = R_\infty$ and the mean value of R_x is

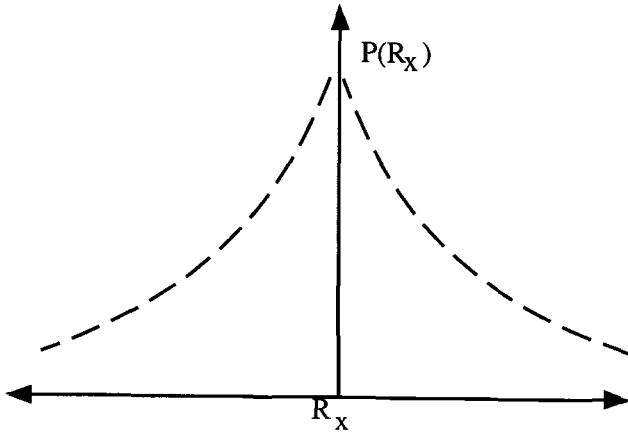


Figure 2.14. The variation of P_x for a one dimensional Gaussian chain.

$$\langle R_x \rangle = \int_{-\infty}^{\infty} R_x P(R_x) dR_x = 0 \tag{2.81}$$

This follows because $P(+R_x) = P(-R_x)$. However, the mean squared value of R_x

$$\langle R_x^2 \rangle = \int_{-\infty}^{\infty} R_x^2 P(R_x^2) dR_x = ZL^2 \quad (2.82)$$

in agreement with previous results (Section 2.4).

2.12.2. Extension to a Three Dimensional Chain

Consider a three dimensional chain composed of Z statistical segments of length L . Suppose these segments can have projections along the x , y and z axes of $\pm L_x$, $\pm L_y$, or $\pm L_z$ where

$$\langle L^2 \rangle = \langle L_x^2 \rangle + \langle L_y^2 \rangle + \langle L_z^2 \rangle \quad (2.83)$$

and

$$\langle L_x^2 \rangle + \langle L_y^2 \rangle + \langle L_z^2 \rangle = \frac{\langle L^2 \rangle}{3} \quad (2.84)$$

Also, since the contribution of a given segment to the extension of the chain in the x direction (called R_x) may be either L_x or $-L_x$, the probability of a projection R_x of the end-to-end length will give a result identical with the solution for the one-dimensional chain (equation 2.79) or

$$P(\langle R_x \rangle) = \frac{1}{\sqrt{2\pi Z \langle L_x^2 \rangle}} \exp\left(-\frac{\langle R_x^2 \rangle}{2ZL_x^2}\right) \quad (2.85)$$

Similarly, for R_y

$$P(\langle R_y \rangle) = \frac{1}{\sqrt{2\pi Z \langle L_y^2 \rangle}} \exp\left(-\frac{\langle R_y^2 \rangle}{2ZL_y^2}\right) \quad (2.86)$$

and for R_z

$$P(\langle R_z \rangle) = \frac{1}{\sqrt{2\pi Z \langle L_z^2 \rangle}} \exp\left(-\frac{\langle R_z^2 \rangle}{2ZL_z^2}\right) \quad (2.87)$$

If one end of a chain is at the origin, the probability of a vector \mathbf{R} being located close to the other end of the chain is

$$P(\mathbf{R}) = P(\mathbf{R}_x)P(\mathbf{R}_y)P(\mathbf{R}_z) \quad (2.88)$$

where

$$\mathbf{R} = \mathbf{R}_x + \mathbf{R}_y + \mathbf{R}_z$$

since for the end-to-end vector to be \mathbf{R} , the x , y and z components must be \mathbf{R}_x , \mathbf{R}_y and \mathbf{R}_z . If the probabilities for the components are independent of each other, then the probability of that they have a joint value of $(\mathbf{R}_x, \mathbf{R}_y, \mathbf{R}_z)$ is the product of the individual probabilities. Thus

$$\begin{aligned} P(\mathbf{R})d\mathbf{R} &= \frac{1}{(2\pi Z)^{3/2} \left(\langle L_x^2 \rangle \langle L_y^2 \rangle \langle L_z^2 \rangle \right)^{1/2}} \exp \left\{ -\frac{1}{2Z} \left[\frac{R_x^2}{L_x^2} + \frac{R_y^2}{L_y^2} + \frac{R_z^2}{L_z^2} \right] \right\} d\mathbf{R} \\ &= \left(\frac{3}{2\pi Z L^2} \right) \exp \left[-3R^2/2ZL^2 \right] dR_x dR_y dR_z \\ &= \frac{\beta^3}{\pi^{3/2}} \exp \left(-\beta^2 R^2 \right) dR_x dR_y dR_z \end{aligned} \quad (2.89)$$

where

$$\beta^2 = \frac{3}{2ZL^2} = \frac{3}{2\sqrt{R^2}} \quad (2.90)$$

and

$$L_x^2 = L_y^2 = L_z^2 = L^2/3$$

The probability of a given scalar distance between ends is found by integrating $P(\mathbf{R})$ over all angular orientations of \mathbf{R} . Transforming from Cartesian to spherical coordinate system (Figure 2.15) simplifies the integration process. In spherical coordinates,

$$dR_x dR_y dR_z = R^2 \sin \theta dR d\theta d\phi \quad (2.91)$$

so that

$$P(R)dR = e^{-\beta^2 R^2} R^2 dR \frac{\beta^3}{\pi^{3/2}} \int_{\phi=0}^{\pi} \int_{\theta=0}^{\pi} \int_0^{\infty} P(\mathbf{R}) \sin \theta dR d\theta d\phi$$

$$= 4\pi \frac{\beta^3}{\pi^{3/2}} \exp[-\beta R^2]^{-\beta^1 R^1} R^2 dR \quad (2.92)$$

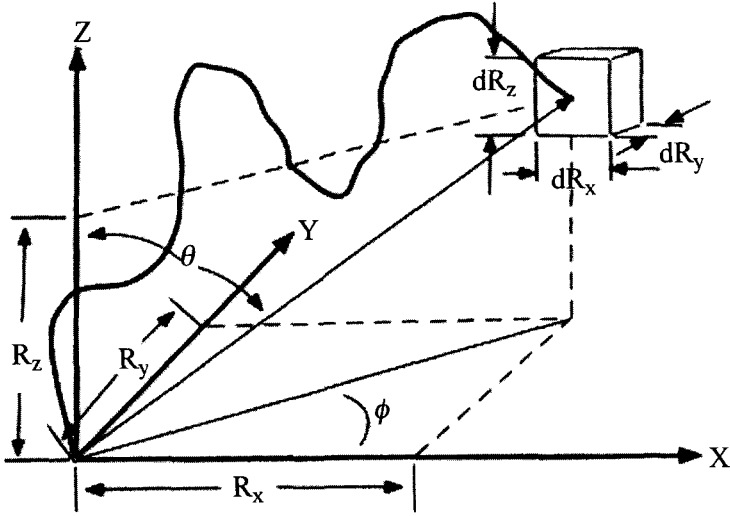


Figure 2.15 Cartesian to Spherical coordinates transformation relations.

It is easily verified that

$$\int_{R=0}^{\infty} P(R) dR = 1 \quad (2.93)$$

and that

$$\langle R^2 \rangle = \int_{R=0}^{\infty} (R^2) P(R) dR = ZL^2 \quad (2.94)$$

This is in agreement with the previous result.

The most probable end-to-end distance $[R_m$, see Figure 2.16] is obtained by differentiation of equation 2.92,

$$\frac{\partial P(R)}{\partial R} = 0 = 4\pi \frac{\beta^3}{\pi^{3/2}} \left[2R e^{-\beta R^2} (-\beta^2 R^2 + 1) \right] \quad (2.95)$$

yielding

$$\langle R_m^2 \rangle = \frac{1}{\beta^2} = \frac{2}{3} \langle R^2 \rangle \quad (2.96)$$

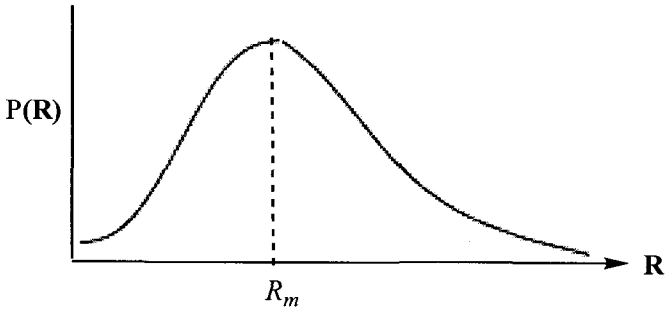


Figure 2.16. The most probable end-to-end distance (R_m) plot.

2.12.3. Extension to Non-Gaussian Case

The failure of the Gaussian statistical theory becomes noticeable when the distance between chain ends assumes values between one third to one half its fully extended chain (or contour) length because of the neglect of higher terms in the expansion and the limitations of Stirling's Approximation as mentioned in Section 2.13.1. Equations based on the following derivations yield calculated values that better agree with experimental data at high elongations, but sacrifice simplicity and general applicability to a variety of polymer structures. As in the Gaussian case, the problem is to determine the probability that one chain end is located in a volume dV at a distance R from the other end.

For the non-Gaussian case, the distribution in angle of the individual chain segments is calculated first. Then, the probability of a given conformation is determined. Finally, the most probable distribution is derived by differentiation, as in the Gaussian case.

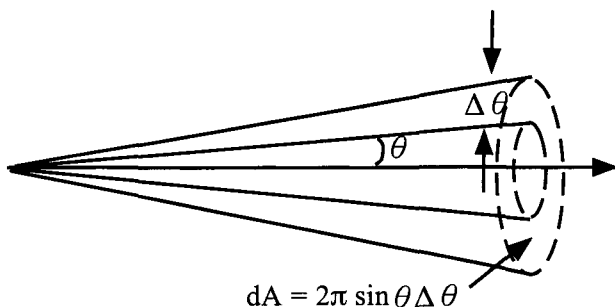


Figure 2.17. a-priori probability of segment being proportional to the size of the volume element.

Consider again, a three-dimensional chain composed of Z statistical segments of length L . These segments are considered to be freely orienting so that the a-priori probability of a segment being oriented at an angle, θ , with respect to \mathbf{R} is just proportional to the size of the volume element (Figure 2.17), or

$$\sum p(\Delta\theta) = C \sin\theta\Delta\theta \quad (2.97)$$

The constant, C , is determined by normalization

$$\sum p(\Delta\theta) = \int_{\theta=0}^{\pi} p(\Delta\theta) = C \int_0^{\pi} \sin\theta d\theta = 1 = 2C \quad (2.98)$$

Thus

$$C = 1/2$$

and

$$p(\Delta\theta) = \frac{1}{2} \sin\theta\Delta\theta \quad (2.99)$$

Now consider a chain in which n_1 segments are oriented with respect to \mathbf{R} in the angular interval $(\Delta\theta_1)$, n_2 in $(\Delta\theta_2)$, etc. The probability of such a distribution is

$$P = C \frac{N!}{n_1! n_2! \dots} \left\{ [p(\Delta\theta_1)]^{n_1} [p(\Delta\theta_2)]^{n_2} \dots \right\} = C \frac{N!}{\prod_i n_i!} \prod_i [p(\Delta\theta_i)]^{n_i} \quad (2.100)$$

It is useful to take logarithms to utilize Stirling's approximation for the factorials (equation 2G.11)

$$\ln P = \ln C + \ln N! - \sum \ln N_i! + \sum n_i \ln p(\Delta\theta_i) = \ln C + N \ln N - N + N \sum [-n_i \ln n_i + n_i \ln p(\Delta\theta_i)] \quad (2.101)$$

since

$$N = \sum n_i \quad (2.102)$$

Thus,

$$\ln P = \ln C + N \ln N + \sum_i n_i \ln \left[\frac{P(\Delta\theta_i)}{n_i} \right] \quad (2.103)$$

We now wish to find the distribution of the n_i 's that maximizes P , that is, one that makes $d \ln P = 0$. Now

$$d \ln P = \sum_i \left[\frac{\partial \ln P}{\partial n_i} \right] dn_i = 0 \quad (2.104)$$

and

$$\left(\frac{\partial \ln P}{\partial n_i} \right) = \ln p(\Delta\theta_i) - \ln n_i - 1 \quad (2.105)$$

However, not all n_i 's are possible. One must maximize $\ln P$ subject to the restriction that N and R are specified. Thus from equation 2.102

$$dN = 0 = \sum dn_i \quad (2.106)$$

If the end-to-end length of the chain is held fixed at a particular R (Figure 2.18), then

$$\sum n_i L \cos \theta_i = R \quad (2.107)$$

so that

$$\sum L \cos \theta_i dn_i = 0 \quad (2.108)$$

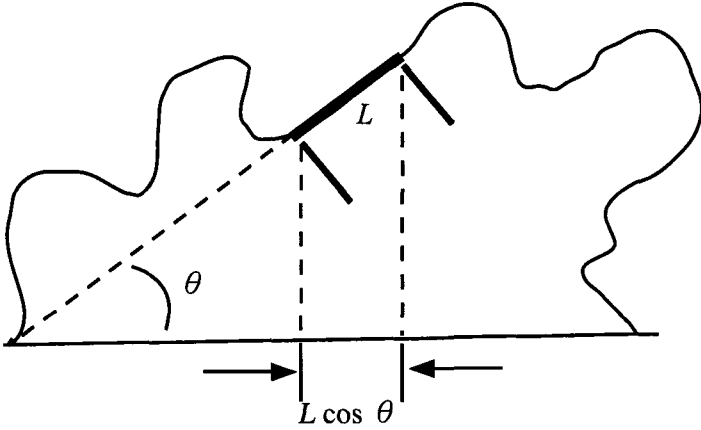


Figure 2.18 Relations used in finding maximum probability.

P must be maximized subject to the constraints of equations 2.106 and 2.108. This is accomplished using Lagrange's method of undetermined multipliers. Equation 2.106 is multiplied by the arbitrary constant $(\alpha - 1)$ and equation 2.108 is multiplied by the arbitrary constant β [not the same β as defined in equation 2.90]. Then these are added to equation 2.104 to give

$$\sum [\ln p(\Delta\theta_i) - \ln n_i + \alpha + \beta \cos \theta_i] dn_i = 0 \quad (2.109)$$

Since this equation must be valid for arbitrary values of dn_i 's, the coefficients must be zero. Thus

$$\ln p(\Delta\theta_i) - \ln n_i + \alpha + \beta \cos \theta_i = 0 \quad (2.110)$$

so

$$n_i = N - p(\Delta\theta_i) e^{\alpha} e^{\beta \cos \theta_i} = \frac{1}{2} \sin \theta e^{\alpha} e^{\beta \cos \theta} \Delta\theta_i \quad (2.111)$$

The coefficients, α and β , may be evaluated from the constraints of equations 2.102 and 2.107,

$$\begin{aligned} \sum n_i = N &= \sum \frac{1}{2} \sin e^\alpha e^{\beta \cos \theta} \Delta \theta_i = \frac{1}{2} e^\alpha \int_{\theta=0}^{\pi} e^{\beta \cos \theta} \sin \theta d\theta \\ &= \frac{e^\alpha}{\beta} \left[\frac{e^\beta - e^{-\beta}}{\beta} \right] = \frac{e^\alpha}{\beta} \left[\frac{\sinh \beta}{\beta} \right] \end{aligned} \quad (2.112)$$

Also

$$\begin{aligned} \frac{R}{L} &= \sum n_i \cos \theta_i = \sum \frac{1}{2} \sin \theta_i \cos \theta_i e^\alpha e^{\beta \cos \theta} \Delta \theta_i \\ &= \frac{1}{2} e^\alpha \int_{\theta=0}^{\pi} e^{\beta \cos \theta} \cos \theta \sin \theta d\theta = \frac{1}{2} \frac{e^\alpha}{\beta^2} \left[\beta (e^\beta + e^{-\beta}) - (e^\beta - e^{-\beta}) \right] \\ &= e^\alpha \left[\frac{\cosh \beta}{\beta} - \frac{\sinh \beta}{\beta^2} \right] \end{aligned} \quad (2.113)$$

Now using equation 2.112 for e^α

$$\frac{R}{L} = \frac{N\theta}{\sinh \theta} \left[\frac{\cosh \beta}{\beta} - \frac{\sinh \beta}{\beta^2} \right] = \left[\coth \beta - \frac{1}{\beta} \right] - N\mathcal{L}(\beta) \quad (2.114)$$

where

$$\mathcal{L}(x) = \coth x - \frac{1}{x} \quad (2.115)$$

is the Langevin function of x . Thus, taking the inverse of the Langevin function,

$$\beta = \mathcal{L}^{-1} \left(\frac{R}{NL} \right) \quad (2.116)$$

The distribution function obtained by combining equations 2.111 and 2.112 is

$$n_i = \frac{N\beta}{\sinh \beta} e^{\beta \cos \theta} \frac{1}{2} \sin \theta_i \Delta \theta_i \quad (2.117)$$

where β is defined by equation 2.116.

Equation 2.117 describes the number of segments making an angle θ_i with respect to the displacement vector. This approach follows the same one used by Langevin and others for calculating the orientation of

dipoles in an electric field or of magnetic species in a magnetic field. One might think of it as the orientation of polymer segments in a mechanical field. This approach will also be used later in the discussion of the optical properties of polymer chains (Chapter 4). Now from equations 2.103 and 2.112

$$\begin{aligned} \ln(P/C) &= N \ln N + \sum n_i \ln \left[\frac{p(\Delta\theta_i)}{n_i} \right] = N \ln N + \sum n_i \ln \left[e^\alpha e^{-\beta \cos\theta_i} \right] \\ &= N \ln N - \alpha \sum n_i - \beta \sum n_i \cos\theta_i = N \ln N - \alpha N - \frac{\beta R}{L} \end{aligned} \quad (2.118)$$

Using equation 2.110

$$= N \ln - \alpha N - \frac{\beta R}{L}$$

Inserting equation 2.117

$$\ln \frac{P}{C} = N \ln N - N \ln \left[\frac{N\beta}{\sinh \beta} \right] - \frac{\beta R}{L} = N \ln N - N \ln N - N \ln \left[\frac{\beta}{\sinh \beta} \right] - \frac{\beta R}{L} \quad (2.119)$$

so that

$$\ln \frac{P}{C} = -N \left[\left(\frac{R}{NL} \right) \beta + \ln \left(\frac{\beta}{\sinh \beta} \right) \right] \quad (2.120)$$

or

$$P = C \exp \left\{ -N \left[\left(\frac{R}{NL} \right) \beta + \ln \left(\frac{\beta}{\sinh \beta} \right) \right] \right\} \quad (2.121)$$

This is a distribution function that is valid for R larger than the Gaussian function of equation 2.92. When $R = R_\infty = NL$

$$\beta = \mathcal{L}^{-1} \left(\frac{R}{NL} \right) = \mathcal{L}^{-1}(1) = \infty \quad (2.124)$$

and $P = 0$ as expected for an extended chain. If the inverse Langevin function and the exponent of equation 2.121 are expanded in series, this leads to

$$P(\mathbf{R}) = C \exp \left\{ -N \left[\frac{3}{2} \left(\frac{R}{NL} \right)^2 + \frac{9}{20} \left(\frac{R}{NL} \right)^4 + \frac{99}{350} \left(\frac{R}{NL} \right)^6 + \dots \right] \right\} \quad (2.123)$$

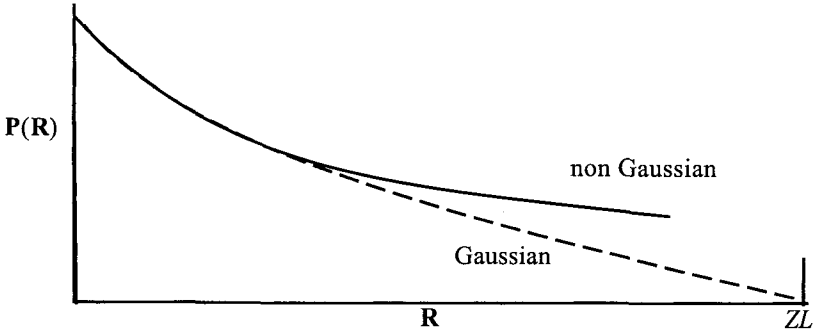


Figure 2.19. Comparison of rubber elasticity models.

At small extensions or for very long chains, $R \ll NL$ and only the first term in the series expansion of the exponent is important, so 2.123 becomes

$$P(\mathbf{R}) = C \exp \left[-\frac{3}{2} \left(\frac{R^2}{NL^2} \right) \right] \quad (2.124)$$

which is similar to equation 2.79. Thus, equations 2.121 or 2.123 represent an improvement over the Gaussian distribution in being more accurate at larger R (see Figure 2.19).

It should be pointed out that, in the non-Gaussian case, $P(R)$ going to zero at R_∞ leads to the force going to infinity (Figure 2.20).

An alternate measure, the radius of gyration, R_g , is derived in Appendix 2C. In the Appendix, the radius of gyration for a linear polymer is shown to be given by the equation

$$\langle R_g^2 \rangle = (1/6) \langle R^2 \rangle \quad (2.125)$$

the effect of branching on $\langle R_g^2 \rangle$ and the Stockmayer branching index are also discussed in the appendices to Chapter 2.

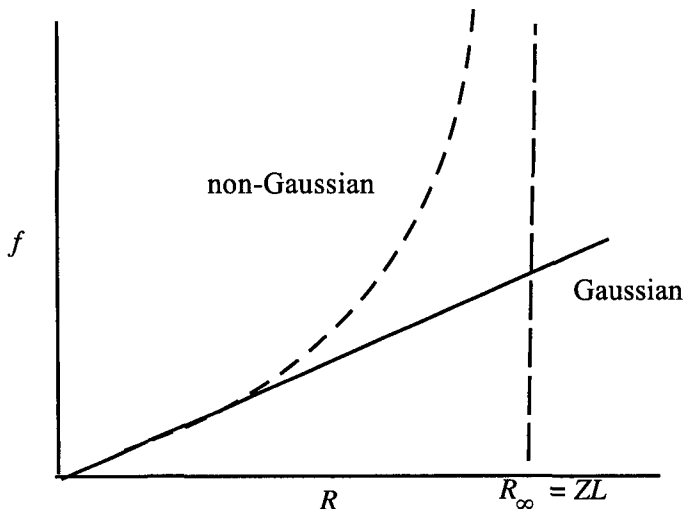


Figure 2.20. Comparison of force-extension curves between the Gaussian and non-Gaussian cases.

References

1. E.B. Wilson, *J. Pure Appl. Chem.* **1962**, *4*, 1
2. K.S. Pitzer, *Discussions Faraday Soc.* **1951**, *10*, 66
3. S. Mizushima, *Structure of Molecules and Internal Rotation*; Academic: New York, **1954**
4. P. Debye, *Polar Molecules*; Dover: New York, **1955**.
5. J.E. Lennard-Jones, *Physica* **1937**, *4*, 941
6. M.V. Volkenstein, *Conformational Statistics of Polymer Chains*; Interscience: New York, **1963**, Chap 2
7. H. Kuhn, *J. Chem. Phys.* **1947**, *15*, 843
8. W.J. Taylor, *J. Chem. Phys.* **1948**, *16*, 257
9. M.V. Volkenstein, Ref. 6, Chap. 4
10. H. Kuhn, *J. Chem. Phys.* **1947**, *15*, 843
11. H. Eyring, *Phys. Rev.* **1932**, *39*, 746
12. W.J. Taylor, *J. Chem. Phys.* **1947**, *15*, 412

TOPICS in POLYMER PHYSICS

13. R. Kubo, *J. Phys. Soc. Japan* **1948**, 3, 119
14. C.M. Tohen, *Phys. Rev.* **1952**, 86, 658
15. J.E. Mark, J.H. Ko, *J. Polymer Sci: Polymer Physics Ed.* **1975**, 13, 222
16. A.A. Christorazum, *Doblady Akad. Nauk. SSSR* **1953**, 79, 999
17. Ching-Tang Au, Chuang-Lui Ju, *J. Chinese Chem. Soc.* **1951**, 18, 110
18. P. J. Flory, *Statistical Mechanics of Chain Molecules*; Interscience: New York, **1969**
19. A. Abe, R.L. Jernigan and P.J. Flory, *J. Am. Chem. Soc.* **1966**, 88, 631
20. F. Heatley, *Polymer* **1972**, 13, 218
21. R.H. Boyd, S.M. Breittling, *Macromolecules* **1972**, 5, 1
22. P.J. Flory, J.E. Mark, A. Abe, *J. Am. Chem. Soc.* **1966**, 88, 639
23. R. DeSantis, H.G. Zachmann, *Colloid and Polymer Sci.* **1977**, 255, 50
24. F.T. Wall, F. Mandel, *J. Chem. Phys.* **1975**, 63, 4592
25. W. Kuhn, F. Grün, *Kolloid Z.* **1942**, 101, 248

Appendix 2A - Statistical Mechanics

Atoms and molecules in all their facets (structure, reaction and properties) form the subject material of chemical science. Classical thermodynamics, on the other hand, describes the energetic interactions between macroscopic systems and takes no cognizance of the molecular constitution of matter. Statistical thermodynamics bridges these two disciplines by using partition functions to calculate the average macroscopic values of thermodynamic functions such as energy or entropy. The concept of a partition function, in which the total energy of a molecule is partitioned or separated into the various contributions from vibrational, rotational and translational energies, is central to statistical thermodynamics. As shown below, the state functions of classical thermodynamics (Appendix 3A) can be derived from partition functions. For the present application, only the partition function for the conformational changes based on bond rotation is considered. The partition function is derived from probability or statistical arguments as would be anticipated considering the large number of molecules comprising even a small sample (recall that 1 mole of a substance contains 6×10^{23} molecules). The first step in the derivation of the partition function is the calculation of the number of ways (N) of distributing n distinguishable molecules over R states. The result (see Appendix 2G) is

$$N = \frac{n!}{n_0! n_1! \dots n_j!} = \frac{n!}{\prod_{s=0}^j n_s} \quad (2A.1)$$

The probability (P) of a given distribution is assumed to be proportional to the number of ways the distribution can occur (the ergodic hypothesis)

$$P = C \frac{n!}{n_1! n_2! \dots n_i!} \quad (2A.2)$$

where C is a constant of proportionality subject to the conditions of a constant number of molecules

$$\sum n_i = N \quad (2A.3)$$

and constant energy

$$\sum n_i \varepsilon_i = E \quad (2A.4)$$

While the average state of a system should be determined by an average over all distributions, the most probable distribution is very much more probable than any other. Therefore, it is a good approximation to just consider this distribution. This may be demonstrated using the more rigorous “method of steepest descents” [1]. To obtain the maximum probability, equation 2A.2 is recast into logarithmic form. Thus

$$\ln P = \ln C + \ln n - \ln n_1! - \ln n_2! \dots \ln n_i! \quad (2A.5)$$

Then, Stirling’s approximation [This approximation does not work well for values of N of the order of 10 or less, but improves with increasing N .]

$$\ln N! = N \ln N - N \quad (2A.6)$$

If $\ln P$ is a function of $n_1, n_2, \dots, n_i, \dots$, then for $\ln P$ to be a maximum,

$$d(\ln P) = (\partial \ln P / \partial n_1) dn_1 + (\partial \ln P / \partial n_2) dn_2 + \dots + (\partial \ln P / \partial n_i) dn_i \quad (2A.7)$$

By differentiating 2A.5 after using Stirling’s approximation,

$$(\partial \ln P / \partial n_i) = -\ln n_i \quad (2A.8)$$

so substituting gives

$$\partial n_1 (\ln n_1) + \partial n_2 (\ln n_2) + \partial n_3 (\ln n_2) + \dots + \partial n_i (\ln n_i) = \partial N = 0 \quad (2A.9)$$

Changes between states in terms of energy and number of molecules, while maintaining the overall values constant, can be expressed in differential form.

From equation 2A.3

$$\partial n_1 + \partial n_2 + \partial n_3 + \dots + \partial n_i = \partial N = 0 \quad (2A.10)$$

and from equation A-4

$$\varepsilon_1 \partial n_1 + \varepsilon_2 \partial n_2 + \varepsilon_3 \partial n_3 + \dots + \varepsilon_i \partial n_i = \partial E = 0 \quad (2A.11)$$

Lagrange's method of undetermined multipliers is now applied to find the maximum in P . Two new variables (α for equation 2A.10 and β for equation 2A.11), the undetermined multipliers, are introduced as restrictions on equation 2A.9. Thus

$$\begin{aligned} \partial n_1 (\ln n_1) + \partial n_2 (\ln n_2) + \partial n_3 (\ln n_3) + \dots + \alpha \partial n_1 + \alpha \partial n_2 + \alpha \partial n_3 + \\ \dots + \beta \varepsilon_1 \partial n_1 + \beta \varepsilon_2 \partial n_2 + \beta \varepsilon_3 \partial n_3 + \dots = 0 \end{aligned} \quad (2A.12)$$

Grouping terms

$$(\ln n_1 + \alpha + \beta \varepsilon_1) \partial n_1 + (\ln n_2 + \alpha + \beta \varepsilon_2) \partial n_2 + (\ln n_3 + \alpha + \beta \varepsilon_3) \partial n_3 + \dots = 0 \quad (2A.13)$$

In general, if one has an equation of the sort

$$Ax + By + Cz + Dw + \dots = 0 \quad (2A.14)$$

where x , y , z and w , can assume any value independently, then the only possible solution is

$$A = B = C = D = \dots = 0 \quad (2A.15)$$

Thus, for all terms in equation 2A.13

$$\begin{aligned} \ln n_1 + \alpha + \beta \varepsilon_1 &= 0 \\ \vdots & \\ \ln n_3 + \alpha + \beta \varepsilon_3 &= 0 \end{aligned} \quad (2A.16)$$

Rearranging terms in equation 2A.14 and taking exponentials

$$n_i = e^{-\alpha} e^{-\beta \varepsilon_i} \quad (2A.17)$$

This result is Boltzmann's distribution, one of the most general equations in physical science.

The multipliers α and β can be determined from the system requirements of constant number and constant energy. Thus substituting equation 2A.15 into equation 2A.3

$$n_i = e^{-\alpha} e^{-\beta \varepsilon_i} + e^{-\alpha} e^{-\beta \varepsilon_2} + \dots = e^{-\alpha} [e^{-\beta \varepsilon_1} + e^{-\beta \varepsilon_2} + \dots] = e^{-\alpha} \sum_1^i e^{-\beta \varepsilon_i} = N \quad (2A.18)$$

or

$$e^{-\alpha} = \frac{N}{\sum e^{-\beta\epsilon_i}} \quad (2A.19)$$

Substituting equation 2A.19 into equation 2A.17

$$n_i = \frac{Ne^{-\beta\epsilon_i}}{\sum e^{-\beta\epsilon_i}} \quad (2A.20)$$

The denominator in equation 2A.18 is the partition function (or the sum over all energy states) discussed at the beginning of this section

$$Q \equiv \sum e^{-\beta\epsilon_i} \quad (2A.21)$$

It can be shown by any of several approaches [2-4] that β meets all the requirements for a parameter, i.e.,

$$\beta = \frac{1}{kT} \quad (2A.22)$$

where k = Boltzmann's constant and T = temperature (in units of degrees Kelvin).

Therefore, equation A-18 can be rewritten

$$n_i = \frac{Ne^{-\beta/kT}}{\sum e^{-\beta/kT}} = \frac{Ne^{-\beta/kT}}{Q} \quad (2A.23)$$

The classical thermodynamic state functions [enthalpy (E), entropy (S), free energy (A)] can be expressed in terms of the partition function as shown in the following derivations.

Combining equation 2A.4

$$E = n_1\epsilon_1 + n_2\epsilon_2 + \dots$$

with equation 2A.20, yields

$$E = (N/Q)[e^{-\beta\epsilon_1} + e^{-\beta\epsilon_2} + \dots] \quad (2A.24)$$

then differentiating

$$\frac{\partial \ln Q}{\partial(1/\beta)} = \frac{1}{Q} \frac{\partial Q}{\partial(1/\beta)} = \frac{1}{Q} \frac{\partial}{\partial \beta} \left[e^{-\beta \epsilon_1} + e^{-\beta \epsilon_2} + \dots \right] \quad (2A.25)$$

since

$$\frac{\partial e^u}{\partial x} = e^u \frac{du}{dx}$$

then equation 2A.25 can be transformed

$$\frac{1}{Q} \left[-\epsilon_1 e^{-\beta \epsilon_1} - \epsilon_2 e^{-\beta \epsilon_2} - \dots \right] = -\frac{E}{N}$$

(from equation 2A.24) or

$$E = -N \frac{\partial \ln Q}{\partial \beta} \quad (2A.26)$$

Converting to kT by use of equation 2A.22

$$E = -N \frac{\partial \ln Q}{\partial \beta} = E = -N \frac{\partial \ln Q}{\partial(1/kT)} \quad (2A.27)$$

where $k = \frac{R}{N_A}$

R = the gas constant

N_A = Avogadro's number

Rearranging equation 2A.27 by use of the relations

$$\frac{\partial \ln Q}{\partial(1/kT)} = \frac{\partial \ln Q}{\partial T} \left(\frac{\partial T}{\partial(1/kT)} \right) \quad (2A.28)$$

and

$$\frac{\partial T}{\partial(1/kT)} = \frac{1}{\frac{\partial(1/kT)}{\partial T}} = \frac{1}{\frac{1}{k} \left(-\frac{1}{T^2} \right)} = -kT^2 \quad (2A.29)$$

Substituting in equation 2A.25

$$E = +kT^2 \frac{\partial \ln Q}{\partial T} \quad (2A.30)$$

From classical thermodynamics, the entropy (S) is related to the specific heat at constant volume (C_v) by

$$S = \int_0^T \frac{C_v dT}{T} \quad (2A.31)$$

where

$$C_v = \left(\frac{\partial E}{\partial T} \right)_v = \frac{\partial \left[kT^2 \frac{\partial \ln Q}{\partial T} \right]}{\partial T} \quad (2A.32)$$

Therefore

$$S = \int_0^T \frac{1}{T} \frac{\partial \left[kT^2 \frac{\partial \ln Q}{\partial T} \right]}{\partial T} dT \quad (2A.33)$$

Equation 2A.31 can be integrated by parts or

$$d(uv) = u dv + v du$$

Then

$$\int u dv = \int d(uv) - \int v du = uv + \int v du \quad (2A.34)$$

Selecting as variables for equation 2A.31

$$u = \frac{1}{T} \quad \text{and} \quad dv = \partial \left[kT^2 \frac{\partial \ln Q}{\partial T} \right] \quad (2A.35)$$

Therefore

$$du = -\frac{1}{T^2} dT \quad \text{and} \quad v = kT^2 \frac{\partial \ln Q}{\partial T} \quad (2A.36)$$

Substituting the terms in equation 2A.36 into equation 2A.34

$$S = \frac{1}{T} kT^2 \frac{\partial \ln Q}{\partial T} \Big|_0^T - \int_0^T \left(kT^2 \frac{\partial \ln Q}{\partial T} \right) \left(-\frac{1}{T^2} dT \right) = \left[kT^2 \frac{\partial \ln Q}{\partial T} + k \ln Q \right]_0^T \quad (2A.37)$$

The Helmholtz free energy (A) is given in classical thermodynamics by

$$A = E - TS \quad (2A.38)$$

Using

$$E = kT^2 \left(\frac{\partial \ln Q}{\partial T} \right)_v$$

and

$$S = kT \frac{\partial \ln Q}{\partial T} + k \ln Q$$

Substituting these terms for E and S into equation 2A.38

$$A = kT^2 \frac{\partial \ln Q}{\partial T} - T \left(kT \frac{\partial \ln Q}{\partial T} + k \ln Q \right) = -kT \ln Q \quad (2A.39)$$

The Gibbs free energy (G) is given in classical thermodynamics by

$$G = A - PV \quad (2A.40)$$

Assuming that the PV term can be treated as a perfect gas

$$A = E - TS$$

$$dA = dE - TdS - SdT = dq - dw - T \left(\frac{dq}{T} \right) = -pdv - SdT \quad (2A.41)$$

$$P = - \left(\frac{\partial A}{\partial V} \right)_T = kT \left(\frac{\partial \ln Q}{\partial V} \right)_T = kT \frac{\partial \ln Q}{\partial V} \quad (2A.42)$$

$$G = -kT \ln Q - kT \frac{\partial \ln Q}{\partial V} \quad (2A.43)$$

Entropy may be expressed in terms of probability (w_0) by use of the following transformations.

Substituting equation 2A.23

$$Q = \sum n_i e^{-\epsilon_i/kT} = w_0 e^{-\epsilon_0/kT} + \dots$$

into equation 2A.37

$$S = \frac{\partial \ln Q}{\partial T} + k \ln Q$$

yields the equation

$$\begin{aligned} S &= kT \left[\frac{\partial \ln w_0 \exp[-\varepsilon_i/kT]}{\partial T} \right] + k \ln [w_0 \exp[-\varepsilon_i/kT]] \\ &= kT \left[\frac{\partial(\varepsilon_i/kT)}{\partial T} \right] + k \ln w_0 + k \ln(e^{\varepsilon_i/kT}) \\ &= kT \left[\frac{\varepsilon_i}{kT^2} \right] + k \ln w_0 + k \left(\frac{\varepsilon_i}{kT} \right) = k \ln w_0 \end{aligned} \quad (2A.44)$$

Equation 2A.44 states that:

The entropy of a molecule is proportional to the logarithm of the number of states accessible to the molecule, and the constant of proportionality is the gas constant divided by Avogadro's number.

References

1. R.H. Fowler, *Statistical Mechanics, 2nd. ed.*; Cambridge University: London, 1936
2. E. Schrödinger, *Statistical Thermodynamics, 2nd. ed.*;
Cambridge University London, 1952
3. M. Dole, *Introduction to Statistical Thermodynamics*; Prentice-Hall: New York, 1954
4. E.A. Guggenheim, *Thermodynamics 3rd. ed.* ; Interscience: New York, 1957

Statistical Thermodynamics of an Ideal Monatomic Gas

A molecule of a gas can be considered as a particle in a box. Its energy levels may be described by quantum mechanics. In one dimension, an integral number of deBroglie half wavelengths must fit into the length of the box, a . That is

$$n(\lambda/2) = a \quad (2A.45)$$

Then, using deBroglie's equation, $\lambda = \hbar/mv$

$$n\hbar/2mv = a \quad (2A.46)$$

or

$$v = n\hbar/2ma \quad (2A.47)$$

Assuming the only energy is kinetic energy, $mv^2/2$, the energy of this n^{th} quantum states is

$$\varepsilon_n = (m/2)[n\hbar/2ma]^2 = n^2 a^2 / 8ma^2 \quad (2A.48)$$

The translation partition function for this one-dimensional system is

$$Q_a = \sum \exp(-\varepsilon_n/kT) = \sum \exp(-\beta_s^2 n^2) \quad (2A.49)$$

For a large number of closely spaced energy levels, one may approximate the sum by an integral, so

$$Q_a = \int \exp(-\beta_s^2 n^2) dn = \pi^{1/2} / 2\beta = (2\pi mkT)^{1/2} a / \hbar \quad (2A.50)$$

where $\beta_s^2 = a^2 / 8ma^2 kT$

The sum is from $n = 1$ to ∞ ; so the limits of integration are from 0 to ∞ in three dimensions. We may consider the molecule to reside in a rectangular box with dimensions, a , b , and c . The three-dimensional partition function then becomes

$$Q = Q_a Q_b Q_c = (2\pi mkT)^{3/2} abc / \hbar^3 \quad (2A.51)$$

where $abc = V$, the volume of the box.

We have seen that the internal energy (2A.30) is

$$E = kT^2 \left(\frac{\partial \ln Q}{\partial T} \right) \quad (2A.52)$$

Now

$$\ln Q = \ln \left[(2\pi mk)^{3/2} / h^3 \right] + (3/2) \ln T + \ln V \quad (2A.53)$$

Then

$$\left(\frac{\partial \ln Q}{\partial T} \right) = 3/(2T) \quad (2A.54)$$

so

$$E = kT^2 (3/2T) = (3/2)kT \quad (2A.55)$$

The heat capacity at constant volume is then

$$C_v = \left(\frac{\partial E}{\partial T} \right)_v = (3/2)k \quad (2A.56)$$

This is the value for a single molecule. For N molecules, it is

$$C_v = (3/2)Nk \quad (2A.57)$$

and for a mole, where $N = N_A$, Avogadro's number

$$C_v = (3/2)N_A k = (3/2)R \quad (2A.58)$$

and R is the gas constant $= N_A k$.

This is in agreement with the value obtained from the kinetic theory of gases.

We have seen that the Helmholtz free energy, A , is

$$A = -kT \ln Q = -kT \left\{ \ln \left[(2\pi mk)^{3/2} / h^3 \right] + (3/2) \ln T + \ln V \right\} \quad (2A.59)$$

The pressure of the gas is then found from

$$P = - \left(\frac{\partial A}{\partial V} \right)_T = kTN \quad (2A.60)$$

Again, this is for a single molecule. For N molecules,

$$P = NkTN = (\text{number of moles}) (RT/V) \quad (2A.61)$$

This is the ideal gas law.

Appendix 2B - Vector Analysis

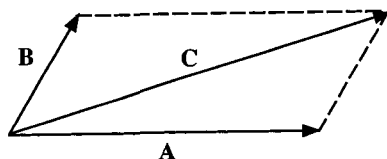


Figure 2B.1. Illustration of the parallelogram rule for vector analysis.

A vector is a quantity that has both magnitude and direction. A common example given in this book is the carbon-carbon bond. Its magnitude is the bond length (1.54 Å for single bonds); its direction is the bond orientation related to an arbitrary reference coordinate system. Vectors are used to describe dipole moments and electromagnetic wave propagation (infrared dichroism, x-ray diffraction and light scattering).

2B.1. Vector Addition

Vectors can be added using parallelogram rule. Consider two vectors (**A** and **B**, Figure 2B.1) that share a common origin. If two lines parallel to these vectors are drawn to form a parallelogram, the diagonal is the sum of these two vectors or the resultant vector, **C**. Mathematically,

$$\mathbf{A} + \mathbf{B} = \mathbf{C} \quad (2B.1)$$

Because vectors have both magnitude and direction, it is convenient to separate a vector into its components by means of the following convention. A unit vector specifies direction. The unit vector is multiplied by a scalar quantity in order to characterize magnitude. For a three dimensional coordinate system, three unit vectors (**i**, **j**, **k**) are set up at right angles to each other to form a unit orthogonal triad (Figure 2B.2). Thus, the vector, **A**, by this convention is

$$\mathbf{A} = a_x \mathbf{i} + a_y \mathbf{j} + a_z \mathbf{k} \quad (2B.2)$$

Similarly,

$$\mathbf{B} = b_x \mathbf{i} + b_y \mathbf{j} + b_z \mathbf{k} \quad (2B.3)$$

The result of adding these two vectors is

$$\mathbf{A} + \mathbf{B} = (a_x + b_x)\mathbf{i} + (a_y + b_y)\mathbf{j} + (a_z + b_z)\mathbf{k} \quad (2B.4)$$

2.B.2 Scalar Product

The scalar or dot product obtained by multiplying two vectors is defined by the operation.

$$\mathbf{A} \cdot \mathbf{B} = |\mathbf{A}||\mathbf{B}|\cos\theta \quad (2B.5)$$

where θ . is the included angle between the vectors (Figure B-2) and $|\mathbf{A}|$ and $|\mathbf{B}|$ are the scalar magnitudes.

Because $\cos\theta = 1$,

$$\mathbf{A} \cdot \mathbf{A} = |\mathbf{A}|^2 \quad (2B.6)$$

The result of multiplying two vectors using a dot product is a scalar quantity.

Since the vectors \mathbf{i} , \mathbf{j} and \mathbf{k} have a magnitude of one by definition and are at right angles to each other.

$$\begin{aligned} (\cos 0^\circ = 1) \quad \mathbf{i} \cdot \mathbf{i} = \mathbf{j} \cdot \mathbf{j} = \mathbf{k} \cdot \mathbf{k} = 1 \\ (\cos 90^\circ = 0) \quad \mathbf{j} \cdot \mathbf{k} = \mathbf{k} \cdot \mathbf{i} = \mathbf{i} \cdot \mathbf{j} = 0 \\ (\cos 90^\circ = 0) \quad \mathbf{k} \cdot \mathbf{j} = \mathbf{i} \cdot \mathbf{k} = \mathbf{j} \cdot \mathbf{i} = 0 \end{aligned} \quad (2B.7)$$

therefore, writing

$$\mathbf{A} \cdot \mathbf{B} = (a_x\mathbf{i} + a_y\mathbf{j} + a_z\mathbf{k}) \cdot (b_x\mathbf{i} + b_y\mathbf{j} + b_z\mathbf{k}) \quad (2B.8)$$

and carrying out the indicated multiplication yields

$$\mathbf{A} \cdot \mathbf{B} = a_x b_x + a_y b_y + a_z b_z \quad (2B.9)$$

because all the cross product terms are equal to zero (equation 2B.7).

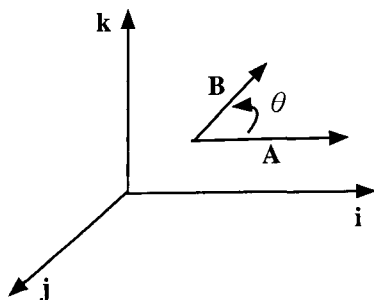


Figure 2B.2 Two vectors set in a unit orthogonal triad

Reference

Banesh Hoffman, *About Vectors*, Dover Press New York, NY (1975)

Appendix 2C - Radius of Gyration

In much of this book, the dimensions of a polymer molecule have been defined in terms of the mean squared distance its ends, $\langle R^2 \rangle$. In this section, a different statistical measure will be introduced called the radius of gyration, R_g , whose mean square radius is defined as

$$\langle R_g^2 \rangle = \frac{1}{Z} \sum_{i=1}^Z \langle r_i^2 \rangle \quad (2C.1)$$

where r_i is a vector measured from the center of gravity of the molecule (Figure 2C.1) defined by

$$\sum r_i = 0 \quad (2C.2)$$

In terms of Physics, $\langle R_g^2 \rangle$ represents the moment of inertia of the molecule.

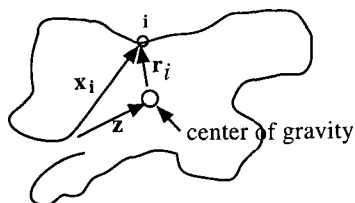


Figure 2C.1 Vector quantities used in describing the radius of gyration of a polymer chain

The use of $\langle R_g^2 \rangle$ is desirable because, for a branched molecule, there are many ends so that $\langle R^2 \rangle$ cannot be easily defined, while $\langle R_g^2 \rangle$ is useful, both the intrinsic viscosity and the angular variation of scattered intensity are closely related by theory to $\langle R_g^2 \rangle$.

The vector z extends from the end segment ($i = 1$) to the center of gravity and the vector r_i from the end segment to the center of gravity to the i^{th} segment (Figure 2C.1).

Now,

$$\mathbf{r}_i = \mathbf{x}_i = \mathbf{z}_i \quad (2C.3)$$

so

$$\sum_{i=1}^Z \mathbf{r}_i = \sum_{i=1}^Z \mathbf{x}_i = \sum_{i=1}^Z \mathbf{z}_i \quad (2C.4)$$

but

$$\sum_{i=1}^Z \mathbf{z} = Z\mathbf{z} \quad (2C.5)$$

so

$$\mathbf{z} = \frac{1}{Z} \sum_{i=1}^Z \mathbf{x}_i \quad (2C.6)$$

The square of the length of \mathbf{z} may be obtained by taking its scalar product with itself

$$\langle z^2 \rangle = \mathbf{z} \cdot \mathbf{z} = \sum_{i=1}^Z \sum_{j=1}^Z \langle (\mathbf{x}_i \cdot \mathbf{x}_j) \rangle \quad (2C.7)$$

Now let us examine

$$\sum_{i=1}^Z \mathbf{r}_i \cdot (\mathbf{r}_i + \mathbf{z}) = \sum_{i=1}^Z (\mathbf{r}_i \cdot \mathbf{r}_i) + z \sum \mathbf{r}_i \quad (2C.8)$$

It follows that

$$\begin{aligned} \sum_{i=1}^Z r_i^2 &= \sum_{i=1}^Z \mathbf{r}_i \cdot (\mathbf{r}_i + \mathbf{z}) \\ &= \sum_{i=1}^Z (\mathbf{x}_i - \mathbf{z}) \cdot \mathbf{x}_i \\ &= \sum_{i=1}^Z x_i^2 - \mathbf{z} \cdot \sum_{i=1}^Z \mathbf{x}_i \end{aligned} \quad (2C.9)$$

using equation 2C.3 for \mathbf{r}_i .

Then

$$\langle R_g^2 \rangle = \frac{1}{Z} \sum_{i=1}^Z \langle x_i^2 \rangle - \frac{1}{Z} \mathbf{z} \cdot \sum_{i=1}^Z \mathbf{x}_i \quad (2C.10)$$

Now, using equation 2C.6 for z

$$\langle R_g^2 \rangle = \frac{1}{Z} \sum_{i=1}^Z x_i^2 - \frac{1}{Z} \mathbf{z} \cdot \sum_{i=1}^Z \mathbf{x}_i \quad (2C.11)$$

Define

$$\langle r^2 \rangle \equiv \frac{1}{Z} \sum_{i=1}^Z \langle x_i^2 \rangle \quad (2C.12)$$

Then, using equation 2C.7

$$\langle R_g^2 \rangle = \langle x^2 \rangle = \langle z^2 \rangle \quad (2C.13)$$

Now define

$$\mathbf{x}_{ij} = \mathbf{x}_i - \mathbf{x}_j \quad (2C.14)$$

Taking the scalar product of \mathbf{x}_{ij} with itself

$$x_{ij}^2 = \mathbf{x}_{ij} \cdot \mathbf{x}_{ij} = (\mathbf{x}_i \cdot \mathbf{x}_j) \cdot (\mathbf{x}_i \cdot \mathbf{x}_j) = x_i^2 + x_j^2 - 2\mathbf{x}_i \cdot \mathbf{x}_j \quad (2C.15)$$

Thus

$$\mathbf{x}_i \cdot \mathbf{x}_j = \frac{1}{2} (x_i^2 + x_j^2 + x_{ij}^2) \quad (2C.16)$$

so, substituting in equation 2C.11

$$\langle R_g^2 \rangle = \frac{1}{Z} \sum_{i=1}^Z \langle x_i^2 \rangle - \frac{1}{2Z^2} \sum_{i=1}^Z \sum_{j=1}^Z \langle x_i^2 \rangle - \frac{1}{2Z^2} \sum_{i=1}^Z \sum_{j=1}^Z \langle x_j^2 \rangle + \frac{1}{2Z^2} \sum_{i=1}^Z \sum_{j=1}^Z \langle x_{ij}^2 \rangle \quad (2C.17)$$

However, in the average (Figure 2C.2)

STATISTICS OF CHAIN CONFORMATIONS

$$\sum_{i=1}^Z \sum_{j=1}^Z \langle x_i^2 \rangle = \sum_{i=1}^Z \sum_{j=1}^Z \langle x_j^2 \rangle = Z \sum_{i=1}^Z x_i^2 \quad (2C.18)$$

so

$$\langle R_s^2 \rangle = \frac{1}{2Z^2} \sum_{i=1}^Z \sum_{j=1}^Z \langle x_{ij}^2 \rangle \quad (2C.19)$$

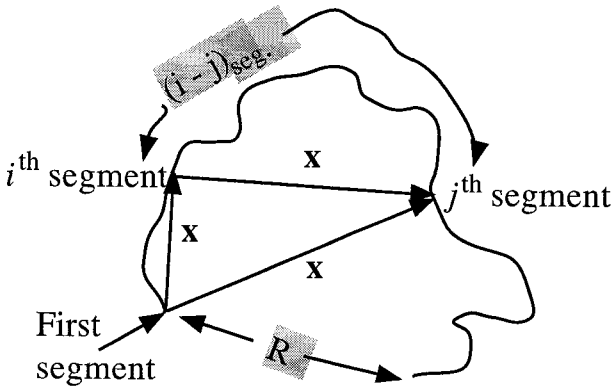


Figure 2C.2.

Now for the end-to-end length of a chain

$$\langle R^2 \rangle = ZL^2 \quad (2C.20)$$

where L is the length of a statistical segment. The same formula applies to $\langle x_{ij}^2 \rangle$, the distance between the i^{th} and j^{th} segment providing $(j - i)$ is large enough. Thus

$$\langle x_{ij}^2 \rangle = |i - j|L^2 \quad (2C.21)$$

where $|i - j|$ is the absolute value of $(i - j)$.

Thus, from equation 2C.19

$$\langle R_s^2 \rangle = \frac{L^2}{2Z^2} \sum_{i=1}^Z \sum_{j=1}^Z |i - j| = \frac{L^2}{2Z^2} \sum_{i=1}^Z \left[\sum_{j=1}^Z (i - j) + \sum_{j=i+1}^Z (j - i) \right] \quad (2C.22)$$

Now from the formula for the sum of the arithmetic series

$$\sum_{i=p}^q i = i \left[\frac{q+p}{2} \right] [q-p] \quad (2C.23)$$

so

$$\begin{aligned} \langle R_g^2 \rangle &= \frac{L^2}{2Z^2} \sum \left\{ \frac{[0+(i-1)][i+1]}{2} + \frac{[(Z-i)+1][Z-i]}{2} \right\} \\ &\cong \frac{L^2}{2Z^2} \sum \left\{ \frac{i^2}{2} + \frac{(Z-i)^2}{2} \right\} \\ &= \frac{L^2}{2Z^2} \sum \left\{ \left[i^2 - Zi + \frac{1}{2}Z^2 \right] \right\} \end{aligned} \quad (2C.24)$$

Now

$$\sum_{i=1}^Z i^2 \cong \int_0^Z i^2 di = \frac{Z^3}{3} \quad (2C.25)$$

so

$$\begin{aligned} \langle R_g^2 \rangle &\cong \frac{L^2}{2Z^2} \left\{ \frac{Z^3}{3} - Z \left(\frac{Z^2}{2} \right) + \frac{1}{2}Z^2(Z) \right\} \\ &= \frac{L^2}{2Z^2} \left\{ \frac{Z^3}{3} - Z \left(\frac{Z^2}{2} \right) + Z^2(Z) \right\} \\ &= \frac{L^2}{6Z^2} Z^3 = \frac{1}{6} ZL^2 = \frac{1}{6} \langle R^2 \rangle \end{aligned} \quad (2C.26)$$

$$\langle R_g^2 \rangle = \frac{1}{6} \langle R^2 \rangle \quad (2C.27)$$

for an unbranched random coil.

The radius of gyration of branched chains (one trifunctional point with equal branch lengths)

$$\langle R_g^2 \rangle = ZL^2 [1/6 - 1/27] \quad (2C.28)$$

The branching index, g , is defined as

$$g = \frac{\langle R_g^2 \rangle_{\text{branched}}}{\langle R_g^2 \rangle_{\text{linear}}} = \frac{ZL^2(1/6 - 1/27)}{ZL^2(1/6)} = 1 - (2/9) = 0.778 \quad (2C.29)$$

As seen from the above, the value of $\langle R_g^2 \rangle$ varies with the chain configuration. The branching index varies similarly with chain configuration

Appendix 2D. Evaluation of $(\mathbf{a}_{m+n} \cdot \mathbf{a}_m)$

Locate the $(\mathbf{a}_m)^{\text{th}}$ bond in a coordinate system in which \mathbf{a}_m lies along the X axis ($\mathbf{a}_m = \mathbf{i}_m$). \mathbf{i}_{m+1} lies in the direction of \mathbf{a}_{m+1} . The y axis of the coordinate system of the $(m+1)$ bond lies in the plane of \mathbf{i}_m and \mathbf{i}_{m+1} and is of course perpendicular to

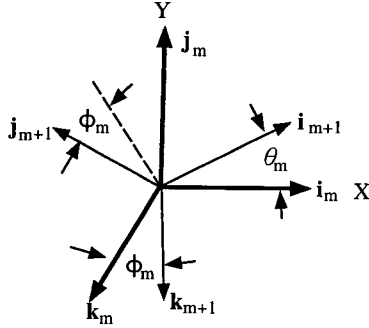


Figure 2D.1. Rotation of coordinate axis used in derivation of equation 2C-41.

\mathbf{i}_{m+1} . \mathbf{k}_{m+1} is perpendicular to \mathbf{i}_{m+1} and \mathbf{j}_{m+1} (Figure 2D.1). θ_m is the angle between \mathbf{i}_m and \mathbf{i}_{m+1} . It follows from this figure that

$$\mathbf{i}_m = (\cos \theta) \mathbf{i}_{m+1} + (\sin \theta) \mathbf{j}_{m+1} \quad (2D.1)$$

$$\mathbf{j}_m = (-\sin \theta \cos \phi_m) \mathbf{i}_{m+1} + (\cos \theta \cos \phi_m) \mathbf{j}_{m+1} + (\sin \theta) \mathbf{k}_{m+1} \quad (2D.2)$$

$$\mathbf{k}_m = (\sin \theta \sin \phi_m) \mathbf{i}_{m+1} + (-\cos \theta \sin \phi_m) \mathbf{j}_{m+1} + (\cos \phi_m) \mathbf{k}_{m+1} \quad (2D.3)$$

Suppose a vector \mathbf{P} is represented in the two coordinate system as

$$\mathbf{P} = c_1 \mathbf{i}_m + c_2 \mathbf{j}_m + c_3 \mathbf{k}_m \quad (2D.4)$$

or

$$\mathbf{P} = c'_1 \mathbf{i}_{m+1} + c'_2 \mathbf{j}_{m+1} + c'_3 \mathbf{k}_{m+1} \quad (2D.5)$$

Now by substituting (2D.1), (2D.2) and (2D.3) into (2D.4), one obtains

$$\begin{aligned} \mathbf{P} = & \left[(\cos \theta)c_1 - (\sin \theta \cos \phi_m)c_2 + (\sin \theta \sin \phi_m)c_3 \right] \mathbf{i}_{m+1} \\ & + \left[(\sin \theta)c_1 + (\cos \theta \cos \phi_m)c_2 - (\cos \theta \sin \phi_m)c_3 \right] \mathbf{j}_{m+1} \quad (2D.6) \\ & + \left[\begin{array}{cc} (\sin \phi_m)c_2 & + (\cos \phi_m)c_3 \end{array} \right] \mathbf{k}_{m+1} \end{aligned}$$

Comparing with ((2D.5), it follows that

$$c'_1 = (\cos \theta)c_1 + (-\sin \theta \cos \phi_m)c_2 + (\sin \theta \sin \phi_m)c_3 \quad (2D.7)$$

$$c'_2 = (\sin \theta)c_1 - (\cos \theta \cos \phi_m)c_2 + (\cos \theta \sin \phi_m)c_3 \quad (2D.8)$$

$$c'_3 = (\sin \phi_m)c_2 + (\cos \phi_m)c_3 \quad (2D.9)$$

The coefficients of this equation define the matrix of the transformation,

$$|A| = \begin{vmatrix} \cos \theta & -\sin \theta \cos \phi_m & \sin \theta \sin \phi_m \\ \sin \theta & -\cos \theta \cos \phi_m & \cos \theta \sin \phi_m \\ 0 & \sin \phi_m & \cos \phi_m \end{vmatrix} = \begin{vmatrix} \alpha_{11} & \alpha_{12} & \alpha_{13} \\ \alpha_{21} & \alpha_{22} & \alpha_{23} \\ \alpha_{31} & \alpha_{32} & \alpha_{33} \end{vmatrix} = |\alpha_{ij}| \quad (2D.10)$$

If a second matrix |B| is

$$|B| = \begin{vmatrix} \beta_{11} & \beta_{12} & \beta_{13} \\ \beta_{21} & \beta_{22} & \beta_{23} \\ \beta_{31} & \beta_{32} & \beta_{33} \end{vmatrix} = |\beta_{ij}| \quad (2D.11)$$

The multiplication of two matrices is defined as

$$|C| = |B||A| = |\gamma_{ij}| \quad (2D.12)$$

where an element of the |C| matrix is obtained by

$$|\gamma_{ij}| = \sum_k \beta_{ik} \alpha_{kj} \quad (2D.13)$$

A vector may be represented by a row matrix

$$\left| \begin{array}{ccc} c'_1 & c'_2 & c'_3 \end{array} \right|$$

or a column matrix

$$\begin{vmatrix} c_1 \\ c_2 \\ c_3 \end{vmatrix}$$

In matrix notation, the set of equations (2D.7), (2D.8), and (2D.9) may be represented by

$$\begin{vmatrix} c'_1 & c'_2 & c'_3 \end{vmatrix} = |A| \begin{vmatrix} c_1 \\ c_2 \\ c_3 \end{vmatrix} \quad (2D.14)$$

Thus, the product of a matrix with a vector gives the components of the vector in a new coordinate system. The product of the matrix and the vector is carried out using the rule ((2D.12) for matrix multiplication, so, for example

$$c'_2 = \sum_{k=1}^3 \alpha_{2k} c_k \quad (2D.15)$$

which is identical with equation 2D.8.

Similarly, if in a third coordinate system

$$P = \sum_{i=1}^3 c''_i \quad (2D.16)$$

where

$$c''_1 = \sum_{j=1}^3 b_{1j} c'_j = \sum_{k=1}^3 \sum_{j=1}^3 [b_{1j} a_{jk} c_k] = \sum_{k=1}^3 \gamma_{1k} c_k \quad (2D.17)$$

It follows that

$$\gamma_{ij} = \sum_{j=1}^3 b_{ij} a_{jk} \quad (2D.18)$$

which is identical with (2D.14). Thus

$$\begin{vmatrix} c_1'' & c_2'' & c_3'' \end{vmatrix} = |C| \begin{vmatrix} c_1 \\ c_2 \\ c_3 \end{vmatrix} = |B| |A| \begin{vmatrix} c_1 \\ c_2 \\ c_3 \end{vmatrix} \quad (2D.19)$$

Let us now apply this to the problem at hand. In the coordinate system of the m^{th} bond

$$\mathbf{a}_m = \begin{vmatrix} 1 \\ 0 \\ 0 \end{vmatrix} \quad (2D.20)$$

while in the coordinate system of the $(m+1)^{\text{st}}$ bond

$$\mathbf{a}_m = |A| \begin{vmatrix} 1 \\ 0 \\ 0 \end{vmatrix} \quad (2D.21)$$

Thus $(\mathbf{a}_{m+1} \cdot \mathbf{a}_m)$ taken in the coordinate system of the $(m+1)^{\text{st}}$ bond is

$$(\mathbf{a}_{m+1} \cdot \mathbf{a}_m) = \mathbf{a}_{m+1} \cdot |A| \begin{vmatrix} 1 \\ 0 \\ 0 \end{vmatrix} = \mathbf{i}_{m+1} \cdot [\alpha_{11} \mathbf{i}_{m+1} + \alpha_{21} \mathbf{j}_{m+1} + \alpha_{31} \mathbf{k}_{m+1}] = \alpha_{11} = \cos \theta \quad (2D.22)$$

If now $|B|$ is the matrix that goes from the coordinate system of the $(m+1)^{\text{st}}$ bond to the $(m+2)^{\text{nd}}$ bond which are related as in Figure 2D.1 so

$$|B| = \begin{vmatrix} \cos \theta & -\sin \theta \cos \phi_{m+1} & \sin \theta \sin \phi_{m+1} \\ \sin \theta & \cos \theta \cos \phi_{m+1} & -\cos \theta \sin \phi_{m+1} \\ 0 & \sin \phi_{m+1} & \cos \phi_{m+1} \end{vmatrix} \quad (2D.23)$$

Then

$$(\mathbf{a}_{m+2} \cdot \mathbf{a}_m) = \mathbf{i}_{m+2} \cdot |B| \begin{vmatrix} 1 \\ 0 \\ 0 \end{vmatrix} = \mathbf{i}_{m+2} \cdot |B| |A| \begin{vmatrix} 1 \\ 0 \\ 0 \end{vmatrix}$$

$$\begin{aligned}
 &= \mathbf{i}_{m+2} \cdot \left| C \begin{array}{c} 1 \\ 0 \\ 0 \end{array} \right| = \mathbf{i}_{m+2} \cdot [\gamma_{11} \mathbf{i}_{m+2} + \gamma_{21} \mathbf{j}_{m+2} + \gamma_{31} \mathbf{k}_{m+2}] = \gamma_{11} \\
 &= \sum_k \beta_{1k} \alpha_{k1} = \beta_{11} \alpha_{11} + \beta_{12} \alpha_{21} + \beta_{13} \alpha_{31} = \cos^2 \theta - \sin^2 \theta \cos \phi_{m+1} \quad (2D.24)
 \end{aligned}$$

This is identical with equation 2.28 obtained for n-butane except the sign of the second term (because of the ϕ defined in Figure 2D.1 differs from that of Figure 2.7 by 180°).

Similarly, if we call $|A| \equiv |A_m|$, $B \equiv |A_{m+1}|$ and define $|A_{m+2}|$ as the matrix to take us from the $(m+1)$ to the $(m+2)$ coordinate system, where in general

$$|A_{m+n}| = \begin{vmatrix} \cos \theta & -\sin \theta \cos \phi_{m+n} & \sin \theta \sin \phi_{m+n} \\ \sin \theta & \cos \theta \cos \phi_{m+n} & -\cos \theta \sin \phi_{m+n} \\ 0 & \sin \phi_{m+n} & \cos \phi_{m+n} \end{vmatrix} \quad (2D.25)$$

so

$$(\mathbf{a}_{m+3} \cdot \mathbf{a}_m) = \mathbf{i}_{m+2} \cdot |A_{m+2}| |A_{m+1}| |A_m| \begin{vmatrix} 1 \\ 0 \\ 0 \end{vmatrix} = \mathbf{i}_{m+2} \cdot |D| \begin{vmatrix} 1 \\ 0 \\ 0 \end{vmatrix} \quad (2D.26)$$

where

$$|D| = |\delta_j| = |A_{m+2}| |A_{m+1}| |A_m| \quad (2D.27)$$

Thus

$$\begin{aligned}
 (\mathbf{a}_{m+3} \cdot \mathbf{a}_m) &= \mathbf{i}_{m+3} \cdot (\delta_{11} \mathbf{i}_{m+3} + \delta_{21} \mathbf{j}_{m+3} + \delta_{31} \mathbf{k}_{m+3}) \\
 &= \delta_{11} = \sum_j \varepsilon_{1j} \gamma_{j1} = \varepsilon_{11} \gamma_{11} + \varepsilon_{12} \gamma_{21} + \varepsilon_{13} \gamma_{31} \quad (2D.28)
 \end{aligned}$$

where

$$|A_{m+2}| = |\varepsilon_{ij}| \quad (2D.29)$$

Thus

$$\begin{aligned}
 (\mathbf{a}_{m+3} \cdot \mathbf{a}_m) &= \cos \theta (\cos^2 \theta - \sin^2 \theta \cos \phi_{m+1}) \\
 &\quad + \sin \theta \cos \phi_{m+2} (\sin \theta \cos \phi_{m+1}) \\
 &\quad - \sin \theta \cos \phi_{m+1} (\sin \theta \cos \phi + \sin \theta \cos \phi \cos \phi_{m+1}) \quad (2D.30)
 \end{aligned}$$

In the approximation of free rotation where all of the θ 's vary randomly

$$(\mathbf{a}_{m+1} \cdot \mathbf{a}_m) = \cos \theta \quad (2D.31)$$

$$(\mathbf{a}_{m+2} \cdot \mathbf{a}_m) = \cos^2 \theta \quad (2D.32)$$

$$(\mathbf{a}_{m+3} \cdot \mathbf{a}_m) = \cos^3 \theta \quad (2D.33)$$

The last equation could be arrived at using

$$(\mathbf{a}_{m+3} \cdot \mathbf{a}_m) = \mathbf{i}_{m+3} \cdot \left\langle A_{m+2} \right\rangle \left\langle A_{m+1} \right\rangle \left\langle A_m \right\rangle \begin{vmatrix} 1 \\ 0 \\ 0 \end{vmatrix} \quad (2D.34)$$

to the approximation that the ϕ 's are independent. Now

$$\langle A \rangle = \langle A_{m+2} \rangle = \langle A_{m+1} \rangle = \langle A_m \rangle = \begin{vmatrix} \cos \theta & -\sin \theta \langle \cos \phi \rangle & \sin \theta \langle \sin \phi \rangle \\ \sin \theta & \cos \theta \langle \cos \phi \rangle & -\cos \theta \langle \sin \phi \rangle \\ 0 & \langle \sin \phi \rangle & \langle \cos \phi \rangle \end{vmatrix} \quad (2D.35)$$

For free rotation where the θ 's vary randomly, $\cos \theta = \sin \theta = 0$, so

$$\langle (\mathbf{a}_{m+1} \cdot \mathbf{a}_m) \rangle = \mathbf{i}_{m+3} = \langle A \rangle^3 \begin{vmatrix} 1 \\ 0 \\ 0 \end{vmatrix} \quad (2D.36)$$

where

$$\langle A \rangle = \begin{vmatrix} \cos \theta & 0 & 0 \\ \sin \theta & 0 & 0 \\ 0 & 0 & 0 \end{vmatrix} \quad (2D.37)$$

$$\langle A \rangle^2 = \begin{vmatrix} \cos^2 \theta & 0 & 0 \\ \sin \theta \cos \theta & 0 & 0 \\ 0 & 0 & 0 \end{vmatrix} \quad (2D.38)$$

$$\langle A \rangle^3 = \begin{vmatrix} \cos^3 \theta & 0 & 0 \\ \sin \theta \cos^2 \theta & 0 & 0 \\ 0 & 0 & 0 \end{vmatrix} \quad (2D.39)$$

so

$$\begin{aligned} \langle (\mathbf{a}_{m+1} \cdot \mathbf{a}_m) \rangle &= \mathbf{i}_{m+3} \cdot \begin{vmatrix} \cos^3 \theta & 0 & 0 \\ \sin \theta \cos^2 \theta & 0 & 0 \\ 0 & 0 & 0 \end{vmatrix} \begin{vmatrix} 1 \\ 0 \\ 0 \end{vmatrix} \\ &= \mathbf{i}_{m+3} [\cos^3 \theta \mathbf{i}_{m+1} + \sin \theta \cos^2 \theta \mathbf{j}_{m+3}] = \cos^3 \theta \end{aligned} \quad (2D.40)$$

$$\langle (\mathbf{a}_{m+n} \cdot \mathbf{a}_m) \rangle = \mathbf{i}_{m+3} = |A|^n \begin{vmatrix} 1 \\ 0 \\ 0 \end{vmatrix} = \mathbf{i}_{m+3} \cdot \begin{vmatrix} \cos^n \theta & 0 & 0 \\ \sin \theta \cos^{n-1} \theta & 0 & 0 \\ 0 & 0 & 0 \end{vmatrix} \begin{vmatrix} 1 \\ 0 \\ 0 \end{vmatrix} = \cos^n \theta \quad (2D.41)$$

Appendix 2E. Restricted Rotation with Symmetrical Barrier

In the case of restricted rotation, the transformation matrix (equation 2.58A) is

$$|A| = \begin{vmatrix} \cos \theta & -\eta \cos \theta & \varepsilon \sin \theta \\ \sin \theta & \eta \cos \theta & -\varepsilon \cos \theta \\ 0 & \varepsilon & \eta \end{vmatrix} \quad (2E.1)$$

where

$$\eta = \langle \cos \phi_m \rangle \quad (2E.2)$$

and

$$\varepsilon = \langle \sin \phi_m \rangle \quad (2E.3)$$

so

$$\langle \mathbf{a}_m \cdot \mathbf{a}_{m+1} \rangle = |\bar{a}_{11}| = \cos \theta \quad (2E.4)$$

Now

$$\langle \mathbf{a}_m \cdot \mathbf{a}_{m+1} \rangle = |A|_{11}^2 \quad (2E.5)$$

etc.

where ($| \cdot |_{11}$) stands for the 1,1 element of the matrix. For a symmetrical potential where $V(Q) = V(-Q)$,

$$\varepsilon = 0 \quad (2E.6)$$

and

$$\eta \varepsilon = 0 \quad (2E.7)$$

For infinitely long chains

$$\begin{aligned} R^2 &= N\ell^2 \left\{ 1 + 2\langle \mathbf{a}_m \cdot \mathbf{a}_{m+1} \rangle + \langle \mathbf{a}_m \cdot \mathbf{a}_{m+2} \rangle + \langle \mathbf{a}_m \cdot \mathbf{a}_{m+3} \rangle + \dots \right\} \\ &= N\ell^2 \left\{ 2 \left[\left(|\bar{A}| + |\bar{A}|^2 + |\bar{A}|^3 + \dots \right)_{11} \right] \right\} = N\ell^2 [1 + 2|S|_{11}] \end{aligned} \quad (2E.8)$$

where the matrix S is

$$|S| = |\bar{A}| + |\bar{A}|^2 + |\bar{A}|^3 + \dots \quad (2E.9)$$

Now the formula for the summation of a geometric series applies to matrices since

$$|S||\mathbf{I}| = |S| = |\bar{A}| + |\bar{A}|^2 + |\bar{A}|^3 + \dots \quad (2E.10)$$

where $|\mathbf{I}|$ is the identity matrix

$$|\mathbf{I}| = \begin{vmatrix} 1 & 0 & 0 \\ 0 & 1 & 0 \\ 0 & 0 & 1 \end{vmatrix} \quad (2E.11)$$

Then

$$|S||\bar{A}| = |\bar{A}|^2 + |\bar{A}|^3 + |\bar{A}|^4 + \dots \quad (2E.12)$$

so that

$$|S||\mathbf{I}| = |S||\bar{A}| = |\bar{A}| \quad (2E.13)$$

and

$$|S| = |\bar{A}| [|\mathbf{I}| - |\bar{A}|]^{-1} \quad (2E.14)$$

If

$$|M| = |\mathbf{I}| - |\bar{A}| \quad (2E.15)$$

the reciprocal of $|M|$ (or $|M|^{-1}$) is

$$|M|^{-1} = \frac{|\hat{M}|}{D} \quad (2E.16)$$

(see, for example, R.N. Hochstrasser, *Molecular Aspects of Symmetry*; Benjamin: NY, 1966, p 30).

$|\hat{M}|$ is the adjoint of matrix $|M|$. This is the matrix of the cofactors of the transpose of $|M|$ (designated $|M|E$ is the determinant of $|M|$).

In equation 2.8, we need the 1,1 element of $|S|$ where

$$|S|_{1,1} = (|\bar{A}| |M|_{1,1}) = \frac{(|\bar{A}| |\hat{M}|_{1,1})}{D} = \frac{1}{D} (\bar{\alpha}_{11} \hat{m}_{11} + \bar{\alpha}_{12} \hat{m}_{21} + \bar{\alpha}_{13} \hat{m}_{31}) \quad (2E.17)$$

where

$$\bar{\alpha}_{ij} = |\bar{A}| \quad (2E.18)$$

$$|\hat{m}_{ij}| = |\hat{M}| \quad (2E.19)$$

Now

$$|M| = \begin{vmatrix} 1 - \cos \theta & \eta \sin \theta & 0 \\ -\sin \theta & 1 - \eta \sin \theta & 0 \\ 0 & 0 & 1 - \eta \end{vmatrix} \quad (2E.20)$$

so

$$|M'| = \begin{vmatrix} 1 - \cos \theta & -\sin \theta & 0 \\ \eta \cos \theta & 1 - \eta \cos \theta & 0 \\ 0 & 0 & 1 - \eta \end{vmatrix} \quad (2E.21)$$

Then

$$\hat{m}_{11} = (+1) \begin{vmatrix} 1 - \eta \cos \theta & 0 \\ 0 & 1 - \eta \end{vmatrix} = (1 - \eta \cos \theta)(1 - \eta) \quad (2E.22)$$

$$\hat{m}_{21} = (-1) \begin{vmatrix} -\sin \theta & 0 \\ 0 & 1 - \eta \end{vmatrix} = +\eta \sin \theta (1 - \eta) \quad (2E.23)$$

and

$$\hat{m}_{31} = (+1) \begin{vmatrix} \sin \theta & 0 \\ (1 - \eta) \cos \theta & 1 - \eta \end{vmatrix} = 0 \quad (2E.24)$$

Also

$$D = (1 - \eta)(1 + \eta)(1 - \cos \theta) \quad (2E.25)$$

Thus, from equation 2.17

$$\begin{aligned}
 |S|_{h1} &= \frac{(\cos \theta)(1 - \eta \cos \theta)(1 - \eta) + (-\eta \sin \theta)(+\sin \theta)(1 - \eta)}{(1 - \eta)(1 + \eta)(1 - \cos \theta)} \\
 &= \frac{\cos \theta - \eta}{(1 + \eta)(1 - \cos \theta)} \quad (2E.26)
 \end{aligned}$$

Therefore, from equation 2E.8

$$R^2 = N\ell^2 \left\{ 1 + \frac{2(\cos \theta - \eta)}{(1 + \eta)(1 - \cos \theta)} \right\} = N\ell^2 \left\{ \frac{(1 + \cos \theta)(1 - \eta)}{(1 - \cos \theta)(1 + \eta)} \right\} \quad (2E.27)$$

η is more usually defined by taking $\phi = 0$ for the trans conformation. In this case, the sign of ϕ is reversed so that equation 2E.27 becomes

$$R^2 = N\ell^2 \left[\frac{(1 + \cos \theta)(1 + \eta)}{(1 - \cos \theta)(1 - \eta)} \right] \quad (2E.28)$$

Appendix 2F. Rotational Isomeric State (RIS) Approximation

2F.1. Introduction

In the rotational isomeric state approximation, a few discrete rotational angles [1,2,3] replace the continuous range of bond rotational angles. Potential energy considerations determine the number and the values of the rotational angles. Potential energy surfaces generated by use of semi-empirical potential functions (Section 2.2) show the potential energy minima for a particular polymer developed for one-dimensional lattices as applied to problems in ferromagnetism (4) are used in the RIS method. The polymer chains can be considered as one-dimensional lattices without loss of rigor. Knowledge of the chain geometry (bond angles and lengths) and the locations and energies of the bond rotational states are required to apply these methods. Bond angles and lengths are available from x-ray diffraction and other techniques mentioned in Chapter 2. The rotational states (number, locations and energies) selected for a given polymer chain are ultimately determined by fitting the results of calculating conformational dependent properties to the experimental data. Thus, the calculated values of r^2 or u^2 and their temperature dependences are compared with experimental measurements.

The rotational state parameters are adjusted until the best agreement with several types of experimental data is obtained. The RIS approximation permits the use of matrix methods based on the following considerations. The conformational partition function (Q_c) (Appendix 2A) is required for averaging over all possible conformations of a polymer chain.

Thus

$$Q_c = \sum_{\phi} \Omega_{\phi} = \prod_{i=2}^{n-1} U_x \eta_{ji} \quad (2F.1)$$

where

$$U_x \eta_{ji} = \exp(-E_x n_{ji} / RT) = \text{the statistical weight of a conformation with } E_{nz}. \quad (2F.2)$$

z refers to the rotational state of bond $i-1$ and n to that of bond i .

Ω_ϕ = the statistical weight of the entire chain.

The partition function is obtained by first forming the product of statistical weights U_n for each chain conformation and then summing over all possible conformations. As written, equation 2F.1 would tax the capacity of high-speed computers for even short chains ($N < 20$ atoms). However, by using the RIS approximation, the evaluation of equation 2.F.1 becomes tractable. Essentially, the sequence of operations described by equation 2.F.1 is reversed (i.e., the conformational statistical weights are first summed and then the sums are multiplied). Present day computers can readily handle this revised sequence.

2F.2. The Conformational Partition Function

The energetics of a polymer chain conformation can be readily specified by its partition function (see Appendix 2A). In the rotational state approximation, the conformational partition function (Q_c) can be expressed as the product of the statistical weights for each bond (U) from 2 to $n-1$ summed over all rotational states. Thus

$$Q_c = \sum_{\text{all states}} [U_2 U_3 \dots U_{n-1}] \quad (2F.3)$$

for an n -bond chain. Alternatively, this sum can be expressed as the product of statistical weight matrices ($|U_i|$) or

$$Q_c = \prod_{i=1}^n |U_i| \quad (2F.4)$$

As an example, the statistical weight matrix for polyethylene with its three-fold rotational states (trans, gauche plus, gauche minus) is

$$|U_i| = \begin{matrix} & \begin{matrix} t & g+ & g- \end{matrix} \\ \begin{matrix} t \\ g+ \\ g- \end{matrix} & \begin{vmatrix} 1 & \sigma & \sigma \\ 1 & \sigma & \sigma\omega \\ 1 & \sigma\omega & \sigma \end{vmatrix} \end{matrix} \quad (2F.5)$$

The potential energy of the trans state has the lowest energy and is assigned a value of one (Section 2B). The statistical weight for the gauche states is

$$\sigma = \exp\left[-(E_t - E_g)/kT\right] \quad (2F.6)$$

$|\mathbf{U}_i|$ refers only to the rotational states of neighboring bonds and the interactions are considered in pair wise fashion. The rows in the $|\mathbf{U}_i|$ matrix denote the $i-1$ bond and the columns, the i^{th} bond.

The statistical weight matrix is raised to the $n-2$ power thereby taking into account all the internal bonds

$$|\mathbf{U}^{n-2}| \quad (2F.7)$$

and the sum of the elements extracted by premultiplying by \mathbf{J}^* and postmultiplying by \mathbf{J}

$$Q_c = \mathbf{J}^T |\mathbf{U}^{n-2}| \mathbf{J} \quad (2F.8)$$

where

$$\mathbf{J}^* = \text{the row specifying the first bond} = \begin{vmatrix} 1 & 0 & 0 \end{vmatrix}$$

$$\mathbf{J} = \text{the column specifying the } n^{\text{th}} \text{ bond} = \begin{vmatrix} 1 \\ 1 \\ 1 \end{vmatrix}$$

Equation 2F.8 is then diagonalized by application of the transformation matrix (A) (Appendix 2.F, equation 2F.1) that transforms the coordinates of bond $i-1$ into those of bond i .

$$\mathbf{A}^{-1} |\mathbf{U}| \mathbf{A} \Rightarrow \quad (2F.9)$$

where

$$\Rightarrow \text{the diagonal matrix} = \begin{vmatrix} \lambda_1 & 0 & 0 \\ 0 & \lambda_2 & 0 \\ 0 & 0 & \lambda_3 \end{vmatrix} \quad (2F.10)$$

with the elements from the secular equation

$$|\mathbf{U}| - \lambda|\mathbf{I}| = 0 \quad (2F.11)$$

where $|\mathbf{I}|$ = the identity matrix
 λ = the eigenvalue

Transposing equation 2F.9

$$|\mathbf{U}| = \mathbf{A} > \mathbf{A}^{-1} \quad (2F.12)$$

and substituting equation 2F.12 into equation 2F.8

$$Q_c = \mathbf{J}^T \mathbf{A} >^{n-2} \mathbf{A}^{-1} \mathbf{J} = \sum_{\text{number of roots}} G_i \ell_i^{n-2} \quad (2F.13)$$

Equation 2F.13 may be approximated for large values of n by

$$Q_c = \lambda_1^{n-2} \quad (2F.14)$$

where λ_1 is the value of the largest eigenvalue.

2E.3. Mean Square Distance

As mentioned previously, R^2 is a common means of specifying chain dimensions. and is calculated from the RIS approximation by the following procedure.

An orthogonal coordinate system is set up for the chain by taking the x -axis as lying along the bond i , the y axis as situated in the plane defined by the bonds $i-1$ and i , and the z_i axis taken at right angles to x_i and y_i to define a right handed system of coordinates (Figure, Appendix 2E.1). As before (Appendix 2D), the coordinates of bond $i-1$ are transformed orthogonally into the coordinates of bond i by the transformation matrix \mathbf{A} .

The total end-to-end vector distance (\mathbf{R}) can be expressed in terms of the bond length vector, \mathbf{l} , by, in vector notation:

$$\mathbf{R} = \sum_{i=1}^n \mathbf{l}_i = \mathbf{l}_1 + \mathbf{l}_2 + \mathbf{l}_3 + \dots + \mathbf{l}_n \quad (2F.15)$$

or, in matrix notation:

$$\mathbf{R} = \sum_{i=1}^n |A_i^{i-1}| \mathbf{l}_i \quad (2F.16)$$

$$= \mathbf{l}_1 + |A_1| \mathbf{l}_2 + |A_2| |A_1| \mathbf{l}_3 + \dots + |A_2| |A_1| \dots A_{n-1} \mathbf{l}_n \quad (2F.17)$$

where \mathbf{l}_j is a column vector or

$$\mathbf{l}_i = \text{col} \begin{vmatrix} \ell & 0 & 0 \\ \ell & 0 & 0 \\ 0 & 0 & 0 \end{vmatrix} = \ell \begin{vmatrix} 1 \\ 0 \\ 0 \end{vmatrix} \quad (2F.18)$$

The mean square distance, in matrix notation, is

$$R^2 = \mathbf{R}^T \mathbf{R} = \sum_j \sum_i \ell_i^T \ell_j \quad (2F.19)$$

where \mathbf{R}^T is the transpose of \mathbf{R}

$$R^T = \sum_{i=1}^n \ell_i^T |A_i^{i-1}|^T \quad (2F.20)$$

and \mathbf{l}_i^T is the transpose or row form of \mathbf{l}_i ,

$$\mathbf{l}_i^T = |l_i \ 0 \ 0| = l_i |1 \ 0 \ 0| \quad (2F.21)$$

Assuming no interaction between the rotational angles on adjacent bonds, and after separation of diagonal terms, equation 2F.19 can be written as

$$R^2 = \sum l_i + \sum_{i < j} l_i^T |A_i| |A_{i+1}| \dots A_{j-i} l_j \quad (2F.22)$$

or

$$\frac{R^2}{nl^2} = 1 + \frac{2}{nl^2} \sum_{i < j} l^T |A|^{j-i} l \quad (2F.23)$$

References

1. M Volkenstein, Configurational Statistics of Polymer Chains;

TOPICS in POLYMER PHYSICS

(translated from the Russian ed. S.N. Timasheff and M.J. Timasheff), Interscience: New York, **1963**

2. K. Nagai, J. Chem. Phys. **1959**, 31, 1169

3. P.J. Flory,

Statistical Mechanics of Chain Molecules; Interscience: New York, **1969**

4. H.A. Kramers, G.H. Wannier, Phys. Rev. **1941**, 60, 252

5. P.J. Flory, Macromolecules. **1974**, 7, 381

Appendix 2G. Random Walk of Gaussian Chains

$P(R)$ equation 2.79 is proportional to the probability that there are x more segments in the positive direction than in the negative direction. This probability is identical with the probability of having x more heads (H) than tails (T) in S coin tosses (1)

For $S = 1$

$$P(H) = \frac{1}{2} \qquad P(T) = \frac{1}{2} \qquad (2G.1)$$

For $S = 2$

$$\begin{aligned} P(HH) &= \frac{1}{2} \cdot \frac{1}{2} = \frac{1}{4} \\ P(HT) &= 2 \cdot \frac{1}{2} \cdot \frac{1}{2} = \frac{1}{2} \\ P(TT) &= \frac{1}{2} \cdot \frac{1}{2} = \frac{1}{4} \qquad \text{etc.} \end{aligned} \qquad (2H.2)$$

Inspection of 2H.1 and 2H.2 demonstrates that the sum of the probabilities for a given number of tosses equals one.

The probabilities for any number of tosses can be computed from

$$P\binom{x}{s} = C_x^s \left(\frac{1}{2}\right)^s \qquad (2G.3)$$

where C_x^s is the number of ways of obtaining x more heads than tails.

An analytic expression for C_x^s can be derived from the following considerations. The number of ways of arranging n objects in n locations is just n factorial. For example, given a men and b women, the total equals n people. No distinction is made as to individuals, thus

$$\frac{n!}{a!b!} = \text{the number of permutations} \qquad (2G.4)$$

Returning to coin tossing, assume that x represents the number of times heads came up than did tails

$$\text{for } x = 0, \text{ the number of heads} = a = \frac{s}{2}$$

$$\text{for } x = x, \text{ the number of heads} = a = \frac{s+x}{2} \quad (2G.5)$$

$$\text{for } x = x, \text{ the number of tails} = b = \frac{s-x}{2} \quad (2G.6)$$

The symbols s and x are related as can be shown by rearranging equations 2G.5 and 2G.6

$$a+b = \left(\frac{s+x}{2}\right) + \left(\frac{s-x}{2}\right) \quad (2G.7)$$

$$a-b = \left(\frac{s+x}{2}\right) - \left(\frac{s-x}{2}\right)$$

therefore, by analogy, the number of ways of obtaining a heads and b tails in s coin tosses is

$$= \frac{S!}{a!b!} \quad (2G.8)$$

or, substituting equations 2G.5 and 2G.6 into equation 2G.8

$$C_x^s = \frac{S!}{\left(\frac{s+x}{2}\right)! \left(\frac{s-x}{2}\right)!} \quad (2G.9)$$

or, referring to equation 2G.3

$$P\binom{s}{x} = \frac{S!}{\left(\frac{s+x}{2}\right)! \left(\frac{s-x}{2}\right)!} \left(\frac{1}{2}\right)^s \quad (2G.10)$$

For any significant number of coin tosses, the use of factorials becomes cumbersome. Stirling [1,2] in the eighteenth century discovered an approximation that greatly simplifies the mathematical computation. Stirling's approximation substitutes logarithms for factorials, thus

$$\ln N! = N \ln N - N \quad N > 10 \quad (2G.11)$$

The approximation improves with increasing values of N . (For $N < 10$, short chains, calculation using factorials gives better results). Taking the logarithms of both sides of equation 2G.10

$$\ln P\binom{s}{x} = \ln S! - S + S \ln \frac{1}{2} - \ln\left(\frac{s+x}{2}\right)! - \left(\frac{s-x}{2}\right)! \quad (2G.12)$$

and applying Sterling's approximation

$$\begin{aligned} \ln P\binom{s}{x} = S \ln S - S + S \ln \frac{1}{2} - \left(\frac{s+x}{2}\right) \ln\left(\frac{s+x}{2}\right) + \left(\frac{s+x}{2}\right) \\ - \left(\frac{s-x}{2}\right) \ln\left(\frac{s-x}{2}\right) + \left(\frac{s-x}{2}\right) \end{aligned} \quad (2G.13)$$

On rearranging terms, the semi final result is:

$$\ln P\binom{s}{x} = \left(\frac{s+x}{2}\right) \ln\left(1 + \frac{x}{s}\right) - \left(\frac{s-x}{2}\right) \ln\left(1 - \frac{x}{s}\right) \quad (2G.14)$$

To obtain the final result, a second approximation is used. This is based on the Taylor power series

$$\ln(1+u) = u - \frac{1}{2}u^2 + \dots \quad (2G.15)$$

$$\ln(1-u) = -u - \frac{1}{2}u^2 + \dots \quad (2G.16)$$

Substituting equations 2G.15 and 2G.16 into equation 2G.14

$$\begin{aligned} \ln P\binom{s}{x} = \left(\frac{s+x}{2}\right) \left[\left(\frac{x}{s}\right) - \frac{1}{2}\left(\frac{x}{2}\right)^2 \right] \\ - \left(\frac{s-x}{2}\right) \left[\left(-\frac{x}{s}\right) - \frac{1}{2}\left(\frac{x}{2}\right)^2 \right] \end{aligned} \quad (2G.17)$$

Rearranging terms and canceling yields.

$$\ln P\binom{s}{x} = \frac{x^2}{2S} \quad (2G.18)$$

$$P\binom{s}{x} = \exp\left(-\frac{x^2}{2S}\right) \quad (2G.19)$$

This equation states that, in S occurrences, the probability that there will be x number of deviations is proportional to an exponential function.

Based on the assumptions used in this derivation, the greater the number of trials or occurrences, the better the probability calculated from equation 2G.19 will agree with experimental data.

Equation 2G.19 is the basis for the Gaussian distribution. Its application to the random walk problem illustrates its usefulness. Setting

$$P\left(\frac{s}{x}\right) = \exp\left(-\frac{x^2}{2S}\right) \quad (2G.20)$$

where $R = XL =$ end to end distance

$$X = \frac{R}{L}$$

$L =$ segment length

and $C =$ a constant of proportionality

Replacing X by R/L as indicated by the Random Walk model

$$P(R) = C \exp\left(\frac{-R^2}{2SL^2}\right) \quad (2G.21)$$

To evaluate C , $P(R)$ is integrated over the limits $-\infty$ to $+\infty$,

$$\int_{-\infty}^{\infty} P(R) dR = 1 = C \int_{-\infty}^{\infty} \exp\left(\frac{-R^2}{2SL^2}\right) dR \quad (2G.22)$$

and equation 2E.22 is simplified by letting

$$y = R \quad a = \sqrt{\frac{1}{2SL^2}}$$

Then substituting

$$\begin{aligned} C \int_{-\infty}^{\infty} \exp\left[\frac{R^2}{2SL^2}\right] dR &= C \int_{-\infty}^{\infty} \exp[-a^2 y^2] dy \\ &= \frac{\sqrt{\pi}}{a} = \frac{1}{C} \end{aligned} \quad (2G.23)$$

Rearranging equation 2G.23

$$1 = \frac{C\sqrt{\pi}}{\sqrt{\frac{1}{2SL^2}}}$$

or

$$C = \frac{1}{\sqrt{2SL^2\pi}} \quad (2G.24)$$

Substituting equation 2G.24 into equation 2G.21

$$P(R) = \frac{1}{\sqrt{2SL^2\pi}} \exp\left[-\frac{R^2}{2SL^2}\right] \quad (2G.25)$$

This is a Gaussian distribution and can be plotted as shown in Figure 2.13. As the number of segments increase, the probability value of R will tend to lie within a narrow size range.

References

1. S. Goldberg, *Probability, An Introduction*; Dover: New York, 1986
2. Sterling, J. *Methods differentials*. 1730.
3. Wells, D., *The Penguin Dictionary of Curious and Interesting Numbers*. Middlesex, England: Penguin Books, p. 45, 1986.

Appendix 2H. Radius of Gyration, Size and Shape

Real objects like polymer molecules often have ill-defined shapes which may change with time and conditions. A problem is one of describing them in terms of a parameter that may be determined experimentally.

We have calculated the scattering from an object of known shape like a sphere for which measurements of the angular dependence of intensity permits a determination of its radius. Similar calculations are possible for other shapes like rods or ellipsoids leading to measures of their size. For a polymer coil, the shape and size is not fixed, so a statistical description is necessary. In addition, chain branching will affect the shape and size of the polymer coil.

A problem is that it is not possible to determine both size and shape separately, so scattering will reveal parameters that depend on some combination of these. A parameter that can be determined is the average radius of gyration, $\langle r_g^2 \rangle$. This section will deal with a description of this quantity, its calculation for a few shapes, and a discussion of how the radius of gyration may be determined from light scattering.

Definition of $\langle r_g^2 \rangle$

Consider an array of points of mass $m_1, m_2, m_3, \dots, m_i, \dots$ located at vector distances $\mathbf{r}_1, \mathbf{r}_2, \mathbf{r}_3, \dots, \mathbf{r}_i, \dots$ from some arbitrary

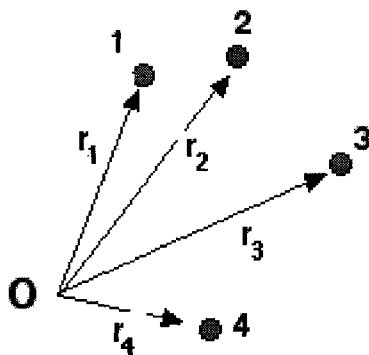


Figure 2H.1. Diagram illustrating the terms used in deriving the radius of gyration.

The origin is then shifted so that it is located at the center of gravity of the distribution defined by

$$\sum m_i r_i = 0 \quad (2H.1)$$

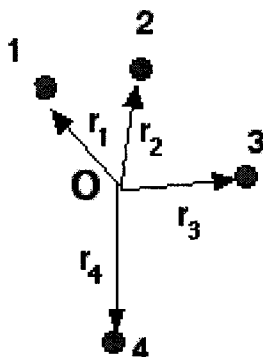


Figure 2H.2. – The arbitrary origin superposed on the center of gravity.

Then, if the r 's are measured from this point,

$$\langle r_g^2 \rangle = \sum m_i r_i^2 / \sum m_i \quad (2H.2)$$

$\langle r_q^2 \rangle$ for a Rigid Rod

Consider a narrow rigid rod of length, L and cross-sectional area, A . It may be divided into segments of length, ΔL (Figure 2H.3). The origin should obviously be taken as the center of the rod. Then, $m_i = \rho A \Delta r$ which will be the same for all segments (where ρ is the density of the rod).

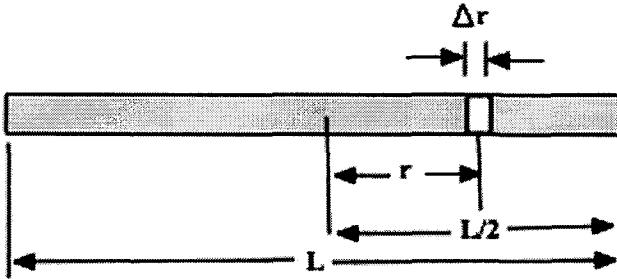


Figure 2H.3. Diagram showing the terms used in deriving the radius of gyration for a rigid rod.

Then
$$\langle r_g^2 \rangle = \frac{\sum r_i^2 \Delta r}{\sum \Delta r} \tag{2H.3}$$

On replacing the sums in equation 2I.3 by integrals, this becomes

$$\langle r_g^2 \rangle = \frac{\int r^2 dr}{\int dr} \tag{2H.4}$$

The limits of integration for equation 2I.4 are from 0 to $L/2$

This becomes

$$\langle r_g^2 \rangle = \left[\frac{r^3}{3} \right] / [r] = \left(\frac{L^3}{24} \right) / (L/2) = L^2/12 \tag{2H.5}$$

$\langle r_q^2 \rangle$ for a Sphere of Radius R

For this, the elements at distances between r_i and $r_i + \Delta r$ will be in the volume of a shell of thickness, Δr and area $A = 4\pi r_i^2$, so $m_{ii} = 4\pi r_i^2 \rho \Delta r$ (Figure 4H.4). The origin should obviously be the center of the sphere.

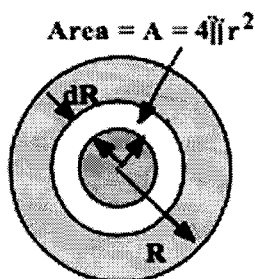


Figure 2H.4. Diagram showing the terms used in deriving the radius of gyration for a sphere.

Thus

$$\langle r_g^2 \rangle = \frac{\sum r_i^4 \Delta r}{\sum r_i^2 \Delta r} \quad (2H.6)$$

Again, replacing the sums in equation 2I.6 by integrals,

$$\langle r_g^2 \rangle = \frac{\int r^4 dr}{\int r^2 dr} = \left[\frac{r^5/5}{r^3/3} \right] \quad (2H.7)$$

where the limits of integration are now from 0 to R. Thus

$$\langle r_g^2 \rangle = \left(\frac{R^5/5}{R^3/3} \right) = \left(\frac{3}{5} \right) R^2 \quad (2H.8)$$

Determination of $\langle r_q^2 \rangle$ from Scattering

The Debye-Bueche theory (Section 4.9) gives

$$I(q) = K \int \gamma(r) \left(\frac{\sin qr}{qr} \right) r^2 dr \quad (2H.9)$$

$\sin x$ may be expressed as a power series

$$\sin x = x - \frac{x^3}{3!} + \frac{x^5}{5!} - \dots \quad (2H.10)$$

Thus

$$I(q) = k \left[\int \gamma(r) r^2 dr - q^2 \int \gamma(r) r^4 dr + q^4 \int \gamma(r) r^6 dr + \dots \right] \quad (2H.11)$$

Now,
$$I(0) = \int \gamma(r) r^2 dr \quad (2H.12)$$

On dividing equation 2H.11 by equation 2H.12

$$\begin{aligned} I(q)/I(0) = & 1 - (q^2/3!) \left[\int \gamma(r) r^4 dr / \int \gamma(r) r^2 dr \right] \\ & + (q^4/6!) \left[\int \gamma(r) r^6 dr / \int \gamma(r) r^2 dr \right] - \dots \end{aligned} \quad (2H.13)$$

For a dilute solution of particles, it may be shown that

$$\gamma(r) = p_{12}(r) \quad (2H.14)$$

where $\gamma(r)$ is the correlation function and $p_{12}(r)$ is the probability that two volume elements separated by distance, r , will both lie within the particle. Using this, the second term in the expansion may be related to $\langle r_q^2 \rangle$. It may be shown that

$$\left[\int p_{12} r^4 dr / \int p_{12} r^2 dr \right] = 2 \langle r_g^2 \rangle \quad (2H.15)$$

Thus, $I(q)$ becomes

$$I(q)/I(0) = 1 - \left[\langle r_g^2 \rangle / 3 \right] q^2 + \dots \quad (2H.16)$$

so $\langle r_q^2 \rangle$ may be determined from the initial slope of a plot of $I(q)/I(0)$ against q^2 .

The low q part of the plot should be linear, but there will be deviations at higher q 's because of the contribution of higher terms of the expansion. This initial slope only depends on $\langle r_g^2 \rangle$ and is independent of shape, so one cannot decide on shape from the value of the initial slope alone. The deviations at higher q are shape dependent, but their resolution into shape and size contributions is difficult, especially if there is a distribution of sizes.

It is important that measurements be made at small enough q so that one can be sure that there are only contributions from the second term

varying as q . For large objects, this may require either going to very small angles or using longer wavelengths of radiation.

One might note that if one uses the equation for the intensity of scattering from a sphere obtained previously (equation 4.55) by summing amplitudes, thus

$$I(U) = K^2 [\sin U - U \cos U]^2 \tag{2H.17}$$

where $U = qR$, and one expands both $\sin U$ and $\cos U$ in series, the coefficient of the q^2 term gives the same value of the radius of gyration of $R^2/6$.

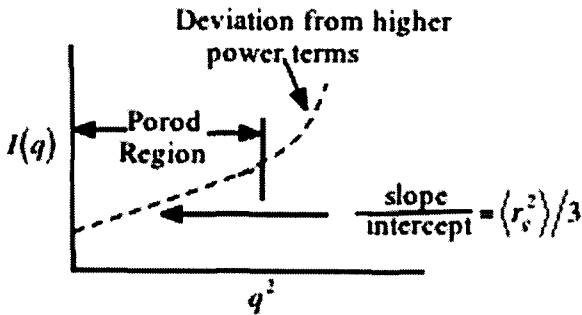


Figure 2H.5. A plot of $K(q)$ versus q^2 used in deriving a value for $\langle r_q^2 \rangle$

A test of whether one has gone to small enough angles is to see whether one is in the "Porod region" by examining the product of $\langle r_q \rangle q$. For a valid measurement, this should be less than one.

While shape cannot be easily established from scattering alone, determining the dependence on molecular weight can be useful. If the molecule was a rod, its length, L , should be proportional to the molecular weight, M , so $\langle r_q^2 \rangle$ should vary as M^2 . However, it may be shown that for random coils, $\langle r_q^2 \rangle = K M$, Thus, if one establishes n in the equation,

$$\langle r_g^2 \rangle = K' M^n \tag{2H.18}$$

from a plot of $\ln \langle r_q^2 \rangle$ against M obtained by measuring $\langle r_q^2 \rangle$ for samples of differing M . For rods, $n = 2$ and for random coils, $n = 1$. A measurement for cellulose acetate, for example, revealed an intermediate

value, indicating that this was a "stiff coil" or a "flexible rod" (for which theories exist.)

Chapter 3

THERMODYNAMICS

3.1. Introduction

Thermodynamics, both classical [Appendix 3.A] and statistical [Appendix 2A], have been applied to many topics in polymer science. The results have provided insights into the origin of rubber elasticity, the nature of polymer crystalline, polymeric heat capacities and the miscibility of polyblends.

This chapter develops the fundamental thermodynamics underlying these and other topics. The equations thus developed provide a theoretical framework for organizing material presented in subsequent chapters.

3.2 Thermodynamics of Elasticity

Equations describing rubber elasticity can be derived in a straightforward fashion from classical thermodynamics based on free energy considerations. Free energy in turn can be related to experimentally accessible quantities as shown in the derivation below.

At constant pressure and temperature, the Gibbs free energy (G) [Appendix 3.A] can be expressed as

$$dG = -dW_e - VdP - SdT \quad (3.1)$$

where $-dW_e$ represents all types of work, other than pressure-volume work, done by the system, P is the pressure, V is the volume, S is the entropy and T is the temperature. The basic equations leading to equation 3.1 are given in Appendix 3A.

The elastic work ($-dW_e$) involved in stretching a one-dimensional chain a distance (dl) on applying a force (f) is

$$dW_e = -fdl \quad (3.2)$$

If the length increases by (dl), the system has work done on it. Conversely, if the length decreases, the system does work. Assuming no other type of work, then

$$dG = \overline{fdl} + VdP - SdT \quad (3.3)$$

Differentiating equation 3.3 with respect to length yields

$$\left(\frac{\partial G}{\partial l}\right)_{P,T} = f \quad (3.4)$$

and with respect to temperature

$$\left(\frac{\partial G}{\partial T}\right)_{l,P} = -S \quad (3.5)$$

Thus, differentiating equation 3.3 with respect to length and using the definition of the state function, G

$$G = H - TS$$

where H = the heat content or enthalpy, an equation for the elastic force at constant temperature and pressure can be obtained

$$f = \left(\frac{\partial G}{\partial l}\right)_{P,T} = \left(\frac{\partial H}{\partial l}\right)_{P,T} - T\left(\frac{\partial S}{\partial l}\right)_{P,T} \quad (3.6)$$

and from the equation

$$G = E - PV - TS$$

where E represents the internal energy

$$f = \left(\frac{\partial E}{\partial l}\right)_{P,T} = \left(\frac{\partial V}{\partial l}\right)_{P,T} - T\left(\frac{\partial S}{\partial l}\right)_{P,T} \quad (3.7)$$

If no change in volume is associated with a length change, the middle term on the right hand side of equation 3.7 equals zero or

$$f = \left(\frac{\partial E}{\partial l}\right)_{P,T} - T\left(\frac{\partial S}{\partial l}\right)_{P,T} \quad (3.8)$$

Equation 3.8 states that the total force on a material may be separated into a force (f_e) related to the internal energy and a force (f_s) associated with entropy effects, or

$$f = f_e + f_s \quad (3.9)$$

Both intermolecular and intramolecular forces contribute to f_e . The intermolecular forces for covalently bonded materials include a) bond bending and stretching, b) forced internal rotation to higher energy conformations and c) pulling chain molecules apart (or pulling them together) against intermolecular forces such as hydrogen bonds or van der Waals forces. On the other hand, f_s arises from intramolecular forces. The entropic force chiefly relates to the decrease in conformational entropy with stretching.

An equation analogous to equation 3.8, but for constant volume and temperature conditions, can be derived from the Helmholtz free energy (A) or

$$f = \left(\frac{\partial E}{\partial l} \right)_{v,T} - T \left(\frac{\partial S}{\partial l} \right)_{v,T} \quad (3.10)$$

The internal energy terms in equations 3.8 and 3.10 are usually not equal, that is

$$\left(\frac{\partial E}{\partial l} \right)_{p,T} \neq T \left(\frac{\partial E}{\partial l} \right)_{v,T} \quad (3.11)$$

This inequality can be shown by an expansion of $(\partial E/\partial l)_{T,P}$ or

$$\left(\frac{\partial E}{\partial l} \right)_{p,T} = T \left(\frac{\partial E}{\partial l} \right)_{v,T} + \left(\frac{\partial E}{\partial V} \right)_{l,T} \left(\frac{\partial V}{\partial l} \right)_{p,T} \quad (3.12)$$

The $(\partial V/\partial l)_{T,P}$ term is usually small for rubbers and is often neglected. But, the term can make a significant contribution to $(\partial E/\partial l)_{T,P}$ because it represents the dilation or volume increase in sample dimensions associated with the decrease in internal pressure on stretching. These arguments also hold for the entropy terms in equations 3.8 and 3.10.

To separate the contributions of the internal energy from the entropy due to the elastic force, the derivatives must be taken at constant volume and temperature. Most force measurements are carried out at constant temperature and pressure because of experimental simplicity. The data are then corrected to constant temperature and volume conditions by one of several approaches [1,2]. For this reason, equation 3.10 will be used in the following discussion.

The two contributions to the elastic force may be experimentally distinguished by the following means: From the Helmholtz free energy analogy to equation 3.4

$$\left(\frac{\partial f}{\partial T}\right)_{v,l} = \left[\frac{\partial}{\partial T}\left(\frac{\partial A}{\partial l}\right)_{v,T}\right]_{v,l} \quad (3.13)$$

Similarly, from equation 3.5

$$-\left(\frac{\partial f}{\partial l}\right)_{v,T} = \left[\frac{\partial}{\partial l}\left(\frac{\partial A}{\partial T}\right)_{v,l}\right]_{v,T} \quad (3.14)$$

Since equations 3.12 and 3.13 differ only in the order of differentiation, they must be equal. This gives the Maxwell-type equation (see Appendix 3A)

$$-\left(\frac{\partial f}{\partial T}\right)_{v,l} = \left(\frac{\partial S}{\partial l}\right)_{v,T}$$

On substituting this equation into equation 3.9, one obtains

$$f = \left(\frac{\partial E}{\partial l}\right)_{v,T} + T\left(\frac{\partial f}{\partial T}\right)_{v,l} \quad (3.15)$$

or, rearranging terms

$$f_e = \left(\frac{\partial E}{\partial l}\right)_{v,T} = f - T\left(\frac{\partial f}{\partial T}\right)_{v,l} \quad (3.16)$$

Thus, from a measurement of the variation of force with temperature, one may determine $(\partial E/\partial l)_{v,T}$ – the internal energy contribution. Again, it should be noted, that because most force-temperature measurements are

THERMODYNAMICS

carried out under constant pressure conditions, corrections are applied to convert the experimental data to constant volume conditions. For rubbers at temperatures above their T_g , one finds experimentally that, to a good approximation,

$$f = KT \tag{3.17}$$

Table 3.1. Thermoelastic Data of Selected Elastomers a.)

(Reference temperature: 30 °C)

Polymer	$\frac{d \ln G_0}{dT} \times 10^3$	Ref.
Poly(ethylene-co-propylene)(EPR)	f_e/f 0.04	a.
Poly(tetrafluoroethylene-co-perfluoropropylene) (Viton A)	0.05	a.
Poly(butadiene-co-styrene) (SBR)	-0.12	a.
Poly(butadiene-co- acrylonitrile) (Hycar)	0.03	a.
Poly(cis-1,4-butadiene) (Budene)	0.10	a.
Poly(cis-isoprene) (natural rubber)	0.18	b.
Poly(2-hydroxypropyl acrylate)	0.53*	c.
Poly(isobutylacrylate)	0.42*	c.
Poly(isobutylmethacrylate)	0.02*	c.

*Reference temperature: 120 °C

a.) E.H. Cirlin, H.M. Gebhard, and M. Shen, *J. Macromol. Sci., Part A* (1971)

b.) M. Shen, *Macromolecules* **1969**, 2, 358

c.) M. Shen, E.H. Cirlin, and H.M. Gebhard, *Macromolecules* **1969**, 2, 682

Thus

$$\left(\frac{\partial f}{\partial T} \right)_{V,l} = K \tag{3.18}$$

and, from equation 3.16

$$f_c = \left(\frac{\partial E}{\partial l} \right)_{V,l} = KT - T(K) = 0 \tag{3.19}$$

An ideal rubber, analogous to an ideal gas for which $(\partial E/\partial V)_T = 0$, has only entropic forces on stretching. The ratio of f_e/f commonly measures the internal energy contribution to the elastic force [3] [also see below]. Real rubbers deviate from ideality as shown for example by the f_e/f data on several rubbers in Table 3.1. Mark [4] has compiled extensive data on f_e/f values obtained under various experimental conditions. These f_e/f data show that internal energy forces usually constitute 5 to 20% of the total elastic force at room temperature. These data also show that the internal energy arises from intramolecular forces. If a chain has a sufficiently large number of segments (x) so as to permit the application of thermodynamics to a single chain, then the force on such a one-dimensional chain behaving as an ideal rubber is

$$f_x = -T \left(\frac{\partial S_x}{\partial \mathbf{R}_x} \right)_{V,T} \quad (3.20)$$

where S_x is the conformational entropy of a chain and \mathbf{R}_x is the vector distance between chain ends. The force of chain contraction in an ideal rubber can be shown to originate in the Brownian motion of its segments (Figure 3.1) just as the pressure in an ideal gas originates from the kinetic movement of the gas molecules. In addition, as with an ideal gas in which the molecular free path changes but the kinetic energy is conserved, the kinetic energy does not change on stretching an ideal rubber only the direction of the force changes. For an unextended chain (Figure 3.1), the end (E) will experience tugs in all directions because of the random motion (like holding a snake by its two ends). If now the application of a force (F) stretches the molecule, Brownian motion will tend to pull the chain in a direction to bring the ends closer together (Figure 3.1) and restore the chain to its more probable (or more coiled) conformation. This is the molecular origin of the entropic elastic restoring force on an ideal rubber.

The conformational entropy of a chain in molecular terms may be calculated from statistical thermodynamics using Boltzmann's equation

$$S_x = k \ln P \quad (3.21)$$

If we now substitute from equation 2.79 for the probability of an end-to-end length of a one-dimensional chain,

$$S_x = k \ln \left(\exp \left[\frac{-R_x^2}{2ZL^2} \right] \right) = \frac{-R_x^2}{2ZL^2} \quad (3.22)$$

and, then from equation 3.20

$$f_x = -T \left(\frac{\partial S_x}{\partial R_x} \right)_{v,T} = \left(\frac{kT}{ZL^2} \right) R_x \quad (3.23)$$

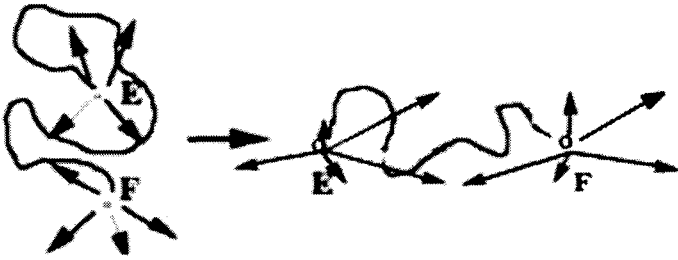


Figure 3.1. Brownian motion of chain segment illustrating effect of extension on average segment dimension.

Thus, the restoring force is proportional to the extension and the one-dimensional chain behaves as a Hookean spring. This important result simplifies the analysis of the normal modes of motion of a polymer. Polymer chain models can be treated mathematically by the much simpler linear differential equations because second order effects are absent. (It should be noted that, while the elastic equation for a polymer chain is identical in form with Hooke's law, the molecular origin of the restoring force is very different).

Equation 3.23 must clearly be valid only at small values of R_x since, when the extended dimensions of the chain approaches R_∞ , the force must increase with R_x , at a greater than linear rate (Figure 3.2). This difference is clearly the result of using the Gaussian approximation for $P(R_x)$. As expected, use of the more accurate distribution function

derived for the non-Gaussian chain (equation 2.123) gives better agreement,

$$P(R_x) = C \exp - N \left[\frac{R}{NL} \beta + \ln \left(\frac{\beta}{\sinh \beta} \right) \right] \quad (3.24)$$

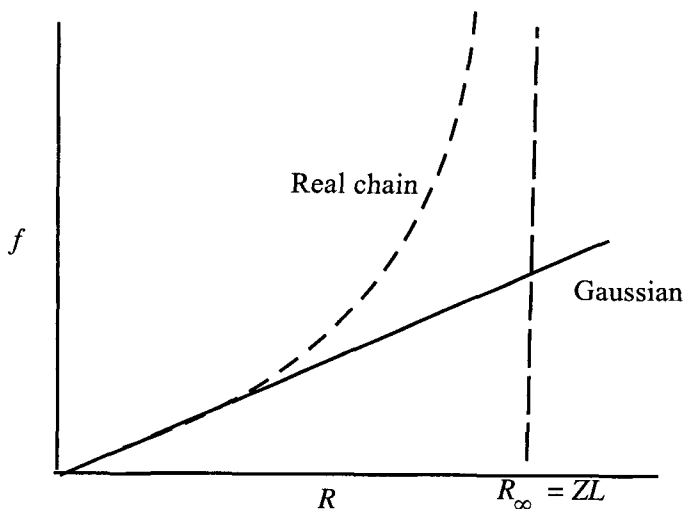


Figure 3.2 Sketch of force against end-to-end distance, R_x , showing the non-linear increase.

substituting into equation 3.21

$$S_x = k \ln C - kN \left[\frac{R}{NL} \beta + \ln \left(\frac{\beta}{\sinh \beta} \right) \right] \quad (3.25)$$

and using equation 3.20 for the case of an ideal rubber (equation 3.39)

$$\begin{aligned}
 f_x &= -T \left(\frac{\partial S_x}{\partial R_x} \right) = kTN \left\{ \frac{\beta}{NL} + \frac{R}{NL} \left(\frac{\partial \beta}{\partial R} \right) + \frac{\sinh \beta}{\beta} \left(\frac{\sinh \beta (\partial \beta / \partial R) - \beta \cosh \beta (\partial \beta / \partial R)}{(\sinh \beta)^2} \right) \right\} \\
 &= kTN \left\{ \frac{\beta}{NL} + \frac{R}{NL} \left(\frac{\partial \beta}{\partial R} \right) + \left[\left(\frac{1}{\beta} \right) - \coth \beta \right] \left(\frac{\partial \beta}{\partial R} \right) \right\} = \left(\frac{kT}{L} \right) \beta = \left(\frac{kT}{L} \right) \mathcal{L}^{-1} \left(\frac{R}{NL} \right)
 \end{aligned}
 \tag{3.26}$$

where $\left[\left(\frac{1}{\beta} \right) - \coth \beta \right] = - \left(\frac{R}{NL} \right)$

If one expands the inverse Langevin function (equation 2.124) in a series

$$\mathcal{L}^{-1}(x) = 3x + \frac{9}{5}x^2 + \frac{297}{175}x^3 + \dots
 \tag{3.27}$$

Then, equation 3.26 becomes

$$f = \left(\frac{3kT}{NL^2} \right) \left[1 + \left(\frac{3}{5} \right) \left(\frac{R}{NL} \right)^2 + \left(\frac{99}{175} \right) \left(\frac{R}{NL} \right)^4 + \dots \right]
 \tag{3.28}$$

Thus, at low elongations, equation 3.28 obeys Hooke's law, but curves upward at higher R values (Figure 3.2). When $R = NL$, the series in equation 3.28 diverges, and f becomes infinite as would be expected for a completely extended chain. In real chains, the breaking force does not reach infinity but breaks at some lower value due to bond breaking.

3.3. Force on a Chain in the Presence of Energy Contributions to Elasticity

Equation 3.26 assumes the ideal rubber case, in which all the force is entropic in origin. Guth and James [5] showed that this result is more general, however, using a method analogous to that used by Debye for describing the orientation of a dipole in an electrical field. Thus, if a segment is oriented at an angle θ to the displacement vector (\mathbf{R}) and a force (f) is applied parallel to \mathbf{R} (Figure 3.3), the component of the force perpendicular to L applied in such a direction as to rotate the segment is

$$f_{\perp} = f \sin \theta
 \tag{3.29}$$

The work of rotation is then

$$dW = f_{\perp} ds = f_{\perp} L d\theta = fL \sin \theta d\theta \quad (3.30)$$

The potential energy, $V(\theta)$, of a segment oriented at an angle θ is then the work of rotation, or

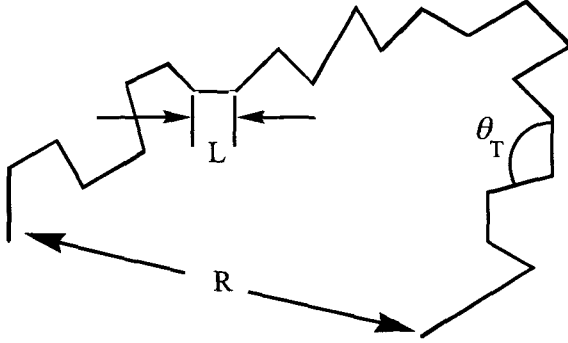


Figure 3.3. Sketch showing the relation of L , θ_T and R for a model chain.

$$\begin{aligned} V(\theta) &= - \int dW = - \int_{\pi/2}^{\theta} fL [\sin \theta d\theta] \\ &= -fL [-\cos \theta]_{\pi/2}^{\theta} = fL \cos \theta \end{aligned} \quad (3.31)$$

The probability $W(\theta)$ of a segment having an orientation angle θ is given by

$$W(\theta) = C e^{(-V(\theta)/kT)} = C e^{(-a \cos \theta)} \quad (3.32)$$

where

$$a = fL/kT \quad (3.33)$$

Thus, the average value of $\cos \theta$ (equation 3.31) is

$$\langle \cos \theta \rangle = \frac{\int_0^{\pi} \cos \theta W(\theta) dW}{\int W(\theta) dW} \quad (3.34)$$

Using this equation, the mean extension of a chain is (Figure 3.3)

$$\langle R \rangle = nL \langle \cos \theta \rangle = \frac{NL \int_0^\pi \cos \theta \exp[-a \cos \theta] \sin \theta d\theta}{\int_0^\pi \exp[-a \cos \theta] \sin \theta d\theta}$$

and, from equations 2.117 through 2.119

$$\langle R \rangle = nL \mathcal{L}(a) NL \mathcal{L}\left(\frac{fL}{kT}\right) \tag{3.35}$$

On taking the inverse of the Langevin function

$$\left(\frac{fL}{kT}\right) = \mathcal{L}^{-1}\left(\frac{\langle R \rangle}{ZL}\right) \tag{3.36}$$

or rearranging terms

$$f = \left(\frac{kT}{L}\right) \mathcal{L}^{-1}\left(\frac{\langle R \rangle}{ZL}\right) \tag{3.37}$$

This is identical with equation 3.26 if $\langle R \rangle = R$. [However, Flory, Hove and Ciferri [6] have pointed out that the inversion process between equation 3.35 and 3.36 is valid only at large n values. For $n < 10$, the error is large.] The entropic origin of force was not assumed in the derivation of equation 3.37 so that this result is generally valid and not restricted to ideal rubbers. The energy contribution to rubber elasticity may be calculated from equation 3.16

$$\left(\frac{\partial E}{\partial l}\right)_{v,T} = f - T \left(\frac{\partial f}{\partial T}\right)_{v,l}$$

and using the expression for f in equation 3.37, for the non-Gaussian case

$$\begin{aligned}
 \left(\frac{\partial E}{\partial R}\right)_{v,T} &= \frac{kT}{L} \mathcal{L}^{-1}\left(\frac{R}{NL}\right) - \frac{kT}{L} \frac{\partial}{\partial T} \left[T \mathcal{L}^{-1} \frac{kT}{L} \right] \\
 &= \frac{kT}{L} \mathcal{L}^{-1}\left(\frac{R}{NL}\right) - \frac{kT}{L} \mathcal{L}^{-1}\left(\frac{R}{NL}\right) - \frac{kT^2}{L} \frac{\partial \mathcal{L}^{-1}\left(\frac{R}{NL}\right)}{\partial T} \\
 &= \frac{kT^2}{L} \frac{\partial \mathcal{L}^{-1}\left(\frac{R}{NL}\right)}{\partial T}
 \end{aligned} \tag{3.38}$$

and for the Gaussian approximation (equation 3.23, modified for three dimensions, hence the factor 3 in the numerator)

$$\begin{aligned}
 \left(\frac{\partial E}{\partial R}\right)_{v,T} &= \frac{3kT}{\langle R^2 \rangle} - T \frac{\partial}{\partial T} \left[T \left(\frac{3kTR}{\langle R^2 \rangle} \right) \right] \\
 &= \frac{3kT}{\langle R^2 \rangle} R - \frac{3kT}{\langle R^2 \rangle} R - 3kTR \left(\frac{\partial [1/\langle R^2 \rangle]}{\partial T} \right) = \frac{3kT^2 R}{\langle R^2 \rangle^2} \left(\frac{\partial \ln R^2}{\partial T} \right)
 \end{aligned} \tag{3.39}$$

If $\langle R^2 \rangle$ is independent of T , then $(\partial E/\partial R)_{v,T} = 0$, and the chain behaves as an ideal rubber.

Based on the above consideration, the term

$$f_e \equiv \left(\frac{\partial E}{\partial R}\right)_{v,T} \tag{3.40}$$

defines the energy contribution to elastic force. Thus, the ratio (from equation 3.39)

$$\left(\frac{f_e}{f}\right) = \frac{\left(\frac{3kTR}{\langle R^2 \rangle}\right) \left(\frac{\partial \ln \langle R^2 \rangle}{\partial T}\right)}{\left(\frac{3kTR}{\langle R^2 \rangle}\right)} = T \left(\frac{\partial \ln \langle R^2 \rangle}{\partial T}\right) \tag{3.41}$$

can be used to calculate the temperature dependence of R^2 . The value of the $\langle R^2 \rangle$ dependence on temperature determined from force-temperature data may be compared with that obtained from solution measurements of R^2 [see Chapter 2.10].

Values of f_e/f can be estimated from extension to the rotational isomeric state model. We have seen, for example, for an atactic chain with a symmetrical energy barrier (Figure 2.5) that (equation 2.50)

$$\langle R^2 \rangle = Nl^2 \left[\frac{1 + \cos \theta}{1 - \cos \theta} \right] \left[\frac{1 + \eta}{1 - \eta} \right] \quad (3.42)$$

where $\eta = \langle \cos \theta \rangle$ and is temperature dependent. In the rotational isomeric approximation, equation 2.59 or

$$\eta = \frac{(\cos 0^\circ) \exp(-V_t/RT) + 2(\cos 120^\circ) \exp(-V_g/RT)}{\exp(-V_t/RT) + 2 \exp(-V_g/RT)} \quad (3.43)$$

where V_t and V_g are the potential energies of the trans and gauche conformations, respectively, then if

$$W = \exp(-\varepsilon/RT) \quad (3.44)$$

where

$$\varepsilon = V_g - V_t \quad (3.45)$$

On substituting the expression for W in equation 3.43, one obtains

$$\eta = \frac{(1 - W)}{(1 + 2W)} \quad (3.46)$$

Then substituting this expression for η into equation 3.42

$$\langle R^2 \rangle = ZL^2 \frac{(1 + \cos \theta)(2 + W)}{(1 - \cos \theta)(3W)} \quad (3.47)$$

After taking logarithms, differentiating with respect to T and using equation 3.41, the equation

$$\frac{f_e}{f} = \frac{-2}{2 + \exp(-\varepsilon/kT)} = \frac{\varepsilon}{RT} \quad (3.48)$$

is obtained.

This equation states that, for an atactic chain with a symmetrical energy barrier, the energy contribution to the total force would originate from transforming a mixture of gauche and trans chain conformers to mainly all gauche conformers – the higher energy state. This was one of the mechanisms proposed at the beginning of this discussion. Both the temperature dependence of retractive force and the swelling data yield the same value of f_e/f . This observation shows that the chain interactions are intermolecular and not intramolecular in origin.

3.4. Solution Thermodynamics

3.4.1. Flory-Huggins Theory

Although this book addresses itself primarily to various topics on solid polymers, some material on dissolved polymers is included in order to comprehend concepts and results that are common to both areas. Thus, the end-to-end vector distance is determined from solution techniques. The concept of theta conditions is better understood from knowledge of solution theory. In addition, as will be shown below, the effect of chain ends and irregularities on polymer crystallinity is similar to the effect of liquid diluents. More recently, the solution concepts of a liquid used for calculating the entropy of mixing and free energy of mixing have been extended to the compatibility of solid polyblends.

To be considered ideal, a low molecular weight liquid must meet three criteria:

- a) the liquid is indifferent to the solvent,
- b) mixing of molecules must be random, and
- c) the molecules of solute and of solvent are of equal size.

Based on these assumptions, the additivity rule for the entropy of mixing can be derived in a few steps.

The free energy of mixing is

$$G_m = H_m - TS_m$$

at constant temperature (T),

$$\Delta G_m = \Delta H_m - T\Delta S_m \quad (3.49)$$

THERMODYNAMICS

since, for an ideal liquid (condition b), $\Delta H_m = 0$. The entropy of mixing may be derived from the Boltzmann equation (Appendix 2A)

$$\Delta S_m = k \ln P \quad (3.50)$$

and, the probability (P) or number of ways of placing N_1 solvent and N_2 solute molecules into a total of N spaces is given by (assuming molecules of equal size)

$$P = C \frac{N!}{N_1! N_2!} \quad (3.51)$$

Taking logarithms

$$\ln P = \ln C + \ln N! - \ln N_1! - \ln N_2! \quad (3.52)$$

and using Stirling's approximation (equation 2.101) to remove factorials

$$\ln P = \ln C + N \ln N - N - N_1 \ln N_1 + N_1 - N_2 \ln N_2 + N_2$$

Since,

$$\Delta S = k \ln P$$

then, from equation 3.52

$$\Delta S_m = -R [n_1 \ln x_1 + n_2 \ln x_{21}] \quad (3.53)$$

where $x_1 =$ mole fraction solvent

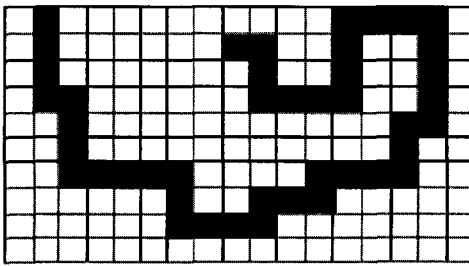


Figure 3.4. Lattice schematic (■ polymer segment).

$$n_1 = \frac{N_1}{N_2}$$

and $R =$ the gas constant

Thus, for low molecular weight solutions, the entropy of mixing is proportional to mole fractions. Deviations from ideality could arise from molecules not being of equal size, from a finite value of ΔH or from a combination of both.

Polymer solutions deviate strongly [7] from ideal behavior. This is not surprising considering the large disparity in size between a polymer molecule and a monomeric solvent molecule. A lattice treatment developed independently by Huggins [8] and by Flory [9] can be used to handle this type of problem. The artificial lattice serves as a device for enumerating the possible combinations of polymer segments and solvent molecules. The polymer segments do not necessarily have the dimensions of a repeat unit because they are arbitrarily constrained to have the same size as the solvent molecule. For the calculation, polymer chains comprising x -segments are added successfully only to a lattice with sites or cells of a size that can fit only one segment.

For the lattice model, Figure 3.4,

let

N_1 = number of solvent molecules = number of solvent cells

N_2 = number of solute molecules

xN_2 = number of solute segments = number of solute cells

$$x = \frac{\text{volume of polymer molecule}}{\text{volume of solvent molecule}} \quad (3.54)$$

The total number of lattice cells is N

$$N = N_1 + xN_2 \quad (3.55)$$

Then the total probability (P) for all polymer molecules is

$$P = [P_1 P_2 P_3 \dots P_{N_2}] \frac{N_1!}{N_1! N_2!} \quad (3.56)$$

where P_1 is the number of ways of putting the first molecule in the lattice, P_2 is the number of ways of putting in the second molecule, etc. P_1 may be calculated by the following procedure. For the first segment of the first molecule, there are N possible locations. For the next segment of this molecule, there are z locations, where z is the coordination

number of the lattice. There are $(z-1)$ possible locations for each succeeding segment.

$$P_1 = N[zp_1][(z-1)p_2][(z-1)p_3] \dots [(z-1)p_{x-1}] \quad (3.57)$$

The p 's are the probabilities that the available cell is already occupied after $(x-1)$ segments have been added. The assumption of the Flory-Huggins theory is that this probability is just the average probability throughout the lattice and is just equal to the fraction of the cells that are still empty.

$$P_1 = \frac{(N-1)}{N} \quad (3.58)$$

$$P_2 = \frac{(N-2)}{N} \quad (3.59)$$

$$P_3 = \frac{(N-3)}{N} \quad (3.60)$$

etc.

This assumption is probably the weakest part of the theory especially at low concentrations, where the local concentration near a polymer molecule is higher than the average concentration.

Restrictions imposed by a lattice moreover can lead to errors in the calculation. The lattice model assumes that segments of the polymer chain occupy successive cells in the lattice. This may not allow for configurations of chains where cells adjacent to filled cells may be occupied by portions of molecules such as side groups [10].

The Flory-Huggins calculation assumes that a segment may enter any unoccupied cell adjacent to itself with equal probability. This assumption does not accommodate chain stiffness, for example, where cells causing chain bending might be assigned different probability than those that do not.

The model also assumes random placement of segments where the probability being placed in a given cell is not dependent upon whether neighboring cells are occupied by solvent molecules or polymer segments. If there are specific interactions, this would not be so.

Now if, for the purpose of simplifying the notation, y is set equal to $(z-1)$

$$y = (z - 1) \quad (3.61)$$

and one neglects the difference between the z in the first term of equation 3.57 and the $(z-1)$ factors, equation 3.57 becomes

$$P_1 = \left(\frac{y}{N}\right)^{x-1} [N(N-1)(N-2)(N-3)\dots(N-x+1)] \quad (3.62)$$

3.4.2. Calculation of P_2

For the first segment of the second molecule, there are $(N-x)$ possible locations. Thus

$$\begin{aligned} P_2 &= [[N-x] [z p_{2x+1}] [(z-1) p_{x+2}] [(z-1) p_{x+3}] \dots [(z-1) p_{2x-1}]] \\ &= \left(\frac{y}{N}\right)^{x-1} [(N-x)(N-2x-1)(N-2x-2)(N-2x-3)\dots(N-2x+1)] \end{aligned} \quad (3.63)$$

Similarly,

$$\begin{aligned} P_3 &= [N-2x] [z p_{2x+1}] [(z-1) p_{2x+2}] [(z-1) p_{2x+3}] \dots [(z-1) p_{2x-1}] \\ &= \left(\frac{y}{N}\right)^{x-1} [(N-2x)(N-2x-1)(N-2x-2)(N-2x-3)\dots(N-3x-1)] \end{aligned} \quad (3.64)$$

Upon substituting these expressions for P_1 , P_2 , P_3 , etc. into equation 3.57, one obtains

$$P = \left(\frac{y}{N}\right)^{x-1} [(N)(N-1)(N-2)(N-3)\dots(N+1)] \frac{N_1!}{N_1! N_2!} = \left(\frac{y}{N}\right)^{N_2(n-1)} \frac{N_1!}{N_1! N_2!} \quad (3.65)$$

When $x = 1$

$$P = \left(\frac{N!}{N_1! N_2!}\right)^{x-1} \quad (3.66)$$

which is the ideal solution result, equation 3.51. Taking logarithms on both sides of equation 3.66, and using Stirling's approximation,

$$\ln P = \left[(x-1)N_2 \right] \ln y - \left[(x-1)N_2 \right] \ln [N_1 + xN_2] + N_1 + xN_2 \ln [N_1 + xN_2] - \left[N_1 + xN_2 \right] - N_1 \ln N_1 + N_1 - N_2 \ln N_2 + N_2$$

rearranging

$$= [N_1 + N_2] \ln [N_1 + xN_2] - N_1 \ln N_1 - N_2 \ln N_2 + [(x-1)N_2] \ln y - (x-1)N_2 \quad (3.67)$$

Substituting equation 3.67 into equation 3.52, the conformational entropy of the solution is

$$S_{12} = k \ln P = k \left\{ [N_1 + N_2] \ln [N_1 + xN_2] - N_1 \ln N_1 - N_2 \ln N_2 + [(x-1)N_2] \ln y - (x-1)N_2 \right\} \quad (3.68)$$

The entropy of mixing is

$$\Delta S_m = S_{12} - S_1 - S_2 \quad (3.69)$$

S_1 may be obtained from S_{12} by setting $N_2 = 0$ to give

$$\Delta S_1 = k \{ N_1 \ln N_1 - N_1 \ln N_1 \} = 0 \quad (3.70)$$

Similarly, if $N_1 = 0$, S_{12} gives S_2 which is

$$\Delta S_2 = k \{ N_2 \ln [xN_2] - N_2 \ln N_2 + [(x-1)N_2] \ln y - (x-1)N_2 \} = 0 \quad (3.71)$$

Thus on substituting equations 3.68, 3.70, and 3.71 into equation 3.69, one obtains

$$\begin{aligned} \Delta S_m &= k \left\{ [N_1 + N_2] \ln [N_1 + xN_2] - N_1 \ln N_1 - N_2 \ln [xN_2] \right\} \\ &= -k \left\{ N_1 \ln \left[\frac{N_1}{N_1 + xN_2} \right] + N_2 \ln \left[\frac{xN_2}{N_1 + xN_2} \right] \right\} \\ &= -k \{ N_1 \ln \phi_1 + N_2 \ln \phi_2 \} \end{aligned} \quad (3.72)$$

where

$$\phi_1 = \frac{N_1}{N_1 + xN_2} = \text{the volume fraction of solvent}$$

$$\phi_2 = \frac{xN_2}{N_1 + xN_2} = \text{the volume fraction of polymer}$$

Equation 3.72 has the same form as equation 3.53. It should be noted that the lattice parameter y is absent in equation 3.72. The equations differ in that equation 3.72 is additive in volume fractions while equation 3.53 for monomeric liquids is additive in mole fractions.

The derivation of equation 3.72 assumes no interaction between polymers. Although the use of a three dimensional lattice to represent a polymer solution is admittedly artificial (particularly regarding the assumption that polymer segments and solvent molecules have the same dimensions), equation 3.72 has proven useful in correlating many experimental results. A major drawback, as mentioned previously, is the assumption that the polymer molecules are randomly distributed on the lattice. This assumption becomes untenable in dilute solutions in which polymer molecules exist as isolated islands surrounded by a sea of solvent. Flory [11], Flory and Krigbaum [12] and Ishihara and Guth [13] have derived expressions for the dilute solution case.

Another assumption is that there are no vacancies or holes in the lattice, i.e., that the change in volume on mixing is zero. Sanchez and Lacombe [14, 15]) have extended lattice calculations to include holes and thereby allowed for the condition that $\Delta V_m \neq 0$.

3.3.3. Entropy of Mixing

The Flory-Huggins treatment can be extended to the calculation of an interaction parameter (χ_1) used in many theories dealing with polymer miscibility. The concept of a theta (or Flory) condition is a major consequence. As mentioned in Chapter 2 in the discussion on chain dimensions, the use of the theta condition removes the complication of long chain interaction in assessing chain conformations.

The expression for the entropy of mixing as derived from the Flory-Huggins treatment is applied in deriving an equation relating the free energy of mixing to the interaction parameter χ_1 . The latter can be

evaluated by any of several techniques, but particularly by osmotic pressure measurements.

The partial molal entropy of mixing $(\Delta S_m)_1$ is defined as

$$\langle (\Delta S_m) \rangle_1 \equiv \left(\frac{\partial \Delta S_m}{\partial n_1} \right)_{n_1, P, T} \quad (3.73)$$

Substituting from equation 3.72

$$\begin{aligned} \langle (\Delta S_m) \rangle_1 &= -R \left[\frac{\partial}{\partial n_1} [n_1 \ln \phi_1 + n_2 \ln \phi_2] \right]_{n_1} \\ &= -R \left[\ln \phi_1 + n_1 \left(\frac{\ln \phi_1}{\partial n_1} \right)_{n_1} + n_2 \left(\frac{\ln \phi_2}{\partial n_2} \right)_{n_1} \right] \end{aligned} \quad (3.74)$$

The partial differentials in equations 3.73 to 3.74 are solved as follows

$$\begin{aligned} \left(\frac{\partial \ln \phi_1}{\partial n_1} \right)_{n_1} &= \frac{1}{\phi_1} \left(\frac{\partial \phi_1}{\partial n_1} \right)_{n_1} = \frac{1}{\phi_1} \frac{\partial \left(\frac{n_1}{n_1 + xn_2} \right)}{\partial n_1} = \frac{1}{\phi_1} \left[\frac{(n_1 + xn_2) - n_1}{(n_1 + xn_2)^2} \right] \\ &= \left[\frac{(n_1 + xn_2)}{n_1} \right] \left[\frac{-xn_2}{(n_1 + xn_2)^2} \right] = \frac{-xn_2}{n_1(n_1 + xn_2)} \end{aligned} \quad (3.75)$$

Similarly,

$$\begin{aligned} \left(\frac{\partial \ln \phi_2}{\partial n_1} \right)_{n_1} &= \frac{1}{\phi_2} \left(\frac{\partial \phi_2}{\partial n_1} \right)_{n_1} = \frac{1}{\phi_2} \left(\frac{\partial \left[\frac{xn_1}{n_1 + xn_2} \right]}{\partial n_1} \right)_{M_1} = \frac{1}{\phi_2} \left[-\frac{xn_2}{(n_1 + xn_2)^2} \right] \\ &= \left[\frac{(n_1 + xn_2)}{xn_2} \right] \left[\frac{-xn_2}{(n_1 + xn_2)^2} \right] = -\frac{1}{n_1 + xn_2} \end{aligned} \quad (3.76)$$

Substituting equations 3.75 and 3.76 into equation 3.74

$$\begin{aligned} \langle\langle \Delta S_m \rangle\rangle_1 &= -R \left[\ln \phi_1 + n_1 \left(\frac{x n_1}{n_1 + x n_2} \right) + n_2 \left(\frac{1}{n_1 + x n_2} \right) \right] \\ &= -R \left[\ln \phi_1 + (x-1) \left(\frac{1}{n_1 + x n_2} \right) \right] \end{aligned} \quad (3.77)$$

Then since,

$$\begin{aligned} \frac{x n_2}{n_1 + x n_2} &= \frac{\phi_2}{x} \\ \langle\langle \Delta S_m \rangle\rangle_1 &= -R \left[\ln \phi_1 + \frac{x-1}{x} \phi_2 \right] \end{aligned} \quad (3.78)$$

The expression for $\langle\langle \Delta H_m \rangle\rangle_1$ derived in Appendix 3B is given by

$$\langle\langle \Delta H_m \rangle\rangle_1 = \left(\frac{\partial \Delta H_m}{\partial n_1} \right) = RT \chi_1 \phi_2^2 \quad (3.79)$$

where χ_1 = the polymer/solvent interaction parameter

Since

$$\langle\langle \Delta G_m \rangle\rangle_1 = \langle\langle \Delta H_m \rangle\rangle_1 - T \langle\langle \Delta S_m \rangle\rangle_1$$

Substituting from equations 3.78 and 3.79 yields

$$\langle\langle \Delta G_m \rangle\rangle_1 = \mu_1 - \mu_1^0 = RT \left[\chi_1 \phi_2^2 + \ln \phi_1 + \frac{x-1}{x} \phi_2 \right] \quad (3.80)$$

where (see Appendix 3C)

$$\mu_1^0 = \left(\frac{\partial G}{\partial n_1} \right)^0 = \text{the chemical potential of the solvent in pure solvent}$$

$$\mu_1 = \left(\frac{\partial G}{\partial n_1} \right) = \text{the chemical potential of the solvent in solution}$$

Several experimental techniques have been used to determine values of the polymer/solvent interaction parameter, see for example Scott and Hildebrand [16] or Orwell [17] who describe these techniques in extensive reviews.

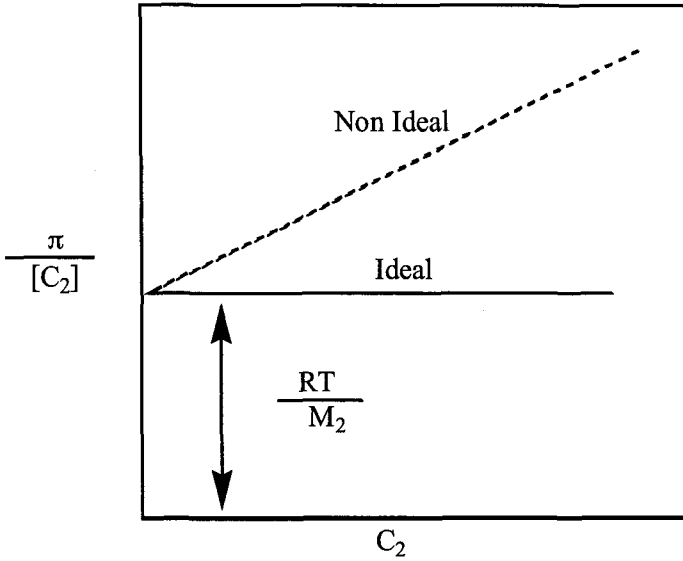


Figure 3.5. Idealized plot of osmotic pressure against solute concentration.

Osmotic pressure (π) given by equation 3.81 is a common techniques used to measure χ_1

$$\pi = RT \left[\frac{C_2}{M_2} + A_2 C_2^2 + \dots \right] \tag{3.81}$$

(This equation is derived in Appendix 3C)

where

$$A_2 = \frac{(\frac{1}{2} - \chi_1)}{\rho_2^2 V_1} = \text{the second virial coefficient}$$

The slope of the plot in Figure 3.5

$$\text{slope} = \frac{RT(\frac{1}{2} - \chi_1)}{\rho_2^2 V_1} \tag{3.82}$$

where V_1 is the molal volume and ρ_2 the solution density yields a value of χ_1 .

Table 3.2 Miscible Polymer Blends

Compatibility Polymers	Criteria	Ref.
1. Polystyrene/Poly(2,6 dimethyl phenylene oxide)	a	1
2. Polystyrene/Poly(vinyl methyl ether)	b	2
3. Polyvinylidene fluoride/Poly(methyl methacrylate)	c	3
4. Polyvinylidene fluoride/Poly(ethyl methacrylate)	c*	3
5. Polyvinyl chloride/random polyester copolymer (tetramethylene ether glycol terephthalate/ tetramethylate terephthalate)	c**	4
3. Polyvinyl chloride/Poly(ethyl methacrylate)	d	5
7. Polyvinyl chloride/Poly-ε-caprolactam	e	6
8. Polyisoprene/Polybutadiene	f	7
9. Polybutylene terephthalate/polycaprolactone		8

* Composition limits

** Temperature limits

Miscibility Criteriaa. Single glass temperature, T_g , observed from DSC measurement

b. Transparent film formed when cast from a selected solvent

c. Single T_g observed for dynamic mechanical measurement

d. Compatible at 30% solids

e. Single T_g f. Single T_g during linear thermal expansion

The value of the slope in Figure 3.5 tracks solution miscibility because of the $(\frac{1}{2} - \chi_1)$ term. This term may be generalized (1) to two parameters $\psi(1 - \theta/T)$ where ψ = an enthalpy term to show the relation between χ_1 and θ . If $(\frac{1}{2} - \chi_1) = 0$ or $\theta = T$, the polymer/solvent combination forms a pseudo ideal or “ θ ” solution in which there is no net interaction. For $\chi_1 < \frac{1}{2}$, the polymer/solvent pair is immiscible and a two phase system results. Polymers are inherently less miscible in solvent liquids than are monomeric substances. Because of their chain structure and the consequent connectivity between chain segments, the possible permutations of segments in liquid mixtures are severely restricted and therefore their entropy of mixing is low. Therefore, even a small positive enthalpy on mixing suffices to render the free energy of mixing positive

and the polymer/solvent combination incompatible. Solubility tends to decrease with increasing polymer molecular weight as would be expected based on the entropy considerations just discussed.

3.5. Polymer Miscibility

The concepts derived from polymer solutions have been extended to considerations of polymer/polymer miscibility Scott [18] discussed the case of two homopolymers dissolved in a common solvent forming an equilibrium mixture and derived expressions for the free energy of mixing, using the Flory-Huggins theory

$$\Delta G_1 = RT \left[\ln \phi_1 + \left(1 - \frac{x_1}{x_2} \right) \phi_2 + x_1 \chi_1 \phi_2^2 \right] \quad (3.83a)$$

$$\Delta G_2 = RT \left[\ln \phi_2 + \left(1 - \frac{x_1}{x_2} \right) \phi_2 + x_1 \chi_1 \phi_2^2 \right] \quad (3.83b)$$

where

$$x_1 = \frac{V_1}{V_2} = \text{degree of polymerization}$$

V_1 = molal volume of polymer 1

V_2 = molal volume of polymer 2

V_0 = molal volume of an idealized polymer molecule

These equations are analogous to equation 3.80, but with the stipulation that the requirement for the existence of a θ condition for a polymer/polymer mixture (a value of χ_1 equal to $1/2$) applies only to the case of infinite molecular weight. The critical value of χ_1 for the theta condition will be somewhat less than $1/2$ for polymers of moderate molecular weights. Also, the compatibility of a polymer/polymer mixture increases as the molecular weights of the individual polymer decreases.

Scott's conclusion that only a few polymer mixtures are miscible agreed with the experimental data then available on ternary systems comprising two polymers in a common solvent [19]. More recent work on newer polymers has revealed several miscible systems (Table 3.2). Criteria for miscibility of a polymer/polymer mixture include optical

transparency, the existence of a single glass temperature for the polymer mixture and shifts in the dynamical mechanical spectra.

The subject of polymer miscibility has received fresh impetus from the development of polyblends, graft and block copolymers and thermoplastic elastomers. In these systems, immiscible polymer chains or blocks covalently bond. Because they are immiscible, the two polymer blocks separate into two microscopic domains or regions in which only one polymer is present, but the presence of covalent bonds prevents complete separation into two microscopic phases. The polystyrene/polyethylene oxide system studied by Benoit was an early example of the effect of the interaction between polymer miscibility and copolymer bonding [20]. Varying the block or graft length, the composition and location of the blocks in the chain can produce different morphologies [21,22]. The limiting cases of morphology are the sphere, the cylinder and the lamella (Figure 3.6).

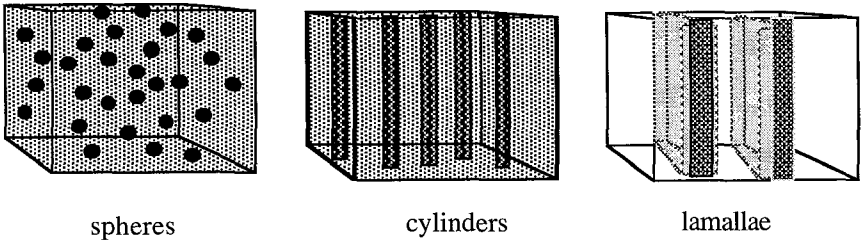


Figure 3.6 Morphology of some polyblends.

Meier [23] has derived equations relating block copolymer morphology to thermodynamics using lattice models. His model explains quantitatively the observations of Merrett [24] on the influence of preferential solvents on the mechanical properties of graft copolymers. Merrett found that, depending on the solvent used in casting films of a natural rubber/poly(methyl methacrylate) graft copolymer, he could obtain either a hard stiff film characteristic of poly(methyl methacrylate) or a soft, flexible film typical of natural rubber. He interpreted these results as follows: a solvent for poly(methyl methacrylate) collapsed the

rubber blocks into discrete domains. On drying, the poly(methyl methacrylate) became the continuous phase interspersed with rubber domains and the film would be hard and stiff. A solvent for natural rubber reversed this order and the dried film would be soft and flexible because the rubber blocks now constituted the continuous phase.

Krause [25] and Helfand [26] have given theories, based on lattice models, for estimating block copolymer miscibilities including the type of interface developed between the microphases in these systems. Coleman, et al. [27] have assessed the validity of solubility parameters in estimating the miscibility of polymer pairs.

3.6. Spinodal Decomposition

Phase separation usually occurs by the mechanism of nucleation and growth. Another mechanism for phase separation, spinodal decomposition, is more common for blends. Blends of miscible polymers are materials in which the phase separation by nucleation and growth is so slow that phase separation spinodal decomposition can occur. Polymer blends and liquid crystals are therefore good candidates for observing spinodal decomposition because the chain structures slow the transition rate. The basis for an experimental approach is shown in Figure 3.7. The upper section in this figure shows a one-phase region. The concave solid line depicts the boundary between the one phase and the two-phase regions for the transition occurring by a binodal (nucleation and growth) mechanism. The dashed line represents the boundary between a binodal transition and a spinodal decomposition transition. The region enclosed by the dashed line constitutes a region in which phase transition by spinodal decomposition is the stable form. The two boundary lines coincide at only one point, T_s .

Figure 3.7 shows an Upper Critical Solution Temperature (UCST) as is predicted by Flory-Huggins theory. This theory as presented cannot predict the Lower Critical Solution Temperature (LCST) sometimes observed. A LCST curve can only be predicted if one has temperature variation of c different from that described in the theory developed here.

The point, T_s , corresponds to the condition that the second derivative of the free energy with respect to composition equals zero. If a point in

the one phase region, say at A, with a composition given by AB could be suddenly cooled to the temperature at B, then the phase transition would occur by spinodal decomposition alone. Experimentally, this is exactly what is done and the technique is called “temperature jump”.

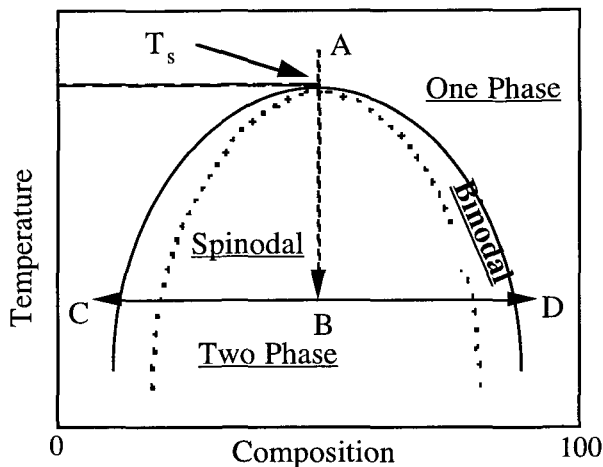


Figure 3.7 Phase diagram showing the spinodal region.

Light scattering (or neutron scattering) measurements can be used to determine the spinodal point using the following procedure. For a constant temperature, the intensity of scattering is measured simultaneously over a range of angles using a special detector. The measurements are repeated for different times. The data are then rearranged to form a plot of scattering against reduced angle at constant time for a series of temperatures (Figure 3.8). The plots are then extrapolated to zero scattering angle, the slope is just the apparent diffusion constant, see equation 3.12. A plot of D_{app} against temperature extrapolated to zero D_{app} (Figure 3.10) yields the spinodal temperature (T_s). Physically, the spinodal temperature represents a state in which the activation energy for spinodal decomposition is zero while that nucleation and growth is precluded because it has an activation energy.

Spinodal decomposition can be divided into three stages depending on the mathematical equations used to describe them and on the degree

of coarsening observed in the developing structure. The Cahn-Hilliard-Cook equation [28] is used to describe the first stage.

$$q_n \propto t^0$$

$$I(q,t) = I(q,t=0)\exp[2R(q)t] \tag{3.84}$$

where $I(q,t)$ = the scattering intensity at time t and scattering angle q

$R(q)$ = the growth rate at angle q

$$q = \frac{\sin \theta}{2} = \text{the reduced scattering angle}$$

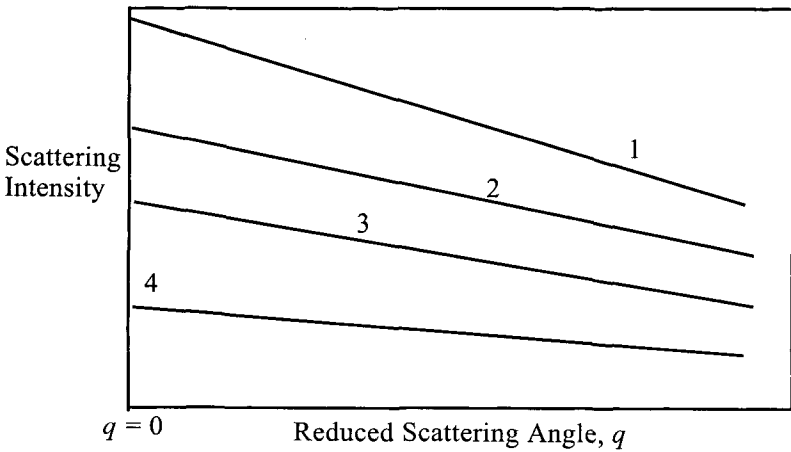


Figure 3.8. Diagram showing series of curves used in extrapolation to determine the limiting scattering angle.

or rearranging by taking logarithms on both sides

$$\log I(q) = 2R(q)t$$

In the first stage, the angle of the scattering maximum remains the same, but the height of the maximum increases.

Then, for a second intermediate stage at longer time, the maximum moves towards smaller angles. This second stage is fit by the relation,

$$R(q) = D_{app} q^2 \left(1 - \frac{q^2}{2q_m^2} \right) \quad (3.85)$$

or, rearranging terms and extrapolating to zero angle.

$$\left. \frac{R(q)}{q^2} \right|_{q=0} = D_{app}$$

so that a plot of $R(q)/q^2$ versus q^2 yields a straight line that can be fit by the straight-line relation, $y = mx+b$ for which the slope is the apparent diffusion, D_{app} (Figure 3.9). A plot of the slope values at several temperatures against temperature extrapolated to the temperature value at zero apparent diffusion yields the spinodal temperature (T_s), as shown in Figure 3.10.

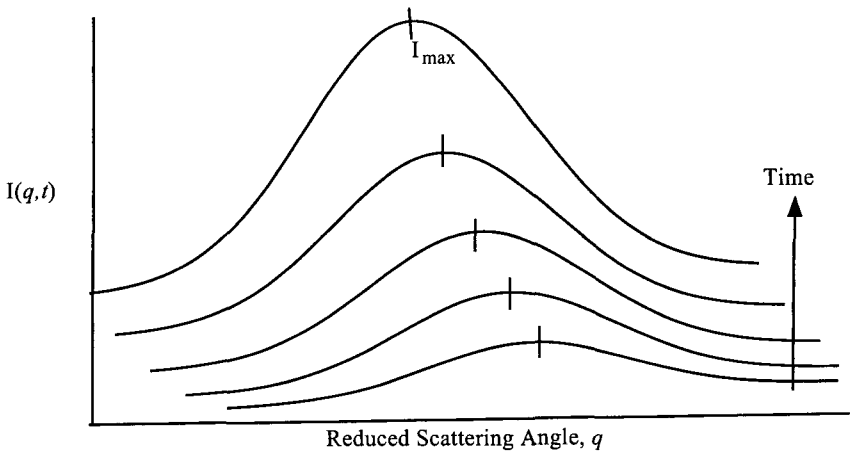


Figure 3.9. Plots showing the increase in scattering intensity with increasing time.

The maximum in the first stage reflects a fluctuation in composition that travels rapidly and forms a web-like structure. The second stage arises from the growth in size of the new phase. In a third stage, the growth of phases is controlled by viscous flow. At the end of the phase separation processes, it is difficult to tell whether they occurred by nucleation and growth or by spinodal decomposition. One must observe

them at earlier stages to tell which process was followed during phase separation.

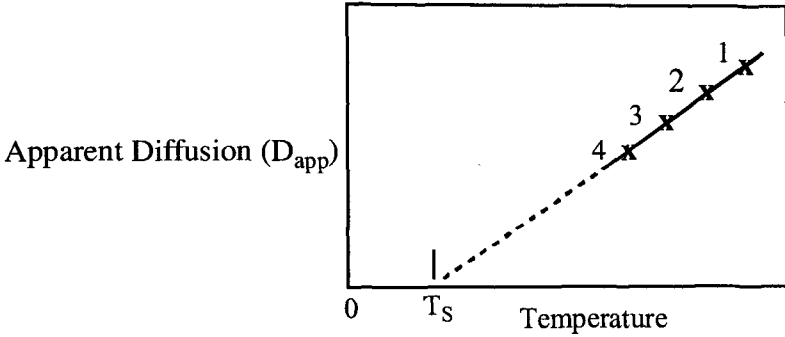


Figure 3.10. Plot showing extrapolation to obtain the spinodal temperature.

In the initial stage, an empirical curve is used to approximate the scattering changes with angle that continually increase with time

$$q_m \propto t^{-\alpha} \quad (3.86)$$

For the intermediate stage, the empirical curve can be approximated by

$$I_m = t^\beta \quad (3.87)$$

In many cases, β is greater than 3 times the value of α

$$\beta > 3\alpha$$

But, for the special case of $\beta = 3\alpha$, the intensity is given by

$$I(q) \cong \langle \eta^2 \rangle S(q) \quad (3.88)$$

where $S(q)$ = the scattering intensity corrected for electronic density,

Since $S(q)$ can be approximated by,

$$S(q) \cong q_n^{-3}$$

therefore

$$I(q) \approx \langle \eta^2 \rangle S(q) \approx \langle \eta^2 \rangle q_n^{-3} \quad (3.89)$$

The quench depth, ε , or

$$\varepsilon = \frac{T - T_s}{T_s} = \frac{\chi - \chi_s}{\chi_s} = \text{quench depth} \quad (3.90)$$

is a measure of the thermodynamic driving force [29,30].

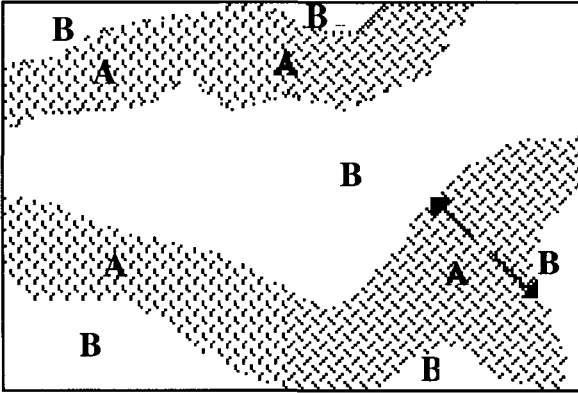


Figure 3.11. Diagram showing spinodal phase (A) superimposed on a binal phase (B) during decomposition.

A third stage is usually observed in which the spinodal structure coarsens (Figure 3.11). This process can be described by an exponential dependence of the maximum intensity and the maximum reduced scattering angle on time, viz.

$$D_{app} = D_c \varepsilon \quad (3.91)$$

where D_c = the diffusion constant for coarsening.

$$\chi_s = \frac{1}{2} \left(\frac{1}{N_{wA} \phi_A} + \frac{1}{N_{wB} \phi_B} \right) \approx \frac{1}{N_{wA}} \quad (3.92)$$

determines the composition of the final spinodal phases, similar to the tie lines found in distillation. A, B are the phases as stated above, N is the weight average and ϕ is the weight fraction. Over time, the two phases change composition along the tie lines and finally achieve the compositions at C and D (Figure 3.7).

3.7. Heat Capacity

Heat capacity (C) is defined by the relation

$$C = \frac{dQ}{dT} \quad (3.93)$$

where dQ = the amount of heat transferred in or out of a system.

dT = the temperature change accompanying the transfer process.

This quantity is more conveniently measured at constant pressure

$$C_p = \left(\frac{\partial H}{\partial T} \right)_p \quad (3.94)$$

where H = the enthalpy, than at constant volume

$$C_v = \left(\frac{dE}{dT} \right)_v \quad (3.95)$$

where E = the internal energy. The two quantities are related by

$$C_v = C_p = T\bar{V} \frac{\alpha^2}{\beta} \quad (3.96)$$

where \bar{V} = the specific volume

$$\alpha = \text{the coefficient of the (cubic) thermal expansion} = \left(\frac{1}{V} \right) \left(\frac{dV}{dT} \right)_p$$

$$\beta = \text{the (isothermal) compressibility} = - \left(\frac{1}{V} \right) \left(\frac{dV}{dP} \right)_T$$

Heat capacity is a quantity used in many areas of polymer studies. It is applied for example in determining the absolute value of entropy (see below), by use of the relation

$$S = S_0 + \int_0^T \frac{C_p}{T} dT \quad (3.97)$$

where S_0 = the value of the entropy at absolute zero, as calculated from third law considerations.

3.8. Thermodynamics of Crystallization

Crystalline polymers never are completely composed of a single crystalline phase. An amorphous or liquid like phase coexists with the crystalline phase. The degree of crystalline and the morphology associated with this two-phase system are covered elsewhere in this book (Chapter 8). The crystalline phase in polymers meets the thermodynamic requirements for a crystal including the existence of a first order transition or melting temperature (T_m). Above this temperature, the polymer chains possess a random, liquid like order. On cooling to a temperature range, which varies for different polymers, below T_m , the chains spontaneously form regions with ordered arrays interspersed by less ordered or amorphous regions. The question of whether semi-crystalline polymers possessed melting points that fit the criterion for reversible first order transitions has engendered much controversy. Early experiments using, for example, specific volume against temperature measurements showed that crystalline polymers melted over a range of temperature. This contrasted with the very narrow melting temperature range found with pure low molecular weight substances such as benzoic acid. In addition, polymers on cooling below the melting point crystallized 10-50°C below T_m suggesting a lack of reversibility. Subsequent measurements such as those of Chiang and Flory [29] and of Mandelkern et al. [30] have met these objections and demonstrated that semi-crystalline polymers undergo a first order transition on melting.

The chain structure of polymers however modifies the manifestations of crystallinity. Strictly speaking, a thermodynamic phase should have properties independent of its size. This is not so for polymer crystals that are small and surface properties that can be very important. Also, because of chain irregularities and non-equilibrium growth conditions, polymer crystals are usually imperfect. X-ray diffraction patterns of polymer crystals, for example, show fewer higher reflections indicating poorer crystal regularity. Another difference is that polymer molecules are usually bigger than the crystals, so interconnection and chain folding affect properties. This results in diffuse interfaces between crystalline and amorphous phases as compared to sharper interfaces for low molecular weight crystals.

Several topics that illustrate the relationships between thermodynamics, polymer structure and polymer crystalline are given below.

3.8.1 Polymer Structure – Melting Point

Several qualitative conclusions can be drawn from free energy considerations on the effect of polymer chain structure on melting point. The melting point is defined as the equilibrium point between the crystalline and molten phases in a polymer. The criterion for thermodynamic equilibrium is

$$\Delta G_m = 0 \tag{3.98}$$

where $\Delta G_m = G_{\text{cryst}} - G_{\text{amorph}}$

= the difference in the Gibbs free energy

since

$$\Delta G = \Delta H - T\Delta S$$

where $\Delta H = H_{\text{amorph}} - H_{\text{cryst}}$

$$\Delta S = S_{\text{amorph}} - S_{\text{cryst}}$$

Then, for equilibrium between the crystalline and amorphous phases to exist at the melting point

$$0 = \Delta G_m = \Delta H_m - T_m \Delta S_m \tag{3.99}$$

or, rearranging terms

$$T_m = \frac{\Delta H_m}{\Delta S_m} \tag{3.100}$$

Both terms on the right side in equation 3.100 are positive because both the enthalpy and entropy are greater in magnitude in the amorphous phase.

From an examination of equation 3.100, one can draw the following conclusions:

i. As ΔH becomes more positive, the melting point increases. A large negative value of ΔH_m accompanies a low H_{cryst} value in which chain

molecules are strongly bonded together. Molecules that contain polar groups such as $-\text{CCO}-$, $-\text{CHCl}-$, $-\text{CHOH}-$, form hydrogen bonds such as nylon or cellulose, or are regular in structure and can pack closely together (linear polyethylene, Teflon or stereoregular polymers) have strong bonding.

ii. As ΔS_m becomes smaller, the melting point increases. This condition exists if there is only a small decrease in order upon melting; a condition that occurs for ordered melts. An ordered melt in turn is associated with stiff chains in the melt (polyphenylene, $-\text{CF}_2-$, KevlarTM). With such cases, the melt is often liquid crystalline rather than amorphous. An equilibrium melting point is one where the crystalline phase transforms into a completely disordered amorphous state. With high molecular weights, this transformation may be slow. Thus, for example, for ultra-high molecular weight polyethylene, the apparent melting point may be extraordinarily high since the melt, which initially forms, retains the orientation imposed by the crystals. In such cases, the melting point depends upon the rate of heating.

iii. Chain orientation also orders the melt thereby raising the melting point because of the decrease in ΔS_m . Examples are natural rubber and poly(ethylene terephthalate) that crystallize on stretching. This topic is discussed in detail below.

iv. Crystals of finite size and defects in crystals result in a lower ΔH_{crys} , a lower ΔH and a lower melting point. This topic is expanded in the next section. It should be realized that the equilibrium state of a crystalline material is one with infinitely large perfect crystals. Thus, crystals of finite size with imperfections represent a non-equilibrium state. In addition, polymer crystals differ from low molecular weight crystals in having diffuse phase boundaries. With annealing, polymer crystal sizes increase and imperfection content decreases as equilibrium is approached with a consequent increase in the melting temperature. In such cases, annealing may occur in the course of slow heating, so the observed melting point may also depend upon the heating rate.

3.8.2. Effect of Diluent and Impurities

An analogy to the effect of salt in water can be made for semi-crystalline polymers. Pure polymer crystal is at equilibrium with its polymer melt at the melting temperature. If the temperature is raised, the molecules move more rapidly so the crystal phase decreases and the melt phase increases. Physically, this change results because fewer molecules return to the crystal; while, the crystal continues to move molecules into the melt at the same rate. On the other hand, below the melting temperature, the molecular motion slows down; the crystal phase increases at the expense of the melt phase.

If impurities are added to the polymer at its melting point, fewer molecules return to the crystal phase because the impurity molecules displace polymer crystal molecules and fewer polymer molecules are able to deposit on the crystal phase. The rate of movement of chain molecules into the melt is not affected by the presence of impurities. So, the melting point of the polymer/impurity composition is lower than that of the pure polymer.

The influence of impurities (chain ends, solvent or co-monomer) on the melting point can also be treated from a consideration of the chemical potential (for further details on chemical potential, see Appendix 3C). At the melting point,

$$\mu_u^c = \mu_u \tag{3.101}$$

where

μ_u^c = the chemical potential (the free energy per mole) of the crystalline phase

μ_u = the chemical potential (the free energy per mole) of the liquid phase

For the crystalline phase, at temperatures below the melting point,

$$\mu_u^0 - \mu_u^c = \left(\frac{\partial G_u}{\partial n} \right)_{T,P} - \left(\frac{\partial G_c}{\partial n} \right)_{T,P} = \left(\frac{\partial \Delta G}{\partial n} \right)_{T,P} \tag{3.102}$$

where μ_u^0 = the chemical potential of the standard state assumed to be that of the pure liquid at the same temperature and pressure.

and n = the number of moles of the chain repeat unit

Since chemical potentials are derived from free energy,

$$\Delta G = \Delta H - T\Delta S = \Delta H_u \left[1 - T(\Delta S_u / \Delta H_u) \right] = \Delta H_u \left[1 - (\Delta s_u / \Delta h_u) \right] \quad (3.103)$$

where

$$\Delta H_u = \left(\frac{\partial \Delta H}{\partial n} \right)_{T,P} \quad (3.104)$$

If we assume that

$$(\Delta s / \Delta h) = (\Delta s^0 / \Delta h^0) = (1/T_m^0),$$

$\Delta s / \Delta h$ refers to the real material
and $\Delta s^0 / \Delta h^0$ refers to the perfect crystal
then

$$\begin{aligned} \Delta G &= \Delta H \left[1 - (T/T_m^0) \right] \\ \mu_u^0 - \mu_u^c &= (\partial \Delta G_u / \partial n)_{T,P} = (\partial \Delta H / \partial n) \left[1 - (T/T_m^0) \right] \\ &= \Delta h \left[1 - (T/T_m^0) \right] \end{aligned} \quad (3.105)$$

If the temperature is not too far below T_m^0 , then

$$\mu_u^0 - \mu_u^c = 0$$

and analogous to equations 3.101 and 3.102

$$\frac{\Delta S_u}{\Delta H_u} = \frac{\Delta S_u^0}{\Delta H_u^0} = \frac{1}{T_m^0} \quad (3.106)$$

where ΔS_u^0 and ΔH_u^0 are the values of ΔS_u and ΔH_u at T_m . Thus,

$$\mu_u^0 - \mu_u^c = \Delta H_m \left(1 - \frac{T}{T_m^0} \right) \quad (3.107)$$

The condition for equilibrium to exist between the crystalline phase and the amorphous phase diluted with monomeric liquid is

$$\mu_u^0 - \mu_u^c = \mu_u^0 - \mu_u \quad (3.108)$$

Equation 3.108 states that the difference in chemical potential between a standard state and the crystalline phase equals the difference in chemical potential between the same standard state and the diluted amorphous polymer unit. An equation similar to equation 3.80 derived from the Flory-Huggins treatment can be applied to the case of an amorphous phase containing diluent

$$\mu_u^0 - \mu_u^c = RT \frac{V_u}{V_1} (\phi_1 - \chi_1 \phi_1^2) \quad (3.109)$$

where V_u = the molar volume of the repeat unit

V_1 = the molar volume of the diluent

ϕ_1 = the volume fraction of the diluent

χ_1 = the polymer/solvent interaction parameter = $\frac{BV_1}{RT}$

At the melting point for a semi crystalline polymer containing diluent, then from equations 3.107, 3.108 and 3.109

$$\Delta H_u \left(1 - \frac{T_m}{T_m^0} \right) = RT_m \left(\frac{V_u}{V_1} \right) \left(\phi_1 - \frac{BV_1}{RT} \phi_1^2 \right) \quad (3.110)$$

or, rearranging terms

$$\frac{V_1}{\phi_1} \left(\frac{1}{T_m} - \frac{1}{T_m^0} \right) = \frac{RV_u}{\Delta H_u} \left(1 - \frac{BV_1}{RT_m} \phi_1 \right) \quad (3.111)$$

The term $(1/T_m - 1/T_m^0)$ is roughly proportional to the amount of diluent present.

The presence of diluent depresses the undiluted melting point (T_m^0). The same polymer will differ in the extent of a melting point depression with changes in diluent due to the presence of the solvent interaction parameter term in equation 3.102 such as shown in Figure 3.12. This term yields a value of B that agrees well with values determined by other techniques (e.g., light scattering or osmotic pressure). The intercept also furnishes a value of the heat of fusion that compares well with values obtained by direct calorimetric measurement. In addition, the diluent approach has the advantage that the degree of crystallinity does not have

to be known, a requirement for the calorimetric measurement. The good agreement supports the model of a two-phase crystalline–amorphous structure on which the derivation of equation 3.109 is based.

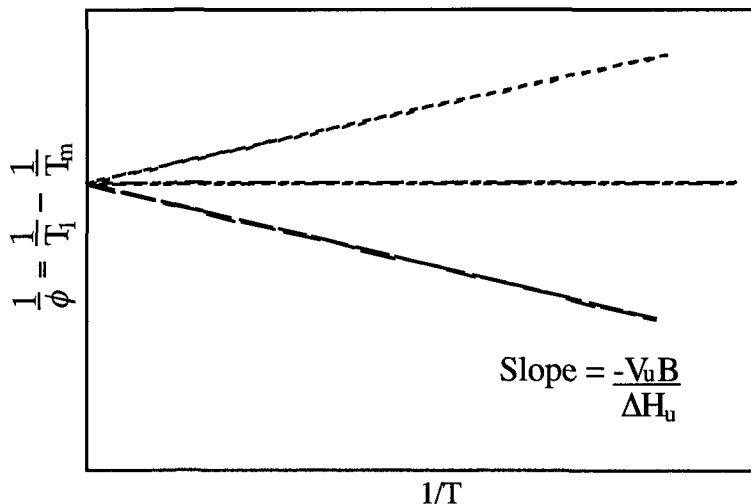


Figure 3.12. Polymer diluent plot showing the same polymer in three different Solvents from equation 3.48.
Value of the slope depends on the value of B.

It should be pointed out that melting points determined using the diluent technique are more likely to be equilibrium melting points since there is mobility in the presence of diluent.

The melting point depression of solid polymers (with no liquid diluent) may be derived from classical solution theory considerations. For ideal solutions of low molecular weight molecules, the equation analogous to equation 3.100 is

$$\mu_u^0 - \mu_u = RT \ln X_2 \quad (3.112)$$

where X_2 = the mole fraction of solute.

If the solution contains only a small fraction of diluent ($\phi_1 \gg 1$), then the following approximations can be made without introducing serious errors:

$$\ln X_2 = -X_1 = -\frac{\frac{\phi_1}{V_1}}{\frac{(1-\phi_1)}{V_u}} = -\frac{V_u}{V_1} \phi_1 \quad (3.113)$$

so that, using equation 3.112

$$\mu_u^0 - \mu_s = RT_m \frac{V_u}{V_1} \phi_1 = \mu_u^0 - \mu_u^c = \Delta H_u \left(1 - \frac{T_m}{T_m^0} \right) \quad (3.114)$$

or rearranging terms

$$\frac{1}{T_m} - \frac{1}{T_m^0} = \frac{R}{\Delta H_u} \frac{V_u}{V_1} \quad (3.115)$$

Equation 3.115 is identical with equation 3.111 when $B = 0$. The diluent or component that depresses the melting point may be a constituent of the polymer itself. For example, if a copolymer consists of A units that crystallize and B units that do not, then equations 3.112, 3.114 and 3.115 give

$$\frac{1}{T_m} - \frac{1}{T_m^0} = \frac{R}{\Delta H_u} \ln X_A \quad (3.116)$$

The assumption that one of the monomer units is excluded from the polymer crystal can entail several consequences. In this case, the, the size of the crystal is limited by the sequence length of the crystallizing monomer units, so the effect of comonomer concentration becomes mixed up with the effect of crystal size. In addition, if one of the units is excluded, it will probably reside at the crystal surface and affect the melting point. In many cases, comonomer units get included in the crystal, for example polypropylene in polyethylene. Thus, the situation is more complicated than what is described by the mathematics in this section.

Equation 3.116 assumes the chain structure is a random copolymer. Similar expressions have been obtained for non-random (block) copolymers and for partly tactic polymers. A second example is chain ends. These may be excluded from crystals and act as impurities in which case equation 3.116 is modified

$$\frac{1}{T_m} - \frac{1}{T_m^0} = \frac{R}{\Delta H_u} \ln(1 - X_E) \quad (3.117)$$

where X_E is the mole fraction of chain ends. For linear chains, there are two ends for X_n monomer units where $\langle X_n \rangle$ is the number average degree of polymerization. Thus,

$$X_E = \frac{2}{\langle X_n \rangle} \quad (3.118)$$

and, from equation 3.129,

$$\frac{1}{T_m} - \frac{1}{T_m^0} = \frac{R}{\Delta H_u} \frac{1}{\langle X_n \rangle} \quad (3.119)$$

A plot based on equation 3.119 predicts that the melting point increases with increasing molecular weight (Figure 3.13). This prediction agrees with experiment [31].

The above discussion is oversimplified since if a chain end is excluded, it must reach the surface. This requirement limits the size of the crystal and affects its surface energy. Exclusion is more likely with slow crystallization. On the other hand, with fast crystallization, chain ends (and comonomer units) might be trapped within in the growing crystal. The derivation then assumes that the molar volume of a chain end is the same as that of a monomer unit, but this is not necessarily so. The effect may depend on the nature of the chain end.

Finite crystal size reduces the equilibrium melting point. For crystals of finite size, the melting point is given by (analogous to equation 3.101)

$$T_m = \frac{\Delta H}{\Delta S_0} \quad (3.120)$$

where

$$\Delta H = \Delta H_0 - \Delta H_{\text{excess}} \quad (3.121)$$

$$\Delta H_{\text{excess per crystal}} = \sigma a^2 \quad (3.122)$$

$$\Delta H = \text{excess per unit volume} = \frac{\sigma a^2}{a^2 l} = \frac{\sigma}{l} \quad (3.123)$$

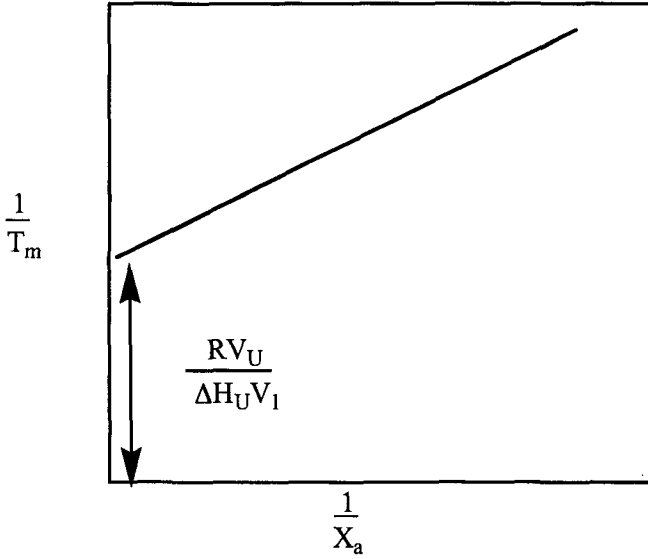


Figure 3.13. Schematic illustrating change in melting temperature with molecular weight (equation 3.137).

The amount of enthalpy per mole associated with the finite crystal surface energy (σ) reduces the equilibrium enthalpy for the infinite crystal (ΔH_0). Thus, from

$$\Delta H_{\text{excess per mole}} = \frac{\sigma}{l} V_m \tag{3.124}$$

where V_m = the molar volume. Substituting equations 3.114 and 3.111 into equation 3.120,

$$T_m = \frac{\Delta H_0 - \frac{\sigma V_m}{l}}{\Delta S_0} \tag{3.125}$$

or, rearranging

$$T_m = T_m^0 \left[\frac{1 - \frac{\sigma V_m}{l \Delta H_0}}{1} \right] \tag{3.126}$$

Thus, the greater the surface free energy and the smaller the crystal, the larger is the melting point depression (Figure 3.14).

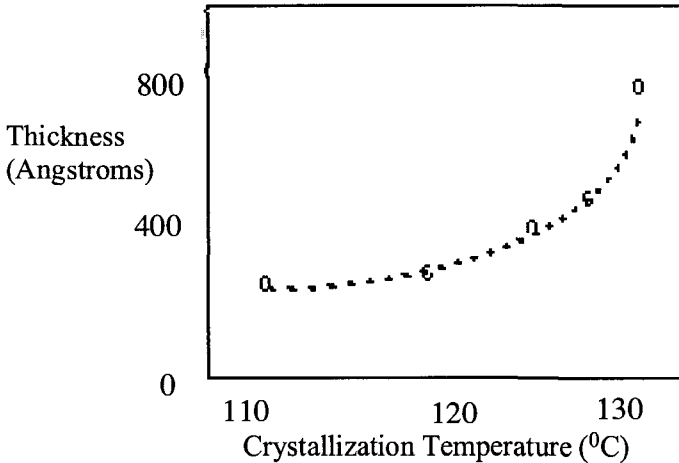


Figure 3.14 Change in melting temperature with crystal (lamellar) thickness
S. Kavesh, J.M Schultz, J. Polymer Sci. **1971**, *9A*, 285.

3.8.3. Crystallization Induced by Stretching

Stretching and preferentially orienting the chains parallel to the stretching direction (Figure 3.15) enhances the ability of polymer chains to crystallize. The parallel chains more readily form crystalline aggregates. Thermodynamic arguments also support this conclusion. Chain entropy decreases with entropy and crystallization will occur when $T\Delta S < \Delta H_f$ for chain structures possessing sufficient regularity.

Flory [32] derived expressions relating the equilibrium degree of crystalline to chain elongation by a statistical segment model of a three-dimensional crosslinked rubber network. The process was assumed to comprise two distinct steps. The network was first elongated at a temperature sufficiently high so that no crystallization occurred. The temperature was then gradually lowered to a temperature at which the elongated network could crystallize. This sequence differs from the usual practice in which elongation and crystallization are carried out simultaneously. The consequences of this difference are discussed below.

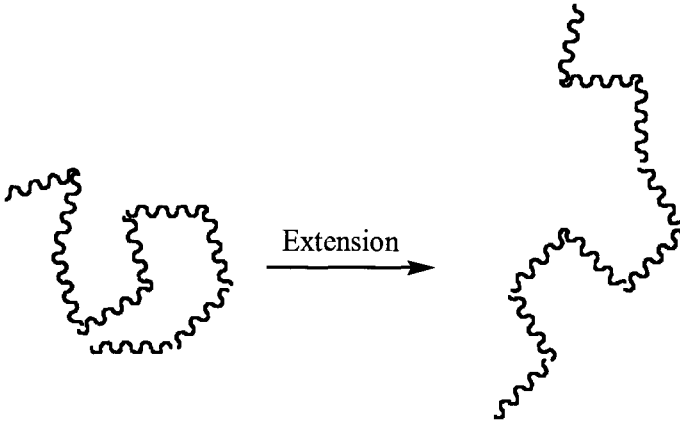


Figure 3.15. Schematic illustrating change chain order on stretching.

This result of this two-step process is

$$X_c = 1 - \left\{ \frac{\frac{3}{2} - f(\alpha)}{\frac{3}{2} - \theta} \right\} \quad (3.127)$$

where

$$f(\alpha) = \left(\frac{6}{\pi} \right)^{1/2} \frac{\alpha}{n^{1/2}} - \frac{\alpha^2 + 1}{2n} \quad (3.128)$$

and α = the elongation ratio

n = the number of statistical segments per cc

$$\theta = \frac{\Delta H_u}{R} \left[\frac{1}{T_m^0} - \frac{1}{T} \right]$$

A plot of equation 3.128 (Figure 3.16) using reasonable values of the parameters for natural rubber shows that i) at a given temperature, the degree of crystalline increases with increasing elongation, ii) for a given value of α , the degree of crystalline decreases with increasing temperature. The maximum at high elongation may or may not be significant because the model assumes a Gaussian chain distribution that becomes invalid at high elongations.

This treatment by Flory which predicts that stretching lowers melting points and promotes the crystallization assumes that extended chain crystals form which is probably true at higher elongations. Extended chain crystallization results in a decrease in force at constant length or an increase in length at constant force. The latter is given to explain the observation that if a rubber band is held stretched between nails which crystallizes; the rubber band can lift off the nails. At lower elongations where chain folded crystals might form, these effects are reversed.

Wu [33] has rederived equation 3.127 using a more general model with two independent parameters: the fraction of the total chain end-to-end distance assigned to the crystalline region and the degree of crystalline. He then analyzed the relative stability of the folded chain versus the extended chain morphology [Chapter 8] as a function of elongation and temperature.

The Flory model also leads to a prediction of the effect of crystallization on the retractive force (α_0) exerted by a stretched rubber

$$\alpha_0 = \frac{\left(\frac{N_c}{V}\right)RT\left[\alpha - \frac{1}{\alpha^2}\right] - \left(\frac{6n}{\pi}\right)^{1/2} X_c}{1 - X_c} \quad (3.129)$$

where α is the elongation ratio, N_c number of chains per unit volume (V), n the number of statistical segments per chain and X_c the degree of crystallinity. This equation predicts a decrease in stress with the onset of crystallization for a stretched rubber sample. Several workers (40) have found this effect.

The results cited above apply to systems in the thermodynamic equilibrium state. For the non-equilibrium state in which elongation and crystallization occur simultaneously, the retractive force or tension increases with elongation [34]. For this case, the crystals formed at a given elongation serve as crosslinks that impede further extension thereby increasing the force required for elongation. Further, the degree of crystalline can attain values greater than the equilibrium value because the increased tension deforms nominally amorphous regions and forces them into crystalline alignment.

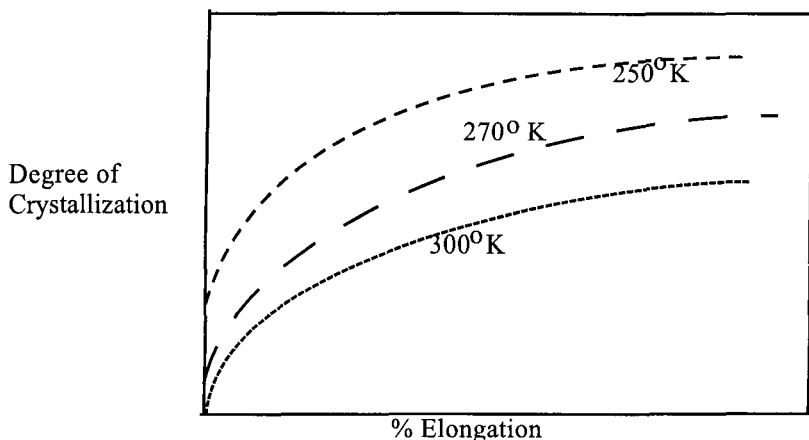


Figure 3.16. Plot of degree of crystalline against elongation at three temperatures For $n=25$, $h=600R$ and $T_{cry}=250^{\circ}$.

At low elongations, crystallization in natural rubber can be very slow. Natural rubber will crystallize slowly, often several months, at no elongation. This rubber crystallized at room temperature is termed “stark rubber” because it is stiff and rather rigid at room temperature in contrast to the flexible sheets of coagulated natural rubber latex usually found at room temperature.

Optical techniques (birefringence and low angle light scattering) have been used to characterize stress-induced crystallization [35]. The crystallization temperature is more important than is elongation in determining the final degree of crystalline.

References

1. P.J Flory, Principles of Polymer Chemistry, Cornell: Ithaca, 1953, Chapter 11
2. M.L. Miller, The Structure of Polymers; Reinhold: New York, 1966, Chapter 7
3. J.J. Aklonis, W.J. McKnight, Introduction to Polymer Viscoelasticity; Wiley (Interscience): New York, 1982
4. J.E. Mark, Adv. Polymer Sci. 1982, 44, 1;
J. Polymer Sci. Macromol. Revs. 1976, 11, 135
5. H.M. James, E. Guth, J. Chem. Phys. 1943, 11, 455
6. P.J. Flory, C.A.J. Hoeve, A. Ciferri, J. Polymer Sci. 1959, 34, 337
7. P.J. Flory, Ref. 1 Chapter 12

TOPICS in POLYMER PHYSICS

8. M.L. Huggins, J. Chem. Phys. **1941**, 9, 440; J. Phys. Chem. **1942**, 10, 151
9. P.J. Flory, J. Chem. Phys. **1941**, 9, 66; *ibid.* **1942**, 10, 51; *ibid.* 1945 15)
10. K.W. Foreman and K.F. Freed, J.Chem. Phys., **1995**, 102, 4663
11. P.J. Flory, Ref. 1, Chapter 12
12. P.J. Flory, W.R. Krigbaum, J. Chem. Phys. **1950**, 18, 1086
13. Ishihara, E. Guth, Adv. in Polymer Sci. **1967**, 5, 233
14. I.C. Sanchez, R.H. Lacombe, J. Phys. Chem. **1976**, 80, 2352
15. R.H. Lacombe, I.C. Sanchez, J. Phys. Chem. **1976**, 80, 2568
16. J.H. Hildebrand, R.L. Scott,
The Solubility of Non Electrolytes, 3rd. Ed.; Dover: New York, **1964**
17. R.A. Orwell, Rubber Chem. And Technol., **1977**, 50, 451
18. R.L. Scott, J. Chem. Phys., **1949**, 17, 279
19. A. Dobry, F. Boyer-Kawenski, J. Polymer Sci., **1947**, 2, 90
20. H. Benoit, J. Polym. Sci. **1964**, C4, 1589
21. M. Shen and H. Kawai, A.I. Ch.E. Journal. **1978**, 24, 1
22. C. Sadron, Angew. Chem. **1963**, 75, 742
23. D.J. Maier, Block and Graft Copolymers;
J.J. Burke, V. Weiss, eds. Syracuse University: Syracuse, **1973**, p 105
24. F.M. Merret, J. Polymer Sci. **1957**, 24, 467
25. S. Krause, Ref. 25, p 143
26. E. Helfand, J. Chem. Phys. **1975**, 62, 999
27. M.M. Coleman, C.J. Serman, D.E. Bhageagar, P.C. Painter, Polymer, **1990**, 31, 1187
28. J. Cahn, J. Chem. Phys. **1965**, 49, 93
29. R. Chaing, P.J. Flory, J. Amer. Chem. Soc. **1961**, **83**, 2857
30. L. Mandelkern, Crystallization of Polymers; McGraw-Hill: New York, **1964**
31. B. Wunderlich and G. Czornyj, Macromolecules. **1977**, 10, 906
32. P.J. Flory, J. Chem. Phys. **1947**, 15, 9
33. W. L. Wu, J. Polymer Sci. Phys. Ed. **1978**, 16, 391; Polym. Eng. Sci. **1979**, 19, 391
34. P.J. Flory, Ref. 1, pp 451-454
35. R.S. Stein, Polym. Eng. Sci. **1976**, 16, 15

Appendix 3A Classical Thermodynamics

Classical thermodynamics deals with the interconversion of energy in all its forms including mechanical, thermal and electrical. Helmholtz [1], Gibbs [2,3] and others defined state functions such as enthalpy, heat content and entropy to handle these relationships. State functions describe closed energy states/systems in which the energy conversions occur in equilibrium, reversible paths so that energy is conserved. These notions are more fully described below. State functions were described in Appendix 2A; however, statistical thermodynamics derived state functions from statistical arguments based on molecular parameters rather than from basic definitions as summarized below.

Assume the existence of two phases separated by a phase boundary or interface. Phases, in this sense, can exist in any of the three states of matter: gaseous, liquid or solid. Their only requirement for existence is that their intensive properties such as pressure and free energy (see below) are the same everywhere within the phase. This assumes that the phases are large in size since the free energy of phases near surfaces will be different. The two phases constitute a system in the thermodynamic sense. At equilibrium, for the conditions of constant temperature and pressure, the following state functions are defined as:

$$G \equiv H - TS \quad (3A.1)$$

$$H \equiv E + PV \quad (3A.2)$$

$$E \equiv dQ - dW \quad (3A.3)$$

where

G = the Gibbs Function

H = the enthalpy or heat content at constant temperature
and pressure

T = the temperature expressed in units of degrees Kelvin

S = the entropy

E = the internal energy at constant temperature and volume

Q = the heat absorbed by the system

W = work done by the system

The first law of thermodynamics is based on the conservation of energy. It can be formulated in several ways. Equation 3A.3 is one way. Another is:

$$\oint dE = 0 \quad (3A.4)$$

which states that, for a reversible process, E depends only on the initial and final states of the system and not on the path/sequence traveled between these states. Therefore, E is a state function.

The second law of thermodynamics defines the maximum amount of work that can be obtained from a system. Entropy is the state function used to express the second law in mathematical terms and is defined, for a reversible process, by

$$dS = \frac{dQ}{T} \quad (\text{analogous to equation 3A.3}) \quad (3A.5)$$

or by,

$$\oint dS = 0 \quad (\text{analogous to equation 3A.4}) \quad (3A.6)$$

Differentiating the state functions defined above leads to a criterion for equilibrium and to the concept of chemical potential (for an example, see Appendices 3A and 3C and equation 3.114). Thus,

$$\text{(From 3A.1)} \quad dG = dH - TdS + VdP \quad (3A.7)$$

$$\text{(From 3A.3)} \quad dE = dQ - dW \quad (3A.8)$$

$$\text{(From 3A.5)} \quad dQ = TdS \quad (3A.9)$$

$$\text{and} \quad dW = PdV \quad (3A.10)$$

These equations hold for reversible processes. Equation 3A.10 assumes that only pressure-volume work is done by or on the system. But, equation 3A.7 can be modified to include other types of work such as stretching a rubber chain (Section 3.2) or charging an electrical condenser.

The Gibbs free energy is a function of temperature and pressure. The following relations show the dependence. Inserting equations 3A.5 and 3A.10 into equation 3A.9,

THERMODYNAMICS

$$dE = TdS - PdV \quad (3A.11)$$

Then, using equation 3A.8

$$dH = TdS - PdV + PdV + VdP = TdS + VdP \quad (3A.12)$$

and substituting equation 3A.12 into equation 3A.7

$$dG = TdS + VdP - TdS - SdT = VdP - SdT \quad (3A.13)$$

At constant pressure and temperature, $dP = dT = 0$; so that the relation

$$dG \equiv 0 \quad (3A.14)$$

defines the condition needed to specify thermodynamic equilibrium at constant temperature and pressure.

For irreversible processes

$$dS > \frac{dQ}{T} \quad (3A.15)$$

and

$$dG < 0$$

If matter is transported between phases A and B, assuming the system is isolated from the rest of the universe (a closed system), the free energy of the system (G) is given by

$$G = G_A + G_B \quad (3A.16)$$

At equilibrium

$$dG = 0 = dG_A + dG_B \quad (3A.17)$$

If there are two components present in the system that are common to both phases, then at equilibrium

$$dG_A = \left(\frac{\partial G_A}{\partial n_{1A}} \right) dn_{1A} + \left(\frac{\partial G_A}{\partial n_{2A}} \right) dn_{2A} \quad (3A.18)$$

where

$$\left(\frac{\partial G_A}{\partial n_{1A}} \right) \equiv m_{1A} = \text{the chemical potential of component 1 in phase A}$$

n_{1A} = the number of moles of component 1 in phase A

Similarly,

$$dG_B = \mu_{1B} dn_{1B} + \mu_{2B} dn_{2B} \quad (3A.19)$$

At equilibrium

$$dG_A = dG_B \quad (3A.20)$$

Equations analogous to those of 3A.7 through 3A.15 may be derived for the conditions of constant temperature and volume. These are based on the Helmholtz free energy (A):

$$A = E - TS \quad (3A.21)$$

From equation (3A.11)

$$dA = TdS - PdV - TdS = -PdV - SdT \quad (3A.22)$$

At constant temperature and volume, $dV = dT = 0$; so that the equation

$$dA = 0 \quad (3A.23)$$

states the condition necessary for the attainment of equilibrium at constant temperature and volume.

Relations, first derived by James Clark Maxwell (the Maxwell equations) can be used to express the state functions of entropy and free energy in terms of physically measurable quantities: the coefficient of volume expansion (α) and the isothermal compressibility (β).

Using equation 3A.13

$$dG = VdP - SdT$$

and equation 3A.22

$$dA = -PdV - SdT$$

and the relations, derived from differential calculus

$$\left\{ \frac{1}{\partial z} \left(\frac{\partial x}{\partial y} \right)_z \right\}_y = \left\{ \frac{1}{\partial y} \left(\frac{\partial x}{\partial z} \right)_y \right\}_z \quad (3A.24)$$

It is shown below that

THERMODYNAMICS

$$-\left(\frac{\partial S}{\partial P}\right)_T = \left(\frac{\partial V}{\partial T}\right)_P - \alpha V \quad (3A.25)$$

and

$$-\left(\frac{\partial S}{\partial V}\right)_T = \left(\frac{\partial P}{\partial T}\right)_V = \frac{\alpha}{\beta} \quad (3A.26)$$

From equation 3A.24

$$\frac{\partial}{\partial T} \left(\frac{\partial V}{\partial V}\right)_T = \frac{\partial}{\partial V} \left(\frac{\partial A}{\partial T}\right)_V \quad (3A.27)$$

since

$$A = -PdV - SdT$$

then

$$\left(\frac{\partial A}{\partial V}\right)_T = -P \quad (3A.28)$$

and

$$\left\{ \frac{\partial}{\partial T} \left(\frac{\partial A}{\partial V}\right)_T \right\}_V = -\left(\frac{\partial P}{\partial T}\right)_V \quad (3A.29)$$

Also

$$\left(\frac{\partial A}{\partial T}\right)_V = -S \quad (3A.30)$$

and

$$\left\{ \frac{\partial}{\partial V} \left(\frac{\partial A}{\partial T}\right)_V \right\}_T = -\left(\frac{\partial S}{\partial V}\right)_T \quad (3A.31)$$

Equating equation 3A.31 with 3A.29, based on 3A.27

$$-\left(\frac{\partial S}{\partial V}\right)_T = -\left(\frac{\partial P}{\partial T}\right)_V = \left(\frac{\partial P}{\partial V}\right) \left(\frac{\partial V}{\partial T}\right)$$

Rearranging

$$-\left(\frac{\partial S}{\partial V}\right)_T = \frac{\left(\frac{\partial V}{\partial T}\right)_P}{\left(\frac{\partial V}{\partial P}\right)_T} = \frac{\alpha}{\beta} \quad (3A.32)$$

Similarly, from equation 3A.24

$$\frac{\partial}{\partial T} \left(\frac{\partial G}{\partial P} \right)_T = \frac{\partial}{\partial P} \left(\frac{\partial G}{\partial T} \right)_P \quad (3A.33)$$

since

$$G = VdP - SdT; \quad \left(\frac{\partial G}{\partial P} \right)_T = V \quad (3A.34)$$

and

$$\left\{ \frac{\partial}{\partial T} \left(\frac{\partial G}{\partial P} \right)_T \right\}_P = \left(\frac{\partial V}{\partial T} \right)_P \quad (3A.35)$$

Also

$$\left(\frac{\partial G}{\partial T} \right)_P = -S \quad (3A.36)$$

and

$$\left\{ \frac{\partial}{\partial P} \left(\frac{\partial G}{\partial T} \right)_P \right\}_T = - \left(\frac{\partial S}{\partial P} \right)_T \quad (3A.37)$$

Equating equations 3A-37 with 3A-35 based on 3A-32

$$+ \left(\frac{\partial S}{\partial P} \right)_T = - \left(\frac{\partial V}{\partial T} \right)_P = \alpha V \quad (3A.38)$$

since

$$\alpha \equiv \frac{1}{V} \left(\frac{\partial V}{\partial T} \right)_P$$

References

1. H. Helmholtz, S.B. Preuss, *Akad. Wiss.* **1882**, *1*, 22
2. J.W. Gibbs, *Collected Works*, Dover Press, New York, **1961**
3. G. Astarita, *Ind. Eng. Chem. Funderm.* **1977**, *16*, 138

Appendix 3B. Heat of Mixing

The heat of mixing is derived from a lattice treatment. But, energy of interaction terms must be considered as well as the probability of molecular placement. Nearest neighbor pairs of molecules are the only energy interactions considered. If the distance between all the nearest neighbors is assumed the same, then the total internal energy of the solution is given by

$$E_{12} = -[N_{11}\epsilon_{11} + N_{12}\epsilon_{12} + N_{22}\epsilon_{22}] \quad (3B.1)$$

where N_{11} = the number of solvent-solvent contacts per cm³

N_{12} = the number of solvent-solute contacts per cm³

N_{22} = the number of solute-solute contacts per cm³

$-\epsilon_{11}$ = the potential energy of a solvent-solvent contact

$-\epsilon_{12}$ = the potential energy of a solvent-solute contact

$-\epsilon_{22}$ = the potential energy of a solute-solute contact

The negative sign is arbitrary and is used so that other quantities such as cohesive energy density will be positive.

The terms in equation 3B.1 are evaluated by the following procedure.

Let

$$N_{11} = \frac{1}{2}N_1zP_{11} \quad (3B.2)$$

where N_1 is the number of solvent molecules per cm³, z is the coordination number of the lattice, the number of lattice sites making nearest neighbor contact with a given site (assuming that a solvent molecule or a segment of a solute molecule occupies each site). P_{11} is the probability that a lattice site about the central site is occupied by a solvent molecule and is assumed to be proportional to the volume fraction of solvent (ϕ_1) or

$$P_{11} = \phi_1 = \frac{N_1}{N_1 + xN_2} \quad (3B.3)$$

where x = the number of lattice sites occupied by a solute molecule

$$= \frac{\text{volume of solute molecules}}{\text{volume solvent molecules}} \quad (3B.4)$$

The factor of $(1/2)$ is necessary in equation (3B.2) since each solvent-solvent contact is counted twice. Similarly, since there are xN_2 solute segments,

$$N_{22} = \frac{1}{2} xN_2zP_{22} \quad (3B.5)$$

where

$$P_{22} = \phi_2 = \frac{xN_2}{N_1 + xN_2} \quad (3B.6)$$

Equation 3B.6 is not as good an approximation as is equation 3B.3 in that a given solute segment site must automatically be surrounded by the neighboring solute segments on the same chain. Thus, P_{22} will be somewhat higher than ϕ_2 , the average volume fraction of segments in solution. Now, let

$$N_{12} = N_1zP_{12} \quad (3B.7)$$

where P_{12} is the probability that a solvent molecule occupies a lattice site. Assume that

$$P_{12} = P_{22} = \phi_2 \quad (3B.8)$$

so that, using equations 3B.8, 3B.6 and 3B.7

$$N_{12} = (xN_1N_2z) / (N_1 + xN_2) \quad (3B.9)$$

Note that the same result can be obtained from

$$N_{12} = xN_2zP_{21} = xN_2zf_1 = N_{12} = (xN_1N_2z) / (N_1 + xN_2) \quad (3B.10)$$

On substituting equations 3B.2, 3B.5 and 3B.9 in 3B.1

$$E_{12} = \frac{z}{(N_1 + xN_2)} \left[\frac{1}{2} N_1^2 \epsilon_{11} + xN_1 \epsilon_{12} + \frac{1}{2} N_2^2 x^2 \epsilon_{22} \right] \quad (3B.11)$$

The ϵ terms in equation 3B.10 are evaluated by an analogous procedure. The internal energy change upon mixing is

$$\Delta E_m = E_{12} - (E_1 + E_2) \quad (3B.12)$$

where E_1 is the internal energy of N_1 molecules of pure solvent, and is given by

$$E_1 = -\frac{1}{2}N_1z\varepsilon_{11} \quad (3B.13)$$

Similarly,

$$E_2 = -\frac{1}{2}xN_2z\varepsilon_{22} \quad (3B.14)$$

so that, on substituting equations 3B.12 and 3B.13 into 3B.12m

$$\begin{aligned} \Delta E_m &= \frac{z}{(N_1 + xN_2)} \left[\left(\frac{1}{2}N_1^2\varepsilon_{11} + xN_1\varepsilon_{12} + \frac{1}{2}N_2^2x^2\varepsilon_{22} \right) \right. \\ &\quad \left. - \left(\frac{1}{2}N_1\varepsilon_{11} + \frac{1}{2}xN_2\varepsilon_{22} \right) \right] (N_1 + xN_2) = -\frac{xzN_1N_2}{(N_1 + xN_2)} \left[\varepsilon_{12} - \frac{1}{2}\varepsilon_{11} - \frac{1}{2}\varepsilon_{22} \right] \end{aligned} \quad (3B.15)$$

Converting

$$= -\frac{xzn_1n_2}{(n_1 + xn_2)} \left[\varepsilon_{12} - \frac{1}{2}\varepsilon_{11} - \frac{1}{2}\varepsilon_{22} \right]$$

where n_i = the number of moles of i

Thus,

$$\Delta E_m = (\Delta\varepsilon)n_1\phi_2 \quad (3B.16)$$

where
$$\Delta\varepsilon = zN_A \left[\varepsilon_{12} - (1/2)\varepsilon_{11} + (1/2)\varepsilon_{11} \right] \quad (3B.17)$$

$$N_A = \text{Avogadro's number} = 6.02 \times 10^{23}$$

and
$$\phi_2 = \frac{xn_2}{n_1 + xn_2} \quad (3B.18)$$

Avogadro's number is inserted into equation 3B.16 to reflect the change from ΔE per molecule to $\Delta\varepsilon$ per mole.

The heat of mixing at constant pressure is

$$\Delta H_m = E_m + P\Delta V_m \quad (3B.19)$$

but according to the lattice model, the volume change upon mixing, ΔV_m , is zero, so that, from equation 3B.15

$$\Delta H_m = (\Delta\varepsilon)n_1\phi_2 \quad (3B.20)$$

This is the ΔH_m per cm^3 . To obtain the molar heat of mixing, this must be multiplied by V_1 , the molar volume

$$\Delta H_m = \frac{RT\chi_1 n_1 \phi_2}{V_1} \quad (3B.21)$$

where χ_1 is an interaction parameter, dependent upon the molecular types, defined by

$$\chi_1 = \frac{(\Delta\varepsilon)V_1}{RT} = \frac{BV_1}{RT} \quad (3B.22)$$

This equation predicts that χ_1 should vary with $1/T$. Experimentally, it is often found that it varies in a manner described by the empirical equation

$$\chi_1 = A + B/T \quad (3B.23)$$

contrary to the above discussion. The meaning of A is uncertain and it is often referred to "an entropic contribution to χ_1 ". This may be a consequence of errors inherent in the theory for the entropy of mixing.

The partial molal heat of mixing is

$$\Delta H_1 = \left(\frac{\partial H_m}{\partial n_1} \right)_{P,T,n_2} V_1 = RT\chi_1 d \left[\frac{xn_1 n_2}{n_1 + xn_2} \right] = RT\chi_1 \left[\frac{x^2 n_2^2}{n_1 + xn_2} \right] = RT\chi_1 \phi_1 \quad (3B.24)$$

This equation is used in deriving equations 3.80 and 3.113.

For athermal solutions ($\Delta\varepsilon = 0$)

$$\varepsilon_{12} = \frac{\varepsilon_{11} + \varepsilon_{22}}{2} \quad \text{and} \quad \chi_1 = 0 \quad (3B.25)$$

so that

$$\langle \Delta H_1 \rangle = 0 \quad (3B.26)$$

For good solvents $\epsilon_{12} > (\epsilon_{11} + \epsilon_{22})/2$ so that χ_1 is negative and $\langle \Delta H_1 \rangle$ is negative. Heat is therefore given off on mixing.

In the absence of specific interaction such as hydrogen bonding

$$\epsilon_{12} = \sqrt{\epsilon_{11}\epsilon_{22}} \quad (3B.27)$$

[This result arises from the London theory of "dispersion forces" and is reviewed in Hildebrand and Scott, Chapter IV. For original work, see

R. Eisenschitz and F. London, *Z. Physik.* **1930**, *60*, 491,

F. London, *Z. Physik.* **1930**, *63*, 245

F. London, *Z. Physik. Chem.* **1930**, *B11*, 222

Trans. Faraday Soc. **1937**, *33*, 8]

For this case

$$\Delta\epsilon = -zA_0 \left[(1/2)\epsilon_{11} - \sqrt{\epsilon_{11}}\sqrt{\epsilon_{22}} + (1/2)\epsilon_{22} \right] = -(1/2)zA_0 \left[\sqrt{\epsilon_{11}} - \sqrt{\epsilon_{22}} \right]^2 \quad (3B.28)$$

A consequence of equation 3B.26 is that $\Delta\epsilon$ and therefore ΔH_m is always positive and heat can only be absorbed on mixing. If heat is evolved, this must mean that there is specific interaction and equation 3.25 is not obeyed (e.g. $H_2SO_4 + H_2O$ where hydration of the H^+ ion and ionization of H_2SO_4 occurs). A positive ΔH_m tends to make a positive contribution to ΔF_m and opposes solution. Therefore the larger the difference between $\sqrt{\epsilon_{11}}$ and $\sqrt{\epsilon_{22}}$, the more positive $\Delta\epsilon$ and the poorer the solubility. This is a quantitative proof of the empirical statement that "like dissolves like"

It should be pointed out that experimentally, one sometimes find that with polymer blends, ΔH_m is sometimes negative, suggesting that in such cases, there are specific interactions between components such as ionic, dipolar or hydrogen bonding. A negative ΔH_m promotes miscibility.

Appendix 3C Osmotic Pressure

Consider an idealized cylinder model containing two compartments separated by a membrane permeable only to the solvent (Figure 3C.1a) Each compartment has a sliding piston. One compartment contains only solvent the other, solvent plus solute. When no outside force acts on the system, solvent will tend to migrate from the compartment containing pure solvent into the solution compartment. As the solvent compartment becomes depleted, the resulting

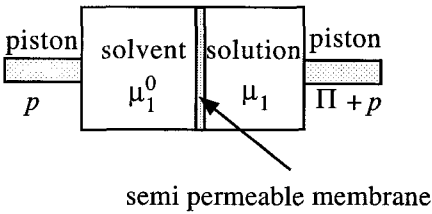


Figure 3C.1a Cylinder

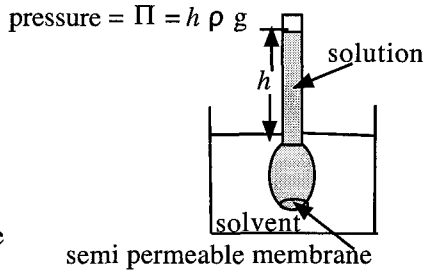


Figure 3C.1b Idealized osmometer.

pressure will slide the piston to the right. The model assumes that a reverse flow of solute molecules does not occur because the membrane is not permeable to solute molecules. The pressure exerted by the solvent can be gauged by measuring the force required to restore the piston to its original position. Osmometers in which the pressure head produces solvent flow through a semi-permeable membrane (Figure 3C.1b) use this principle. Osmotic pressure (π) is defined as the pressure required to stop solvent flow. The chemical potentials for this process are defined as

$$\mu_1^0 \equiv \left(\frac{\partial G}{\partial n_1} \right)_{T,P} = \text{the solvent chemical potential in pure solvent} \quad (3C.1)$$

$$\mu_1 \equiv \left(\frac{\partial G}{\partial n_1} \right)_{T,P} = \text{the solvent chemical potential in solution at 1 atmos. pres.} \quad (3C.2)$$

When $\mu_{0,1} > \mu_1$, solvent flows through the semi-permeable membrane.
At equilibrium,

$$\mu_1^0 \equiv \mu_1 + \Delta\mu_1 \quad (3C.3)$$

where $\Delta\mu_1$ = the increase in μ_1 , because of the applied pressure.

$\Delta\mu_1$ can be evaluated by integrating over pressure

$$\mu_1 = \int_p^{p+\Pi} \left(\frac{\partial\mu_1}{\partial P} \right)_{T,n_1,n_2} dP \quad (3C.4)$$

Rearranging

$$\left(\frac{\partial\mu_1}{\partial P} \right)_{T,n_1,n_2} = \left[\frac{\partial}{\partial P} \left(\frac{\partial G}{\partial n_1} \right)_{T,P,n_2} \right]_{T,n_1,n_2} = \left[\left\{ \frac{\partial}{\partial P} \left(\frac{\partial G}{\partial n_1} \right) \right\}_{T,P,n_2} \right]_{T,n_1,n_2} \quad (3C.5)$$

and

$$\left(\frac{\partial G}{\partial P} \right)_{T,n_1,n_2} = V \quad (3C.6)$$

since

$$dF = VdP - SdT$$

Thus

$$\left(\frac{\partial\mu_1}{\partial P} \right)_{T,n_1,n_2} = \left(\frac{\partial V}{\partial n_1} \right)_{T,P,n_2} - \bar{V}_1 \quad (3C.7)$$

where \bar{V}_1 = the partial molal volume which is assumed to have a constant value.

Substituting \bar{V}_1 into equation 3C.4

$$\Delta\mu_1 = \int_p^{p+\Pi} [\bar{V}_1] dP = \bar{V}_1 dP = \Pi \bar{V}_1 = \mu_1^0 - \mu_1 \quad (3C.8)$$

Thus

$$\mu_1^0 - \mu_1 = \Pi \bar{V}_1$$

where

THERMODYNAMICS

$\mu_1^0 - \mu_1$ = the difference in chemical difference

Π = the work to move a mole of solvent from pure solvent to solution
or

$$\Pi = \frac{\mu_1^0 - \mu_1}{\bar{V}_1} \quad (3C.9)$$

Osmotic pressure is thus the work required to move a mole of solvent from pure solvent through the membrane. From the Flory-Huggins equation (3.80)

$$\Pi = \frac{\mu_1^0 - \mu_1}{\bar{V}_1} = -\frac{RT}{\bar{V}_1} \left[\ln \phi_1 + \left(1 - \frac{1}{x}\right) \phi_2 + \chi_1 \phi_2^2 \right] \quad (3C.10)$$

Equation 2Cm.10 can be transformed into a more tractable form by the following operations. If we let

$$\ln \phi_1 = \ln [1 - \phi_2] \quad (3C.11)$$

and expand $\ln [1 - \phi_2]$ by a Taylor's series

$$\ln [1 - \phi_2] \cong -\phi_2 - \frac{1}{2} \phi_2^2 \quad (3C.12)$$

Then substitute into equation 3C-10

$$\Pi = \frac{RT}{\bar{V}_1} \left[-\phi_2 - \frac{1}{2} \phi_2^2 + \left(1 - \frac{1}{x}\right) \phi_2 + \chi_1 \phi_2^2 \right] = \frac{RT}{\bar{V}_1} \left[\frac{1}{x} \phi_2 + \left(\frac{1}{2} - \chi_1\right) \phi_2^2 \right] \quad (3C.13)$$

The following definitions are used to modify equation 3C.13 into experimentally accessible quantity

$$\phi_2 = \frac{\text{volume solute}}{\text{volume solution}} = \frac{\text{wt. solute}}{\text{volume solute}} \frac{\text{volume solute}}{\text{wt. solute}}$$

$$\frac{1}{\rho_2} \quad c_2$$

and

$$\begin{aligned}
 x &= \frac{\text{volume mole fraction}}{\text{weight mole polymer}} \\
 &= \frac{\text{volume mole polymer}}{\text{volume mole solvent}} \frac{\text{weight mole polymer}}{\text{volume mole solvent}} \\
 &\quad \frac{1}{\rho_2} \quad \nearrow \quad \quad \quad \frac{M_2}{V_1} \quad \nearrow
 \end{aligned}$$

Thus

$$\Pi = \frac{RT}{\bar{V}_1} \left[\frac{\rho_2 \bar{V}_1}{M_2} \frac{c_2}{\rho_2} + \left(\frac{1}{2} - \chi_1 \right) \frac{c_2}{\rho_2} \right] \quad (3C.14)$$

For low concentrations, \bar{V}_1 can be approximated by V_1 , so that

$$\Pi = RT \left[\frac{c_2}{M_2} + \left(\frac{1}{2} - \chi_1 \right) \frac{c_2^2}{\rho_2^2 V_1} \right] = RT \left[\frac{c_2}{M_2} + A_2 c_2^2 \right] \quad (3C.15)$$

where $A_2 = \text{the second virial coefficient} = \frac{(1/2) - \chi_1}{\rho_2^2 V_1}$

Chapter 4

OPTICS

4.1. Introduction

The optical properties of polymers are important in terms of both their applications as technological materials and the information obtained on their structure. For example, many applications ranging from packaging film to glazing materials require transparent polymers. At a higher technology level, the transmission of information by fiber optics, the use of optical discs for storing music, video and computer data and the use of non-linear optical devices in “optical switches” are common applications. Means for obtaining transparency are therefore a prime concern in these applications. The structural information gleaned from optical techniques ranges over a broad size distribution from the molecular level examined by neutrons and x-rays to the macroscopic sizes visible to the unaided eye. Thus, a hierarchy of structural sizes can be constructed based on optical data. In addition, optical techniques have the advantages of being non-destructive, specific and rapid.

The subject matter of this chapter deals with the interaction of radiation with matter. While most of the discussion deals with electromagnetic radiation, much of the formalism also applies to “matter waves” or deBroglie waves such as those associated with electron beams or neutrons. Although the equations describing this interaction are valid for all classes of materials, the treatment in this chapter is restricted to solid polymers. Chapter 5 treats the properties of polymers in terms of their intrinsic electrical behavior. The material in this chapter is also limited because only the case of the response of materials when subject to radiation of constant frequency (or wavelength) without gain or loss of energy to the system is discussed. The effect of varying frequency

because of its importance is described in a separate chapter on spectroscopy (Chapter 6). This chapter addresses primarily the topics of refraction and its offshoot, double refraction or birefringence, scattering phenomena including diffraction, light absorbance and fluorescence.

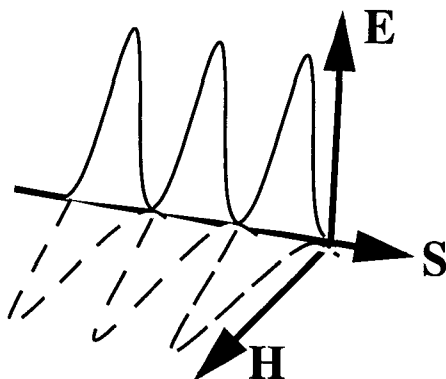


Figure 4.1. Diagram showing the relation between the magnetic and the electrical fields for plane polarized light.

4.2. Nature of Electromagnetic Waves

Electromagnetic radiation consists of simultaneous fields varying periodically with position and time. In free space, these fields act perpendicularly to each other and to the direction of propagation of the wave. The direction of polarization of the radiation is defined as being parallel to the electrical field. For unpolarized light, the polarization direction varies randomly about the propagation direction; while for plane polarized light, the field is restricted to a plane containing the propagation direction (Figure 4.1). For the interaction of the wave with matter, it is usually sufficient to consider only the effect of the electrical field. With circularly polarized light, the direction of polarization rotates about the propagation direction, either clockwise or counter clockwise in phase with the wave. It may be generated by two perpendicular plane polarized waves differing in phase by $1/4$ wavelength. The wavelength of the radiation is the distance between corresponding points on the wave.

The velocity of propagation (c) is the product of the wave length (λ) and the frequency (ν), the number of waves per unit time, or

$$c = \lambda\nu \quad (4.1)$$

c has a value of 3.00×10^8 m/s in free space. The electromagnetic spectrum covers a wide wavelength span from 10^{-10} m, the x-ray region, to $\approx 10^5$ m, the low frequency radio region. Visible light with wavelengths from roughly 300 nm (violet) to 800 nm (red) constitutes only a small fraction of the electromagnetic spectrum. When electromagnetic radiation impinges on matter, the radiation may follow one of several paths depending upon the wavelength and the material characteristics. It may be reemitted – the so-called elastic process – as scattered radiation. Scattering causes losses in transmitted energy, and in the limit of periodic structures and radiation with wavelengths of the same magnitude as the structural periodicity, leads to diffraction effects. The interaction of the radiation with molecules of the medium results in a decrease in the velocity of the waves leading to refraction phenomena. Finally, the molecule may absorb radiation. The absorbed energy may be transferred to other modes of motion and subsequently dissipated as heat. Another possibility is that part of the energy may be transferred to or from other modes and may be emitted as a photon of higher or lower frequency. If the transfer occurs with phonons, Brillouin lines result. Transfer between molecular energy levels leads to Raman lines. If the excited state is electronic, fluorescence occurs, or for high level states, phosphorescence. Energetic (x-ray or uv) photons can produce dissociation of chemical bonds leading to chemical reactions or may eject photoelectrons (XPS) [x-ray photoelectron spectroscopy] or ESCA [electron spectroscopy for chemical analysis]). Fluorescence is observed with the transfer of the residual energy to electronic modes; whereas, Raman scattering is associated with energy transfer to or from rotational or vibrational modes.

4.3. Refraction

The interaction between electrical fields and matter can be described in terms of polarizability (Chapter 5). The dipole moments induced in matter by electrical fields slow down wave propagation. The result of

polarizability on a macroscopic level is refraction. Electromagnetic radiation traversing a polarizable medium is slowed down from its velocity in vacuum, c , to a lower velocity in the material, v_m . The refractive index (η) is defined as the ratio

$$\eta = \frac{c}{v_m} \quad (4.2)$$

The frequency of propagation is constant and does not change between vacuum and the medium, so that, from equations 4.1 and 4.2,

$$\eta = \frac{c}{v_m} = \frac{v\lambda_0}{v\lambda} = \frac{\lambda_0}{\lambda} \quad (4.3)$$

where λ_0 is the wavelength in vacuum and λ , that in the medium. The refractive index for visible light is usually greater than one. For a typical polymer, η may be of the order of 1.5. Values less than one can be encountered with x-rays and neutrons.

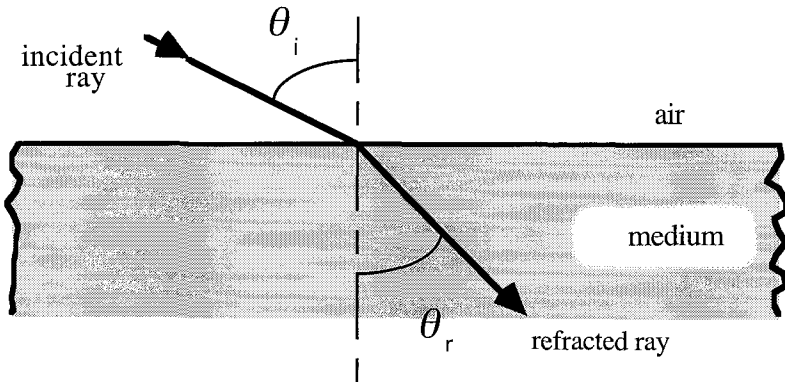


Figure 4.2. Relation between the angle of incidence and the angle of refraction
As is exemplified in Snell's Law.

The retardation or slowing down of electromagnetic radiation in passing through a medium results in bending of the rays at a planar boundary. This bending or changes in direction of the radiation rays can be used to measure η , from Snell's Law

$$\eta = \frac{\sin \theta_i}{\sin \theta_r} \quad (4.4)$$

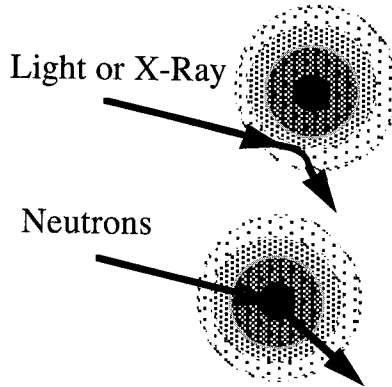


Figure 4.3. Diagrams showing that x-rays and light scattering involve extra-nuclear scattering, while neutron scattering depends on the nature of the atomic nucleus.

where θ_i is the incident angle and θ_r , the refraction angle (Figure 4.2). For light rays, the formation of an image in the optical microscope depends on this phenomenon. However, because x-rays are only slightly retarded in traversing a medium, the refractive index is so close to one that the amount of bending is small. Because of its low refractive index and absorption by most materials, no material analogous to glass in optical microscopy is available to refract x-rays. However, devices such as x-ray microscopes have been constructed by employing reflection optics or zone plates. Neutron radiation also shows the phenomenon of refraction although its origin differs from that of electromagnetic radiation. The neutron beam interacts with the nucleus (and not the extra nuclear electrons, (see Figure 4.3). Also, the scattering intensity of neutrons does not regularly increase with atomic number as occurs with x-rays or light, but varies in a more complex manner related to nuclear structure. The interaction of neutrons with matter is weak. This has advantages in that many materials are transparent to neutrons simplifying experimental design as well as exhibiting minimal background hazards.

On the other hand, since the low energy neutron radiation used for scattering is not ionizing, its detection is difficult. The fact that neutron radiation is usually not ionizing results in its being less of a biological hazard and presents less danger to the experimenter than x-rays do.

The refractive index is related to the polarizability per unit volume, P , by the Lorenz-Lorentz equation (Appendix 5B)

$$\frac{\eta^2 - 1}{\eta^2 + 2} = \left(\frac{4}{3}\right)\pi P \quad (4.5)$$

where $P = N\alpha$ = the polarizability per unit volume

$\alpha = m/E$ = the molecular polarizability

and

N = the number of molecules per unit volume

The P or polarizability term is that for the radiation of light wave frequencies and does not include contributions from dipole orientation as might happen at low frequencies.

In defining $\alpha = m/E$, one is assuming linear optics. In general,

$$M = \alpha E + \alpha' E^2 + \alpha'' E^3 + \dots \quad (4.6)$$

where α' and α'' are hyperpolarizabilities. At the low intensities of light we are considering, E is sufficiently small that the higher terms be neglected. At the higher intensities obtainable with lasers, E is sufficiently large that these terms must be considered, giving rise to the important area of non-linear optics described later in this Chapter (4.12).

In deriving this equation, the effect of the surroundings of a molecule (internal field) is taken into account by assuming that it resides within a spherical cavity (Lorenz field). This assumption can restrict the applicability of this equation. The macroscopic quantity, P , is related to the microscopic quantity, the molecular polarizability (assumed in this case to be isotropic so that α and P are scalar quantities)

$$P = \sum (\alpha_m)_i \quad (4.7)$$

where $(\alpha_m)_i$ is the molecular polarizability of the i^{th} molecule and the summation is carried out over all molecules in the unit volume. Equation 4.7 assumes that the molecule is located at the center of an isotropic

force field. For an anisotropic force field, the refractive index varies with the polarization direction. In this case, equation 4.6 can be applied to each direction using a different refractive index. The change in refractive index corresponding to small changes in polarizability can be found by differentiation,

$$\frac{6\eta d\eta}{(\eta^2 + 2)^2} = \left(\frac{4}{3}\right)\pi dp \quad (4.8)$$

Thus, for small refractive index differences,

$$\Delta\eta = \eta_1 - \eta_2 = \frac{2}{9}\pi \frac{(\langle\eta\rangle^2 + 2)^2}{(\langle\eta\rangle)} (P_1 - P_2) \quad (4.9)$$

where $\Delta\eta$ refers to the averaged value of η_1 and η_2 and $\Delta\eta$ is the birefringence. The equation becomes a poor approximation when $\Delta\eta$ is large or when higher order terms in ΔP are neglected. Equation 4.9 relates refractive index, birefringence and polarizability. It also shows that birefringence can be calculated from the polarizability difference. Details of this calculation are presented in Section 4.8.

4.4. Scattering

Light scattering and polarizability arise from fluctuations in refractive index associated with the outer electrons. X-ray scattering depends on fluctuations in electron density where all the electrons contribute equally. Thus, there are polarization effects in light scattering but not in x-ray scattering. Neutron scattering, by contrast, is related to fluctuations in neutron scattering wavelength usually related to fluctuations in the correlation of various isotropic species. The electrical field (E) from electromagnetic radiation incident upon an atom can be expressed as

$$E = E_0 \cos \omega t \quad (4.10)$$

where E_0 is the amplitude of the incident field and ω , the angular frequency ($2\pi\nu$). If the polarizability of the atom in an isotropic force field is given by α , a dipole moment, m , will be induced

$$m = \alpha E = E_0 \alpha \cos \omega t \quad (4.11)$$

This assumes that the frequency of the radiation is less than the resonant frequency so that the dipole vibrates in phase with the field. According to electromagnetic theory [1], this oscillating dipole will serve as a source of secondary radiation (scattering) of amplitude

$$E_s = \frac{1}{c^2 r} \frac{d^2 m_i}{dt^2} \cos \phi \quad (4.12)$$

where c is the velocity of light, (Figure 4.6) and r is the distance of the observer from the scatterer. The angle ψ is that between the dipole moment and the plane of the polarization seen by the observer.

Substituting equation 4.11 into 4.12 gives

$$E_s = -\frac{\alpha E_0 \omega^2}{c^2 r} \cos \psi \cos(\omega t) \quad (4.13)$$

for the electrical field amplitude at the scattering center, and

$$E_s = -\frac{\alpha E_0 \omega^2}{c^2 r} \cos \psi \cos(\omega t - \phi) \quad (4.14)$$

where ϕ is a phase angle which takes into account the distance, d , a wave must travel to reach the observer or

$$\phi = \frac{2\pi d}{\lambda} = \frac{\omega d}{c} \quad (4.15)$$

The distance, d , is measured from an arbitrary reference point and may include a portion of the distance traveled by the incident beam as well as by the scattered beam. These equations assume that the electric field at the scattering point is not modified on crossing dielectric boundaries. This assumption is referred to as the ‘‘Rayleigh-Gans approximation’’. Deviations from this assumption can be treated in simple cases such as in the Mie scattering from spheres.

Equation 4.14 was derived for the Rayleigh scattering case – the limit in which the frequency of the light is small compared to that of the resonance frequency of the electrons. For x-ray scattering, the frequency of the radiation is higher than resonance. In this limit, the case of Thomson scattering holds and

$$E_s = -\frac{q^2 \pi E_0}{m_0 c^2 r} \cos \psi \cos(\omega t - \phi) \quad (4.16)$$

where q is the electronic charge and m_0 the electronic mass. Thus, all electrons scatter x-rays equally, so that the x-ray scattering ability of an atom just depends on the number of electrons given by its atomic number, Z . At these high frequencies, the force on the electrons is largely a result of the momentum rather than the restoring forces arising from chemical bonding. This explains why x-scattering does not depend on the arrangement of chemical bonds, and hence, does not depend on orientation nor result in "x-ray birefringence". It should be noted that Thomson scattering is independent of frequency and polarizability while Rayleigh scattering is dependent on frequency and polarizability. Thus, more polarizable molecules (larger, conjugated, more aromatic) are better Rayleigh scatterers than others. The x-ray scattering ability of an atom just depends upon the number of electrons it possesses as given by its atomic number. Neutron scattering depends upon nuclear properties. Hence, hydrogen is a strong neutron scatterer although it is a weak electron scatterer. In both cases, the scattering equation may be compressed from a trigonometric form to a complex exponential form

$$(E_s)_j = K_j \exp[i(\omega t - \phi_j)] \quad (4.17)$$

where the subscript, j , refers to the scattering from the j^{th} object and K_j is proportional to the scattering power of the j^{th} scatterer. For a collection of scattering objects, the total field strength of the scattered waves is additive, or,

$$E_s = \sum (E_s)_j = E_0 \sum K_j \exp[i(\omega t - \phi_j)] \quad (4.18)$$

This expression is the basic equation in scattering theory for two reasons. First, all scattering phenomena (light, x-ray, and neutron) can be interpreted in terms of this equation. These techniques differ mainly in the structural entities that contribute to the K_j term. For light, as pointed out previously, the refractive index or polarizability is the principal contributor. For x-rays, the electron density is important, and, for neutrons, the nature of the scattering nucleus [2]. Secondly, equation

4.18 represents a starting point for the discussion of the interference problem presented below.

4.4.1. Intensity of Light Scattering for an Isolated Atom or Molecule

The intensity of light scattering for an isolated atom or molecule is proportional to the mean squared amplitude (product of the scattered intensity and its complex conjugate in complex exponential notation)

$$I_s = K \langle E_s^2 \rangle \quad (4.19)$$

where the proportionality constant, K , is equal to $c/4\pi$ for electromagnetic radiation and c is the speed of light. Combining equations 4.14 and 4.19,

$$I_s = K \frac{\alpha^2 E_0^2 \omega^4}{r^2 c^4} \cos \psi \langle \cos^2(\omega t - \phi) \rangle \quad (4.20)$$

The average is over all values of time. Thus, the relation

$$\langle \cos^2(\omega t - \phi) \rangle = \langle \cos^2 x \rangle = \frac{\int_0^{2\pi} \cos^2 x dx}{\int_0^{2\pi} dx} = \frac{1}{2} \quad (4.21)$$

holds, so that equation 4.20 can be simplified to

$$I_s = K \frac{\alpha^2 E_0^2 \omega^4}{2r^2 c^4} \cos^2 \psi \quad (4.22)$$

Since the incident intensity is given by

$$I_0 = K \langle E^2 \rangle = K E_0^2 \langle \cos^2 \omega \pi \rangle = \frac{1}{2} K E_0^2 \quad (4.23)$$

The ratio of the scattered to incident intensity is given by

$$\frac{I_s}{I_0} = \frac{\alpha^2 \omega^4}{c^4 r^2} \cos^2 \psi \quad (4.24)$$

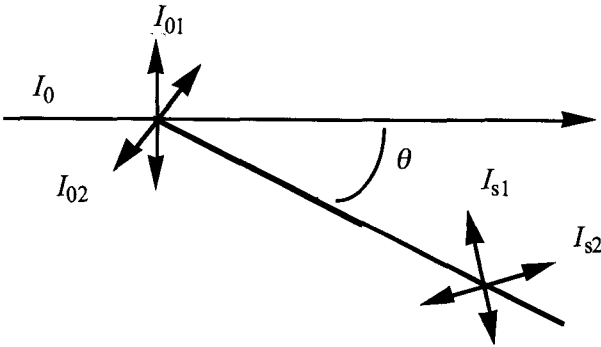


Figure 4.4. Resolution of a plane unpolarized incident beam into polarized components.

4.4.2. Effect of the Polarization of Light

Equation 4.24 is valid only for a plane polarized light beam. For unpolarized incident light, the beam is resolved into two polarized components at right angles to each other and to the transmitted light beam (Figure 4.4). The scattered intensity can thus be expressed as

$$I_s = I_{s1} + I_{s2} \quad (4.25)$$

or, on substituting equation 4.25 into 4.24

$$\frac{I_s}{I_0} = \frac{\alpha^2 \omega^4}{c^4 r^2} \frac{(\cos^2 \psi_1 + \cos^2 \psi_2)}{2} \quad (4.26)$$

From Figure 4.4, it can be seen that $\psi_1 = \theta$ and $\psi_2 = 0^\circ$ so that

$$\frac{I_s}{I_0} = \frac{\alpha^2 \omega^4}{c^4 r^2} \frac{(1 + \cos^2 \theta)}{2} \quad (4.27)$$

The frequency term may be converted to wavelength by means of the relations

$$\frac{\omega^4}{c^4} = \frac{16\pi^4 \nu^4}{c^4} = \frac{16\pi^4}{\lambda^4} \quad (4.28)$$

and on substituting in equation 4.26

$$\frac{I_s}{I_0} = \frac{8\pi^4 \alpha^2}{\lambda^4 r^4} (1 + \cos^2 \theta) \quad (4.29)$$

This equation states that:

(i) $I \approx 1/\lambda^4$ this relation states that shorter wavelengths scatter more than longer ones. Thus, if the incident light is white, the short wave lengths (blue) scatter more than the long ones (red). It should be noted that violet would be scattered even more strongly. However, the sky looks blue because the sensitivity of the eye decreases as one increases frequency in going from blue to violet. Therefore, the light from a clear sky is blue due to scattering by gas molecules in the atmosphere. Also, sunsets are red because the transmitted light from the sun that has passed through the atmosphere and has lost the higher frequency blue-violet component because of scattering. It also might be pointed out that Polaroid™ filters are useful for taking photographs of clouds, since they can make the polarized blue light from the sky appear dark, whereas the white light arising from scattering by the larger water droplets in the clouds is not (as will be discussed later) so its intensity is not reduced by the filter.

(ii) At $\theta = 0^\circ$ the scattering comprises both polarization components of the incident beam. At $\theta = 90^\circ$, the scattered light is one half as intense because it arises from only one component E_{01} . Consequently, the scattered light at 90° will be plane polarized [specifically vertically polarized with the electrical vector vibrating perpendicular to a plane defined by the directions of propagation of the incident beam and the scattered beam (Figure 4.4)] (Appendix 4A). The polarization of scattered light from the sky may be demonstrated by viewing the blue sky through Polaroid™ sunglasses. Complete polarization at 90° is only true if the scattering is from isotropic molecules. Actually, the atmosphere is composed of O_2 and N_2 molecules that are anisotropic leading to partial polarization as discussed later in this chapter.

4.4.3. The Scattering Intensity for a Collection of Scattering Objects

The amplitude of scattering from a collection of objects is found by summing the amplitudes from the components, taking phase differences into account. For random locations of such objects, phases will be

random. Then, intensities are additive. The result for N identical randomly oriented molecules (see equation 4B.10) is

$$\frac{I_s}{I_0} = \frac{8\pi^4 N \alpha^2}{\lambda^4 r^4} (1 + \cos^2 \theta) \quad (4.30)$$

is similar to equation 4.29 except for the inclusion of the term N . A modified form of equation 4.30 is conveniently used to express the scattering power of a system in terms of the "Rayleigh Ratio" defined as

$$R \equiv \frac{(I_s/I_0)r^2}{V_s(1 + \cos^2 \theta)} \quad (4.31)$$

where V_s is the scattering volume. In terms of the Rayleigh Ratio, equation 4.30 becomes

$$R = \frac{8\pi^4}{\lambda^4} \left(\frac{N}{V} \right) \frac{\alpha^2}{V_s(1 + \cos^2 \theta)} \quad (4.32)$$

It should be noted the R is independent of θ only if it is divided by the term $(1 + \cos^2 \theta)$ (for unpolarized light).

Thus, in this case, the scattering serves as a means for counting the number of molecules per unit volume (N/V). It is apparent that α is greater for larger molecules that scatter more. A simple theory for scattering of uniform spheres of radius R_s gives $\alpha = R_s^3$, so that R is proportional to the molecular radius or the molecular weight. It is of historical interest that this equation was used to estimate an approximate value of Avogadro's number from the scattering intensities of gases. One of first determinations was done by Raman's group [3].

The above treatment is valid for molecules that are small compared to the

$$E_s = k \frac{E_0 \omega^2}{c^2 r} \cos \psi \sum_j \alpha_j \cos(\omega t - \phi_j) \quad (4.33)$$

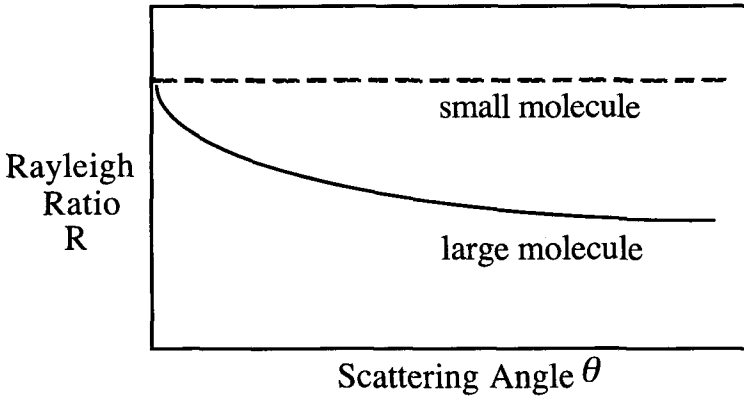


Figure 4.5. Variation of Rayleigh Ratio with scattering.

wavelength of the incident beam. Thus, in equation 4.16, the volume term was assumed to act as a point scattering source. The polarizability term α in equation 4.33 represents the total polarizability of the molecules in a volume element and it is assumed that all parts of a molecule are sufficiently close so that the spacing term d_j / λ may be taken as the same for all molecules. This leads to the prediction that the Rayleigh Ratio value is independent of the scattering angle θ (Figure 4.5). For molecules having dimensions comparable with the wavelength, phase differences will occur between waves scattered from different regions of the molecule. These phase differences result in an angularly dependent reduction in scattered intensity. This reduction may be expressed using of an interference factor $P(\theta)$ such that

$$(R - R_0) = (R - R_0)_0 P(\theta) \quad (4.34)$$

where $(R - R_0)_0$ is the Reduced Rayleigh ratio neglecting intramolecular effects and R_0 is the Rayleigh ratio of the solvent of a solution.

It follows, from this expression, that

$$P(\theta) = \frac{\left\langle \left[\sum_j \alpha_j \cos(\alpha\pi - \phi_j) \right]^2 \right\rangle}{\left\langle \left[\sum_j \alpha_j \cos \alpha\pi \right]^2 \right\rangle} \quad (4.35)$$

where the summation is over all parts of a molecule and $\langle \rangle$ denotes an average.

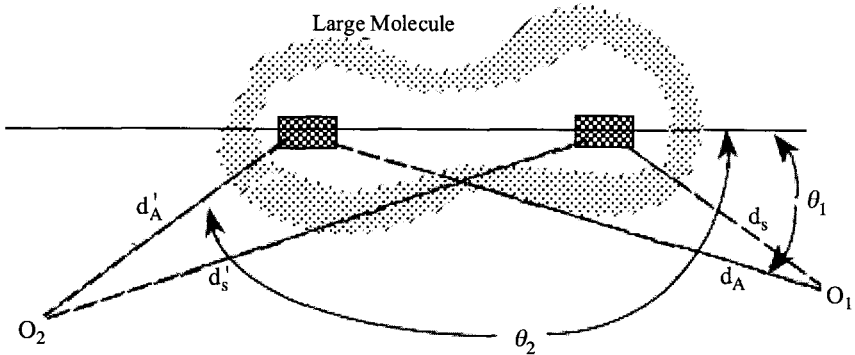


Figure 4.6. Variation of $P(\theta)$ with change in scattering.

The nature of $P(\theta)$ may be qualitatively deduced as follows. The diagram in Figure 4.6 shows that, for scattering in the forward direction at angle θ_1 , to 0, the path difference between the rays from elements A and B of the molecule ($d_B - d_A$) is less than that at the backward angle θ_2 to observer O₂, ($d_B - d_A$). So, a greater phase difference occurs at θ_2 , and if the dimensions of the molecule are something less than a wavelength, destructive interference occurs and $P(\theta) < 1$. If the molecular dimensions are much greater than a wavelength, destructive and constructive interference occur leading to maxima and minima in $P(\theta)$. These may be experimentally seen from samples in which the scattering objects are of uniform size with white light, the maxima and minima occur at different θ 's for different λ 's, so colors are seen. With a distribution of sizes, the maxima and minima occur at different θ 's, so they are "washed out". Thus, only a uniform drop in intensity with θ is usually observed. For $\theta = 0^\circ$, no path difference exists, ($d_B - d_A$), and $P(\theta) = 1$. Thus, this technique may be used to estimate size, since with increasing molecular size, the phase difference decreases more rapidly with increasing angle and therefore $P(\theta)$ decreases more rapidly with scattering angle (Figure 4.7).

Equation 4.16 gives the total amplitudes of scattering from a collection of objects and represents a logical starting point for an

exposition of interference phenomena associated with molecular size. From equation 4.12, an alternate form of equation 4.18

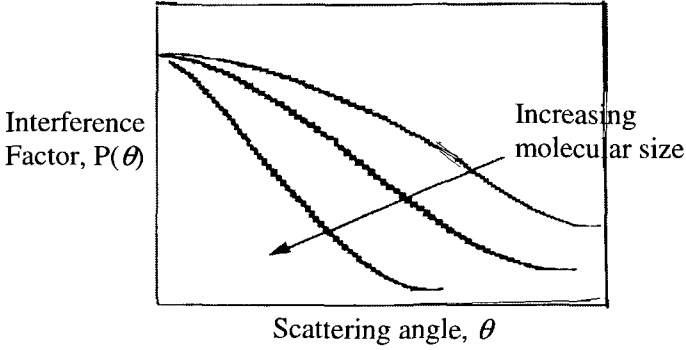


Figure 4.7. Angular variation of the interference factor $P(\theta)$ in different molecular sizes.

$$E_s = E_0 \sum_j K_j \exp[i\omega(t - [d_j/c])] = E_0 \sum_j K_j \exp[i\omega t] \exp[-i\omega d_j/c] \quad (4.36)$$

may be derived as follows.

From Figure 4.8, the following relations can be deduced

$$d_j = A + B \quad (4.37)$$

$$A = \mathbf{r}_j \cdot \mathbf{s}_0; \quad B = D - C; \quad C = \mathbf{r}_j \cdot \mathbf{s}_1 \quad (4.38)$$

Thus

$$d_j = \mathbf{r}_j \cdot \mathbf{s}_0 + D - \mathbf{r}_j \cdot \mathbf{s}_1 = D + \mathbf{r}_j \cdot (\mathbf{s}_0 - \mathbf{s}_1) = D + (\mathbf{r}_j \cdot \mathbf{s}) \quad (4.39)$$

where $\mathbf{s} = \mathbf{s}_0 - \mathbf{s}_1$ = the propagation or scattering vector

\mathbf{s}_0 = the unit vector in the incident ray direction

\mathbf{s}_1 = the unit vector in the scattered ray direction

\mathbf{r}_j = the vector to the j^{th} scattering element

On substituting the expression for d_j in equation 4.39 into equation 4.36

$$E_s = E_0 \exp[i\omega t] \exp[ikD] \sum_j A_j \exp[-ik(\mathbf{r}_j \cdot \mathbf{s})] = F \exp[i\omega t] \exp[ikD] \quad (4.40)$$

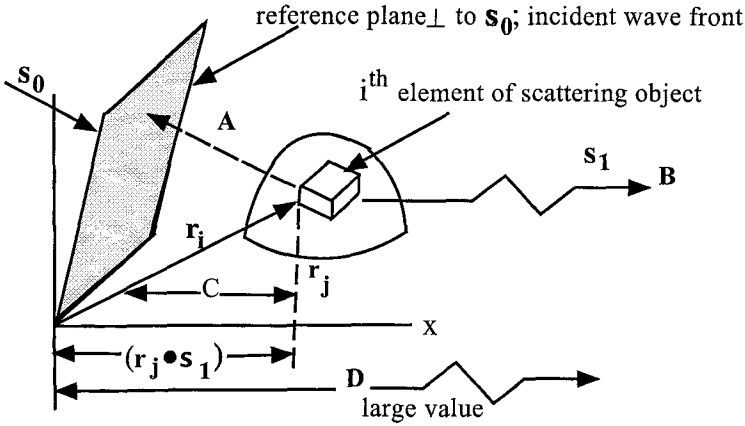


Figure 4.8. Relationships between vectors \mathbf{s}_1 and \mathbf{s}_0 and a scattering angle.

where $i = (-1)^{1/2}$ and $F = \sum_j A_j \exp[-ik(\mathbf{r}_j \cdot \mathbf{s})]$ is the structure or form factor for the object that is a characteristic of the object's geometry in calculating the form factor in terms of system geometry. As an example, consider F for a system composed of spherically symmetric scatterers.

For a medium regarded as a continuum consisting of an infinite number of infinitesimal elements, the summation in equation 4.40 may be replaced by an integral

$$F = \sum_j K_j \exp[-ik(\mathbf{r}_j \cdot \mathbf{s})] = \int_r \rho(\mathbf{r}) \exp[-ik(\mathbf{r}_j \cdot \mathbf{s})] d^3\mathbf{r} \quad (4.41)$$

where $\rho(\mathbf{r}) d\mathbf{r}$ is the amplitude scattered by a three dimensional element with a volume $d^3\rho$. In polar coordinates (Figure 4.9), this volume element becomes

$$d^3\mathbf{r} = r^2 \sin\psi dr d\psi d\phi \quad (4.42)$$

so that, on substituting in equation 4.41

$$F = \int_{x=0}^{\infty} \int_{\psi=0}^x \int_{\phi=0}^{2x} \rho(r, \psi, \phi) \exp[-ik(\mathbf{r}_j \cdot \mathbf{s}) \cos \psi] r^2 \sin \psi d\phi dr \quad (4.43)$$

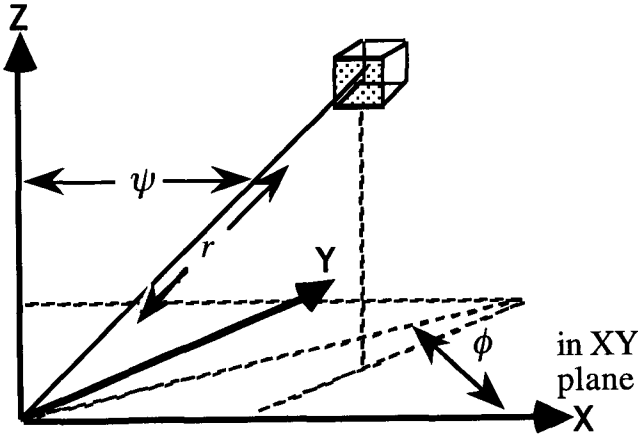


Figure 4.9. Polar coordinate system for locating the position of a scattering volume.

For spherically symmetric systems, $\rho(r, \psi, \phi)$ is independent of the angles ψ and ϕ so that

$$\rho(r, \psi, \phi) = \rho(r) \quad (4.44)$$

and from the definition of a dot product

$$\mathbf{r}_j \cdot \mathbf{s} = rs \cos u \quad (4.45)$$

where u is the angle between \mathbf{r} and \mathbf{s} . In the present case, we may rotate the coordinate system so that $u = \psi$ since, for a spherically symmetric system, this may be done without changing ρ and

$$F = \int_{x=0}^{\infty} \rho(r) \int_{\psi=0}^x \exp[-ik \cos \psi] \sin \psi d\psi \int_{\phi=0}^{2x} d\phi r^2 dr \quad (4.46)$$

Since

$$\int_{\phi=0}^{2\pi} d\phi r^2 dr = 2\pi \quad (4.47)$$

then

$$F = \int_{r=0}^{\infty} \rho(r) r^2 dr \int_{\psi=0}^{\pi} \exp[-ikr \cos \psi] \sin \psi d\psi \quad (4.48)$$

The second integral in equation 4.48 when integrated by parts yields

$$\begin{aligned} \int_{y=0}^{\pi} \exp[-ikr \cos y] \sin y dy &= -\frac{1}{a} \int_{-a}^a e^y dy = \frac{1}{a} e^y \Big|_{-a}^a \\ &= \frac{e^a - e^{-a}}{a} = \frac{e^{ihr} - e^{-ihr}}{ihr} \end{aligned} \quad (4.49)$$

Equation 4.49 may be simplified by noting that

$$\sin x = \frac{e^{ix} - e^{-ix}}{2i} \quad (4.50)$$

The expression for the form factor becomes,

$$F = 4\pi \int_{r=0}^{\infty} \rho(r) \frac{\sin qr}{qr} r^2 dr \quad (4.51)$$

where $q = \frac{4\pi}{\lambda} \sin \theta$

The interference factor described previously (equation 4.34) may be expressed in terms of the structure factor as

$$P(\theta) = \frac{\int_{x=0}^{\infty} \rho(r) \frac{\sin qr}{qr} r^2 dr}{\int_{x=0}^{\infty} \rho(r) r^2 dr} \quad (4.52)$$

Using the following approximations, the scattering from an isolated sphere may be calculated from equation 4.51. This derivation neglects the influence of the sphere surface in distorting the electrical field. This is valid provided the radius and scattering power are not too high (the Rayleigh-Gans-Debye approximation). Also, the derivation also assumes

the sphere be uniform, so that $\rho(r) = \rho_0$ and surrounded by non-scattering material so that $\rho(r) = 0$ if $r > R$. With these assumptions, equation 4.51 becomes

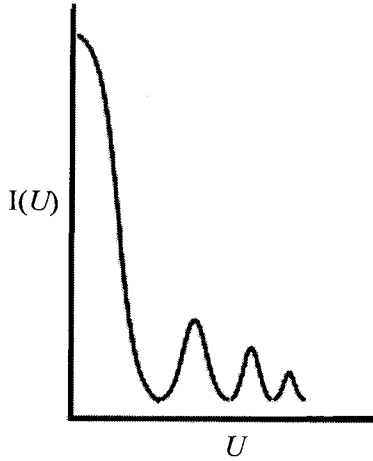


Figure 4.10. Sketch showing the dependence of $I(U)$ on U .

$$F_{sp} = 4\pi\rho_0 \int_{r=0}^R \frac{\sin qr}{qr} r^2 dr \quad (4.53)$$

Changing variables, $x = qhr$

$$F_{sp} = \frac{4\pi\rho_0}{q^3} \int_{x=0}^{qR} x \sin(x) dx \quad (4.54)$$

Integrating by parts gives

$$F_{sp} = \frac{4\pi\rho_0}{q^3} [\sin U - U \cos U] = V_{sp} \rho_0 \Phi(U) \quad (4.55)$$

where V_{sp} = the sphere volume

$$F(U) = \text{the sphere scattering function} = \frac{3}{U^3} [\sin U - U \cos U]$$

The sphere scattering function shows a damped response with maxima and minima (Figure 4.10). Equations 4.53 - 4.55 are valid if the sphere is surrounded by non-scattering material. For the case where the

sphere is surrounded by uniform scattering mattering of scattering amplitude, ρ_s , then the same equations would result except that instead of ρ_0 , the expression $(\rho_0 - \rho_s)$ would be substituted. Then the intensity depends on the contrast, $(\rho_0 - \rho_s)^2$. Thus, the scattering goes to zero when $\rho_s = \rho_0$ (contrast matching). This also illustrates the reciprocity principle where the scattering remains the same if the scattering powers of the medium and the surroundings are interchanged, so that spheres of a solid in a liquid scatter the same as spheres of liquid in a solid.

The parameter U is a measure of the scattering angle and depends upon the ratio of R to λ .

$$U = qR = 4\pi(R/\lambda)\sin(\theta/2) \quad (4.56)$$

Equation 4.56 also shows F is proportional to the sphere volume, V_{sp} or to R^3 so the intensity varies as R^6 . Thus, the scattered intensity increases greatly with sphere size, and if there is a distribution of sizes, the scattering is dominated by the larger ones. This dependence indicates why it is essential to remove larger dust particles when studying molecules by scattering techniques. A sphere 10X as large as another will scatter 1,000,000X as much.

4.5. Diffraction

Diffraction is a special case of scattering that arises when spacings are regular. The spacing between atoms in crystals is on the order of angstroms (10^{-10} m). The wavelengths of electrons, x-rays, and neutrons are in the same range.

The “wave-vector Bragg” equation describes diffraction phenomenon and can be derived using the reciprocal lattice approach as shown in the next section.

4.5.1. The Reciprocal Lattice

Consider a crystal unit cell (Figure 4.11) defined by the three lattice vectors, \mathbf{a}_1 , \mathbf{a}_2 and \mathbf{a}_3 (not necessarily orthogonal).

We shall also define a set of “unit” reciprocal lattice vectors, \mathbf{b}_1 , \mathbf{b}_2 and \mathbf{b}_3 by

$$\mathbf{b}_1 = \frac{\mathbf{a}_2 \times \mathbf{a}_3}{[\mathbf{a}_1 \mathbf{a}_2 \mathbf{a}_3]} \quad \mathbf{b}_2 = \frac{\mathbf{a}_3 \times \mathbf{a}_1}{[\mathbf{a}_1 \mathbf{a}_2 \mathbf{a}_3]} \quad \mathbf{b}_3 = \frac{\mathbf{a}_1 \times \mathbf{a}_2}{[\mathbf{a}_1 \mathbf{a}_2 \mathbf{a}_3]} \quad (3.57)$$

Here $[\mathbf{a}_1 \mathbf{a}_2 \mathbf{a}_3]$ is the “triple product” defined by

$$[\mathbf{a}_1 \mathbf{a}_2 \mathbf{a}_3] = (\mathbf{a}_1 \times \mathbf{a}_2) \cdot \mathbf{a}_3 = \mathbf{a}_1 \cdot (\mathbf{a}_2 \times \mathbf{a}_3) \quad (3.58)$$

and is the volume of the unit cell, V_u .

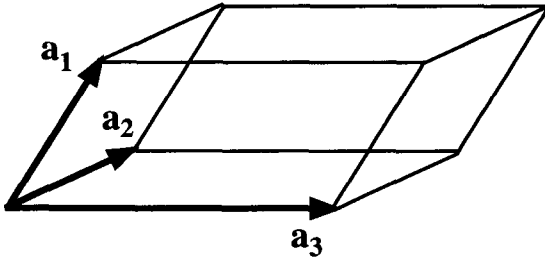


Figure 4.11 Diagram of a crystal cell defined by three lattice vectors.

Recall that $\mathbf{A} \cdot \mathbf{B} = AB \cos \theta_{AB}$ for a scalar product (Figure 4.12)

$$\mathbf{A} \times \mathbf{B} = AB \sin \theta_{AB} \mathbf{k} \quad (\text{for a vector product})$$

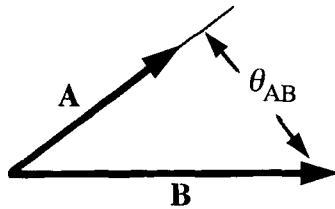


Figure 4.12. Diagram showing the angular relation between vectors \mathbf{A} and \mathbf{B} .

\mathbf{k} is a unit vector perpendicular to \mathbf{A} and \mathbf{B} and in the direction of a right handed screw rotating from \mathbf{A} to \mathbf{B}

Let us now define a “reciprocal lattice” vector, \mathbf{H} , by

$$\mathbf{H} = h_1 \mathbf{b}_1 + h_2 \mathbf{b}_2 + h_3 \mathbf{b}_3 \quad (4.59)$$

h_1 , h_2 and h_3 are integers called the “Miller Indices” (often designated h, k, l) whose nature will be described later and which describe the orientation of crystal planes.

Let us consider the scalar product $\mathbf{a}_1 \cdot \mathbf{H}$

$$\mathbf{H} = h_1 \mathbf{b}_1 + h_2 \mathbf{b}_2 + h_3 \mathbf{b}_3 \quad (4.60)$$

Consider the term

$$(\mathbf{a}_1 \cdot \mathbf{b}_1) = \mathbf{a}_1 \cdot \frac{\mathbf{a}_2 \times \mathbf{a}_3}{[\mathbf{a}_1 \mathbf{a}_2 \mathbf{a}_3]} = \frac{[\mathbf{a}_1 \mathbf{a}_2 \mathbf{a}_3]}{[\mathbf{a}_1 \mathbf{a}_2 \mathbf{a}_3]} = 1 \quad (4.61)$$

Similarly

$$(\mathbf{a}_2 \cdot \mathbf{b}_2) = (\mathbf{a}_3 \cdot \mathbf{b}_3) = 1 \quad (4.62)$$

It also follows that

$$(\mathbf{a}_1 \cdot \mathbf{b}_2) = \mathbf{a}_1 \cdot \frac{\mathbf{a}_3 \times \mathbf{a}_1}{[\mathbf{a}_1 \mathbf{a}_2 \mathbf{a}_3]} = 0 \quad (4.63)$$

since $(\mathbf{a}_3 \times \mathbf{a}_1)$ lies perpendicular to \mathbf{a}_1 so its dot product with \mathbf{a}_1 is zero.

By similar reasoning, it follows that

$$(\mathbf{a}_1 \cdot \mathbf{b}_3) = 0 \quad (4.64)$$

and in general

$$(\mathbf{a}_i \cdot \mathbf{b}_j) = \delta_{ij} \quad (4.65)$$

where δ_{ij} is the “Kronecker delta” defined by

$$\delta_{ij} = \begin{cases} \delta_{ij} = 1 & \text{if } i = j \\ \delta_{ij} = 0 & \text{if } i \neq j \end{cases} \quad (4.66)$$

Thus

$$\mathbf{a}_1 \cdot \mathbf{H} = h_1 \quad (4.67)$$

similarly

$$\mathbf{a}_2 \cdot \mathbf{H} = h_2 \quad (4.68)$$

and

$$\mathbf{a}_3 \cdot \mathbf{H} = h_3 \quad (4.69)$$

This may be compared with the modified equations for constructive interference for a three-dimensional crystal

$$\mathbf{a}_1 \cdot (\mathbf{s}/\lambda) = n_1$$

$$\mathbf{a}_2 \cdot (\mathbf{s}/\lambda) = n_2$$

$$\mathbf{a}_3 \cdot (\mathbf{s}/\lambda) = n_3$$

It is evident that these equations are of the same form and are identical if

$$\mathbf{H} = (\mathbf{s}/\lambda) \quad (4.70)$$

and

$$h_1, h_2, h_3 = n_1, n_2, n_3 \quad (4.71)$$

4.5.2. Interpretation of the Vector Bragg Equation

Equation 4.70 is referred as the “Vector Bragg Equation” which expresses the relationship between \mathbf{H} , a vector characterizing a crystal plane, and \mathbf{s} , a vector characterizing the scattering geometry, for constructive interference to occur. Such a vector equation implies two conditions:

The directions of \mathbf{H} and \mathbf{s} are the same.

Their magnitudes are equal

The first condition defines the orientation of a crystal necessary for diffraction to occur. The second condition leads to the conventional “scalar” Bragg equation,

$$n\lambda = 2d \sin \theta_B \quad (4.72)$$

where

n = the order of the diffraction

d = the distance between crystal planes, and

θ_B = the Bragg angle ($\theta/2$),

where θ is the scattering angle between the incident ray, s_0 and the scattered ray, s_1

This defines a set of θ 's corresponding to the set of d 's. We may now interpret the vector Bragg equation

$$\mathbf{H} = (\mathbf{s}/\lambda) \tag{4.73}$$

We see that the vector, \mathbf{H} , is perpendicular to the (h_1, h_2, h_3) crystal plane (Appendix 4C). It must be parallel to the vector, \mathbf{s} , whose nature we will now examine. From its definition

$$\mathbf{s} = \mathbf{s}_1 - \mathbf{s}_0 \tag{4.74}$$

Since \mathbf{H} is perpendicular to the crystal plane and \mathbf{H} is parallel to \mathbf{s} , \mathbf{s} must be perpendicular to the crystal plane. Therefore, triangles ABC and DBC (Figure 4.13) are congruent,

$$\theta_1 = \theta_2 = \theta/2 = \theta_B \tag{4.75}$$

Therefore, the Bragg diffraction angle θ_B is equal to one half the incident ray, s_0 , and the scattered ray, s_1 .

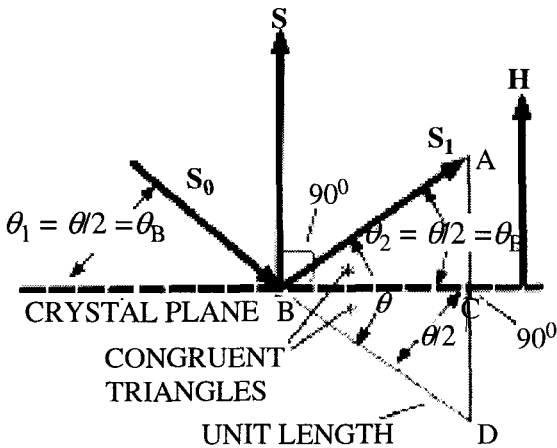


Figure 4.13. Relationships used in deriving the Vector Bragg equation.

4.5.3. The Distance Between Crystal Planes

Since, see Appendix 4D,

$$H = |\mathbf{H}| = 1/d \quad (4.76)$$

it follows that

$$1/d^2 = H^2 = \mathbf{H} \cdot \mathbf{H} \quad (4.77)$$

Now

$$\mathbf{H} = h_1 \mathbf{b}_1 + h_2 \mathbf{b}_2 + h_3 \mathbf{b}_3 = \sum h_i \mathbf{b}_i \quad (4.78)$$

so

$$1/d^2 = \sum_i \sum_j h_i h_j (\mathbf{b}_i \cdot \mathbf{b}_j) = \sum h_i^2 \mathbf{b}_i^2 + \sum_{i \neq j} \sum h_i h_j (\mathbf{b}_i \cdot \mathbf{b}_j) \quad (4.79)$$

Since the crystal system is specified by the \mathbf{a}_1 's and determines the \mathbf{b}_1 's, this permits the calculation of the d 's for any $(h_1 h_2 h_3)$ plane of a crystal.

Orthorhombic crystals have their axes perpendicular. Thus, since \mathbf{b}_1 is perpendicular to \mathbf{a}_2 and \mathbf{a}_3 , it will be parallel to \mathbf{a}_1 . Then \mathbf{b}_1 , \mathbf{b}_2 and \mathbf{b}_3 will be perpendicular to each other, so

$$(\mathbf{b}_i \cdot \mathbf{b}_j) = b_i b_j \delta_{ij} \quad (4.80)$$

where δ_{ij} = the Kronecker delta (equation 4.100)

Since, for an orthorhombic crystal,

$$\mathbf{b}_1 = \frac{\mathbf{a}_2 \times \mathbf{a}_3}{[\mathbf{a}_1 \mathbf{a}_2 \mathbf{a}_3]} = \frac{a_2 a_3}{a_1 a_2 a_3} (\mathbf{a}_1 / a_1) = (1/a_1) (\mathbf{a}_1 / a_1) \quad (4.81)$$

where (\mathbf{a}_1 / a_1) is a unit vector in the \mathbf{a}_1 direction. Thus

$$b_1 = (1/a_1) \quad (4.82)$$

Similarly,

$$b_2 = (1/a_2) \text{ and } b_3 = (1/a_3) \quad (4.83)$$

so

$$1/d^2 = \sum h_i^2 b_i^2 + \sum_{i \neq j} \sum h_i h_j (\mathbf{b}_i \cdot \mathbf{b}_j) \quad (4.84)$$

For the special case of a cubic crystal, $a_1 + a_2 + a_3 = a$, so

$$1/d^2 = (1/a^2) \sum_i h_i^2 \quad (4.85)$$

and

$$d = \frac{a}{\sqrt{h_1^2 + h_2^2 + h_3^2}} \quad (4.86)$$

4.5.4. The Diffraction Phenomenon in One Dimension

To illustrate the diffraction phenomenon in one dimension, consider a linear array of identical scattering objects separated by a distance, a . The sum over the atoms in equation 4.41

$$F = K \left[1 + e^{ik(\mathbf{a} \cdot \mathbf{s})} + e^{ik(2\mathbf{a} \cdot \mathbf{s})} + e^{ik(3\mathbf{a} \cdot \mathbf{s})} + \dots \right] \quad (4.87)$$

This equation predicts a maximum in scattering when the phase differences between waves scattered from the different particles are integral multiples of the wavelength.

$$k(\mathbf{a} \cdot \mathbf{s}) = n(2\pi) \quad (4.88)$$

since

$$\exp^{n(2\pi)} = 1$$

and the scattering from all the atoms will be in phase, or

$$\mathbf{a} \cdot \mathbf{s} = n\lambda \quad (4.89)$$

where n , the multiplicity factor, is an integer commonly termed the order of the diffracted ray. The scattering peak sharpens as the number of objects, N , in the linear array increases. For very large numbers, the peak is restricted to a small, angular range. On the other hand, the broadening of diffraction peak with a smaller number of objects provides a means for

the determination of crystal size. For smaller crystals, N is less and the diffraction peaks are broader.

An extension of this concept to three-dimensional crystals provides a means for measurement of crystal size from the width of diffraction peaks. Larger crystals lead to sharper peaks. The numerous sharp peaks observed at discrete angles for this scattering form a diffraction pattern. For radiation incident at an angle θ_2 to the array, the scattering angle θ_q (Figure 4.14) is given, from equation 4.89, by

$$a(\cos \theta_1 - \cos \theta_2) = n\lambda \quad (4.90)$$

Since

$$\mathbf{a} \cdot \mathbf{s} = \mathbf{a} \cdot [\mathbf{s}_1 - \mathbf{s}_2]$$

$$\mathbf{a} \cdot \mathbf{s}_1 - \mathbf{a} \cdot \mathbf{s}_2 = a(\cos \theta_1 - \cos \theta_2) \quad (4.91)$$

As illustrated in Figure 4.14, vectors for the two angles sweep out conic sections in three dimensions on rotation. The apices of the cones join at the diffracting surface. In addition, as shown in Figure 4.14, the intersection of the diffracting cones with a photographic film yields the characteristic x-ray diffraction pattern. In 2 or 3 dimensions, a corresponding equation must be obeyed in each direction, each defining a set of cones as the locus of constructive interference in that direction.

The condition for constructive interference in all dimensions is a set of the common intersection of these cones, defined by the simultaneous solution of the respective equations. Thus, the equations represent one form of the scattering conditions required for diffraction to occur in three dimensions

$$\mathbf{a} \cdot \mathbf{s} = 2a \sin \theta \cos \alpha = h\lambda$$

$$\mathbf{b} \cdot \mathbf{s} = 2b \sin \theta \cos \beta = k\lambda \quad (4.92)$$

$$\mathbf{c} \cdot \mathbf{s} = 2c \sin \theta \cos \gamma = \ell\lambda$$

where α , β and γ are the direction cosines of the vector \mathbf{s} , i.e., of the normal to the reflecting plane determined by the coordinate system \mathbf{a} , \mathbf{b} and \mathbf{c} . If $d(hkl)$ is the spacing of the lattice, then

$$d(hkl) = \frac{a}{h} \cos \alpha = \frac{b}{k} \cos \beta = \frac{c}{l} \cos \gamma \quad (4.93)$$

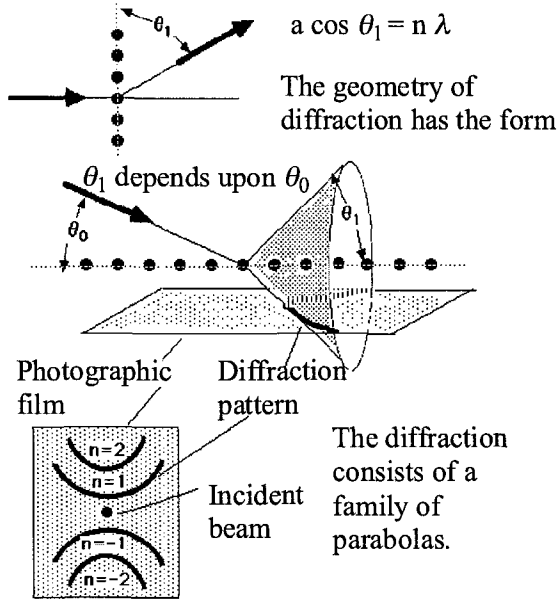


Figure 4.14 Diagram showing Bragg diffraction condition for one-dimension.

because the direction of s is normal to the reflecting plane. On substituting equation 4.83 into 4.92, the Bragg equation based on the reflection condition

$$2d(hkl) \sin \theta = n \lambda \quad (4.94)$$

for the diffraction of x-rays from a crystal lattice is obtained. The Bragg equation express the interference conditions that must be met simultaneously so that a maximum be observed with a three-dimensional periodic structure or diffraction grating.

Klug and Alexander [4], James [5] and Kakudo and Kasai [6] cover in monographs the spacing for different unit cells, the intensity, the application of the reciprocal lattice to the structural assignments, and other topics regarding diffraction.

This formalism also permits the calculation of diffracted intensities. We have seen (equation 4.40) that

$$F = \sum K_j \exp(\mathbf{q} \cdot \mathbf{r}_j) \quad (4.95)$$

and since

$$\mathbf{q} = k\mathbf{s} = \left(2\pi/\lambda\right)\lambda\mathbf{H} = 2\pi\mathbf{H} \quad (4.96)$$

and

$$\mathbf{r}_j = x_j\mathbf{a} + y_j\mathbf{b} + z_j\mathbf{c} \quad (4.97)$$

Then

$$\mathbf{q} \cdot \mathbf{r}_j = 2\pi\left[\mathbf{H} \cdot (x_j\mathbf{a}_1 + y_j\mathbf{a}_2 + z_j\mathbf{a}_3)\right] \quad (4.98)$$

but, for example

$$\mathbf{H} \cdot \mathbf{a}_1 = (h_1\mathbf{b}_1 + h_2\mathbf{b}_2 + h_3\mathbf{b}_3) \cdot \mathbf{a}_1 = h_1 \quad (4.99)$$

since

$$\mathbf{b}_i \cdot \mathbf{a}_j = \delta_{ij} \quad (4.100)$$

where δ_{ij} = the Kronecker delta.

The Kronecker delta has a value of 1 when i equals j and has a value of 0 when i is not equal to j .

Thus

$$\mathbf{q} \cdot \mathbf{r}_j = 2\pi(h_1x_{1j} + h_2x_{2j} + h_3x_{3j}) \quad (4.101)$$

and

$$F = \sum K_j \exp\left[2\pi i(h_1x_{1j} + h_2x_{2j} + h_3x_{3j})\right] \quad (4.102)$$

While the sum should be over the entire crystal, it is sufficient to carry it out over only a unit cell since the diffraction condition requires that rays from different unit cells be in phase. Thus, from knowledge of the location of atoms in a unit cell, the intensity of diffraction may be calculated.

4.6. Absorption

From a quantum mechanical viewpoint, absorption requires that the photon energy be equal to the difference between the energies of two states in the system, or

$$\hbar\nu = E_2 - E_1 \quad (4.103)$$

where \hbar is Planck's constant, E_1 and E_2 are the energies of the lower and the higher states and ν is the photon frequency. The classical mechanical equivalent of this is that the frequency of re-radiation corresponds to the resonance frequency of the electrons of the absorbing system. The energy level difference for absorption is greatest for x-rays where inner shell electrons are involved and decreases as the electromagnetic spectrum is traversed towards lower frequencies where transitions between energy levels involving outer electrons of the atoms take place. The energy in the infrared region is absorbed as molecular vibrations or rotations. Electronic resonances lead to absorption of x-rays (inner electrons), ultraviolet, or visible light while vibrational or rotational resonances in molecules result in absorption of infrared (from the near to the far) radiation.

The absorption can be characterized by a transition moment, i.e., a vector parallel to the direction of the polarization of the radiation that is absorbed. The transition moment intensity depends upon the symmetry of the electronic or molecular motion associated with the absorption process. Thus, for the vibrational motion of a diatomic molecule, the transition moment induced in the molecule is parallel to the molecular axis and only occurs when the two atoms are different and so possess a dipole moment. A polyatomic molecule, on the other hand, may absorb at several frequencies, each having a transition moment characteristic of a process involving a particular motion of a molecule. The electronic motions in the x-ray and ultraviolet regions couple directly or resonate with transition moments of the radiation.

The extinction coefficient, ϵ , of a material with thickness, l , is defined as

$$\epsilon = (1/l) \ln(I_0/I_t) \quad (4.104)$$

where I_t is the transmitted intensity and I_0 the incident intensity. This coefficient can be related to the extinction coefficient for a particular mode, a_i , with its associated transition moment by

$$\varepsilon_i = a_i \cos^2 \theta_i \quad (4.105)$$

where θ_i is the angle between the transition moment axis and the polarization direction of radiation (Figure 4.6).

For an isotropic body, the extinction coefficient is independent of the polarization direction of the incident radiation beam. However, for an oriented structure, the extinction coefficient depends on the polarization direction and three principal extinction coefficients ε_1 , ε_2 , ε_3 may be specified. For uniaxial orientation of the body, only two of these are independent. The dichroism, D , is the ratio of extinction coefficients associated with principal direction of absorption, viz.

$$D \equiv \frac{\varepsilon_1}{\varepsilon_2} \quad (4.106)$$

For uniaxial orientation, it may be shown that [7]

$$\frac{D-1}{D+2} = \frac{\langle 3\cos^2\theta - 1 \rangle}{2} = f_M \quad (4.107)$$

where f_M is the orientation function for the transition moment.

4.7. Fluorescence

As mentioned previously, absorbed radiation may be re-emitted at a different frequency because part of the energy from the incident beam transfers to other electronic or molecular states and the balance may be emitted as a photon of lower frequency. The change in energy for the photon is given by

$$\hbar(\nu_a - \nu_c) = \Delta E \quad (4.108)$$

where ν_a is the vibrational frequency and ν_c the emitted frequency. The intensity of the polarized fluorescent light for oriented systems depends upon both the orientation of the transition moments for absorption and for re-emission. If the absorbed radiation is polarized in the direction of

the unit vector \mathbf{P} and the emitted radiation is viewed with an analyzer transmitting radiation polarized along the unit vector \mathbf{A} , the intensity of the emitted light is [8]

$$I = K(\mathbf{M}_a \cdot \mathbf{P})^2 (\mathbf{M}_e \cdot \mathbf{A})^2 \quad (4.109)$$

where \mathbf{M}_a is the unit vector along the absorption transition direction, \mathbf{M}_e the unit vector along the emission transition moment direction (Figure 4.15) and K is proportionality constant. If the \mathbf{M} 's are parallel and \mathbf{P} and \mathbf{A} are parallel to each other, equation 4.101 reduces to

$$I_{11} = \langle K \cos^4 \theta_m \rangle \quad (4.110)$$

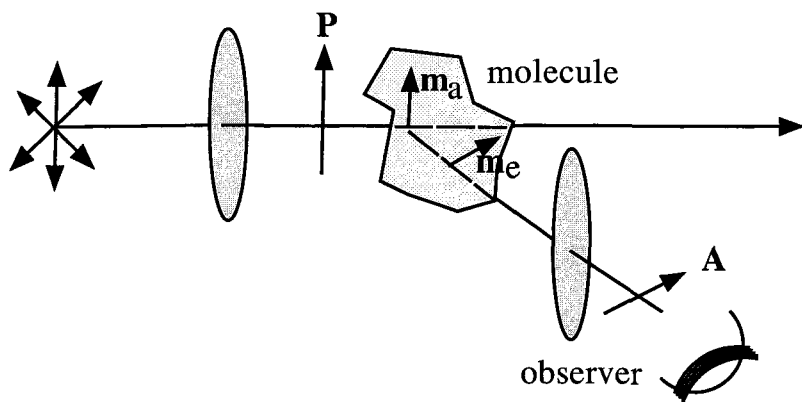


Figure 4.15 Diagram illustrating relationships between vectors in fluorescence and Raman scattering.

where θ_m is the angle between the common transition moment direction and the polarization direction. The condition that \mathbf{M}_a and \mathbf{M}_e be parallel requires that the molecule not move during the lifetime of the excited state. Examination as to whether or not this condition is met can provide information about dynamics. Thus, this component of fluorescence (also Raman scattering) depends upon the fourth moment of the orientation angle, in contrast to the second moment dependence found with birefringence and dichroism. Other polarized components of fluorescence depend upon both the second and fourth moments. Bower [9]

and Kimura and Desper [10] have presented general analyses of the relation between fluorescence and molecular orientation.

For fluorescence, the transition occurs between different energy states of the electrons. For Raman scattering, the transition involves molecular or rotational energy states so that the displacement of a Raman line from the incident frequency corresponds to the frequency of a molecular transition. Raman and infrared spectra cover transitions in the same spectral region of the electromagnetic spectrum, but the Raman measurements are made using visible light techniques. However, the selection rules or the requirements for absorption to occur differ for the two techniques. Infrared absorption requires the presence of a change in net dipole moment in the molecule whereas Raman scattering requires a change in molecular polarizability. The techniques are complementary because often functional groups in the same molecule fulfill only one of these requirements.

4.8. Birefringence

Birefringence techniques are capable of measuring the stress in materials. Brewster's Law states that the birefringence of a material is proportional to the stress applied to the material. The constant of proportionality calculated from Brewster's Law is termed the stress-optical coefficient (SOC) and is

$$SOC = \frac{\Delta\eta}{\sigma} = \frac{2\pi}{45kT} \frac{(\langle\eta\rangle^2 + 2)^2}{\langle\eta\rangle} (b_1 - b_2) \quad (4.111)$$

This equation predicts that the birefringence is directly proportional to the applied stress, inversely proportional to temperature and independent of the degree of crosslinking and elongation. Experiments [11–15] have confirmed these predictions. Brewster in 1816 first observed the proportionality that is the basis for the photoelastic analysis of structures. The stress-optical coefficient is expressed in units of Brewsters (10^{-13} cm²/dynes). The above theory is formulated in terms of the anisotropy ($b_1 - b_2$) – a property of the statistical segment that is a mathematical idealization of the real chain (Chapter 2). Work has been done in attempting to attach a molecular significance to this quantity.

This effort has tried to relate the statistical segment anisotropy $(b_1 - b_2)_s$ to the anisotropy of the monomer unit $(b_1 - b_2)_m$. The latter quantity is calculated from the assumption that bond polarizability tensors are additive. The number of monomer units in the statistical segment, Z_0 , may then be estimated from the relation

$$Z_0 = \frac{b_1 - b_2}{(b_1 - b_2)_m} \quad (4.112)$$

The parameter Z_0 is a measure of chain stiffness. In the statistical segment model, the greater the number of monomers in a segment, the fewer the segments for a given length and the stiffer the chain [16] (Chapter 2.6).

If one assumes a configuration for the monomer unit, one may calculate its polarizability using the relation analogous to equation 7.33

$$(b_1)_n = \sum_j \left[(b_1 - b_2)_j \cos^2 \theta_{ij} + (b_2)_j \right] \quad (4.113)$$

where $(b_1)_j$ and $(b_2)_j$ are the principal polarizabilities of the j^{th} bond that lie at an angle θ_{ij} with the i^{th} axis (Figure 4. 12). It is necessary, for this calculation to assume a reference monomer configuration that establishes the geometry for specifying the θ_{ij} angles. This equation of tensor additivity of polarizability assumes that each bond approximates the external field which is not modified by the arrangement of surrounding bonds (other than as described by the Lorenz field). The Lorenz field is based on a spherical cavity model that may not be appropriate. Bond polarizability values determined by independent techniques are also required. Different values are found depending upon the method of measurement. Values obtained from gas phase measurements [17] are often lower than those calculated from data on the refractive indices of crystalline solids [18]. Internal field effects [19] can account for this divergence. Values of $(b_1 - b_2)$ can also be obtained from streaming birefringence measurements and are in approximate agreement with those obtained from the stress optical coefficient measurements. These differences again may be understood by consideration of differences in the internal field. Expressions in terms of bond polarizabilities suffer in

that they do not consider the effect of one part of a molecule on another. Thus, this formalism predicts that the SOC for polyisobutylene is zero in contrast to the appreciable value found experimentally. There also have been attempts to calculate internal fields in crystals.

The difficulty arises from the assumption that all C-C bonds make an equivalent contribution to polarizability. In fact, the contribution of the bonds in the main chain differs from those of the CH₃ group. These errors are particularly serious in molecules with electron delocalization, where equal polarizability of main chain bonds to the side chain bonds is a poor approximation.

The idealization involved in the statistical segment model renders calculation of the anisotropy of polarizability difficult. Newer theoretical techniques avoid this problem by summing over bond polarizabilities directly using actual parameters such as bond angles and potentials opposing rotation about single bonds. Thus, in equation 4.114, the summation is taken over principal polarizabilities of bonds rather than statistical segments using the rotational isomeric state models of Flory (20-22) and Nagai (23,24) (Appendix 2F). For these calculations, the anisotropy of the segment is given by

$$(b_1 - b_2)_s = \frac{3}{2} \sum_{i=1}^n \frac{\langle \mathbf{r}^T \mathbf{a}_i \mathbf{r} \rangle}{\langle r^2 \rangle_0} \quad (4.114)$$

where \mathbf{r}^T is the transpose (i.e., the row form) of the end-to-end vector \mathbf{r} and \mathbf{a}_i is the traceless tensor representing the anisotropy of the polarizability associated with the group i of the chain. This is defined by the expression

$$\mathbf{a}_i = a_i - \mathbf{a}_i |\mathbf{E}| \quad (4.115)$$

where \mathbf{a}_i is the polarizability tensor a_i is the average scalar polarizability and $|\mathbf{E}|$ the identity matrix. The summation is taken over all groups in the chain. The symbol $\langle \rangle_0$ denotes averages over the free unperturbed chain. The sum is evaluated using matrix multiplication methods and is given by

$$\sum_{i=1}^n \langle \mathbf{r}^T a_i \mathbf{r} \rangle = 2Z^{-1} \sum_{i=1}^n |Q_i| \quad (4.116)$$

where Z is the conformational partition function evaluated by serial multiplication of the statistical weight matrices and $|Q_i|$ is the generator matrix [20, 21, 25]. The $|Q_i|$ term includes the structural data for group i , bond lengths, angles and rotational barriers as well as $@_i$ and U_i for group i .

The result of the evaluation for a polyethylene chain is

$$(b_1 - b_2)_s = A_{cc}(b_1 - b_2)_{cc} + A_{ch}(b_1 - b_2)_{ch} \quad (4.117)$$

For tetrahedral bonding, Smith and Mortensen [26] have shown that the ratio of A_{ch}/A_{cc} is equal to 2. For the actual values determined for a polyethylene chain of $\langle \text{CCC} = 112^\circ$ and $\langle \text{HCH} = 109.5^\circ$ and a carbon-carbon bond length of 0.153 nm, the value of A_{ch}/A_{cc} was 1.88 ± 0.02 [27] in good agreement with the value of 1.87 proposed by Nagai [23]. Thus, equation 4.147 may be expressed by

$$(b_1 - b_2) = A_{cc} \Gamma_{pm} \quad (4.118)$$

where Γ_{pm} is the effective anisotropy of the methylene group defined by

$$\Gamma_{pm} = (b_1 - b_2)_{cc} - 1.88(b_1 - b_2)_{ch} \quad (4.119)$$

The geometric factors are included in the quantity A_{cc} , whereas the values of bond anisotropy comprise Γ_{pm} . The statistical calculations made using weighing factors of the rotational isomeric states consistent with the chain dimensions yield a value of $A_{cc} = 4.0 \pm 0.6$. It is also possible to relate the variation of the stress-optical coefficient with temperature to the derivative $d(\ln A_{cc})/dT$ [equal to $-1.25 (\pm 0.25) \times 10^{-3} \text{K}^{-1}$ for a polymethylene chain]. By fitting data on cross linked polyethylene samples swollen with decalin (with volume fraction polymer of 0.33) for which $(b_1 - b_2)^3 = 4.0 \text{ \AA}^3$, a value of $1.0 (\pm 0.2) \text{ \AA}^3$ is found. It might be noted that this value of G_{pm} is roughly twice the value of $0.54 (\pm 0.05)$ as obtained from light scattering depolarization of n-alkanes in CCl_4 [28, 29]. The difference is probably because the polyethylene SOC measurements were made in a solvent that is not

isotropic (because of the difficulty in finding suitable solvents). It should be noted that in order to obtain molecular anisotropies from solid-state measurements that may be compared with theoretically calculated values, it is necessary that the solid be swollen with an isotropic solvent. An isotropic solvent separates chains from each other by decreasing the internal field anisotropy as well as disrupting “nematic ordering” which probably occurs in polymers that are not swollen with an isotropic solvent.

4.9. Scattering from Inhomogeneous Media

The basic expression for scattering from a collection of scattering objects (equation 4.18) is

$$E_s = e^{i\omega t} \sum K_j e^{i\phi} = e^{i\omega t} F \quad (4.120)$$

The structure of the scattering system determines the magnitude of F , termed the form factor.

The intensity of scattering obtained by taking the product of the field strength and complex conjugate is given by

$$I_s = \frac{c}{4\pi} E_s E_s^* = \frac{c}{4\pi} FF^* \quad (4.121)$$

where the asterisk represents the complex conjugate,

The central problem of describing the scattering from a system revolves around calculating the form factor in terms of the system geometry. Two approaches are taken in calculating: the model and the statistical approach.

The first uses a model of the scattering system to evaluate equation 4.121. This approach works best for a system composed of a dilute, randomly dispersed arrangement of discrete scattering particles that have a definite shape. Also, if the distribution of interparticle distance can be stated, interparticle interference effects can be included in this approach. The model approach is used in deriving equations 4.51 and 4.55. More specifically, this approach is the basis of the electron and the x-ray scattering techniques for determining the structure of small molecules. Van de Hulst [30] and Chu [31] have covered in detail the effects of

particle size, and of the refractive index difference between a particle and its surroundings.

The statistical approach is applied to systems that assume a continuum model with a large number of scattering objects that are not regularly arranged in space. In this case, the scattering can better be described in terms of fluctuations from uniformity. A perfectly homogeneous medium does not scatter light because destructive interference results in cancellation of scattered waves. This may be demonstrated geometrically in the following way. Consider two scattering elements, A and B, of a uniform medium (Figure 4.8). If A and B are identical, the scattered rays E_{SA} and E_{SB} , will have equal amplitudes. It is possible to choose the distance between A and B, d_{AB} , such that E_{SA} and E_{SB} , are 180° out of phase and thus at the location of the observer, the two rays will just cancel other. All pairs of volume elements (except for those within a layer near the walls of thickness comparable with the wavelength) may be paired in this way so that the total scattered amplitude may be shown to be zero.

For real media, the polarizabilities of A and B will not be the same and their scattered amplitudes will differ so that the cancellation will not be complete. Thus, the observed scattering from a condensed (solid or liquid) phase is a consequence of incomplete cancellation resulting from fluctuations in uniformity. With increasing fluctuations, the medium becomes more optically heterogeneous with a concomitant enhancement in scattering. Four kinds of fluctuations may occur:

- i.) Density fluctuations: there may be a different number of molecules in A and B.
- ii.) Concentration fluctuations: in a multicomponent medium, the composition of the molecules in A and B may differ.
- iii.) Orientation fluctuations: for anisotropic molecules, the average orientation of the molecules in elements A and B may differ resulting in a difference in their scattering ability. [Orientation fluctuations are discussed in detail in Appendix 4E.]
- iv.) Chirality fluctuations in the case of optically rotatory media where the rotation of the plane of polarized light may vary among volume elements.

A theory due to Einstein [32] that was later generalized by Debye [33] describing the scattering from a fluctuating medium. Debye and Bueche [34] later formulated the scattering for an isotropic medium having no macroscopic orientation. The deviation in scattering power, ρ_i , at position, \mathbf{r}_i from the average $\langle \rho \rangle$ was expressed in terms of the fluctuation η_i defined as

$$\eta_i = \rho_i - \langle \rho \rangle \quad (4.122)$$

The scattered intensity is then

$$I = K \sum_i \sum_j \rho_i \rho_j e^{ik(\mathbf{r}_i \cdot \boldsymbol{\sigma})} = K \iint \rho(r_i) \rho(r_j) e^{ik(\mathbf{r}_{ij} \cdot \boldsymbol{\sigma})} d^3 r_i d^3 r_j \quad (4.123)$$

in the approximation of a continuous medium where the scatterers are isotropic and the fluctuations are small enough so that the Rayleigh-Gans approximation may be employed. Here $\rho(r_i) d^3 r_i$ represents the scattering contribution from those elements included in the volume element $d^3 r_i$ (which is assumed to be small enough so that all elements scatter in phase). Then

$$\begin{aligned} I &= K \iint [\eta(r_j) - \langle \rho \rangle] [\eta(r_i) - \langle \rho \rangle] e^{ik(\mathbf{r}_i \cdot \boldsymbol{\sigma})} d^3 r_i d^3 r_j \\ I &= K \iint \eta(r_i) \eta(r_j) e^{ik(\mathbf{r}_i \cdot \boldsymbol{\sigma})} d^3 r_i d^3 r_j - \langle \rho \rangle \int \eta(r_i) e^{ik(\mathbf{r}_{ij} \cdot \boldsymbol{\sigma})} d^3 r_i d^3 r_j \\ &\quad - \langle \rho \rangle \int \eta(r_j) \exp^{ik(\mathbf{r}_{ij} \cdot \boldsymbol{\sigma})} d^3 r_i d^3 r_j + \langle \rho \rangle^2 \int \exp^{ik(\mathbf{r}_{ij} \cdot \boldsymbol{\sigma})} d^3 r_i d^3 r_j \end{aligned} \quad (4.124)$$

The last term is zero since this represents the scattering from a uniform medium. The second and third terms are also zero since these represent an average over the product of $\eta(r_i)$ (or $\eta(r_j)$) with $\exp[ik(\mathbf{r}_{ij} \cdot \boldsymbol{\sigma})]$. The four terms are positive or negative with equal probability in a manner not correlated with r_{ij} . Thus

$$I = K \iint \eta(r_i) \eta(r_j) \exp[ik(\mathbf{r}_{ij} \cdot \boldsymbol{\sigma})] d^3 r_i d^3 r_j \quad (4.125)$$

Now, for an unstructured medium, the average value of the product $\langle \eta(\mathbf{r})_i \eta(\mathbf{r})_j \rangle$ depends only on \mathbf{r}_{ij} and not individually on \mathbf{r}_i or on \mathbf{r}_j . Thus, the integration over \mathbf{r}_i and \mathbf{r}_j may be replaced by one over

$$\begin{aligned}
 I &= K \iint \langle \eta(\mathbf{r}_i) \eta(\mathbf{r}_j) \rangle_{ij} \exp^{ik(\mathbf{r}_{ij} \cdot \boldsymbol{\sigma})} d^3 \mathbf{r}_i d^3 \mathbf{r}_j \\
 I &= K \iint \langle \eta(\mathbf{r}_i) \eta(\mathbf{r}_j) \rangle_{ij} \exp^{ik(\mathbf{r}_{ij} \cdot \boldsymbol{\sigma})} d^3 \mathbf{r}_{ij} \int d^3 \mathbf{r}_i \\
 I &= KV \iint \langle \eta(\mathbf{r}_i) \eta(\mathbf{r}_j) \rangle_{ij} \exp^{ik(\mathbf{r}_{ij} \cdot \boldsymbol{\sigma})} d^3 \mathbf{r}_{ij} \quad (4.126)
 \end{aligned}$$

where V is the scattering volume of the sample given by

$$V = \int d^3 \mathbf{r}_i \quad (4.127)$$

One then introduces a correlation function defined as

$$\gamma(\mathbf{r})_{ij} = \frac{\langle \eta(\mathbf{r}_j) \eta(\mathbf{r}_i) \rangle_{r_{ij}}}{\langle \eta^2(\mathbf{r}_i) \rangle} \quad (4.128)$$

This function decreases from unity at $\mathbf{r}_{ij} = 0$ where $h(\mathbf{r}_i) = h(\mathbf{r}_j)$ to zero as $\mathbf{r}_{ij} \rightarrow \infty$, since in a medium not having long range structure, there will be no correlation between $h(\mathbf{r}_i)$ and $h(\mathbf{r}_j)$ when the volume elements are far apart. The rate at which $\gamma(\mathbf{r}_{ij})$ decreases with \mathbf{r}_{ij} characterizes the scattering entity.

Then

$$I = KV \langle \eta^2 \rangle \int \gamma(\mathbf{r}_{ij}) \exp[ik(\mathbf{r}_{ij} \cdot \boldsymbol{\sigma})] d^3 \mathbf{r}_{ij} \quad (4.129)$$

This is the three dimensional form of the Debye-Bueche equation which may be used to describe the scattering of oriented systems. For samples

having spherical symmetry, one may integrate over the angular coordinates of \mathbf{r}_{ij} to give

$$I = 4\pi KV \langle \eta^2 \rangle \int_{r=0}^{\infty} \gamma(r) \frac{\sin qr}{qr} r^2 dr \quad (4.130)$$

where $r = |\mathbf{r}_{ij}|$. Here the geometry of the system is described by the one-dimensional function, $\gamma(r)$.

For many systems, $\gamma(r)$ has a simple functional form

$$\gamma(r) = \exp(-r/a_c) \quad (4.131)$$

where a_c is a correlation distance equal to the average value of a_1, a_2 and a_3 (Figure 4.16). Debye, Anderson and Brumberger [35] show that this form may be derived for a random, two-phase system having sharp boundaries.

Equation 4.130 is the usual form of the Debye-Bueche equation. This equation generally describes the scattering from a spherically symmetrical system provided a suitable expression can be found for the correlation function. For many systems, an exponential correlation function is adequate

$$I = K' \langle \eta^2 \rangle \frac{a_c^3}{(1 + a_c^2 q^2)^2} \quad (4.132)$$

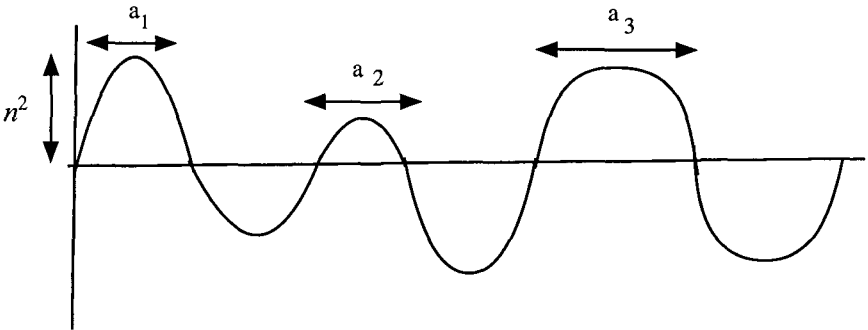


Figure 4.16 Idealized plot showing the fluctuation parameters n^2 and a_c .

In this case, a plot of $I^{-1/2}$ vs. q^2 should be linear with a slope/intercept = a_c^3 . The interpretation of a_c must be made using the approach of Porod [36] who showed

$$1/a_c = \phi_1 / \langle l_2 \rangle + \phi_2 / \langle l_1 \rangle \quad (4.133)$$

for a two-phase system in which ϕ_1 and ϕ_2 are the volume fractions. Here $\langle l_1 \rangle$ and $\langle l_2 \rangle$ are the average chord lengths of random lines drawn through the respective phases. When ϕ_2 is small, ϕ_1 approaches unity so $1/a_c = 1/l_2$ or $a_c = \langle l_1 \rangle$. In this case of dilute phase 2, a_c is a measure of its size, analogous to the measurement of the dimensions of molecules in dilute solution. When the phases are present in about equal amounts, where $\phi_1 = \phi_2 = 1/2$

$$1/l_c = 2 \left[1/\langle l_1 \rangle + 1/\langle l_2 \rangle \right] \quad (4.134)$$

so

$$l_c = 1/2 \left[\frac{\langle l_1 \rangle \langle l_2 \rangle}{\langle l_1 \rangle + \langle l_2 \rangle} \right] \quad (4.135)$$

in which case a_c represents a "harmonic average" phase size.

The quantity $\langle \eta^2 \rangle$ may also be readily interpreted for a two-phase system. It may be shown to be

$$\langle \eta^2 \rangle = \phi_1 \phi_2 (\rho_1 - \rho_2)^2 \quad (4.136)$$

where ρ_1 and ρ_2 represent the scattering power of the phases. This means the refractive index for the optical spectra or the polarizability for the electronic fields. It is evident that the intensity, proportional to $\langle \eta^2 \rangle$, passes through a maximum when $\phi_1 = \phi_2 = 1/2$.

The Debye-Bueche equation is more general than just for light scattering and applies also to x-ray and neutron scattering, but in these cases, the ρ 's and the K 's will be different.

The correlation function, $\gamma(r)$, may be generally be determined by the Fourier transform of $I(q)$

$$\gamma(r) = \frac{K''}{\langle \eta^2 \rangle} \int_{r=0}^{\infty} I(q) \frac{\sin qr}{qr} q^2 dq \quad (4.137)$$

While, mathematically, one should integrate over q from 0 to ∞ , this is not experimentally possible, since q cannot exceed the value of $q_{\max} = 4\pi/\lambda$ when $\sin(q/2) = 1$. The resulting error is referred to as a "termination error" which is often not too large.

At $r = 0$, $\gamma(r) = 1$ and $\sin(qr)/qr = 1$ so

$$\langle \eta^2 \rangle = K'' \int_0^{\infty} I(q) q^2 dq = K'' Q \quad (4.138)$$

The quantity, Q , is called the "invariant" or "total integral" and may be used as a means for m

Review articles cited [2,37] describe the application of scattering techniques to the elucidation of structural information on polymeric solids in more detail.

4.10. Quasi-elastic Light Scattering

The Raleigh scattering from a stationary object occurs at the same frequency as the incident light. However, just as the sound from a moving source is shifted upward or downward as frequency is shifted upward or downward depending upon whether it is moving towards or away from the observer, frequency shifts also occur from a moving scatterer. Thus, the frequency spectrum is broadened from a system undergoing Brownian motion by an amount dependent upon mobility; this phenomenon of "quasi-elastic light scattering" (QELS) provides a means of determining diffusion coefficients of molecules in solutions as well as mobility in emulsion bulk polymers. For example, there is an increase in the width of the frequency spectrum upon heating through the glass temperature as mobility increases. In favorable cases, translational

and rotational motion may be distinguished by observing polarization behavior.

Quasi-elastic techniques can also be applied to other types of scattering. For example, as facilitated by the spin echo technique, the method may be applied to neutron scattering to look at mobility of smaller regions at larger wavelength light. Isotropic labeling permits studies of motions of selected parts of molecules.

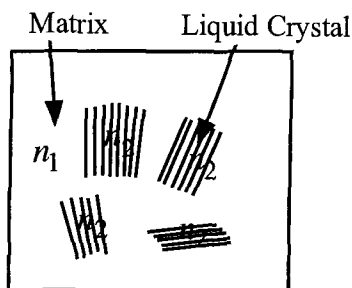


Figure 4.17. Sketch illustrating the mismatch between the refractive indices and the crystal orientation fluctuation.

4.11. Variation of Scattering with Electric Fields

The change in light scattering of conventional polymers with electric and magnetic fields is small. However, much larger effects may be obtained with liquid crystalline systems that have cooperative orientation. As with Kerr effect devices (see Section 4.14), more rapid orientation times desirable for display devices are obtained using low molecular weight or side chain polymer liquid crystals.

A way of combining the desirable mechanical properties of polymer with the rapid response times of low molecular weight liquid crystals is through use of polymer dispersed liquid crystals. These consist of droplets or domains of low molecular weight liquid crystals or a polymer matrix. In the absence of fields, these may be highly scattering as a consequence of both orientation fluctuations within the liquid crystal as well as refractive index mismatch between the liquid crystal and the matrix (Figure 4.17). With proper design, both sources of scattering may be reduced upon applying a field, which produces molecular orientation. A typical device may exhibit a light scattering change from 5% to 85%

upon application of a field. Since the orientation is usually produced through interaction with induced dipoles, alternating current voltages, often quite modest (10-50 volts) may be employed. The use of alternating current has the advantage in that with sufficiently high frequency, turbulence will not result because of conductivity of ionic impurities.

Turbulence can be employed to advantage in bistable switchable devices. The above devices require the electrical field to be on to remain transparent. However, with a properly designed smectic polymer - low molecular weight mixture, the orientation remains for a considerable time after a high frequency electrical pulse is applied. When a low frequency pulse is used, the ensuing conductivity produces turbulence, which brings the device back to a turbid state. Thus, the system is rendered transparent by a high frequency pulse and turbid by a low frequency pulse. It is not necessary to apply a voltage in the intervening time period.

4.12. Non-Linear Optics

The previous material in this chapter dealt with the linear response of the material to the electromagnetic field. As described by equation 4.5, for example, the electric field as measured by the polarizability (\mathbf{P}) induced in an atom is linearly related to the amplitude of the incident electric field amplitude (E) by proportionality constant, the polarizability (α). The advent of high intensity lasers giving radiation with high intensities leading to high electrical fields has increased the range of response in an atom beyond the linear range [37]. In addition, non-linear birefringences have also been observed.

The reason for frequency multiplication with non-linear optics may be seen from the realization that the amplitude of the scattered light is given by

$$E_s \approx \frac{d^2 n}{dt^2} \quad (4.139)$$

If

$$m = \alpha E + \beta E^2 + \gamma E^3 + \dots \quad (4.140)$$

and

$$E = E_0 e^{i\omega t} \quad (4.141)$$

then

$$\frac{dm}{dt} = E_0 \left[i\omega\alpha e^{i\omega t} + 2i\omega^2\beta e^{2i\omega t} + 3i\omega^3\gamma e^{3i\omega t} + \dots \right] \quad (4.142)$$

and

$$\frac{d^2m}{dt^2} = -E_0 \left[\omega^2\alpha e^{i\omega t} + 4\omega^2\beta e^{2i\omega t} + 9\omega^2\gamma e^{3i\omega t} + \dots \right] \quad (4.143)$$

Thus E_s will have components at double, 2ω , triple, 3ω , etc. of the incident frequency dependent upon the magnitudes of β and γ .

Materials with appreciable values of β leading to frequency doubling are called second-order Non Linear Optics (NLO) materials. Such materials lack a center of symmetry since the magnitude of the induced M is different for $+E$ and $-E$. Molecules of this sort typically have donor and acceptor groups on opposite sides of the molecule making it easier for electrons to move in one direction than the other. Of course, to be active, the molecule must be oriented. With polymers, this can be accomplished by “poling” where the material is subjected to an electric field above its glass temperature and been quenched with the field on so as to “freeze” the molecule in their ordered state.

Third order NLO materials are often molecules in which the electrons are delocalized as with conjugated molecules. It may be shown that as the size of the region of delocalization increases, γ increases more rapidly than α .

NLO materials find use in optical recording devices. To improve resolution, it is desirable to use higher frequency light. Frequency multiplication with NLO provides a means by which higher frequency light can be obtained from a laser.

NLO can also be used for optical switches. Since polarizability of NLO materials increases with field strength, refractive index also varies. Thus, as light intensity changes, an interface may pass from a transmitter to a totally reflecting regime, so one beam of light may be used to switch or modulate a second one.

Most materials with nonlinear optical (NLO) properties are inorganic such as lithium borate. Only a few low molecular weight organic compounds with nonlinear optical properties have been reported. Recently the preparation of a thermoset copolymer of 4-nitro-1,2-phenylenediamine (NPDA) and bisphenol-A diglycidyl ether (Bis-A) with NLO properties has been reported [38, 39, 40, 41]. This area overlaps with electrical effects in that pi charge conjugation along the chain backbone and non centro-symmetric separation of the positive and negative charges seem to be required to observe non linear behavior in polymers, The polysilane family [42] represents one specific polymer type that shows these characteristics and these chains exhibit non-linear optical behavior.

4.13. Piezo-Electric Materials

As with NLO materials, molecules with a permanent dipole moment may be “poled” by thermally exciting them through their glass temperature in an electrical field. Such materials with “frozen-in” dipole orientation have polarization charge on their surface. They may be distorted upon applying a voltage or, in turn, they generate a voltage upon distortion. Thus, they may serve as transducers.

Such poled materials are generally birefringent and birefringence will vary when an electric field is applied. Thus, when placed between crossed polarizers, the transmission of light will vary with applied voltage. With appropriate optics, the birefringence change can provide a means for rotating the direction of polarization with applied field.

Such “piezo-electric modulation” is useful for devices such as polarimeters and spectrometers where one wishes to study optical phenomenon as a function of polarization.

Piezo-electric polymers are often materials like the β form of poly(vinylidene fluoride) in which the unit cell has a residual dipole moment.

Chapter 5.4 contains additional material on piezo-electricity.

4.14. Kerr Effect

We have seen that molecules may be oriented in an electric field. If these molecules are anisotropic, such orientation produces birefringence. This is the Kerr effect. The orientation may occur because molecules have a permanent dipole moment, or else they may arise because of an anisotropic induced dipole moment with molecules having anisotropic polarizabilities.

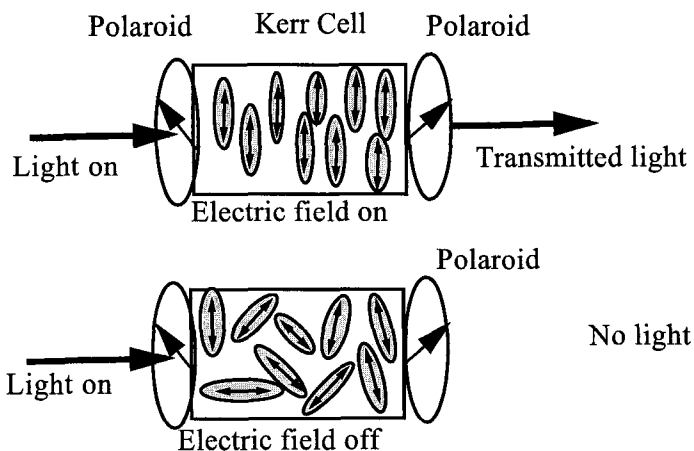


Figure 4.18. Sketch of Kerr Cell illustrating application as a light beam switch.

A Kerr cell can be used to switch or modulate a light beam by placing it between crossed polars (Figure 4.18). This effect finds use in electro optical devices.

Kerr effects can be very large with liquid crystalline systems where cooperative orientation can occur. This finds use in display devices. Generally, low molecular liquid crystals are employed because of their more rapid orientation times. However, polymers with liquid crystal forming side chains are sometimes used. The advantage of polymers is their mechanical integrity.

A similar phenomenon occurs with magnetic fields and is related to the anisotropy of magnetic susceptibility.

References

1. R.W. Ditchburn, *Light*, Interscience: New York, **1953** Appendix VII-B
2. J.S. Higgins, R.S. Stein, *J. Appl. Cryst.* **1978**, *11*, 346
3. C.V. Raman, *Indian J. Phys.*, **2**, *1*, (1927)
4. A.P. Klug, L.E. Alexander, *X-Ray Diffraction Procedures*; John Wiley: New York, **1954**
R.W. James, *The Optical Principles of the Diffraction of X-Rays*; G. Bell and Sons, Ltd: London, **1962**
6. M. Kakudo, N. Kasai, *X-Ray Diffraction of Polymers*; Elsevier: New York, **1972**
7. R.D.B. Fraser, *J. Chem. Phys.* **1953**, *21*, 1511
8. Y. Nishijima, Y. Onogi, T. Asai, *Rep. Prog. Polym. Phys. Jpn.* **1965**, *8*, 31
9. D.I. Bower, *J. Polymer Sci. Part A-2* **1972**, *10*, 2135
10. C.R. Desper, I. Kimura, *J. Appl. Phys.* **1967**, *38*, 4225
11. L.R.G. Treloar, *The Physics of Rubber Elasticity*, 3rd. Ed.; Oxford **1975**
12. A.N. Gent, V.V. Vickery, *J. Poly.Sci.Part A-2.* **1967**, *5*, 547
13. A.N. Gent, *Macromolecules.* **1969**, *2* 262
14. D.W. Saunders, *Trans. Faraday Soc.* **1956**, *52*, 1414
15. M. Fukuda, G.L. Wilkes, R.S. Stein, *J. Polymer Sci. Part A-2.* **1971**, *9*, 1417
16. R.S. Stein and R.J. Volungis, *J. Chem. Phys.*, **1955**, *23*, 1179
17. K.G. Denbigh, *Trans. Faraday Soc.* **1940**, *36*, 936
18. C.W. Bunn, R. deDaubeny, *Trans. Faraday Soc.* **1954**, *50*, 1173
19. R.S. Stein, *J. Polymer Sci. Part A-2.* **1969**, *7*, 1021
20. P.J. Flory, *Statistical Mechanics of Chain Molecules*; Interscience: New York, **1969**, Chapter IX
21. P.J. Flory, R.J. Jernigan, A.E. Tonelli, *J. Chem. Phys.* **1968**, *48*, 3822
22. M.H. Liberman, Y. Abe, P.J. Flory, *Macromolecules* **1972**, *5*, 550
23. K. Nagai, *J. Chem. Phys.* **1964**, *40*, 2818; *ibid.* **1968**, *49*, 421
24. K. Nagai and T. Isikawa, *J. Chem. Phys.* **1966**, *45*, 3128
25. P.J. Flory, *J. Chem. Phys.* **1972**, *56*, 826
26. R.P. Smith, E.M. Mortensen, *J. Chem. Phys.* **1960**, *32*, 502
27. Y. Abe, A.E. Tonelli, P.J. Flory, *Macromolecules.* **1970**, *3*, 294
28. G.D. Patterson, P.J. Flory, *J. Chem. Soc., Faraday Trans.* **1970**, *2*, 68
29. R.S. Stein, *Rubber Chem and Technol.* **1976**, *49*, 458
30. H.C. Van de Hulst, *Light Scattering by Small Particles*: Wiley: New York, **1957**
31. B. Chu, *Laser Light Scattering*, 2nd Ed., Academic Press, **1991**
32. A. Einstein, *Ann. d. Physik.* **1910**, *33*, 1275
33. P. Debye, *J. Appl. Phys.* **1944**, *15*, 338 ; *J. Phys. Colloid Chem.* **1947**, *51*, 18
34. P. Debye, A.M. Bueche, *J. Appl. Phys.* **1949**, *20*, 518
35. P. Debye, H.R. Anderson, H. Brumberger, *J. Appl. Phys.* **1957**, *28*, 679
36. G. Porod, *Z. Kolloid* **1952**, *125*, 51-122
37. P.N. Butcher, D. Cotter, *The Elements of Non-Linear Optics*, Cambridge: NY **1990**

OPTICS

38. M. Eich, B. Reck, D.Y. Yoon, C.G. Wilson, G.C. Bjorklund,
J. Appl. Phys., **1989**, 66(7), 1, 3241
39. D. Jungbaur, B. Reck, R. Tweig, D.Y. Yoon, C.G. Wilson, J.D. Swalen,
Appl. Phys. Lett. **1990**, 56(26), 2610
40. E. Infeld, G. Rowlands, *Nonlinear Waves, Solitons and Chaos*,
Cambridge:New York, **1990**
41. G.M. Carter, Y.I. Chen, M.F. Rubner, D.J. Sandman, M.K. Thakur, S.K. Tripathy,
Nonlinear Optical Properties of Organic Molecules and Crystals;
D. Chemla, J. Zyss, Eds., Academic: New York, **1987**, Vol. 2, pp. 85–120
42. R.D. Miller, J. Michl, *Chem. Rev.* **1989**, 89, 1359

Appendix 4A Depolarization of Scattering

The prediction that the scattering of vertically polarized incident light at $\theta = 90^\circ$ is completely vertically polarized is only true if the scatterer is isotropic and its polarizability is a scalar. In this case, the induced dipole will lie in the same direction (vertical) as the incident field. For anisotropic molecules, polarizability is a tensor, so the induced dipole is not necessarily vertical (Figure 4A.1).

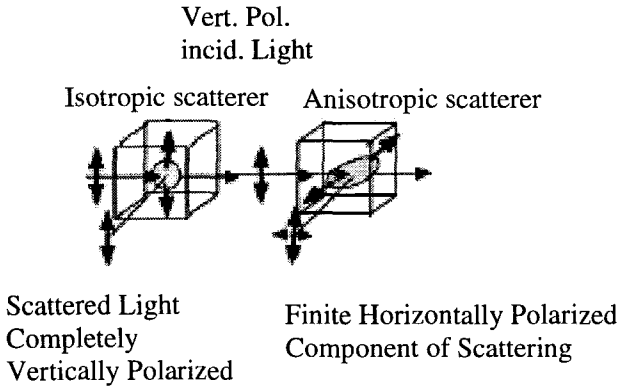


Figure 4A.1 Diagram illustrating depolarization of scattering

Let us consider the scattering from a molecule with its optic axis in the direction of the unit vector, \mathbf{a} , and with principal polarizabilities, α_1 and α_2 (Figure 4A.2).

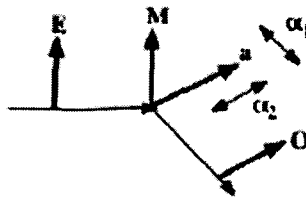


Figure 4A.2 Diagram relating terms in equation 4A.2

The induced dipole moment, \mathbf{M} , induced by the electrical field, \mathbf{E} , is

$$\mathbf{M} = \delta(\mathbf{a} \cdot \mathbf{E})\mathbf{a} + \alpha_2\mathbf{E} \quad (4A.1)$$

where δ is the (uniaxial) molecular anisotropy defined as

$$\delta = \alpha_1 - \alpha_2 \quad (4A.2)$$

From this equation for the induced dipole moment

$$\mathbf{M} = \delta(\mathbf{a} \cdot \mathbf{E})\mathbf{a} + \alpha_2 \mathbf{E} \quad (4A.3)$$

and the previously obtained equation for the scattered amplitude in the direction of \mathbf{M}

$$\mathbf{E}_s = \mathbf{E}_0 \frac{-\alpha \omega^2 \mathbf{E}_0 e^{j\omega t} \omega^2}{c^2 \mathbf{r}} \cos \psi \quad (4A.4)$$

We can obtain the result by replacing the polarizability, α , by the effective polarizability for the anisotropic system defined by

$$\alpha_{\text{eff}} = (\mathbf{M} \cdot \mathbf{O}) / \mathbf{E} \quad (4A.5)$$

so that insertion in the above equation gives

$$\mathbf{E}_s = \mathbf{E}_0 \frac{-[(\mathbf{M} \cdot \mathbf{O}) / \mathbf{E}]^2 \omega^2}{c^2 \mathbf{r}} \cos \psi \quad (4A.6)$$

Here, \mathbf{O} is a unit vector perpendicular to the direction of propagation of the scattered ray and in the direction of the electric field transmitted by an analyzing polarizer. For randomly oriented molecules, the Rayleigh factor becomes

$$R(\theta) = (\mathbf{N}/V_s) \left(\omega^4 / c^4 \right) \left\langle (\mathbf{M}_i \cdot \mathbf{O})^2 (\mathbf{M}_j \cdot \mathbf{O})^2 \right\rangle \quad (4A.7)$$

Let us consider the case of H_V polarization at a scattering angle, θ , of 90° . In this case

$$\mathbf{E} = E \mathbf{k}, \quad \mathbf{O} = \mathbf{i} \quad \text{and} \quad \cos^2 \psi = 1 \quad (4A.8)$$

Thus

$$R_H(90^\circ) = (\mathbf{N}/V_s) \left(\omega^4 / c^4 \right) \delta^2 \left\langle (\mathbf{a}_i \cdot \mathbf{k})(\mathbf{a}_j \cdot \mathbf{k})(\mathbf{a}_i \cdot \mathbf{i})(\mathbf{a}_j \cdot \mathbf{i}) \right\rangle \quad (4A.9)$$

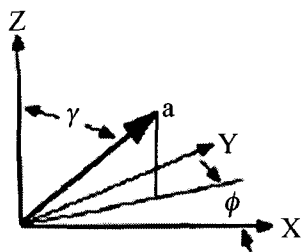


Figure 4A.3 Diagram showing the angular relations in deriving equation 4A.11

The unit vector, \mathbf{a} , may be described in terms of its angular coordinates, ϕ and γ , defined as

$$\langle (\mathbf{a}_i \cdot \mathbf{k})(\mathbf{a}_j \cdot \mathbf{k})(\mathbf{a}_i \cdot \mathbf{i})(\mathbf{a}_j \cdot \mathbf{i}) \rangle$$

$$= \langle \sin \gamma_i \cos \gamma_i \cos \phi_i \cdot \sin \gamma_j \cos \gamma_j \cos \phi_j \rangle = \langle \sin^2 \gamma_i \cos^2 \gamma_i \cos^2 \phi_i \rangle \quad (4A.10)$$

assuming that there is no correlation between the orientation of the i^{th} and the j^{th} scatterers. (The case of correlation will be considered later.) If there is no correlation between γ and ϕ and there is uniaxial orientation so all values of ϕ are equally probable,

$$\langle \sin^2 \gamma_i \cos^2 \gamma_i \cos^2 \phi_i \rangle = \langle \sin^2 \gamma_i \cos^2 \gamma_i \times \cos^2 \phi_i \rangle$$

$$= (1/2) \langle \sin^2 \gamma_i \cos^2 \gamma_i \rangle = (1/2) [\langle \cos^2 \gamma_i \rangle - \langle \cos^4 \gamma_i \rangle] = (1/2) [(1/3) - (1/5)] = 1/15 \quad (4A.11)$$

assuming random orientation in γ . Thus,

$$R_{H_v}(90^\circ) = (\mathbf{N}/\mathbf{V}_s)(\omega^4/\mathbf{c}^4)(1/15)\delta^2 \quad (4A.12)$$

For isotropic molecules, $\delta = 0$ and $\mathbf{R}_{H_v}(90^\circ) = 0$. A measure of $\mathbf{R}_{H_v}(90^\circ)$ serves to give δ^2 . If the molecules are polar and, for example, an electrical field tend to line up the molecules in the vertical direction, $\langle \cos^2 \gamma_i \rangle$ and $\langle \cos^4 \gamma_i \rangle$ can be calculated as before and will both approach unity so $\mathbf{R}_{H_v}(90^\circ)$ will approach zero.

Appendix 4B Scattering from a Collection of Molecules

For a collection of molecules, equation 4.14 must be generalized to give

$$E_s = \sum (F_s)_s = -\frac{E_0 \omega^2}{c^2 r} \cos \psi \sum_{i=1}^N \alpha_i \cos(\omega t - \phi_i) \quad (4B.1)$$

(It is assumed that all of the molecules are close enough together that the distance to the observer, r , may be taken as the same for all of them.)

On calculating the intensity of scattering from this equation, one obtains

$$(I_s/I_0) = (16\pi^4/\lambda^4 r^2) \left\langle \left[\sum_i \alpha_i \cos(\omega t - \phi_i) \right]^2 \right\rangle \quad (4B.2)$$

Now

$$\sum \alpha_i \cos(\omega t - \phi_i) = \sum \alpha_i [\cos \omega t \cos \phi_i + \sin \omega t \sin \phi_i] \quad (4B.3)$$

so

$$\langle \sin^2 \omega t \rangle = \langle \cos^2 \omega t \rangle = 1/2 \quad (4B.4)$$

and

$$\langle \sin \omega t \cos \omega t \rangle = 0 \quad (4B.5)$$

so

$$\begin{aligned} \left\langle \left[\sum \alpha_i \cos(\omega t - \phi_i) \right]^2 \right\rangle &= \frac{1}{2} \sum_i \sum_j \alpha_i \alpha_j [\cos \phi_i \cos \phi_j + \sin \phi_i \sin \phi_j] \\ &= \frac{1}{2} \sum_i \sum_j \alpha_i \alpha_j \cos(\phi_i - \phi_j) \end{aligned} \quad (4B.6)$$

But

$$\phi_i - \phi_j = \frac{2\pi}{\lambda} (d_i - d_j) = \frac{2\pi}{\lambda} d_{ij} \quad (4B.7)$$

so

$$(I_s/I_0) = \frac{8\pi^4}{\lambda^4 r^2} \left[\sum_i \sum_j \alpha_i \alpha_j \cos(2\pi d_{ij}/\lambda) \right] (1 + \cos^2 \theta) \quad (4B.8)$$

A special case of interest is where all molecules are identical and are randomly located. In this case $\alpha_i = \alpha_j = \alpha$ and the sum in equation 4.7 may be separated into two terms, one for which $i = j$ and the other for which $i \neq j$

$$\sum_i \sum_j \alpha_i \alpha_j \cos(2\pi d_{ij}/\lambda) = \sum_i \alpha_i^2 + \sum_{i \neq j} \cos(2\pi d_{ij}/\lambda) = N\alpha^2 \quad (4B.9)$$

Thus

$$(I_s/I_0) = \frac{8\pi^4 N\alpha^2}{\lambda^4 r^2} (1 + \cos^2 \theta) \quad (4B.10)$$

The scattering power of a system is conveniently expressed in terms of the "Rayleigh Ratio" defined as

$$R = \frac{(I_s/I_0)r^2}{V(1 + \cos^2 \theta)} \quad (4B.11)$$

where V is the volume of the scattering system. Thus,

$$R = \frac{8\pi^4}{\lambda^4} (N/V)\alpha^2 \quad (4B.12)$$

The molecular polarizability, α , may be related to the refractive index, η , by the Lorenz-Lorentz equation (Appendix 5B).

$$\frac{\eta^2 - 1}{\eta^2 + 1} = \frac{4}{3} \pi (N/V)\alpha \quad (4B.13)$$

For a dilute gas, $n \approx 1$, so $\eta^2 + 2 \approx 3$ and

$$\eta^2 - 1 = 4\pi(N/V)\alpha \quad (4B.14)$$

Using this value of $(N/V)\alpha$ in equation 4.B12 gives

OPTICS

$$R = \frac{(\eta^2 - 1)^2 \pi^2}{2\lambda^4 (N/V)} \quad (4B.15)$$

Now

$$\frac{N}{V} = \frac{\rho N_A}{M_2} \quad (4B.16)$$

where ρ is the density of the gas, $N_A = 6.02 \times 10^{23}$ and M_2 is the molecular weight of the gas molecules. Thus

$$R = \frac{(\eta^2 - 1)^2 \pi^2 M_2}{2\lambda^4 \rho_A} \quad (4B.17)$$

This equation applies to a gas where the molecules move about independently so that the second term of equation 4.09 is zero. It may be tested by measuring R for a gas of known refractive index. It has been used as a means of determining the value of Avogadro's number, N_A .

Appendix 4C The Nature of the Reciprocal Vector \mathbf{H}

The reciprocal lattice vector, \mathbf{H} , is defined by,

$$\mathbf{H} = h_1 \mathbf{b}_1 + h_2 \mathbf{b}_2 + h_3 \mathbf{b}_3 \quad (4C.1)$$

where h_1 , h_2 and h_3 are the Miller Indices of a plane. We shall show that \mathbf{H} is perpendicular to the plane. The Miller indices are defined as integers giving the reciprocal of the fraction of the unit lengths, \mathbf{a}_1 , \mathbf{a}_2 and \mathbf{a}_3 intercepted by the crystal plane closest to the origin. Thus, the plane with the index, h_1 , intercepts the \mathbf{a}_1 axis a distance a_1/h_1 from the origin.

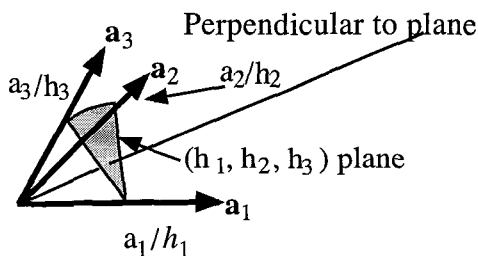


Figure 4C.1. Diagram showing the distance d from origin to crystal plane.

Consider a vector, \mathbf{P} , lying in the (h_1, h_2, h_3) plane,

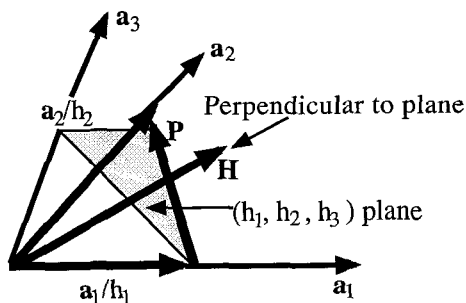


Figure 4C.2 . Sketch showing vector \mathbf{P} in the (h_1, h_2, h_3) plane.

This is given by

$$\mathbf{P} = (\mathbf{a}_1/h_1) - (\mathbf{a}_2/h_2) \quad (4C.2)$$

If \mathbf{H} is perpendicular to the plane, then \mathbf{H} and \mathbf{P} must be perpendicular and $\mathbf{H} \cdot \mathbf{P} = 0$. This is

$$\begin{aligned} & [h_1 \mathbf{b}_1 + h_2 \mathbf{b}_2 + h_3 \mathbf{b}_3] \cdot [(\mathbf{a}_1/h_1) - (\mathbf{a}_2/h_2)] \\ &= h_1 [(\mathbf{a}_1 \cdot \mathbf{b}_1)/h_1] - h_1 [(\mathbf{a}_2 \cdot \mathbf{b}_1)/h_1] \\ &+ h_2 [(\mathbf{a}_1 \cdot \mathbf{b}_2)/h_1] - h_1 [(\mathbf{a}_2 \cdot \mathbf{b}_2)/h_1] \\ &+ h_3 [(\mathbf{a}_1 \cdot \mathbf{b}_3)/h_1] - h_1 [(\mathbf{a}_2 \cdot \mathbf{b}_3)/h_1] \\ &= [1-0] + [0-1] + [0-0] = 0 \end{aligned} \quad (4C.3)$$

Thus, \mathbf{H} is perpendicular to the (h_1, h_2, h_3) plane.

Appendix 4D The Magnitude of the Reciprocal Vector H

The distance between crystal planes corresponds to the distance of the (h_1, h_2, h_3) plane from the origin.

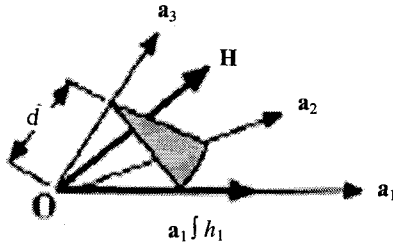


Figure 4D.1 Diagram showing the distance d from origin to crystal plane

where d = distance of plane from origin

Now the scalar product of two vectors, **A** and **B** is

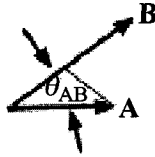


Figure 4D.2 Projection of vector **A** on vector **B**

$$\mathbf{A} \cdot \mathbf{B} = AB \cos \theta_{AB} \quad (4D.1)$$

This may be interpreted as the product of the magnitude of **B** with the projection of **A** on **B**. Since d is the projection of \mathbf{a}_1/h_1 on **H**,

It follows that

$$\begin{aligned} (\mathbf{a}_1/h_1) \cdot \mathbf{H} &= dH = (\mathbf{a}_1/h_1) \cdot [h_1 \mathbf{b}_1 + h_2 \mathbf{b}_2 + h_3 \mathbf{b}_3] \\ &= h_1 (\mathbf{a}_1 \cdot \mathbf{b}_1) / h_1 + 0 + 0 = 1 \end{aligned} \quad (4D.2)$$

so

$$dH = 1 \quad (4D.3)$$

and

$$H = 1/d = s/\lambda = 2\sin \theta_B$$

Appendix 4E Orientation Fluctuations

The equation for a system with orientation fluctuations

$$\mathbf{R}_H[q] = 4\pi K_L V \langle \delta^2 \rangle \int_0^\infty f(r) \frac{\sin qr}{qr} r^2 dr \quad (4E.1)$$

where

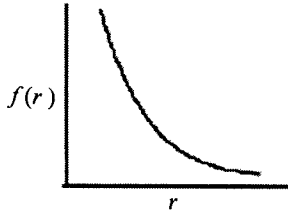


Figure 4E.1. Diagram showing exponential dependence of $f(r)$ on r .

$$f(r) = \frac{3 \langle \cos^2 \theta \rangle - 1}{2} \quad (4E.2)$$

involves the mean-squared anisotropy, $\langle \delta^2 \rangle$, of the scattering element and its correlation function in orientation, $f(r)$. $f(r)$ behaves in a similar manner to $\gamma(r)$. It represents the probability that two optic axes a distance, r , apart are parallel. As with $\gamma(r)$, an exponential orientation correlation function often suffices.

$$f(r) = e^{-r/a_0} \quad (4E.3)$$

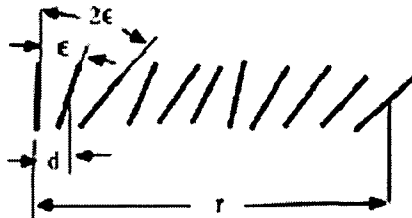


Figure 4E.2. Diagram illustrating the quantities used in deriving equation 4E.5.

A model for an exponential orientation correlation function has been proposed.

[R.S. Stein and S.N. Stidham, J. Appl. Phys. **35**, 42 (1964)]

This model involves a “random walk” in orientation and gives

$$\mathbf{a}_0 = \mathbf{d}/2\epsilon^2 \quad (4E.4)$$

For such a correlation function, a_0 , may be determined from a “Debye-Bueche type” plot. The orientation correlation function may be generally determined by Fourier inversion.

The theory also leads to an expression for the V_V intensity

$$\mathbf{R}_v[\mathbf{q}] = 4\pi K_L V \left[\langle (\Delta\rho_i)^2 \rangle \int_0^\infty \gamma(\mathbf{r}) \frac{\sin qr}{qr} \mathbf{r}^2 d\mathbf{r} + (4/45) \langle \delta^2 \rangle \int_0^\infty f(\mathbf{r}) \frac{\sin qr}{qr} \mathbf{r}^2 d\mathbf{r} \right] \quad (4E.5)$$

Thus, it is seen that the V_V scattering depends on both the orientation and the density fluctuations. By measuring both components of polarization, it is possible to separate the two contributions.

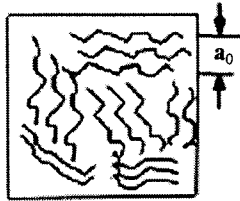


Figure 4E.3. Sketch showing the orientation correlation function model.

Some observations are:

For liquid crystalline polymers and volume, crystalline polymers, most of the scattering arises from orientation fluctuations.

For non-volume filling crystalline polymers, there is an appreciable contribution arising from the difference in scattering length of the crystalline and amorphous phases. This gives rise to a (V_V) scattering maximum during the course of crystallization.

The above theory predicts a cylindrically symmetrical scattering pattern (independent of μ). This is a consequence of the “random

orientation fluctuation" assumption made in its derivation where $f(r)$ depends only on the magnitude of \mathbf{r} and not upon the angle between \mathbf{r} and \mathbf{a} . The theory has been generalized.

[R.S. Stein, P.F. Erhardt, S.B. Clough and G. Adams,
J. Appl. Phys. **37**, 3980 (1966)]

Appendix 4F Scattering from Concentration Fluctuations

The concentration fluctuation contribution to the scattering from dilute solutions is given by

$$I_c(q) = K(\partial\alpha/\partial c)^2 \langle (\Delta c)^2 \rangle \quad (4F.1)$$

To calculate $\langle (\Delta c)^2 \rangle$, one proceeds as with density fluctuations to give

$$\langle (\Delta c)^2 \rangle = \int P(\Delta c) (\Delta c)^2 d(\Delta c) / \int P(\Delta c) d(\Delta c) \quad (4F.2)$$

where $P(\Delta c)$ is given by a Boltzmann distribution,

$$P(\Delta c) = C \exp[-w(\Delta c)] / kT \quad (4F.3)$$

where $w(\Delta c)$ is the work required to produce a concentration fluctuation, (Δc) .

The change in G involved in a concentration change may be given in terms of the chemical potential, μ .

$$\Delta G = \int \mu_1 d(\Delta n_1) \quad (4F.4)$$

where

$$\mu_1 = (\partial G / \partial n_1)_{P,T} \quad (4F.5)$$

where n_1 is the number of moles of solvent. Consider a volume element of size v ,

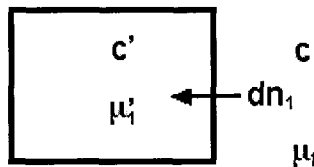


Figure 4F.1 .Change in chemical potential due to moment of solvent into the volume element.

If dn_1 moles of solvent move into the volume element where the chemical potential is n_1' from outside the volume element where the chemical potential is μ_1 , the change in free energy is

$$dG = \mu_1' dn_1 - \mu_1(-dn_1) \quad (4F.6)$$

Let x be the instantaneous value of n_1 which goes from n_1 to n_1' . Then $\Delta n_1 = n_1' - n_1$ so

$$\Delta G = \int dG = \int (\mu_1' - \mu_1) dx \quad (4F.7)$$

where the limits of integration are from $x = n_1$ to $x = n_1'$. Now, by expanding μ_1 in a power series in $(x - n_1)$ and neglecting higher terms small fluctuations, one obtains

$$\mu_1' = \mu_1 + (\partial\mu/\partial n_1)(x - n_1) \quad (4F.8)$$

giving

$$\Delta G = \int (\partial\mu/\partial n_1)(x - n_1) dx = (\partial\mu/\partial n_1) \int (x - n_1) dx \quad (4F.9)$$

assuming $(\partial\mu/\partial n_1)$ to be independent of concentration. This gives

$$\begin{aligned} \Delta G &= (\partial\mu/\partial n_1) \left[(x^2/2) - n_1 x \right]_{n_1}^{n_1'} \\ &= (\partial\mu/\partial n_1) \left[(n_1'^2/2) - n_1 n_1' - (n_1^2/2) - n_1^2 \right] \\ &= (1/2)(\partial\mu/\partial n_1) (n_1' - n_1)^2 = (1/2)(\partial\mu/\partial n_1) (\Delta n_1)^2 \end{aligned} \quad (4F.10)$$

It might be noted that this equation is analogous to that for the work for stretching a Hookean spring by an amount, ΔL , which is $(1/2)K\Delta L^2$ where K is the force constant of the spring. Here, $(\partial\mu/\partial n_1)$ is the effective "force constant" expressing the resistance of a solution to a concentration change.

Now, Δn may be related to Δc since c is given by

$$c = n_2 M_2 / v = n_2 M_2 / (n_1 V_1 + n_2 V_2) \cong n_2 M_2 / n_1 M_1 \quad (4F.11)$$

where n_2 and M_2 are the number of moles and molecular weight of the solute. V_1 and V_2 are the molar volumes of the two components. The approximation is valid in dilute solution where $n_1 V_1 \gg n_2 V_2$.

Then

$$\left(\frac{\partial c}{\partial n_1}\right) = -n_2 M_2 / V_1 n_1^2 = -c/n_1 = -cV_1/v \quad (4F.12)$$

Thus

$$(n_1)^2 = (v^2/c^2 V_1^2)(\Delta c)^2 \quad (4F.13)$$

Now

$$\left(\frac{\partial \mu_1}{\partial n_1}\right) = \left(\frac{\partial \mu_1}{\partial c}\right)\left(\frac{\partial c}{\partial n_1}\right) = -\left(\frac{\partial \mu_1}{\partial c}\right)(cV_1/v) \quad (4F.14)$$

so

$$\Delta G = -(N_A)/2 \left(\frac{\partial \mu_1}{\partial c}\right)(v/vV_1)(\Delta c)^2 \quad (4F.15)$$

Avogadro's number, N_A , is required in the above equation since ΔG is required in amount/mole. One notes that ΔG depends parabolically upon Δc and is the same for positive and negative fluctuations in concentration.

This result may then be substituted into the equation for $P(\Delta c)$ giving

$$\begin{aligned} P(\Delta c) &= C \exp\left\{-\left(N_A/2RT\right)\left[-\left(\frac{\partial \mu_1}{\partial c}\right)\right](v/cV)(\Delta c)^2\right\} \\ &= C \exp(-ay^2) \end{aligned} \quad (4F.16)$$

where $y = (\Delta c)$ and

$$a = \left(N_A/2RT\right)\left[-\left(\frac{\partial \mu_1}{\partial c}\right)\right](v/cV) \quad (4F.17)$$

This leads to

$$\left\langle(\Delta c)^2\right\rangle = (1/2a) = RTcV/\left[-\left(\frac{\partial \mu_1}{\partial c}\right)\right]vN_A \quad (4F.18)$$

It is noted that $\left\langle(\Delta c)^2\right\rangle$ varies inversely with v , the size of the volume element. The smaller the volume element, the bigger the fluctuation.

Evaluation of $(\partial\alpha/\partial c)$

In the derivation of the Lorenz-Lorentz equation, we showed that

$$\eta^2 - 1 = 4\pi K_i P = 4\pi K_i \alpha / \nu \quad (4F.19)$$

where η is the refractive index N , the number of molecules per unit volume and K_i , the internal field factor that we found, for a spherical cavity is

$$K_i = E_{int}/E_{appl} = (\eta^2 + 2)/3 \quad (4F.20)$$

P is the polarization per unit volume and α is the polarizability of the volume element of volume, ν .

Then

$$2\eta(\partial\eta/\partial c) = 4\pi K_i(\partial\alpha/\partial c)/\nu \quad (4F.21)$$

We are assuming that the internal field does not fluctuate. On substituting into the equation for $I_c(q)$, one obtains

$$I_c(q) = K(1/\nu)(\nu/2\pi K_i)\eta^2(\partial\eta/\partial c)^2 RTcV/\{N_A[-(\partial\mu_1/\partial c)]\} \quad (4F.21)$$

The constant, K , may be evaluated referring to the electromagnetic of scattering. If the scattering is measured in units of the "Rayleigh Ratio", R , defined as

$$R_c(q) = I_c(q)/I_0 V_s \quad (4F.22)$$

where I_0 is the incident intensity and V_s is the scattering volume. Then

$$R_c(q) = 2\pi^2\eta^2(\partial\eta/\partial c)^2 RTcV_1/\{\lambda^4[-(\partial\mu_1/\partial c)]\} \quad (4F.23)$$

Evaluation of $[-(\partial\mu_1/\partial c)]$

The chemical potential, μ , may be related to the osmotic pressure, Π , by (Appendix 3C)

$$\Pi = (\mu_{10} - \mu_1)/V_1 \quad (4F.24)$$

where μ_{10} is the chemical potential of the solvent. Thus

$$\left(\frac{\partial \Pi}{\partial c}\right) = -\left(\frac{1}{V_1}\right)\left(\frac{\partial \mu_1}{\partial c}\right) \quad (4F.25)$$

Therefore, light scattering can provide information about osmotic pressure (without the need of having a membrane). The osmotic pressure varies with concentration according to

$$\Pi = cRT\left[\left(1/M_2\right) + A_2c + \dots\right] \quad (4F.26)$$

where M is the molecular weight of the solute and A_2 is the second virial coefficient expressing the deviation from ideality. For an ideal solution, this reduces to van Hoff's equation.

$$\Pi = cRT/M_2 \quad (4F.27)$$

conventionally used to determine the molecular weight of low MW species from osmotic pressure. It is noted that the higher the molecular weight, the fewer the number of molecules and the lower the osmotic pressure. The precision becomes too low for practical use for molecular weights greater than about 10,000.

By differentiating equation,

$$\left[-\left(\frac{\partial \mu_1}{\partial c}\right)\right] = V_1RT\left[\left(1/M_2\right) + 2A_2c + \dots\right] \quad (4F.28)$$

The result may then be used in the equation for light scattering.

Molecular Weight from Light Scattering

On using the above result for the chemical potential change, one obtains

$$R_c(q) = Hc/\left[\left(1/M_2\right) + 2A_2c + \dots\right] \quad (4F.29)$$

This gives for ideal solutions,

$$R_c(q) = HcM_2 \quad (4F.30)$$

It is evident that the scattering arising from concentration fluctuations increases with concentration, and, in contrast to osmotic pressure, increases with molecular weight. Hence, it is a good technique for studying polymers.

This equation can be used to explain the average molecular weight obtained by light scattering. For a multicomponent mixture, the above equation generalizes to

$$R_c(q) = H \sum c(M_2)_i \quad (4F.31)$$

where the sum is over all molecular weight species present. The “average molecular weight” obtained from light scattering $\langle M_{LS} \rangle$ is

$$R_c(q) = Hc \langle M_{LS} \rangle \quad (4F.32)$$

where c is the total concentration

$$c = \sum c_i \quad (4F.33)$$

Thus,

$$\langle M_{LS} \rangle = \frac{\sum c_i M_i}{\sum c_i} = \frac{\sum \eta_i M_i^2}{\sum \eta_i M_i} \quad (4F.34)$$

This is a weight average molecular weight, $\langle M_w \rangle$, which might be contrasted with a number average, $\langle M_n \rangle$, (obtained from osmotic pressure) defined as

$$\langle M \rangle = \frac{\sum n_i M_i}{\sum n_i} \quad (4F.35)$$

Upon rearranging, the equation, it becomes

$$Hc/R_c(q) = (1/M_2) + 2A_2c + \dots \quad (4F.36)$$

Thus, a plot of $Hc/R_c(q)$ versus c has an intercept of $(1/M_2)$ and a slope of $2A_2$ (twice the slope of a corresponding osmotic pressure plot).

To use this method, one must obtain the value of H . This requires:

1. That absolute intensity be measured. The apparatus must be calibrated.
2. The value of $(\partial n / \partial c)$ be known. This is relatively independent of molecular weight and primarily depends upon the chemical nature of the polymer and the solvent. For known/solvent pairs, values may be found in the literature. Otherwise, it can be

obtained from the slope of a plot of refractive index versus concentration, or else, directly, using a differential refractometer.

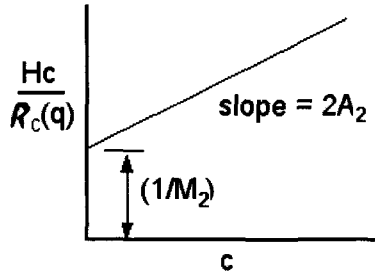


Figure 4F.3. Plot of $HC/R_c(q)$ against c .

This consideration is valid for small molecules where the assumption that there is no correlation among fluctuations of nearby volume elements is valid. Such correlation lead to interference among scattered rays from different parts of large molecules causing a decrease in scattered intensity with increasing scattering angle. The effect of this discussed in the next section.

Dealing with Large Molecules

We used the result in the above discussion that

$$I(q) = K \langle (\Delta A)^2 \rangle \quad (4F.37)$$

which a special case of the more general equation

$$I(q) = K \langle (\Delta A)_i (\Delta A)_j \rangle = K \langle (\Delta A)^2 \rangle P(q) \quad (4F.38)$$

where, for spherical symmetry

$$P(q) = \int \gamma(r) [\sin(qr)/qr] r^2 dr \quad (4F.39)$$

giving, at small q in the Guinier approximation,

$$P(q) = 1 + \langle R_g^2 \rangle / 3q^2 + \dots \quad (4F.40)$$

Obviously, at sufficiently small $\langle R_g^2 \rangle$, this approaches unity. For larger $\langle R_g^2 \rangle$, it approaches unity as $q \rightarrow 0$. A problem is whether one can collect data at sufficiently small $q = (4\pi/\lambda)\sin(\theta/2)$ to reach this limit.

Smaller q 's can be reached by going to smaller θ 's or larger λ 's.

Thus, in dealing with large molecules, it is necessary to extrapolate data to $q = 0$ to correct for this intermolecular interference effect. To get the proper molecular weight from a $Hc/R(q)$ plot, one must carry out a "double extrapolation", both to $c \rightarrow 0$ and $q \rightarrow 0$. One way of doing this is by a "Zimm Plot".

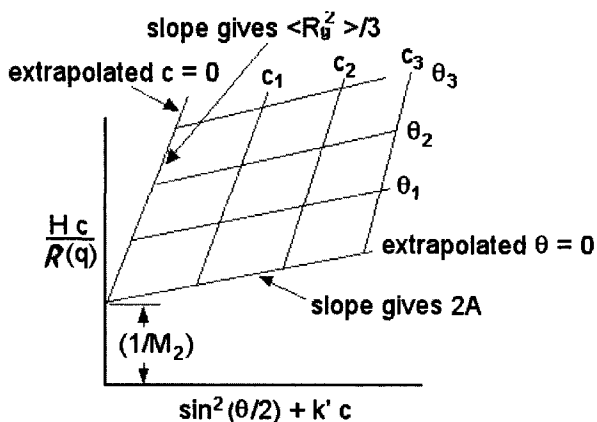


Figure 4F.4. Zimm Plot "double extrapolation".

Software now exists to automatically carry out a Zimm Plot. One makes measurements at a number of angles and concentrations and inserts these in the program. Values of M_2 , $\langle R_g^2 \rangle$ and A_2 are then calculated. The connection between scattering and molecular weight is discussed further in Appendix 4G.

Extensions to Other Kinds of Radiation

The theory developed here is not limited to light scattering, but also applies to x-ray and neutron scattering, provided the appropriate values

of K and A are used. The selection may be made so as to achieve the desired contrast and wavelength to best suit the problem at hand. For example, as will be shown, contrast for neutron scattering can be controlled by isotropic substitution.

Extensions to Concentrated Solution and Bulk Polymers

The equation

$$\langle (\Delta c)^2 \rangle = (1/2a) = RTcV / \left\{ - \left[\left(\frac{\partial \mu_1}{\partial c} \right) \right] v N_A \right\} \quad (4F.41)$$

is not limited to dilute solutions, so long as the appropriate values of μ_1 is used. While the theory exists, light scattering is not normally carried out on concentrated solutions and bulk polymers because of the difficulty of removing impurities such as dust which can be appreciably contribute to the scattering. However, such measurements are now possible using neutron scattering since by replacing hydrogen by deuterium, the molecular contrast can be enhanced so that it can appreciably exceed that due to impurities.

Effect of Anisotropy and Orientation

The preceding discussion was limited to isotropic unoriented systems in which the scattering power (such as polarizability) was a scalar and where there was spherical symmetry. The effect of anisotropy (where, for example, polarizability is a tensor quantity) will be discussed later.

Appendix 4G Why Concentration Fluctuations Relate to Molecular Weight

For a given concentration, c , the number of molecules/cm³, N , becomes less as the molecular weight, M , increases.

$$N = (c/M) N_{AV} \quad (4G.1)$$

Thus, for low molecular weight,

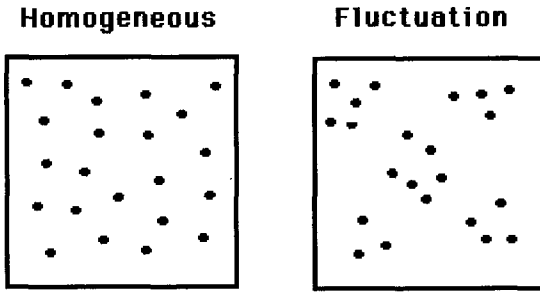


Figure 4G.1. Molecular distribution for low molecular polymers.

while for high molecular weight.

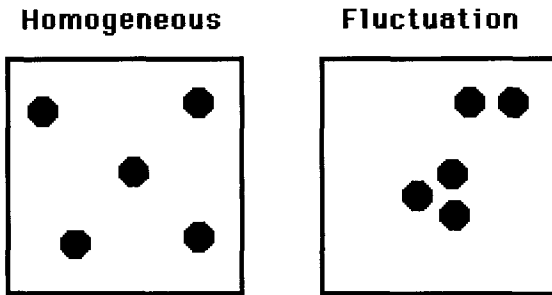


Figure 4G.2. Molecular distribution for high molecular polymers.

The amount of fluctuation, and hence the intensity of scattering, is greater for a fewer number of large molecules.

How to Measure the Size of an Elephant

Assume that two elephants weigh as much as 50 people. Both may fluctuate in mass.

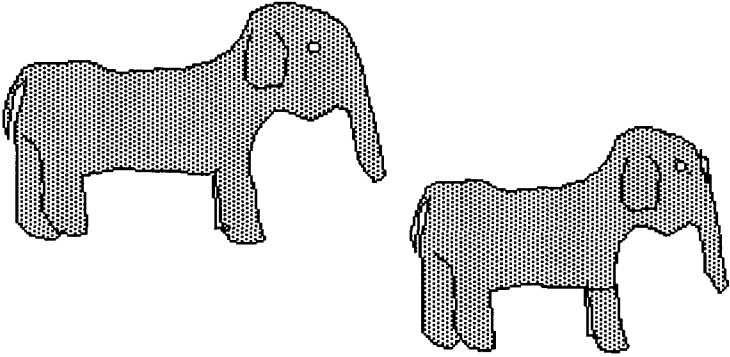


Figure 4G.3. The elephants represent high molecular weight polymers.

while, for people,

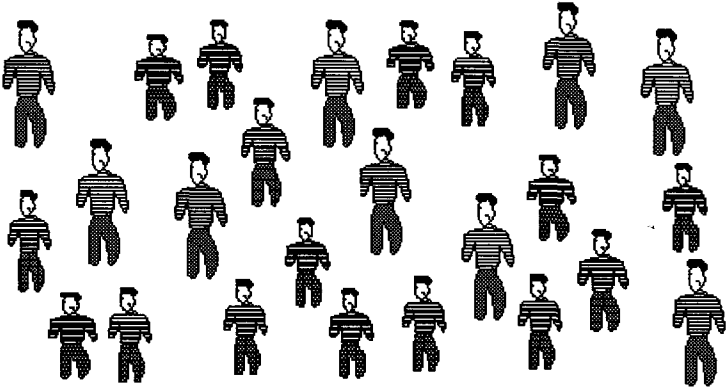


Figure 4G.4. The elephants represent low molecular weight polymers.

The group of people is obviously more homogeneous. As a scattering experiment, a baseball thrown into the group of people would hit someone most of the time.

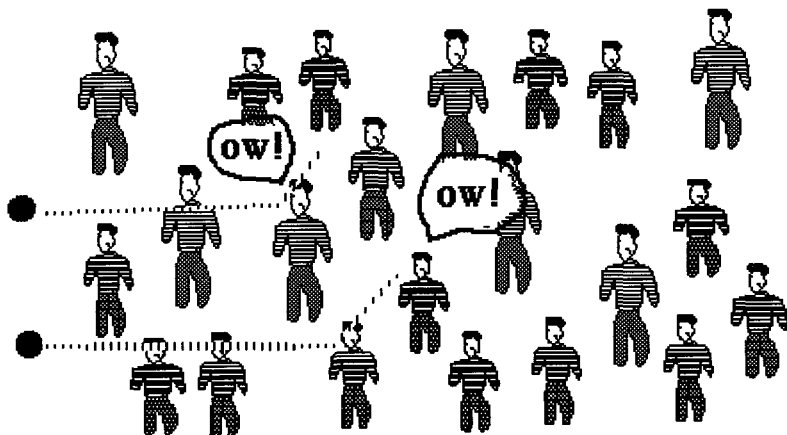


Figure 4G.5. A baseball thrown into people will probably hit at least one person.

The same experiment with the elephants will give misses most of the time, but occasionally, it will produce a big reaction.

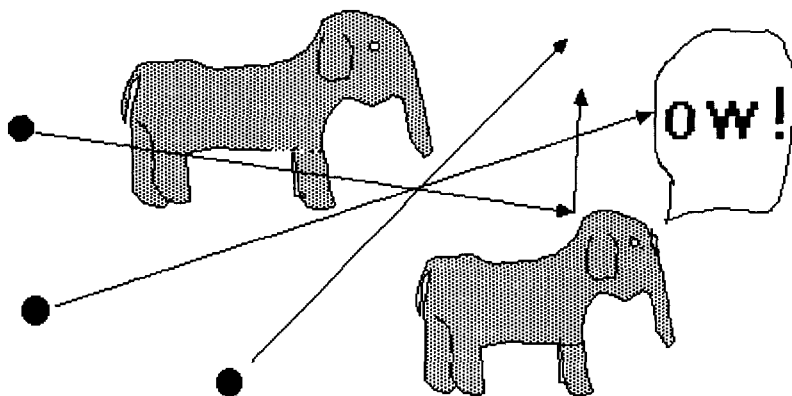


Figure 4G.6. The probability that a baseball will strike an elephant is much less.

ANOTHER WAY OF LOOKING AT IT -

The work required to produce a concentration fluctuation, ΔG , is energy expended in forcing the solvent to move against the osmotic pressure, Π

OPTICS

The greater ΔG , the lower $P(\Delta c)$, the lower $\langle(\Delta c)^2\rangle$, and the less the scattering. Now according to van't Hoff's equation

$$\Pi = (c/M_2)RT \quad (4G.2)$$

so high $M_2 \rightarrow$ low $\Pi \rightarrow$ high scattering. That is, for osmotic pressure,

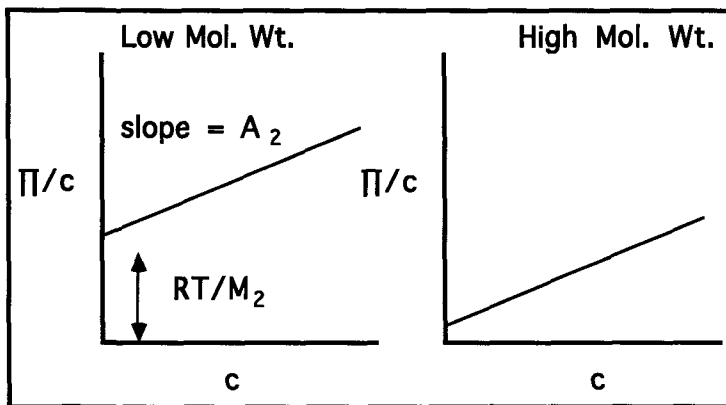


Figure 4G.7. For osmotic pressure, scattering decreases as molecular weight increases.

while for light scattering,

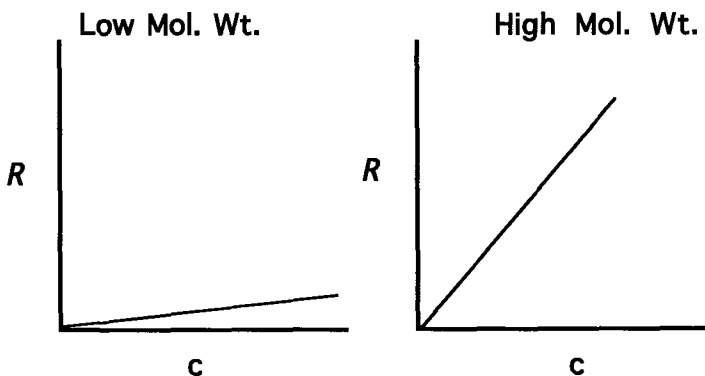


Figure 4G.8. For light scattering, scattering increases with increasing molecular weight.

50

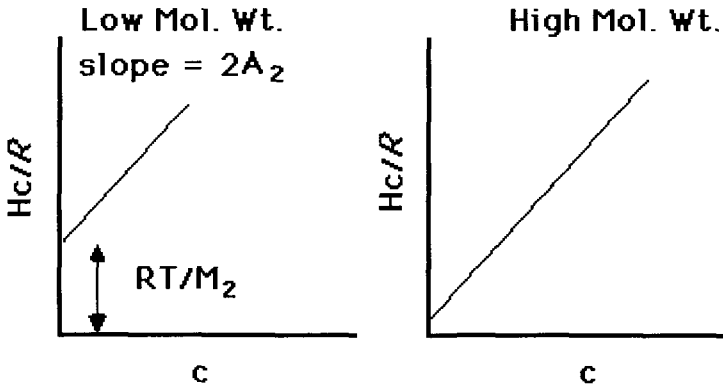


Figure 4G.9. Comparison of scattering behavior by two techniques.

Thus, polymers, having high molecular weight, give low osmotic pressure but high light scattering. For this reason, light scattering is the preferred technique for polymer studies.

Chapter 5

ELECTRICAL PROPERTIES

5.1 Introduction

This chapter discusses the electrical properties of solid polymers in terms of the interaction between electromagnetic fields and matter as measured by electrical apparatus. The interaction between electromagnetic fields and matter that gives rise to scattering, absorption, and reflection phenomena is the subject of the previous chapter on optics. The electrical interaction for polymers discussed in this chapter encompasses a variety of behavior from insulators on one end through semi-conductors to materials with conductivities in the metallic region. Insulators resist the flow of electrical current and therefore have high dielectric coefficients. This high resistance has led to the application of polymer films as dielectric separators in capacitors. The phenomena of piezoelectricity, pyroelectricity and static electricity are associated with the dielectric character of most polymers. An important application of the piezoelectric effect in polymers is the use of poly(vinylidene fluoride) film as transducers in microphones, speakers and similar electro-acoustical devices.

Ordinarily, polymers have very low conductivity and serve as insulators. They can serve the very important function of separating conductors from each other and preventing transfer of electrons between them. While such is useful for everyday use such as insulating power lines, polymers also serve more "high tech" applications such as in making printed circuit boards on which computer components are formed by processes such as lithography. The trend is for such devices to become increasingly smaller so as to permit more complex circuitry to

occupy less space. This means that conductors must be spaced more closely but still separated by insulators. One asks if there is a limit to the smallness of such insulators. There is, since Ohm's law as applied to describe the resistance of macroscopic insulators no longer works when dimensions approach the atomic scale. Then, the phenomenon of "quantum mechanical tunneling" occurs whereby electrons can pass through insulators in a manner not permitted by classical considerations. This places limits on materials and dimensions suitable for insulator applications,

For computer applications, the rate at which data can be transmitted determines the speed of computer performance. This is determined by the "time constant" of the electronics that describes the rate at which an electrical pulse decays that determines the possible interval between pulses. This time constant is proportional to the capacitance of the circuits that relates to the dielectric constants of their components. For this purpose, polymers are attractive, since they generally have lower dielectric constants than their non-polymeric alternatives. For this consideration, knowledge of the relationship between dielectric constant and molecular structure is essential.

This chapter first derives the basic equations relating dielectric behavior to polymeric structure. The equations defining the change in dielectric behavior with frequency and temperature are then developed. The application of dielectric phenomena to polymeric structures is described next with particular emphasis on piezoelectricity. Finally, the relation between static electricity and polymer structure is discussed.

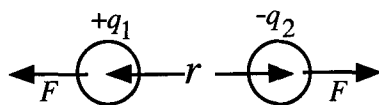


Figure 5.1. Diagram illustrating the force-distance relation between two electrical charges.

5.2. Dielectrics

5.2.1. Dielectric Constant

ELECTRICITY

The dielectric constant (ϵ) of a material may be defined using Coulomb's Law, which expresses the force, F , between two point charges, q_1 and q_2 , separated by distance, r , as (Figure 4.1)

$$F = \frac{q_1 q_2}{\epsilon r^2} \quad (5.1)$$

In vacuum, $\epsilon = 1$ in electrostatic units (ESU) when F is measured in dynes and r in cm., in which case, Coulomb's Law becomes

$$F = \frac{q_1 q_2}{r^2} \quad (5.2)$$

so

$$\epsilon = F_0 / F \quad (5.3)$$

where F_0 is the force between charges in vacuum. Hence, a dielectric shields the charges from each other and reduces the force. For air, $\epsilon = 1.00059$ and for water, $\epsilon = 80$. Thus, the force between ions in aqueous solutions is substantially reduced as a result of their being surrounded by polar water molecules. This is the principal reason for water being an excellent solvent for ionic species, in that it shields oppositely charged ions from each other and permits them to function independently.

The electrical field strength, \mathbf{E} , is defined as the force on a charge of +1 ESU and is a vector quantity. At a distance, r , away from a charge, q , Coulomb's Law gives

$$\mathbf{E} = \frac{q}{\epsilon r^2} \quad (5.4)$$

or

$$\mathbf{E} = \frac{q}{\epsilon} \frac{\mathbf{r}}{r^3} \quad (5.5)$$

and \mathbf{E} is oriented in the direction of \mathbf{r} .

The electromagnetic displacement (\mathbf{D}) is the value of \mathbf{E} in a vacuum when $\epsilon = 1$. For a dense medium, the two quantities are related by

$$\mathbf{D} = \epsilon \mathbf{E} \quad (5.6)$$

The dielectric properties of a material are also important in capacitor applications. The capacitance (C) of a body is defined as

$$C = \frac{q}{V} \quad (5.7)$$

where V is the voltage in electrostatic units. The capacitance increases with increasing values of the dielectric constant (Figure 5.2).

To understand equation 5.6, one must first introduce the concept of "lines of force", Φ . One may then show that the number of lines emanating from a point charge, Q , in vacuum is

$$\Phi = \mathbf{D}A = \left(Q/r^2\right)(4\pi r^2) = 4\pi Q \quad (5.8)$$

where \mathbf{D} is the number of lines of force per unit area (Appendix 5A)

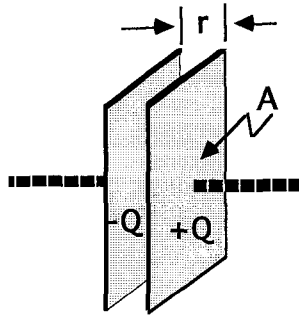


Figure 5.2. Schematic diagram of a parallel plate condenser with plate Area A and charge Q .

For a point charge, these lines are in the direction of the force that is radially outward, whereas for a parallel plate condenser, they are perpendicular to the plates (except near the edges) (Figure 5A.5). Therefore, for such a condenser, \mathbf{D} in the region between the plates is

$$\mathbf{D} = \Phi/A \quad (5.9)$$

and

$$\mathbf{E} = \mathbf{D}/\epsilon = 4\pi/\epsilon A \quad (5.10)$$

The voltage between the plates is the work necessary to carry a unit charge from one plate to the other, separated by distance, s , and is

ELECTRICITY

$$V = \mathbf{F}s = \mathbf{E}s \quad (5.11)$$

Since \mathbf{E} is the force on a unit charge. Thus,

$$\mathbf{E} = V/s = 4\pi Q/\epsilon A \quad (5.12)$$

Thus

$$C = Q/V = \epsilon A/4\pi s \quad (5.13)$$

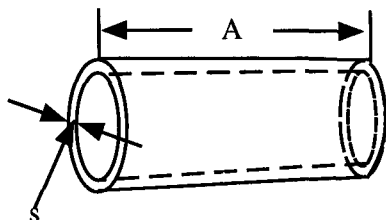


Figure 5.3. Rolled sheet showing the relation of area A to thickness s .

The capacitance then is proportional to ϵ and A , and inversely proportional to s . Thus one way to make a condenser of high capacitance is to roll up a conducting film separated by a thin spacer into a tube giving a large A and small s . (Figure 5.3).

The flux density per unit area in the presence of the dielectric, \mathbf{E} , is less than that in its absence, \mathbf{D} , because of the opposing lines of flux arising on the surface of the dielectric from its polarization. This polarization charge density, P , gives rise to the flux density, $4\pi P$, so that

$$\mathbf{E} = \mathbf{D} - 4\pi\mathbf{P} \quad (5.14)$$

and

$$\epsilon = \mathbf{D}/\mathbf{E} = 1 + 4\pi(\mathbf{P}/\mathbf{E}) \quad (5.15)$$

or

$$\epsilon - 1 = 4\pi(\mathbf{P}/\mathbf{E}) \quad (5.16)$$

Now the polarization charge density arises from the N dipoles of moment, μ per cm^3 lying in the volume of the dielectric a distance, L , from its surface. Thus,

$$\mathbf{P} = NqL = N\mu \quad (5.17)$$

where $\mu = qL$

In the absence of permanent dipoles, μ arises from the induced dipole moment of the atoms or molecules having a polarizability, α , and experiencing an effective field, \mathbf{E}_{eff} . So $\mu = \alpha\mathbf{E}_{\text{eff}}$. The effective field is related to the applied field by

$$\mathbf{E}_{\text{eff}} = \mathbf{D} - 4\pi\mathbf{P} + \mathbf{E}_{\text{int}} = \mathbf{E} + \mathbf{E}_{\text{int}} \quad (5.18)$$

The internal field, \mathbf{E}_{int} , is that arising from the charges on the surface of the cavity within which a molecule resides. This was calculated by Lorenz using the assumption that the cavity was spherical as shown in Appendix 5B giving rise to

$$\mathbf{E}_{\text{int}} = (4/3)\pi\mathbf{P} = (\varepsilon - 1)\mathbf{E}/3 \quad (5.19)$$

Thus,

$$\mathbf{E}_{\text{eff}} = \mathbf{E} + (\varepsilon - 1)\mathbf{E}/3 = \mathbf{E}[3 + (\varepsilon - 1)]/3 = \mathbf{E}(\varepsilon + 2)/3 \quad (5.20)$$

Then

$$\varepsilon - 1 = 4\pi N\alpha(\mathbf{E}_{\text{eff}}/\mathbf{E}) = 4\pi N\alpha(\varepsilon + 2)/3 \quad (5.21)$$

or

$$\frac{\varepsilon - 1}{\varepsilon + 2} = (4/3)\pi N\alpha \quad (5.22)$$

This is the Clausius-Mosotti equation.

At high frequencies, it can be shown [1] that $\varepsilon = \eta^2$ where η is the refractive index. Substitution of this relation into equation 5.22 yields

$$\frac{\eta^2 - 1}{\eta^2 + 2} = \frac{4\pi}{3} N\alpha \quad (5.23)$$

or the Lorenz-Lorentz equation that is a link between the bulk and the molecular optical properties. The Lorenz-Lorentz equation is often expanded as, by substitution from equation 5.21

$$\frac{\eta^2 - 1}{\eta^2 + 2} = \frac{4\pi}{3} \frac{\rho}{M} N_A \alpha \quad (5.24)$$

This equation represents the starting point for molecular refraction discussed in Chapter 4.

5.2.2. Orientation of permanent dipoles

The preceding discussion has to do with induced dipoles; whereas, the relaxation studies deal with the motions of parts of polymer chains that have different relaxation times for orientation. Many polymers such as polyvinyl fluoride, polyvinyl chloride and nylons have permanent dipoles that may be reoriented on the application of an applied field. The response of the oriented permanent dipoles will vary with the strength of the applied field.

5.2.3. Dielectric Loss

The Boltzmann superposition principle holds for dielectric as well as mechanical phenomena (Appendix 8A). One means of applying this principle to dielectrics is the differential equation

$$t \frac{dD(t)}{dt} + D(t) = \tau \epsilon_0 \frac{dE(t)}{dt} + \epsilon_0 E(t) \quad (5.25)$$

where $D(t)$ is the time dependent electric displacement, $E(t)$ the corresponding electric field and τ the dielectric relaxation time. The equation for alternating current voltage imposed across a dielectric body has the form

$$E(t) = E_0 e^{i\omega t} \quad (5.26)$$

and for the corresponding displacement

$$D(t) = D_0 e^{i(\omega t - \delta)} \quad (5.27)$$

where ω is the angular frequency and δ is the dielectric loss angle analogous to the mechanical loss angle. Substituting equations 5.26 and 5.27 into equation 5.25 and solving

$$\varepsilon = \varepsilon_{\infty} + \frac{\varepsilon_0 - \varepsilon_{\infty}}{1 + i\omega\tau} \quad (5.28)$$

ε^* is the complex dielectric constant, ε_0 the static or low frequency value of the dielectric constant, ε_{∞} the limiting value at high or optical frequencies and τ is the relaxation time or the time required for the stress to relax to $1/e$ of its initial value. Equation 5.28 summarizes the basic frequency dependence in dielectrics as shown by the following derivation. ε^* may be written as

$$\varepsilon^* = \varepsilon' + i\varepsilon'' \quad (5.29)$$

where ε' is the in phase or energy storage component and ε'' the out of phase or energy dissipating component of the energy absorbed by the dielectric at different frequencies. ε^* may be separated into its real and imaginary components by multiplication of equation 5.28 by $(1 - i\omega\tau)/(1 - i\omega\tau)$ yielding

$$\varepsilon' = \varepsilon_{\infty} + \frac{\varepsilon_0 + \varepsilon_{\infty}}{1 + \omega^2\tau^2} \quad (5.30)$$

$$\varepsilon'' = (\varepsilon_0 - \varepsilon_{\infty}) \frac{\omega\tau}{1 + \omega^2\tau^2} \quad (5.31)$$

The dielectric loss tangent ($\tan \delta$) analogous to the mechanical case is obtained from the ratio

$$\tan \delta = \frac{\varepsilon''}{\varepsilon'} \quad (5.32)$$

and, from equations 5.31 and 5.32

$$\tan \delta = \frac{(\varepsilon_0 - \varepsilon_{\infty})i\omega\tau}{\varepsilon_0 + \varepsilon_{\infty} + \omega^2\tau^2} \quad (5.33)$$

Equations 5.30 through 5.33 are termed the Debye equations and contain the basic framework used for the analysis of the frequency dependence of polymer dielectrics [2]. Thus, for example, integration of equation 5.33 assuming a single relaxation time yields

$$\int_{-\infty}^{\infty} \tan \delta d \ln \nu = \left[\frac{(\epsilon_0 - \epsilon_\infty)}{(\epsilon_0 \epsilon_\infty)^{1/2}} \right] \frac{\pi}{2} \quad (5.34)$$

The area under a plot of $\tan \delta$ against $\ln \nu$ provides a measure of the relaxation process.

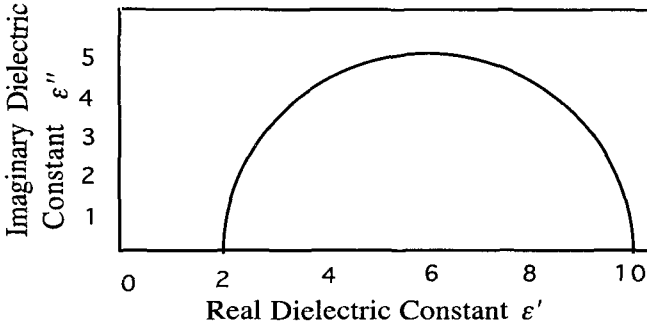


Figure 5.4. Schematic diagram of an idealized Cole-Cole plot for a single relaxation time.

Cole and Cole [3] have shown how the real and the imaginary components of the complex dielectric constant may be evaluated by an Argand diagram in which each point corresponds to one frequency. This diagram plots ϵ'' as the ordinate and ϵ' the abscissa (Figure 5.4). The shape of the plot is given by

$$\left[\frac{\epsilon' - (\epsilon_0 - \epsilon_\infty)}{2} \right]^2 + (\epsilon'')^2 = \left(\frac{\epsilon_0 - \epsilon_\infty}{2} \right)^2 \quad (5.35)$$

obtained from the rearrangement of equations 5.30 and 5.31. Thus, a plot of ϵ'' against ϵ' yields a semi-circle of radius $(\epsilon_0 + \epsilon_\infty)/2$ with its origin lying at a distance $(\epsilon_0 + \epsilon_\infty)/2$ along the abscissa based on equation 5.35.

A distribution of dielectric relaxation times is observed for most materials analogous to what is found for mechanical relaxation processes. The single relaxation time used in equations 5.30 and 5.31 is therefore replaced by an integral, or

$$\varepsilon'(\omega) = \varepsilon_{\infty} + (\varepsilon_0 - \varepsilon_{\infty}) \int_0^{\infty} \left[\frac{\phi(\tau)}{1 + \omega^2 \tau^2} \right] d \ln \tau \quad (5.36)$$

And

$$\varepsilon''(\omega) = (\varepsilon_0 - \varepsilon_{\infty}) \int_0^{\infty} \left[\frac{\phi(\tau) \omega \tau}{1 + \omega^2 \tau^2} \right] d \ln \tau \quad (5.37)$$

where $\phi(\tau)d \ln$ is the fraction of the change in dielectric constant originating from mechanisms having relaxation times between $\ln \tau$ and in $\tau + d(\ln \tau)$. The simple relations used to obtain the Cole-Cole plot in Fig. 5.4 for a single relaxation time are not valid for a distribution of relaxation times. For the latter case, Cole and Cole [3] therefore proposed the empirical relations

$$\varepsilon'(\omega) = \varepsilon_{\infty} + (\varepsilon_0 - \varepsilon_{\infty}) \left[\frac{1 + (\omega \tau_0)^{\beta} \cos(\beta \pi / 2)}{1 + 2(\omega \tau_0)^{\beta} \cos(\beta \pi / 2) + (\omega \tau_0)^{2\beta}} \right] \quad (5.38)$$

and

$$\varepsilon''(\omega) = (\varepsilon_0 + \varepsilon_{\infty}) \left[\frac{(\omega \tau_0)^{\beta} \cos(\beta \pi / 2)}{1 + 2(\omega \tau_0)^{\beta} \cos(\beta \pi / 2) + (\omega \tau_0)^{2\beta}} \right] \quad (5.39)$$

β is a parameter with limits $0 < \beta < 1$. The limit of $\beta = 1$ corresponds to the single relaxation time case. As with mechanical relaxations, the frequency at $\omega = 1/\tau_0$ is that of maximum loss.

References 4 and 5 give details on experimental procedures and results for individual polymers. The use of dielectric techniques to monitor orientational changes in an ethylene-carbon monoxide 1:1 alternating copolymer is described in reference 6.

5.3. Piezo- and Pyroelectric Effects

The polarization induced in polymer dielectrics by the application of an electric field or by other charging treatments can, in a few cases, persist for long (ca. months) periods at room temperature. The polymers thus treated are termed electrets. Polymer films that have been subjected to this polarization treatment or poled manifest piezoelectric and

pyroelectric phenomena. Piezoelectricity (or pressure electricity) refers to the generation of electric current on the application of a stress (or pressure) to a material. (The reverse effect, a change in sample dimensions on application of electrical stress, also occurs in piezoelectric materials). Pyroelectricity (or thermal electricity) is an analogous phenomenon in which the application of heat causes the generation of electricity in certain materials.

Piezoelectricity links the fields of electricity and acoustics. Piezoelectric materials are key components in acoustic transducers such as microphones, loudspeakers, transmitters, burglar alarms and submarine detectors. The Curie brothers [7] in 1880 first observed the phenomenon in quartz crystals. Langevin [8] in 1916 first reported the application of piezoelectrics to acoustics. He used piezoelectric quartz crystals in an ultrasonic sending and detection system – a forerunner to present day sonar systems. Subsequently, other materials with piezoelectric properties were discovered. These included the crystal Rochelle salt [9], the ceramics lead barium titanate/zirconate (pzt) and barium titanate [10] and the polymer poly(vinylidene fluoride) [11]. Other polymers such as nylon 11 [12], poly(vinyl chloride) [13] and poly(vinyl fluoride) [14] exhibit piezoelectric behavior, but to a much smaller extent. Strain constants characterize the piezoelectric response. These relate a vector quantity, the electrical field, to a tensor quantity, the mechanical stress (or strain). In this convention, the film orientation direction is denoted by 1, the width by 2 and the thickness by 3. Thus, the piezoelectric strain constant d_{13} refers to a polymer film held in the orientation direction with the electrical field applied parallel to the thickness or 3 direction. The requirements for observing piezoelectricity in materials are a non-symmetric unit cell and a net dipole movement in the structure. There are 32-point groups, but only 30 of these have non-symmetric unit cells and are therefore capable of exhibiting piezoelectricity. Further, only 10 out of these twenty point groups exhibit both piezoelectricity and pyroelectricity. The piezoelectric strain constant, d , is related to the piezoelectric stress coefficient, g , by

$$d = e_x g \quad (5.40)$$

and the dielectric constant at stress level x , ϵ_x . The piezoelectric strain constant, d , relates the applied electric field to the resultant (units of meters per volt. the piezoelectric stress coefficient, g , relates the stress applied to a crystal to the resultant electric field in the crystal (units of volts meters per Newton).

5.4. Piezo-Electric Coefficient

To determine the factors that influence the efficiency of piezoelectric materials, one starts with the voltage equation

$$V = Q/C \tag{5.41}$$

where V = Voltage

Q = the electric charge

C = the capacitance

Differentiating equation 5.41 by s , the thickness of the piezoelectric material

$$\left(\partial V/\partial s\right) = Q\left[\partial(1/C)/\partial s\right] \tag{5.42}$$

Then, substituting the capacitance equation,

$$C = \frac{4\pi s}{\epsilon A} \tag{5.43}$$

into equation 5.42

$$= Q \frac{\partial}{\partial s} \left[\frac{4\pi s}{\epsilon A} \right] = \frac{4\pi Q}{\epsilon A} = \frac{4\pi \mathbf{P}}{\epsilon} \tag{5.44}$$

where s = the condenser spacing

A = Condenser plate area

\mathbf{P} = Polarizability

ϵ = Dielectric constant

The response of the piezoelectric material to sound waves or variation of voltage to stress is given by

$$\left(\partial V/\partial \sigma\right) = \left(\partial V/\partial s\right)\left(\partial s/\partial \sigma\right) \tag{5.45}$$

Since Young's Modulus = $Y = s(\partial \sigma/\partial s)$

Thus

$$(\partial V/\partial \sigma) = \frac{4\pi A s P}{\epsilon Y} \quad (5.46)$$

An advantage of polymers is that they have low ϵ and Y values as well as high polarizability. Thus, polymers can provide sensitive piezoelectric detectors with large areas.

Thus, the greater the dielectric constant, the greater is the piezoelectric effect. This is true only when comparing polymers with similar symmetry. There are certainly high dielectric constant polymers that are not piezoelectric. The electric displacement, \mathbf{D} , (equation 5.6) for the combined effects of stress and temperature is given by the linear relation

$$\mathbf{D} = d_x + e_x \mathbf{E} - p_x \Delta T \quad (5.47)$$

where \mathbf{E} is the electrical field strength, ΔT the temperature difference and p_x the piezoelectric coefficient.

The poling operation enhances piezoelectric effects in polymers in contrast to the case with other materials. As mentioned previously, poly(vinylidene fluoride) (PVDF) shows the greatest response to poling of any polymer. By way of background, the crystallinity of PVDF₂ ranges between 30 and 40% [15]. The non-polar α -crystal phase forms preferentially on initial extrusion of PVDF film. Subsequent drawing or orientation increases the amount of the polar β -crystal phase at the expense of the α phase. Poling however may result in increasing the amount of the β -crystal phase [16]. Orienting the polymer prior to poling may be desirable since this can align the polar groups in such a way they are then more prone to poling. Higher crystallinity is also desirable for poling since the crystals orient better than do the amorphous regions. In addition, efforts have been made to increase the β -crystal phase by modifying the crystallization conditions. For example, the amount of the β -crystal phase of PVF₂ can be increased by blending with PMMA to supplement the effect of poling on its concentration.

The reasons for the superiority of pvdf film as a piezoelectric material are obscure. Other polymers such as Nylon 11 are similar in structural

characteristics: a non-symmetric unit cell, chain conformation and crystallinity, but do not respond to poling to the same degree.

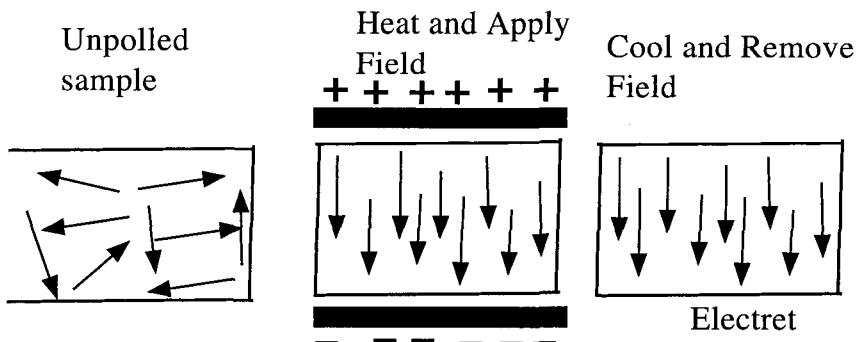


Figure 5.5. Diagram of a typical poling assembly in which permanent dipoles are aligned to form electrets.

In one common poling procedure, the polymer film is placed between two electrodes and a direct current is applied to the assembly (Figure 5.5). Films are usually covered with a thin metal (aluminum, nickel, gold or silver) layer before poling to reduce surface contact resistance. Samples are commonly heated to a temperature below the melting point, held at temperature while the electrical field is applied and then cooled in the presence of the field. As an example [17], poly(vinylidene fluoride) film (6 mm thick) was plated with aluminum, placed between electrodes with the film orientation parallel to the electrodes surfaces, heated to 110°C and a voltage of 5×10^5 volts/cm applied for 45 minutes. Poling can also be accomplished with treatment of polymer film samples by corona discharge at room temperature [18] or by plasma treatment at room temperature [19].

References

1. See, for example, A. von Hippel, Handbook of Physics; E.U Condon, H. Odishaw, Eds. McGraw-Hill: New York, 1958, 4-109, 114
2. P. Debye, *Polar Molecules*; Dover: New York, 1945, Chapter 2
3. R.H. Cole, K.S. Cole, *J. Chem. Phys.* 1941, 9, 341
4. V.V. Daniel, *Dielectric Relaxation*; Academic: New York, 1967
5. N.G. McCrum, B.E. Read, G. William, *Anelastic Effects*; Wiley: New York, 1967
6. P.J. Phillips, G. Kleinheins, R.S. Stein, *J. Polymer Sci.:Part A-2* .1972, 10, 1593

ELECTRICITY

7. J. Curie, P. Curie, *Compt. Rend.* **1880**, *91*, 294, 383, 387
8. W.G. Cady, *Piezoelectricity*; Dover: New York, **1964**
9. A.M. Nickolson, J. A. Anderson, *Rep. Nat. Res. Council*, (**Apr. 1918**)
10. B. Wul, I.M. Goldman, *Comp. Rend. Acad. Sci. USSR* **1945**, *46*, 139, **1945**, *49*, 177
11. H. Kawai, *Japan. J. Appl. Phys.* **1969**, *8*, 975
12. S. Edelman, L.R. Grisham, S.C. Rothe, J. Cohen, *J. Acoust. Soc. Am.* **1970**, *48*, 1040
13. R. Hayakawa, Y. Wada, *Adv. in Polymer Sci.* **1973**, *11*, 1
14. H. Sussner, Y. Wadw, *J. Polymer Sci.: Polymer Phys. Sci. Ed.* **1978**, *16*, 529
15. P.E. Bloomfield, R.A. Ferren, P.F. Radiice, H. Stefanou , O.S. Sprout,
Naval Res. Rev. **1 May 1978**, *31*
16. S. Kobayashi, K. Yahagi, *Japan. J. Appl. Phys.* **1979**, *18*, 261
17. P.D. Southgate, *Appl. Phys. Letters* **1976**, *28*, 250
18. J.E. McKinney, G.T. Davis, *Am. Chem. Soc. ORPL Reprints.* **1978**, *30(1)*, 271
19. R. Elsdon, F.R.G. Mitchell, *J. Phys. D:Appl. Phys.* **1976**, *9*, 1445

Appendix 5A. Lines of Flux

5A.1. Electrical Field Strength

The electrical field strength is a vector in the direction of and equal in magnitude to the force on a unit positive charge.

Thus the field strength, \mathbf{E} , at a distance, r , from a charge, $+q$, in a material with a dielectric constant, ϵ , is

$$E = q / \epsilon r^2 \quad (5A.1)m$$

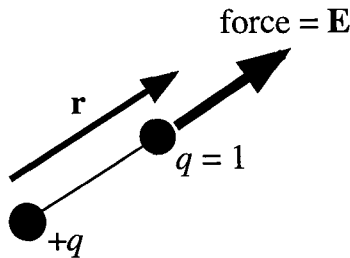


Figure 5A.1. Diagram showing the relations used in deriving the electric field strength.

5A.2. Electric displacement and Flux Density

\mathbf{D} = Displacement = Field Strength in a vacuum ($\epsilon = 1$)

$$\mathbf{D} = e\mathbf{E} \quad (5A.2)$$

Lines of flux are in the direction of \mathbf{D} with a number/cm² equal to \mathbf{D}

Lines of flux between two opposite charges flow from positive charge to negative charge (Figure 5.A.2)

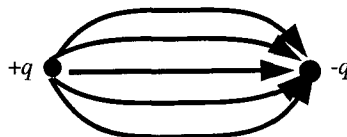


Figure 5A.2. Sketch showing the lines of flux between two charges, one positive and one negative.

ELECTRICITY

Number of lines of flux passing through the surface of a sphere with a charge $+q$ at its center (Figure 5A.3)

$$\Phi = \mathbf{D} \cdot \mathbf{A} = \epsilon \mathbf{E} \cdot \mathbf{A} = \epsilon \left[q / \epsilon r^2 \right] \left[4 \pi r^2 \right] = 4 \pi q \quad (5A.3)$$

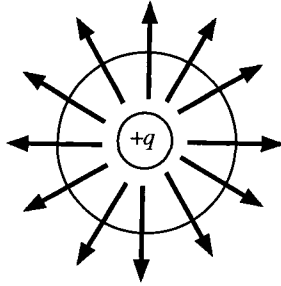


Figure 5A.3. Sketch showing the lines of flux passing through the surface of a sphere.

The lines of flux are continuous. Their number is independent of the radius of the sphere, so that the number of flux lines is constant

The lines of flux are not shape dependent (Figure 5A.4)

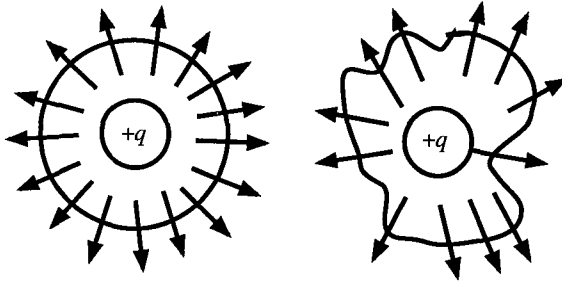


Figure 5A.4. Diagram illustrating independence of shape on lines of flux.

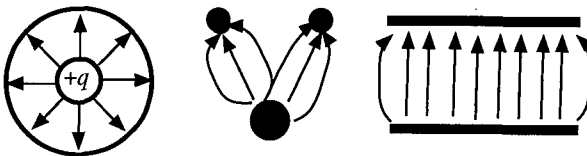


Figure 5A.5. Diagrams showing different types of electric field configurations.

Lines of flux can only start at positive charges and end at negative charges. They must be continuous and will minimize their curvature (Figure 5A.5).

5A.4. The Electrostatic Potential (Voltage)

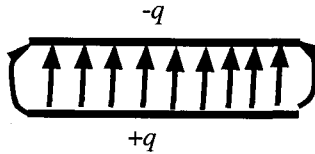


Figure 5A.6. Lines of flux between parallel plates.

The potential $V(x)$ at point x is the potential energy required to bring a unit positive charge from infinity to x , or

$$V(x) = \int_{\infty}^x \mathbf{F} \cdot d\mathbf{r} = \int_{\infty}^x \mathbf{E} \cdot d\mathbf{r} \quad (5A.4)$$

where \mathbf{F} = the force vector

\mathbf{r} = the displacement vector

since the force on a charge of q is

$$\mathbf{F} = q\mathbf{E} \quad (5A.5)$$

and $q = +1$

Example: What is the potential at a distance, r , from a charge q ?

$$V(r) = \int_{\infty}^r \mathbf{E} \cdot d\mathbf{r} = \int_{\infty}^r \frac{q}{\epsilon r^2} = \frac{q}{\epsilon} \left[\frac{1}{r} \right] = \frac{q}{\epsilon r} \quad (5A.6)$$

5A.5. The Field between Parallel Plates

Assume $a \gg s$; Area = $A = a b$

Number of lines of flux = $\Phi = 4\pi Q$

$$\mathbf{D} = \text{Flux density} = 4\pi Q/A$$

ELECTRICITY

$$\mathbf{E} = \text{Field strength} = \mathbf{D}/\epsilon = 4\pi Q/\epsilon A$$

$$\mathbf{V} = \text{Potential} = \mathbf{F}s = \mathbf{E}s = [4\pi Qs]/\epsilon A$$

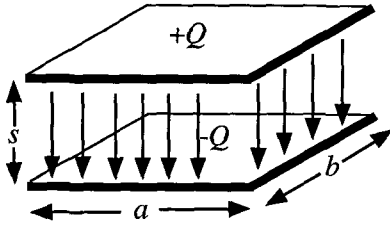


Figure 5A.7. The electrical field between parallel plates.

Appendix 5B. Lorentz Calculation, Internal Field Correction

The inner electric field produced by material between the plates reduces the total electric field (Figure 5B.1)

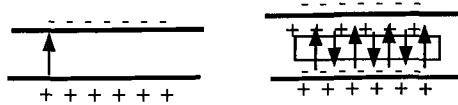


Figure 5B.1. Charge distribution between capacitor plates without and with material between capacitor plates.

E_{int} is the internal field

Thus

$$\epsilon - 1 = 4\pi N\alpha \left(E_{int} / E_{eff} \right) \quad (5B.1)$$

To evaluate (E_{int} / E_{eff}) , we will adopt the model of Lorentz and assume that the molecule is in a spherical cavity in the dielectric

This involves the following assumptions:

The cavity must be at least as large as the molecule.

The molecule must be approximately spherical so as it fits in the cavity.

The material outside the cavity must be uniform.

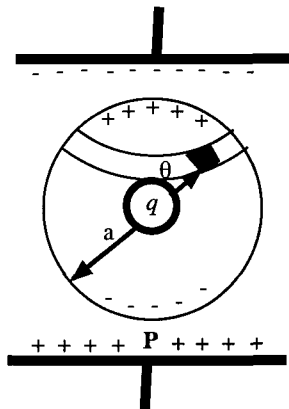


Figure 5B.2. Sketch showing a spherical field around a charge used in the Lorentz calculation.

Figure 5B.3 relates the Cartesian coordinates to the spherical coordinates used in this derivation.

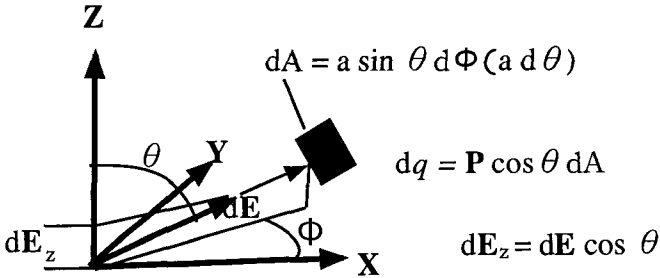


Figure 5B.3. Spherical coordinates used in deriving equation 5B.4.

Now the x and y components of the field are zero because of symmetry, and only the z component remains which is

$$E_z = \int dE \cos \theta = P \int_0^{2\pi} \int_0^\pi \cos^2 \theta \sin \theta d\phi d\theta = (4/3)\pi P \quad (5B.4)$$

Now

$$E_{int} = D - (\text{Field from flat surface}) + (\text{Field from spherical cavity})$$

$$-D - 4\pi P + (4/3)\pi P - E + (4/3)\pi P \quad (5B.5)$$

We have seen that P (equation 5.16) can be given by

$$4\pi P = (\epsilon - 1)E \quad (5B.6)$$

Thus

$$E_{int} = E + (\epsilon - 1)E/3 - (\epsilon - 1)/3 \quad (5B.7)$$

so

$$(E_{int}/E) = (\epsilon - 1)/3 \quad (5B.8)$$

This is the Lorenz internal field factor which is 0 in a vacuum ($\epsilon - 1$) and greater than one in a real media.

For (E_{int}/E) on rearranging equation 5B.07, we obtain

$$\frac{\epsilon - 1}{\epsilon + 2} = \frac{4}{3} \pi N \alpha \quad (5B.9)$$

This is the Clausius-Mosotti equation which relates the macroscopic dielectric constant, molecular polarizabilities and condensed matter.

Chapter 6

SPECTROSCOPY

6.1. Introduction

The change in absorption or emission of waves by matter with frequency (or wavelength) of impinging waves forms the subject matter of spectroscopy. The best known and most intensively studied wave phenomena are those associated with the interaction of electromagnetic waves (ultraviolet, visible and infrared) and matter. Molecules absorb radiation, from a quantum mechanical viewpoint, by excitation from a lower (E_1) to a higher electronic or molecular energy level (E_2) through absorption of a photon of frequency ν . The energy-frequency relation is given by the Bohr equation

$$\Delta E = E_2 - E_1 = h\nu = h \frac{c}{\lambda} \quad (6.1)$$

where h = Planck's constant,
c = the velocity of light
and λ = the wavelength.

The energies calculated from equation 6.1 for the infrared and Raman frequencies lie in the range of the vibrational and rotational motions of molecules. Infrared and Raman spectroscopy provide structural information once the various absorption bands are assigned to specific molecular vibrations. Similarly, the energies associated with the visible and ultraviolet radiation lie in the range of electronic transitions within the atoms and provide information about chemical bonding. Electromagnetic radiation is the most widely used because of the availability of sources and detectors and the interpretation of the data in

terms of structure. Other techniques however based on neutron scattering, acoustical, dynamic mechanical and nuclear magnetic resonance also provide valuable information on polymer structure and properties.

This chapter treats principally the vibrational spectra determined by infrared and Raman spectroscopy. The means used to assign infrared absorption bands are outlined. Also, the rationale for the selection of permitted absorption bands is described. The basis for the powerful technique of Fourier Transform Infrared (FTIR) is presented in Appendix 6A. Polyethylene is used to illustrate both band assignment and the application of selection rules because its simple chain structure and its commercial importance have made polyethylene the most thoroughly studied polymer. The techniques of nuclear magnetic resonance, neutron inelastic scattering and ultraviolet spectroscopy are briefly described. The areas of dielectric loss and dynamic mechanical loss are not presented in this chapter, but material on these techniques can be found in Chapters 5.

6.2. General Background

The basic wave equation (6.2) states that the product of the frequency (ν) and the wave length (λ) is equal to the wave velocity, or

$$c = \lambda\nu \quad (6.2)$$

(in the case of electro-magnetic radiation, c equals the velocity of light)

Radiation is described either by its wavelength (micrometers for the infrared range, or those of frequency in reciprocal length or wave number). From a wave standpoint, the absorption of energy introduces a decrease in the amplitude of the wave as it transverses the medium. This decrease is associated with a loss of energy in the transmitted wave. From a classical viewpoint, the absorption may be considered to occur when the frequency of the radiation equals a resonant frequency of electronic or molecular motion in the medium. The absorption may be characterized by a transition moment, a vector in the direction of the dipole moment (or polarizability) change of the absorbing species. The absorption depends on the component of this transition moment along the polarization direction of the oscillating electric field. A polyatomic

molecule may absorb at several frequencies, each corresponding to a particular electronic or molecular motion in the medium with each having its characteristic transition moment. At first glance, one might reasonably expect long chain molecules with large numbers of atoms to show many absorption bands. However, the periodicity and symmetry of polar molecules usually reduces the number of absorbing frequencies and simplifies polymer spectra compared to those of low molecular weight compounds.

Beer's Law states that the reduction in intensity, dI , of the wave in passing through the increment of thickness, dl , is given by

$$-(dI/dl) = \epsilon I_0 \quad (6.3)$$

where I_0 and I_l are the incident and transmitted beam intensities [1] respectively and the extinction coefficient is ϵ . Integrating

$$I(l) = I_0 e^{-\epsilon l} \quad (6.4)$$

The extinction coefficient is obtained on rearranging equation 6.4

$$\epsilon = \left(\frac{1}{l}\right) \ln\left(\frac{I_0}{I_l}\right) \quad (6.5)$$

This quantity may be related to the absorbance a_i along the associated transition moment by

$$\epsilon_i = a_i \cos^2 \theta_i \quad (6.6)$$

where θ_i is the angle between the transition moment axis and the direction of polarization of the radiation (Figure 6.1) of the i^{th} absorption band.

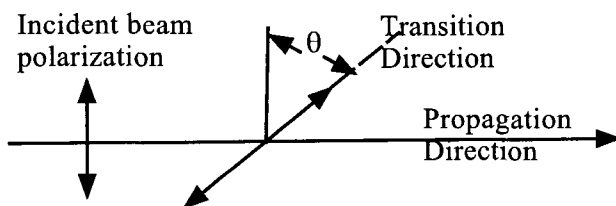


Figure 6.1. Relation between the bond transition moment and the incident beam polarization direction.

6.3. Infrared

In molecular terms, absorption in the infrared occurs classically by interaction between the incident radiation field and dipoles (see Chapter 4) in the medium. These dipoles, as in the case of the chlorine-carbon atom dipoles in poly(vinyl chloride), absorb due to the dipole moment varies along with the vibration. The equations of motions for these atoms (nuclei) are for point masses vibrating (or rotating) in the $400\text{-}2000\text{ cm}^{-1}$ frequency range. The simplest model uses point masses linked by weightless springs that obey Hooke's law. Also, the masses oscillate in simple harmonic motion about an equilibrium configuration. For the infrared region, the masses are of atomic magnitude; the links are the bonds between atoms. Then, from Hooke's law (which assumes that the force varies linearly with the displacement)

$$F = f x \quad (6.7)$$

where f is a force constant or constant of proportionality, F is the applied force, and x the associated bond deformation. A consequence of solution of the equation of motion is that the total energy, E , is conserved so that the sum of the potential energy, V , and the kinetic energy, K , is constant during the vibration

A linear molecule composed of three atoms (Figure 6.2) is described by the equation

$$\underbrace{\frac{m_1 v_1^2}{2} + \frac{m_2 v_2^2}{2} + \frac{m_3 v_3^2}{2}}_{\text{kinetic energy}} + \underbrace{\frac{f(x_2 - x_1)^2}{2} + \frac{f(x_3 - x_2)^2}{2}}_{\text{potential energy}} = E \quad (6.8)$$

where m_i represents the atomic mass, v_i the vibration for the i^{th} atom. The equation of motion for atom 1 is given by

$$m_1 \frac{d^2 x_1}{dt^2} - f(x_2 - x_1) = 0 \quad (6.9)$$

Similar equations can be written for atoms 2 and 3 (Appendix 6B). Solving equations 6.8 and 6.9 as written above in terms of Cartesian coordinates is cumbersome due to interaction terms between the various motions. Transforming the Cartesian coordinates into a set of normal coordinates as described in Appendix 6B greatly simplifies the mathematical manipulation because each vibration is expressed in terms of only one normal coordinate. The Cartesian coordinates can then be expressed as a linear combination of normal coordinates ($B_1B_2B_3$) with the result that

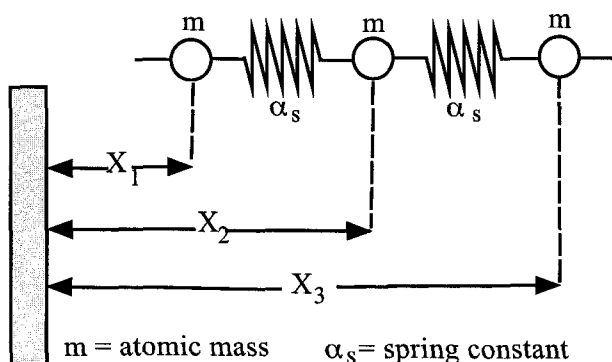


Figure 6.2. Coordinate system for a three state linear molecule.

$$x_1 = \frac{1}{3}B_1 + \frac{1}{2}B_2 \cos \omega_2 t + \frac{1}{6}B_3 \cos \omega_3 t \quad (6.10)$$

$$x_2 = \frac{1}{3}B_1 + \frac{1}{3}B_3 \cos \omega_3 t \quad (6.11)$$

$$x_3 = \frac{1}{3}B_1 + \frac{1}{2}B_2 \cos \omega_2 t + \frac{1}{6}B_3 \cos \omega_3 t \quad (6.12)$$

These linear combinations show the type of vibration, symmetric or anti symmetric, and are thus useful in assigning absorption frequencies to specific molecular vibrations.

In writing the equations of motion for a chain of N atoms, matrix notation is preferred for conciseness. In matrix notation, the potential energy can be written as

$$2|V| = |\bar{x}^T| f |\bar{x}| \quad (6.13)$$

where $|\bar{x}|$ is the column vector of the Cartesian coordinates
or, for a three-atom molecule,

$$|\bar{x}| = \begin{vmatrix} x_1 \\ x_2 \\ x_3 \end{vmatrix} \quad (6.14)$$

f_{ij} is an element in a square 3×3 matrix and $|\bar{x}^T|$ is the transpose or row vector of $|\bar{x}|$

$$\bar{x}^T = | x_1 \quad x_2 \quad x_3 | \quad (6.15)$$

Similarly, the expression for the kinetic energy in matrix notation is given by

$$2K = \dot{\mathbf{x}}^T |\mathbf{M}| \dot{\mathbf{x}} \quad (6.16)$$

where $|\dot{\mathbf{x}}|$ is the column vector of the velocities, $\dot{\mathbf{x}}$, expressed in Cartesian coordinates or

$$|\dot{\mathbf{x}}| = \begin{vmatrix} \dot{x}_1 \\ \dot{x}_2 \\ \dot{x}_3 \end{vmatrix} \quad (6.17)$$

$|\mathbf{M}|$ is the 3×3 diagonal matrix (Appendix 6B) of the atomic masses and $|\dot{\mathbf{x}}^T|$ is the transpose or row vector of $|\dot{\mathbf{x}}|$

$$\dot{\mathbf{x}}^T = | \dot{x}_1 \quad \dot{x}_2 \quad \dot{x}_3 | \quad (6.18)$$

The extension from the three atom, one-dimensional case to that of an isolated polymer chain of finite length is straightforward. As before, the linear chain is composed only of equal masses, m , separated by a constant distance, d (the repeat distance). Hookian springs with force constants, f , join the masses. Again, the chain is assumed to vibrate in only one dimension, say the x-axis. The equation of motion for the n^{th} mass, when it is displaced from its equilibrium position, is (analogous to equation 6.9)

$$m_n \frac{d^2 x_n}{dt^2} - f(x_{n+1} - x_{n-1} - 2x_n) = 0 \quad (6.19)$$

Solutions to equation 6.19 take the form of

$$x_n = A \exp[i(\omega t + knd)] \quad (6.20)$$

where k is termed the wave vector whose modulus is equal to $2\pi/\lambda$, and t is the time. Differentiation of equation 6.20 and substitution into equation 6.19 yields a solution only if the condition

$$\omega = \left(4f/m\right)^{1/2} \sin(kd/2) \quad (6.21)$$

is met. A plot of $\omega(k)$ against f , called the dispersion curve, given by Equation 6.21, has the properties common to all harmonic waves and is not restricted to only the case of atomic vibration. It describes a wave propagating along the chain with a wavelength of $2\pi/k$. Each mass vibrates with frequency $\omega(k)$. The allowable vibration frequencies that can propagate along the chain are restricted to a band between $\omega = 0$ and $\omega_{\max} = (4f/m)^{1/2}$ corresponding to $k = 0$ and $k = +\pi/d$ respectively. At $k = 0$, all masses move in phase with each other so that the chain motion is one of translation (equation 6B.30). Between the k limits, traveling waves move along the chain. At $k = \pm\pi/d$, the masses are out of phase with each other and a standing wave of length $l = 2d$ is set up. The interval between $+\pi/d$ and $-\pi/d$ is termed the first Brillouin zone [1]. Repetition of a vibration occurs when the value of k is greater than $+\pi/d$ or less than $-\pi/d$. The existence of a bound between $\pm\pi/d$ simplifies the mathematical description for isolated polymer chains in that only some chain subunit, and not the entire chain, need be considered.

In principle, use of a suitable coordinate transformation can convert equations 6.13 and 6.16 into secular equations and the vibrational frequencies calculated [2,3] if all the force constants are known. However, the observed frequency bands are commonly much fewer than the number of force constants. Calculations therefore concentrate on assuming values for the force constants and refining the best fit to the observed frequencies. Selection rules reduce the number of force constants required in the frequency calculations. These rules determine whether a given molecular vibration is active and are based on molecular

symmetry considerations. For a vibrational mode to be active in the infrared, the change in the dipole moment, m , set up during the vibration must have a component along the vibrational direction (Figure 6.3).

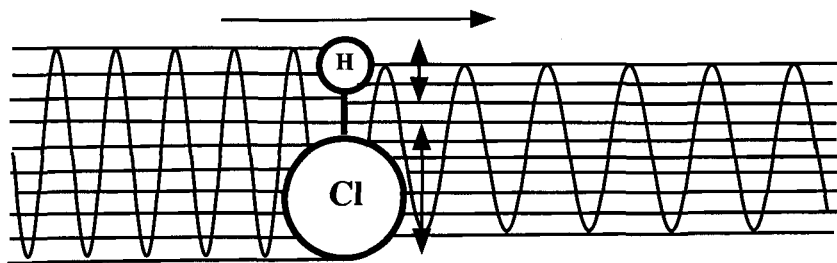


Figure 6.3. Infrared active vibration showing change in the dipole moment.

Polyethylene furnishes a good example of the simplification produced from symmetry considerations. The idealized molecule consists of methylene groups linked in a linear chain. The number of degrees of freedom for a chain with N atoms is $3N$. Of these, three are assigned to translation and three to rotation so that $3N-6$ remain to be assigned to vibrational modes of motion. Taking the ethylene moiety ($N=6$) as the repeat unit, the number of vibrational degrees of freedom in polyethylene is 12. Since a normal coordinate describes each vibration (Appendix 6B), and one coordinate characterizes a mode, interaction terms are eliminated. Appendix 6C presents the nomenclature denoting the vibrational modes. The vibrations are commonly referred to by their changes in skeletal geometry such as methylene stretching, bending, twisting or wagging. These vibrations can be either symmetrical or anti-symmetrical with respect to a center of gravity. The usual convention for a Cartesian coordinate system places the chain axis along the x axis, the plane of the carbon atoms is then used to define the y axis and the z axis is taken as perpendicular to this plane (Figure 6.4). Only eight of the twelve methylene vibrations in polyethylene result in a dipole change: three along the x -axis, three along the y -axis and two along the z -axis. Their approximate location in the polyethylene spectrum may be estimated from the magnitude of the force constants associated with a

particular vibrational mode. Thus, the observation that the stretching modes are found at higher frequencies (2900 cm^{-1} than are the bending 1500 cm^{-1}) modes correlates with their respective force constants (4.6×10^5 dynes/cm for stretching 0.35×10^5 dynes/cm for bending). The use of a polarized (Chapter 4) incident infrared beam facilitates interpretation of the spectrum in that vibrational symmetry determines the polarization of an absorption band.

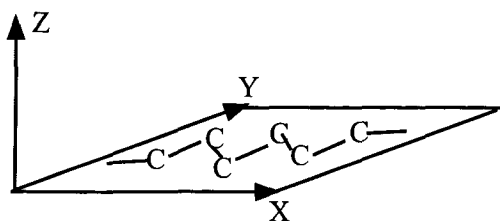


Figure 6.4. Relation between a chain axis and a Cartesian coordinate system.

The main absorption bands of the polyethylene spectrum have been assigned to the different infrared active modes [4-6], but details, particularly in the fingerprint region of $700\text{--}600\text{ cm}^{-1}$, remain to be worked out because of interactions between vibrational modes. Several references [2,3,6,7,8] give details on the mathematical apparatus used to interpret the infrared spectra of polymers.

Vibrational spectra are interpreted at several levels of sophistication. The simplest level compares the spectrum of an unknown polymer with those of known polymers. A good match or correspondence between absorption bands in the spectra of a known and an unknown polymer in the fingerprint region ($700\text{--}600\text{ cm}^{-1}$) constitutes strong evidence that the two polymers are identical. The numerous infrared bands originate from many types of atomic motions and slight changes in structure or composition result in perceptible spectral changes such as frequency shifts and band intensity variations. Another level combines structural information obtained from other techniques (x-ray, chemical analysis, mechanical and thermal properties) with the location of infrared absorption bands in compounds with homologous structures in order to assign the origin of a particular band to a specific vibration. Thus, in the

polyethylene spectrum, the 2860–2900 cm^{-1} doublet is assigned to methylene CH_2 stretching modes based on comparison with n-paraffin structure and chemical structure data. The most difficult level in interpretation of infrared spectra involves calculation of band frequency based on vibrational motion. Molecular symmetry, Raman spectrographic and polarization data are used as aids in interpretation. In principle, the dynamical equations for vibratory motion worked out by physicists over the last century (Rayleigh [9], Brillouin [1], Herzberg [7]) should be capable of being applied to infrared data by scaling the equations to atomic dimensions. In practice, the interactions between vibratory motions, the imperfections present in real chains and the selection of force constants present formidable difficulties in calculating the infrared band frequencies of polymers.

Assignment may be aided from studies of the polarization behavior of oriented polymers. For example, when polyethylene is stretched, the chain of carbon atoms become oriented in the stretching direction. As a result, the plane of the C-H bonds of the CH_2 groups will be perpendicular to this direction. Consequently, the CH_2 bending vibration will result in absorption polarized perpendicular to the stretching direction while the wagging vibration leads to absorption for parallel polarization.

Assignments may also be aided by isotopic substitution. For example, replacements of H by its isotope, D, doubles the mass but little effect on force constants, Consequently, vibrations involving it are shifted to lower frequencies by a predicable amount.

Deuterium substitution is also used in fiber optics. For fiber optics communication, it is necessary to have fibers of high transparency to avoid attenuation of signals. Optical fibers are conventionally made from very pure glass, but polymeric fibers are often of interest because of their lighter weight and superior mechanical properties. These have the disadvantage that they offer greater attenuation arising from scattering from impurities and density fluctuation, but sometimes arise from absorption due to the tails of infrared bands which extend into the visible. One approach to this is to employ deuterated polymers so as to shift these infrared band to lower frequencies.

Normal coordinate calculations on polymers are discussed in Appendix 6B.

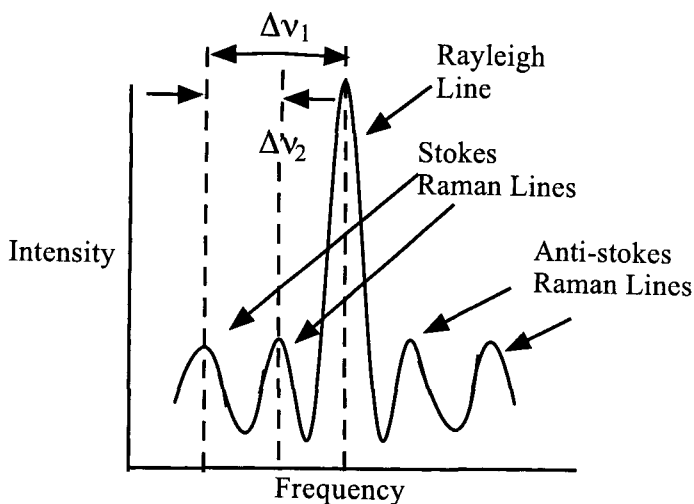


Figure 6.5. Diagram showing the relation between the transmitted beam and the Stokes and anti-Stokes lines.

6.4. Raman

Raman scattering is a technique for studying vibrational spectra that has gained in popularity with the availability of lasers that generate coherent, intense, parallel light beams. Prior to their use, light sources such as mercury arcs were necessary. These were cumbersome and of lower intensity than is available with lasers, so data acquisition times were long. Consequently, the technique was not widely used. The major portion of the scattered radiation has the same wavelength as that of the incident beam (Chapter 4). However, for certain molecules, a portion of the incident radiation is absorbed at one frequency ν_a and scattered at a lower frequency ν_e (Anti Stokes line) or at a higher frequency (Stokes line) (Figure 6.5). The absorption occurs from energy transitions between vibration and rotational states. The equation describing the absorption process in Raman scattering is given by

$$\Delta E = \hbar(\nu_a - \nu_e) \quad (6.22)$$

where \hbar is Planck's constant. A change in polarizability of the molecular bonds characterizes the absorption process in molecular terms. Thus, the electric field, E , incident on a diatomic molecule, with an electric field E_0 of a frequency ν_0 is given by

$$E = E_0 \sin 2\pi\nu_0 t \quad (6.23)$$

The incident field induces a periodic oscillation of the bonding electrons with time. The bond therefore acquires an induced dipole or electric moment vector

$$\alpha E = \mathbf{P} = \alpha E_0 \sin 2\pi\nu_0 t \quad (6.24)$$

where α is the polarizability. The molecule acts as a Hertzian oscillator and radiates energy. If the polarizability is constant with no variation over time, the energy is radiated in the form of electromagnetic waves at a constant frequency ν_0 . If however, the oscillation produces a periodic variation in bond polarizability, then it is assumed that equation 6.24 may be expressed by a series of the form

$$E_0 \sin 2\pi\nu_0 t \left[\alpha_0 + \left(\frac{d\alpha}{dq} \right) s \cos(2\pi\nu t + \varepsilon) + \left(\frac{1}{2} \right) \left(\frac{d^2\alpha}{dq^2} \right) s^2 \cos^2(2\pi\nu t + \varepsilon) + \dots \right] \quad (6.25)$$

where s is the amplitude of the normal coordinate q specifying a particular vibration and ε is the phase of the vibration. It is further assumed that the change in polarizability may be approximated by the first two terms in equation 6.25. On truncating and rearranging, equation 6.24 becomes

$$\alpha E = \alpha_0 E_0 \sin 2\pi\nu_0 t + E_0 s \left(\frac{d\alpha}{dq} \right)_0 \sin 2\pi\nu_0 t + \cos(2\pi\nu t + \varepsilon) \quad (6.26)$$

By using the trigonometric identity,

$$\sin A \cos B = \left(\frac{1}{2} \right) \left[\sin(A + B) + \sin(A - B) \right] \quad (6.27)$$

and rearranging, equation 6.25 is transformed to

$$\alpha E = \left(\frac{1}{2}\right) \left[\sin\{2\pi(\nu_0 + \nu)t + \varepsilon\} + \sin\{2\pi(\nu_0 + \nu)t - \varepsilon\} \right] \quad (6.28)$$

The radiation scattered from Raman active molecules thus has three components: the central line at a frequency ν_0 due to Rayleigh scattering and two ancillary lines displaced to either side: the Stokes ($\nu_0 + \nu$) and the anti-Stokes ($\nu_0 - \nu$) lines (Figure 6.6). The magnitude of the shift and the peak intensity can be related to molecular vibrations using normal coordinate analysis and other mathematical tools discussed in Section 6.3.

	Active Mode	Vibration Direction
	IR active	
	Raman active	
	Raman active	
	IR active	
	Both modes active	
	Both modes active	
	Both modes active	

Figure 6.6. Raman and infrared active frequencies.

The complexity of Raman spectra for polymers is reduced as with infrared spectra because vibrations of the same type superimpose. In addition, as with infrared spectroscopy, selection rules aid in determining which molecular vibrations are active. However, the criterion for Raman activity is a change in bond polarizability with molecular vibration or rotation in contrast to the infrared criterion of a change in dipole moment (Figure 6.6). This means that, for molecules such as carbon dioxide that show both a change in dipole moment and a change in polarizability,

additional information about their atomic structure may be obtained by using both infrared and Raman measurements.

The number of normal modes is reduced by symmetry considerations. For polyethylene, with a center of symmetry in the repeat unit, vibrational modes that are infrared active are Raman inactive and vice versa. Eight modes are active: four in the infrared [$1A_u$, $1B_{1u}$, $2B_{2u}$ and $2B_{3u}$] (Appendix 6C) and four in the Raman [$3A_{2g}$, $2B_{1g}$, $2B_{2g}$ and $1B_{1g}$] with the A_u mode being inactive in both. Thus, only four normal modes out of a possible twelve are associated with the normal modes of vibration in the polyethylene repeat unit.

Thus, Raman spectroscopy complements infrared in that normal modes not observable by infrared spectroscopy may be accessed. For molecules having a center of symmetry, Raman and infrared bands are mutually exclusive in that normal modes observed by one technique are not seen by the other.

There are experimental advantages to Raman spectroscopy in that conventional glass optics can be employed and better detectors are available for visible radiation than for infrared (although there have been impressive developments in the latter stimulated by military needs). Also, infrared absorbencies are such that very thin samples are usually necessary; whereas, thicker samples can be employed with Raman. Also, laser beams can be focused to illuminate small areas making it possible to study the spatial variation of the spectra. Fiber optics can be employed to "pipe" the incident radiation to the desired position in the sample and to collect the scattered light.

There are disadvantages to the Raman technique. Many samples contain fluorescent impurities or are inherently fluorescent. This fluorescence leads to background radiation, which often makes the observation of Raman spectra difficult. However, methods have been devised, for example using high resolution monochromators, which help circumvent this problem.

Also, phase separated or crystalline samples exhibit intense Rayleigh scattering, rendering difficult the observation of the Raman satellites in the presence of this intense central band.

6.5. Ultraviolet and Visible

The energy associated with ultraviolet ($\nu = 200\text{--}400\text{ nm}$) and visible ($\nu = 400\text{--}700\text{ nm}$) light photons can be calculated from equation 6.1 and lies in the region of electronic transitions. In contrast to the relatively small number of vibrational and rotational transitions available to nuclei (the basis for infrared and Raman spectra), electrons possess a multitude of transition states. Electrons can move from any of a number of ground states to many accessible excited states on absorption of a photon. In comparison to an infrared spectrum that typically shows many sharp absorption bands, a typical ultra-violet spectrum has only a few broad absorption bands. The frequency at which the band has a maximum (ν_{\max}) and the intensity of the absorption (ϵ_{\max}), the extinction coefficient (see equation 6.5) at ν_{\max} characterizes these bands. For polyvinyl alcohol, the maximum in the spectra shifts from the ultraviolet to the visible regions of the electromagnetic spectrum as the alcohol group is systematically removed from the main polymer chain and the number of conjugated double bonds increases (10). This same process is used to produce one type of PolaroidTM film. Polyethylene is rendered more biodegradable by introducing C=O groups in polyethylene to absorb ultraviolet light and lead photo degradation. As with infrared and Raman spectra, the ultraviolet and visible intensities vary with the orientation of a polarized light source.

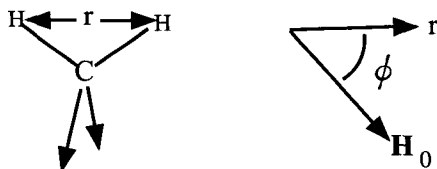


Figure 6.7. Diagrams showing the relation between the distance of the hydrogen atom, r , the applied magnetic field, H_0 and ϕ the angle between H_0 and r .

Ultraviolet dichroism has been applied to polymer orientation studies [11,12]. Quantitative analysis of the amount of conjugated unsaturated structure in rubbers can also be determined from ultraviolet and spectroscopic data. Conjugated systems such as polyenes or aromatics

lower the electronic frequencies to the ultraviolet range. These compounds thus can be measured by fluorescence.

The development of unsaturation as a result of polymer degradation (as with poly(vinyl chloride) which can do so by losing HCl) which often develops a yellowish color as it ages. To obtain colorless polymer, it is necessary to avoid such changes and to eliminate impurities which may absorb in the visible.

6.6. Nuclear Magnetic Resonance

Certain atomic nuclei possess spin angular momentum and a resulting magnetic moment (\mathbf{u}_0). When placed in a magnetic field, these nuclei can occupy one of two spin states, either with or against the field direction [13]. The proton, with a spin quantum number of 1/2, is a prominent example of a nucleus with a magnetic moment. Other nuclei with a magnetic moment are carbon¹³, fluorine¹⁹, silicon²⁹ and phosphorous³¹.

The energy absorbed or emitted (ΔE) in the transition between energy levels by nuclei with spin is given by

$$\Delta E = g(\mathbf{u}_0 \cdot \mathbf{H}_0) \quad (6.29)$$

where \mathbf{H}_0 is the applied magnetic field and g is the spectroscopic splitting factor (with a value of 2 in the case of the proton). The frequency (ν_0) at which a particular transition occurs is given on combining equations 6.1 and 6.29 by

$$\hbar\nu_0 = 2\mathbf{u}_0 \cdot \mathbf{H}_0 \quad (6.30)$$

where \hbar is Planck's constant. Nuclear magnetic resonance measurements may thus be performed by varying either the frequency or the magnetic field strength. Typically, the magnetic field strength is varied (or swept) while the frequency is held constant and the energy change in the form of a resonant absorption peak between the magnetic field strength and the fixed frequency is recorded.

Commercial spectrometers commonly sweep in the field strength range between 9000 and 23,000 Gauss. Newer equipment is capable of generating field strength of 60,000 to 220,000 Gauss with a concomitant narrowing of the absorption bands. Calculations based on equation 6.30 show that, a frequency of 40 Mc/sec (the radio region of the

electromagnetic spectrum) gives rise to a proton resonance at a magnetic field strength of 10,000 Gauss. The dipole-dipole interaction between pairs of identical nuclei of spin 1/2 (e.g. protons) broadens the absorption line into a band (H) characterized by the expression.

$$H = \frac{3u}{r^3} (\cos^2 \beta - 1) \quad (6.31)$$

where r is the distance between protons and β is the angle between a line joining the protons and O (Figure 6.7). The magic spinning angle technique (14) is based on equation 6.29. The nuclei are oriented at a beta value of 56.3° by an auxiliary magnetic field in order to minimize H and thereby narrow the absorption band [14]. The band broadening may be calculated either from the line width at half the peak intensity or by the second moment of the NMR curve defined by

$$S_2 = \frac{\int_{-\infty}^{\infty} (H - H_0)^2 f(H) dH}{\int_{-\infty}^{\infty} f(H) dH} \quad (6.32)$$

where S_2 represents the mean-square deviation of the field from the center of the line H_0 . The NMR technique is used to characterize polymer transitions (Chapter 3), polymer orientation and to estimate the degree of crystallinity (Chapter 8). It is particularly suited for the study of chain configuration or microstructure and atomic motion because of its high sensitivity and selectivity to protons and carbon¹³.

6.7. Neutron Inelastic Scattering (NIS)

The condition that the incident and scattered radiation have the same wavelength defines elastic scattering. Inelastic scattering, on the other hand, involves a shift in scattered radiation frequency associated with the motion of the scattering atoms. This shift originates from the Doppler effect. The broadening of scattered radiation frequency compared to a monochromatic neutron incident beam characterizes the spectrum of vibrational motions of the atoms or molecules involved in the scattering process. If such motions are quantized, as in the vibrational transitions in solids, discrete frequency shifts occur resulting in Brillouin spectra [14].

Neutron scattering involves interactions of a neutron beam with atomic nuclei (Figure 4.3). The wave like nature of a beam of neutron particles each with mass M_n is incorporated in the deBroglie equation which states that the wave length of a neutron beam, λ , is inversely proportional to the particle velocity, v , or

$$\lambda = \frac{\hbar}{M_n v} \quad (6.33)$$

where \hbar is Planck's constant. The neutron source temperature determines the velocity, a range of wavelengths and hence a spectrum can be generated by use of equipment such as a rotating channel monochromator [15,16]. In contrast to scattering by electromagnetic radiation in which the scattering power increases roughly with increasing atomic number, the scattering power of a neutron beam varies in an erratic fashion with atomic number. A great advantage of neutron scattering is that hydrogen scatters much more strongly than does deuterium.

As shown in Table 6.1, the scattering power may be changed by isotopic substitution, in this case, the replacement of hydrogen by deuterium with negligible effects on chemical structure. Thus, NIS measurements are particularly useful for studying hydrogen-containing compounds that include most of the common polymers.

Table 6.1 Comparison of the Scattering Intensity for Hydrogen and Deuterium

Species	Neutron Scattering Length
	cmx10 ¹²
Hydrogen	-0.372
Deuterium	+0.667
CH ₂	-0.083
CD ₂	+1.109

A second advantage is that the frequency distribution or density of vibrational states can be obtained from these measurements. These data complement those determined from infrared and Raman measurements.

A disadvantage is that the frequency can be measured only up to roughly 600 cm^{-1} because of source intensity limitations. The energy of thermal neutrons lies in the same range as that of the chain lattice vibrations. Neutrons in this energy range can either gain or lose energy when traversing a medium. In addition, the possibility exists that interference effects (Chapter 4) may occur between the scattered neutron beams. If these effects are observed, the scattered beam is said to be coherent; if not, the beam is incoherent. For solid polymers, analysis of the energy distribution of an incoherent, inelastically scattered neutron beam furnishes information [17,18] on the low frequency internal and lattice vibrations ($\approx 15\text{ cm}^{-1}$).

References

A general reference to Spectroscopy is: E.B. Wilson, Jr., J.C. Decius and P.C. Cross,
Molecular Vibrations; Dover, New York, 1980

Specific references are:

1. Leon Brillouin,
Wave Propagation in Periodic Structures, 2nd. Ed; Dover: New York, 1953
2. G. Zerbi, *Appl. Spec. Rev.* **1969**, 2, 193
3. S. Bhagavatam and T. Venkatarayudu,
Theory of Groups and its Application to Physical Problems,
3rd ed.; Andra University: Waltair, India, 1962
4. K. Holland-Moritz and H.W. Siesler, *Appl. Spec. Rev.* **1976**, 11, 1
5. R. Zbinden, *Infrared Spectroscopy of High Polymers*; Academic: New York, 1955
6. S. Krimm, *Adv. in Polymer Science.* **1960**, 2, 51
7. G. Herzberg, *Infrared and Raman Spectra of Polyatomic Molecules*;
Van Nostrand: Princeton, N.J, 1945
8. H.W. Siesler and K. Holland-Moritz, *Infrared and Raman Spectra of Polymers* ;
Dekker: New York, 1980
9. Lord Rayleigh, *The Theory of Sound, Vol.1 2nd Ed.*; Dover: New York, 1945
10. R.S. Stein and Y. Shindo, *J. Poly. Sci., Part B* **1967**, 5, 737
11. R. Yamada, R.S. Stein, *J. Polymer Sci.* **1964**, B2, 1131
12. Y. Shindo, B.E. Read, R.S. Stein, *Macromol. Chem.* **1964**, 118, 272
13. F.A. Bovey, *Nuclear Magnetic Resonance Spectroscopy*; Academic: New York, 1969
14. J. Schaefer, E.O. Stejskal, R. Buchdahl, *Macromolecules.* **1975**, 8, 291
15. W.L. Earl, D.L. VanderHart, *Macromolecules.* **1979**, 12, 762
16. A. Mononachie, R.W. Richards, *Polymer.* **1978**, 19, 739
17. D.G.H. Ballard, J. Shelten, *J. Cryst. Growth.* **1980**, 48, 169
18. P.R. Griffiths, J.A. deHaseth, *Fourier Transform Infrared Spectroscopy*,

TOPICS in POLYMER PHYSICS

Wiley-Interscience: New York, 1986

Appendix 6A Fourier Transform Infrared (FTIR)

The infrared absorption frequencies may be determined either by direct measurement using a grating or prism to separate individual frequencies or by indirect measurement using a Michelson interferometer.

The direct method records frequencies individually after they are separated. Slits for collimating the beam are required in order to resolve the frequencies properly. Collimation discards most of the beam intensity so that the transmitted beam intensity is low with a consequent low signal to noise ratio. In order to increase intensity, scanning times are lengthened. The dispersive technique however requires relatively simple equipment and, for many samples, furnishes thoroughly adequate spectra. However, for conditions in which the sample has high absorbance or whose properties are changing rapidly, the Fourier transform infrared (FTIR) technique is preferred [1,2]. The technique measures the intensity distribution generated by a Michelson interferometer. The interference conditions are obtained by comparing the intensities after the incident light amplitude has been split by mirrors and then recombined. The distance that one beam travels is held fixed x_1 and the distance of the second x_2 is varied by means of a movable mirror. The changing path distance $\Delta (= x_2 - x_1)$ thus results in a shifting interference pattern or interferogram. The recombined amplitude (A) over the frequency range Δ_m is given (Chapter 4) by

$$A = rTA_0 \left\{ \exp[i(\omega t - 2\pi\nu x_1)] + \exp[i(\omega t - 2\pi\nu x_2)] \right\} d\nu \quad (6A.1)$$

where r is the reflection coefficient and T the transmission coefficient of the beam splitter. The intensity at a given path difference is obtained by squaring the amplitude or, more exactly, multiplying the amplitude by its complex conjugate

$$I(\Delta) = A(\Delta, \nu) \times A^*(\Delta, \nu) \quad (6A.2)$$

On substituting equation 6A.1 into 6A.2, and using the relation

$$\exp[i(\omega t - 2\pi\nu x_1)] = \sin(\omega t - 2\pi\nu x_1) + i \cos(\omega t - 2\pi\nu x_1) \quad (6A.3)$$

the intensity can be expressed by

$$I(\Delta) = 2A_0^2(rT)^2 \left\{ 1 + \cos[2\pi(x_2 - x_1)\nu] \right\} d\nu \quad (6A.4)$$

The total intensity at any path difference is obtained by integrating over the frequency range, or

$$I(\Delta) = \int_0^\infty I(\Delta, \nu) d\nu = 2(rT)^2 \left[\int_0^\infty A_0^2(\nu) d\nu + \int_0^\infty A_0^2(\nu) \cos(2\pi\Delta\nu) d\nu \right] \quad (6A.5)$$

The intensity at zero path difference $I(0)$ is equal to the first term on the right hand side of equation A.5

$$I(0) = 2|rT|^2 \int A_0^2(\nu) d\nu \quad (6A.6)$$

The interference pattern in terms of intensity can thus be expressed as

$$I(\Delta) - \frac{1}{2}I(0) = 2|rT|^2 \int_0^\infty A_0^2(\nu) \cos(2\pi\Delta\nu) d\nu \quad (6A.7)$$

The frequency distribution $A(\nu)$ can be obtained by performing a Fourier transformation [3] on equation 6A.7. This theorem states that, the periodic, orthogonal functions [3] $I(\Delta)$ and $B(\nu)$ are related by the symmetrical integral equations

$$I(\Delta) = \int_0^\infty B(\nu) \cos(2\pi\Delta\nu) d\nu \quad (6A.8)$$

and

$$B(\nu) = \int_0^\infty I(\Delta) \cos(2\pi\Delta\nu) d\Delta \quad (6A.9)$$

On performing a Fourier transformation on equation 6A.7, the frequency distribution $F(\nu)$ can be extracted from the interferogram

$$I(\Delta) = \int_0^\infty B(\nu) \cos(2\pi\Delta\nu) d\nu \quad (6A.10)$$

$B(\nu)$ is generated by multiplying each data point by $\cos(2\pi\nu\Delta)$ at each ν value thereby entailing a great deal of computational labor. This redundancy however improves the signal to noise ratio since the signal increases linearly with the number of points, N , while the noise increases as the square root of N . For a 1 cm^{-1} resolution over a 3600 cm^{-1} range, the signal to noise ratio improves by a factor of 60 for the FTIR

compared to the dispersive technique. Scanning speeds are limited only by the rate of mirror movement and not by energy considerations as happens sometimes with dispersive instruments. A complete scan can thus be done in seconds. The FTIR technique became feasible for routine applications with the development of microcomputers that could be dedicated to one spectrometer and the invention of short cuts in solving Fourier transforms such as the Cooley-Tukey algorithm [4]. The Fourier transform technique data are obtained in digital form in contrast to the analog data obtained by the dispersive technique. Data in digital form can be readily used by computers to subtract one spectrum from another or to add additional scans to a spectrum to improve the signal to noise ratio.

This technique has given added impetus to the examination of polymer problems such as the interaction between carbon black and rubber [5], the influence of plastizer on poly(vinyl chloride) properties [5] and chain orientation [6].

References

1. R.J. Bell, *Introductory Fourier Transforms*; Academic: New York, 1972
2. J.L. Koenig, *Applied Spectroscopy*, 1975, 29, 293
3. H. Margenau, G.M. Murphy, *The Mathematics of Physics and Chemistry*, 2nd. ed.; D. van Nostrand: Princeton, N.J. 1954
4. J.W. Cooley, J.W. Tukey, *Math. Comput.* 1965, 19, 297
5. M.M.Coleman, P.C. Painter, *Applications of Polymer Spectroscopy*, E.G.Brame.jr, Ed., Academic: New York, 1978
6. B.Jasse, J.L. Koenig, *J. Polymer Sci.:Polymer Phys. Ed.* 1979, 17, 799

Appendix 6B. Normal Coordinate Analysis

Many problems in vibration analysis are difficult to solve using a Cartesian co-ordinate system. These coordinates change in a complex manner with the translation, vibration and rotation of molecules or other bodies because of interaction terms. When Cartesian coordinates are transformed into normal coordinates, as shown below, the interaction terms disappear and a motion can be expressed in terms of a single normal coordinate.

Consider a one dimensional approximation of a triatomic linear molecule represented by identical mass points with mass, m , linked by weightless Hookian springs with force constants, a_s , (Figure 6.2). The equations of motion for this system is given (equation 6.9) by

$$m \frac{\partial^2 x_1}{\partial t^2} - \alpha_s (x_2 - x_1) = 0 \quad (6B.1)$$

$$m \frac{\partial^2 x_2}{\partial t^2} - \alpha_s (x_2 - x_1) - \alpha_s (x_3 - x_2) = 0 \quad (6B.2)$$

and

$$m \frac{\partial^2 x_3}{\partial t^2} - \alpha_s (x_3 - x_2) = 0 \quad (6B.3)$$

These are Newton's equations for the forces on the three atoms. For ease in manipulating coefficients later on, equation 6B.1 is multiplied by an arbitrary constant C_1 , B-2 by C_2 and B-3 by C_3 , or

$$C_1 m \frac{\partial^2 x_1}{\partial t^2} + C_2 m \frac{\partial^2 x_2}{\partial t^2} + C_3 m \frac{\partial^2 x_3}{\partial t^2} - C_1 (x_2 - x_1) - C_2 f (x_3 - 2x_2 - x_1) - C_3 f (x_2 - x_3) = 0 \quad (6B.4)$$

Rearranging terms

$$C_1 m \frac{\partial^2 x_1}{\partial t^2} + C_2 m \frac{\partial^2 x_2}{\partial t^2} + C_3 m \frac{\partial^2 x_3}{\partial t^2} - \alpha_s [(C_2 - C_1)x_1 - (C_1 - 2C_2 - C_3)x_2 - (C_2 - C_3)x_3] = 0 \quad (6B.5)$$

SPECTROSCOPY

At this point, if the coordinates in equation 6B.5 are transformed into a set of normal coordinates, q , that constitute a linear combination of the x 's, the equation of motion can be simplified. That is, if

$$q = \sum_{i=1}^3 h_i x_i = h_1 x_1 + h_2 x_2 + h_3 x_3 \quad (6B.6)$$

then the equation of motion can be written as

$$\frac{\partial^2 q}{\partial t^2} + \lambda q = 0 \quad (6B.7)$$

where λ is the root, characteristic value or eigenvalue for equation 6B.7 (24). This is a typical wave equation (see Chapters 4) for which a solution (1) is

$$q = A e^{i\omega t} \quad (6B.8)$$

where ω equals $2\pi\nu$ (ν is the frequency) and A , a constant amplitude. The term in λ may be evaluated by substituting equation 6B.8 in equation 6B.7

$$-\omega^2 A e^{i\omega t} + \lambda e^{i\omega t} = 0 \quad (6B.9)$$

or

$$\lambda = \omega^2 \quad (6B.10)$$

The coefficients in equation 6B.5 and h in equation 6B.6 may be related by the following procedure. Substituting 6B.6 into 6B.7, yields

$$h_1 \frac{\partial^2 x_1}{\partial t^2} + h_2 \frac{\partial^2 x_2}{\partial t^2} + h_3 \frac{\partial^2 x_3}{\partial t^2} + \omega^2 h_1 x_1 + \omega^2 h_2 x_2 + \omega^2 h_3 x_3 = 0 \quad (6B.11)$$

Then, on comparing equations 6B.5 and 6B.11 and rearranging terms, the result may be written in the form

$$(U+1)C_1 + UC_2 + C_3 = 0 \quad (6B.12)$$

$$C_1 + UC_2 + C_3 = 0 \quad (6B.13)$$

$$C_2 + (U+1)C_3 = 0 \quad (6B.14)$$

where

$$U = \frac{m\omega^2}{f} = 2 \quad (6B.15)$$

Solving for C_1 by the method of determinants (25) gives

$$C_1 = \frac{\begin{vmatrix} 0 & 1 & 0 \\ 0 & U & 1 \\ 0 & 1 & U+1 \end{vmatrix}}{\begin{vmatrix} U+1 & 1 & 0 \\ 1 & U & 1 \\ 0 & 1 & U+1 \end{vmatrix}} \quad (6B.16)$$

The number is obviously equal to zero. C_1 will be different from zero only if the denominator is zero. Similar considerations apply to C_2 and C_3 . Thus, non-zero solutions for C_1 , C_2 and C_3 exist only for solutions of the secular equation

$$\begin{vmatrix} U+1 & 1 & 0 \\ 1 & U & 1 \\ 0 & 1 & U+1 \end{vmatrix} = 0 = U(U+1)^2 - 2(U+1) = (U+1)(U+2)(U-1) \quad (6B.17)$$

Equation 6B.17 has three solutions $U = -1, -2, +1$. The corresponding values of ω (from equation 6B.15) are $f/m, 0$ and $3f/m$. For the solution $\omega_1 = 0$, substituting into equations 6B.12, 6B.13 and 6B.14,

$$C_1 = C_2 = C_3 = C \quad (6B.18)$$

and

$$h_1 = cm = h_2 = h_3 \quad (6B.19)$$

Thus, the normal coordinate, q , is given (equations 6B.6 and 6B.8) by

$$q_1 = cm(x_1 + x_2 + x_3) = Ae^{i\omega_1 t} = A_1 \quad (6B.20)$$

Similar substitutions for $\omega_2^2 = (\alpha_s/m)$ and $\omega_3^2 = (3\alpha_s/m)$ yields

$$q_2 = cm(x_1 - x_3) = A_2 \exp^{i\omega_2 t} = A_2 \cos \omega_2 t \quad (6B.21)$$

SPECTROSCOPY

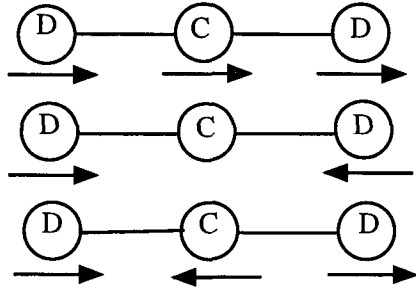


Figure 6B.1 . Normal modes of vibration for a triatomic molecule, labels C and D show different atoms.

and

$$q_3 = c_m(x_1 - 2x_2 + x_3) = A_3 \cos \omega_3 t \quad (6B.22)$$

respectively. If now,

$$B_i = A_i / c_m \quad (6B.23)$$

equations 6B.18, 6B.19 and 6B.20 become

$$x_1 + x_2 + x_3 = B_1 \quad (6B.24)$$

$$x_1 - x_3 = B_2 \cos \omega_2 t \quad (6B.25)$$

$$x_1 - 2x_2 + x_3 = B_3 \cos \omega_3 t \quad (6B.26)$$

The Cartesian coordinates x_1, x_2, x_3 can be expressed on rearranging equations 6B.24, 6B.25 and 6B.26 as motions that are combinations of normal modes

$$x_1 = \frac{1}{3} B_1 + \frac{1}{2} B_2 \cos \omega_2 t + \frac{1}{6} B_3 \cos \omega_3 t \quad (6B.27)$$

$$x_2 = \frac{1}{3} B_1 - \frac{1}{3} B_3 \cos \omega_3 t \quad (6B.28)$$

$$x_3 = \frac{1}{3} B_1 - \frac{1}{2} B_2 \cos \omega_2 t + \frac{1}{6} B_3 \cos \omega_3 t \quad (6B.29)$$

The B terms represent the relative amounts of the various modes contributing to a given motion and they are determined by the initial conditions.

Thus, for $B_2 = B_3 = 0$ (from equations 6B.27 to 6B.29)

$$x_1 = x_2 = x_3 = \frac{1}{3}B_1 \quad (6B.30)$$

This motion corresponds to a translation of the molecule (top line Figure 6B.1).

For $B_1 = B_3 = 0$

$$x_1 = -\frac{1}{2}B_2 \cos \omega_2 t \quad (6B.31)$$

$$x_2 = 0 \quad (6B.32)$$

$$x_3 = -\frac{1}{2}B_2 \cos \omega_2 t \quad (6B.33)$$

corresponding to symmetric stretching (middle line Figure 6B.1). This normal mode is Raman active because the vibration is symmetrical.

For $B_1 = B_2 = 0$

$$x_1 = x_3 = \frac{1}{6}B_3 \cos \omega_3 t \quad (6B.34)$$

$$x_2 = -\frac{1}{3}B_3 \cos \omega_3 t \quad (6B.35)$$

corresponding to an anti-symmetric mode of vibration (bottom line Figure 6B.1). This normal mode is infrared active because the dipole moment is an unsymmetrical vibration.

These are the three normal modes of this molecule. Each motion is expressed in terms of only one normal coordinate. Any other motion can be represented as a linear combination of these normal modes. These arguments can be extended to the case of long polymer chains.

References

1. H. Margenau, G.M. Murphy ; *The Mathematics of Physics and Chemistry, 2nd. Ed.* Van Nostrand: Princeton, N.J. 1953
2. L. Brillouin, *Wave Propagation in Periodic Structures, 2nd. Ed;* Dover: New York 1953

Appendix 6C. Spectrographic Notation

The symmetry operations of rotation, reflection, inversion and glide reflection obey all the tenets of group theory [3,5]. Matrix equations can express the results of these operations. The trace or spur of diagonal matrices (Appendix 3D) is particularly valuable in condensing the information contained in symmetry operations on polymer chain subunits. The terms irreducible representation, symmetry type, and species are also used in denoting the trace [12].

The line group concept was formulated for a one-dimensional chain [14]. The species for the operations on a molecular line group are denoted as follows:

A and B represent the species group symmetric and non-symmetric respectively to an axis of symmetry. The subscript g (German gerade-even) denotes a species symmetric with respect to a center of symmetry or an inversion operation while the subscript u (German ungerade-odd) refers to a species non-symmetric to a center of symmetry. The subscripted number refers to the number of symmetry operations in a given operation.

Thus, the notation B_{1g} for polyethylene stands for a symmetry species that is non-symmetric with respect to a symmetry axis, is symmetric with respect to an inversion operation and has only one irreducible representation.

Chapter 7

THE RUBBERY STATE

7.1. Introduction

Rubbers are fascinating materials for study (as well as having enormous importance in technological applications) because they combine characteristics typical of the three states of matter. Uncrosslinked, they resemble liquids in their flow behavior. Crosslinked, they are able to recover their original dimensions after being severely deformed (stretched, compressed or sheared) above their glass temperatures. Rubbers or elastomers however resemble solids in their resistance to flow and to maintain their shape, if crosslinked and below their glass temperature, when subjected to deformation. Finally, as mentioned below, an explanation for their response to deformation can be described in terms of the behavior of a perfect gas.

As stated in Chapter 1, the rubbery state is unique to polymeric materials. Material classes such as silicates or organic liquids are capable of forming glasses and other classes such as metals or ceramics form polycrystalline aggregates. This uniqueness is associated with the extensible one-dimensional chain and sheet structures possessed by polymers, in contrast to the rigid two-dimensional (graphite) or three dimensional (diamond, metals) structures characteristic of other materials. As discussed in Chapter 2, the single isolated polymer chain extends from its equilibrium conformation on the application of a force because of free rotation about the backbone bonds. This extension reduces the chain entropy because fewer conformations are available to the chain at the larger end-to-end distance (Figure 7.1). On removal of the force, the increase in chain entropy from the larger number of conformations now available to the chain favors chain contraction. Based

on these thermodynamic arguments, the contractive force is proportional to the distance between chain ends (equation 7.1) so long as the chain does not approach complete extension and its statistics are Gaussian. In addition, internal energy contributes little or nothing to the retractive force as is true for an “ideal rubber”. For a real rubber, there may be an internal energy contribution. In the bulk polymer, the application of a tensile force can lead to slippage between chains, large-scale flow and ultimate sample fracture. The amount of flow however can be regulated by the insertion of crosslinks between chains. A small number of crosslinking junction points suffice to suppress large-scale chain flow without sacrificing the chain extension on a local scale required for elastomeric behavior.

In summary, the requirements for a material to exhibit rubber-like properties are:

1. a long chain structure with little or no hindrance to rotation between chain segments.
2. low intermolecular interactions [1].
3. the formation of an extended network structure by a few crosslinking points between chains.

This chapter deals with the properties of large assemblages of rubber chains, in contrast to the thermodynamic properties of isolated chains considered in Chapter 3. The chains are considered to be only lightly crosslinked; at most, to the extent that there is sufficient chain length between crosslinks so that Gaussian random chain statistics are applicable. Equations are also derived relating the network structure produced by crosslinking to deformation and to swelling – the two most important means of characterizing a network structure. In most cases, it is difficult to predict the number of crosslinks formed from the chemistry of the crosslinking reaction, so other means are needed for their determination. The equations derived below for solvent swelling of rubbers or for rubber deformation can be used to estimate the number of crosslinks a quantity important in many rubber applications. The thermodynamics of rubber elasticity is discussed in Chapter 3.

7.2. Force - Extension Relation for Rubbers

7.2.1. Simple Case

The equation of state for rubber networks (analogous to the equation of state for a perfect gas) may be derived in only a few steps. As shown previously, the force (f) on a single chain is described by the equation 3.23

$$f = \frac{3kT}{\langle R^2 \rangle_0} R \quad (7.1)$$

where R is the distance between chain ends and k is Boltzmann's constant. Let us consider a solid composed of such chains in terms of a simple model proposed by James and Guth (2) in which a cube of a rubbery solid has initial dimensions, L_0 , in the unstretched, and $L_x L_y L_z$ in the stretched state (Figure 7.1). There are a total of N chains. It is assumed that $(N/3)$ chains run parallel to each of the three coordinate axes that is,

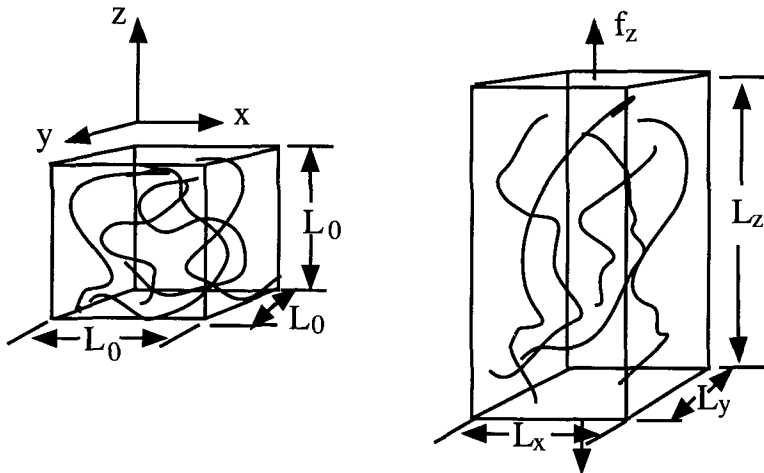


Figure 7.1 Dimensional changes on stretching an isotropic cube.

$$N_x = N_y = N_z = \frac{N}{3} \quad (7.2)$$

The contractile force (f_z) of the chains in the N_z direction is then $3N_z kTL_z / \langle R^2 \rangle_0$. If the contractile force were not balanced by an opposite and equal force, the network would collapse. For an incompressible rubber, the source of this opposing force is the volume of the chain that is assumed to exert a hydrostatic force P equal in all directions. Thus the balance of forces on the face normal to f_s gives

$$f_z + PL_x L_y = \frac{3N_z kTL_z}{\langle R^2 \rangle_0} \quad (7.3)$$

where f_z is the applied force in the z direction.

For a face normal to the X axis, there is no external force and

$$PL_x L_y = \frac{3NkTL_x}{\langle R^2 \rangle} \quad (7.4)$$

Solving for P and using equation 7.2 gives

$$P = \frac{3NkTL_x}{\langle R^2 \rangle L_x L_y} \quad (7.5)$$

This is then substituted in (7.3) to give

$$f_z + \frac{NkTL_x^2 L_y}{\langle R^2 \rangle_0 L_x L_y} = \frac{NkTL_x}{\langle R^2 \rangle} \quad (7.6)$$

and rearranging terms

$$f_z = \frac{NkT}{\langle R^2 \rangle} \left[L_z - \frac{L_x^2}{L_z} \right] \quad (7.7)$$

Now, the extension ratio, α , (for example for the z axis) is defined as

$$\alpha_z = L_z / L_0 \quad (7.8)$$

If the extension occurs at constant volume, (the material is incompressible)

$$L_x L_y L_z = L_0^3 \quad (7.9)$$

Also, if the network is initially isotropic, then the contraction in the X and Y directions will be equal so that

$$L_x = L_y \quad (7.10)$$

and equation 7.9 becomes

$$(\alpha L_0)L_y^2 = L_0^3 \quad (7.11)$$

or

$$L_x = L_y = \frac{L_0}{\alpha^{1/2}} \quad (7.12)$$

Substituting equation 7.12 into equation 7.7

$$f_z = \frac{NkT}{\langle R^2 \rangle} \left[\alpha L_0 - \frac{(L_0^2/\alpha)}{\alpha L_0} \right] = \frac{NkTL_0}{\langle R^2 \rangle} \left[\alpha - \frac{1}{\alpha^2} \right] \quad (7.13)$$

This equation is in the proper functional form for rubber elasticity and predicts the correct functional relationship between f and α . However, the relationship between the number of hypothetical chains in this network and the number of actual chains is not clear from our discussion but James and Guth [2] thoroughly explore this relationship.

7.2.2. Consideration of Network Crosslinks

A more exact calculation involves the calculation of the energy stored in a rubber network because of network deformation. This stored energy is expressed in terms of the Helmholtz free energy (A) and is derived from entropy considerations. The force-extension relation can then be calculated by taking the derivative of A with respect to elongation, as described below and in Chapter 3.2.

Consider a network that is crosslinked with ν crosslinking points per cm^3 , each of functionality, f . A network chain will be defined as that element of the network between two adjacent crosslinking points. There are N_0 such network chains (this network chain is to be distinguished from the original chain, the molecular entity present before the introduction of crosslinking points). Since f network chains emanate

from each crosslinking point and each chain is shared by two crosslinking points

$$\frac{N_0}{V} = \frac{fv}{2} \quad (7.14)$$

If, as is most common, $f = 4$,

$$\frac{N_0}{V} = 2v \quad (7.15)$$

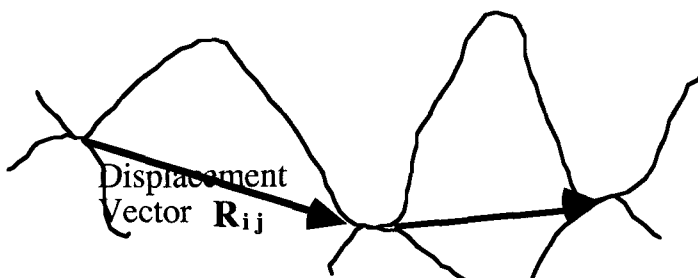


Figure 7.2 Definition of a network displacement vector.

A network displacement vector is that vector which connects two adjacent crosslinking points. This will be designated as \mathbf{R}_{ij} where j is the number of statistical segments for the network chain associated with the i^{th} vector (Figure 7.2).

Now assume that the chain distributions are in their most probable (which is assumed to be Gaussian) conformations at the time the crosslinks are introduced. (This is not always so, as in the case of crosslinking in the swollen state as will be discussed below.) The number, N_{ij} , of displacement vectors of type \mathbf{R}_{ij} (in the unstretched state) is

$$N_{ij} = N_j P_{ij} \quad (7.16)$$

where

$$P_{ij} = \left(\frac{\beta_j^3}{\pi^{3/2}} \right) \exp[-\beta_j^2 R_i^2] \quad (7.17)$$

N_j is the number of network chains per cm^3 having j statistical segments and P_{ij} is the probability that a chain of j segments will have a vector distance, \mathbf{R}_j between its ends. Also

$$\beta_j^2 = \frac{3}{2jL^2} \quad (7.18)$$

where L is the statistical segment length. It should be noted that it is possible to modify the derivation at this point to accommodate situations where the crosslinks were introduced in other than the most probable fashion. This would occur, for example, for elastomers crosslinked in a deformed, a swollen or a crystalline state. (These cases are discussed below.) Also, entanglements are neglected so that the conformations available to a chain are not restricted by the requirement that the chain cannot pass through another chain. The quantity, N_j is related to the statistics of introduction of crosslinks. In a regular copolymer of a di- and polyfunctional monomer, this may be a fairly sharp distribution function. A more common situation, however, is that in which the crosslinks are randomly introduced in which case.

$$N_j = N_c(1-q)q^{j-1} \quad (7.19)$$

where q is the probability that a segment is not crosslinked. It is noted that

$$\sum_{j=1}^{\infty} N_j = N_c \quad (7.20)$$

Let Ω be the number of conformations of a network and W_{ij} be the number of conformations of a chain of j segments with distance R_i between its ends. Then

$$\Omega = \frac{CN_c!}{\prod_{ij} N_{ij}!} \prod W_{ij}^{N_{ij}} \quad (7.21)$$

where, as we have seen

$$W_{ij} = \frac{\beta_j^3}{\pi^{3/2}} \exp[-\beta_j^2 R_i^2] \quad (7.22)$$

THE RUBBERY STATE

The factorial terms arise from the assumption that the network chains are identical and indistinguishable. The derivation can be generalized to the case of a distribution in N_j . In the unstretched state, where $\Omega = \Omega_0$, the entropy is

$$S_0 = k \ln W = k \ln C + N_c \ln N_c - N_c - \sum_{ij} N_{ij} \ln N_{ij} + \sum_{ij} N_{ij} + \sum_{ij} N_{ij} \ln W_{ij} \quad (7.23)$$

Using Stirling's approximation (equation 2G.10).

$$\sum_{ij} N_{ij} = \sum_i N_i \int P_{ij} dP_{ij} = N_0(1-q) \sum_{j=1}^{\infty} q^{j-1} \int_{R_j}^{\infty} \frac{\beta_j^3}{\pi^{3/2}} \exp[-\beta_j^2 R_i^2] dR_i = N_c \quad (7.24)$$

$$s_0 = k \left[\ln C + N_c \ln N_c + \sum_{ij} (N_{ij})_0 \ln \frac{W_{ij}}{(N_{ij})_0} \right] \quad (7.25)$$

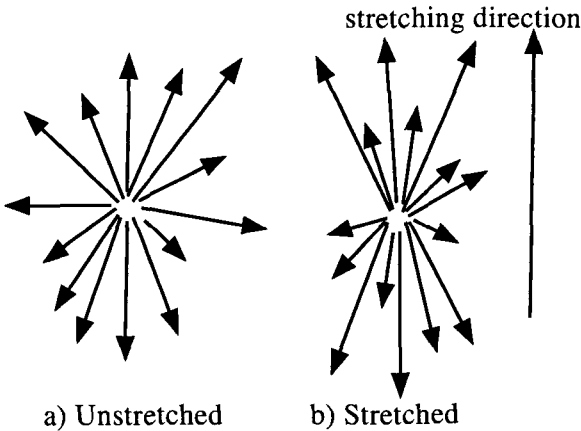


Figure 7.3. Transformation of chain vectors on stretching.

The use of Stirling's approximation assumes a sufficiently large value of N_{ij} . This assumption fails at high degrees of crosslinking and high extensions. The failure leads to "non-Gaussian" behavior. Note the similarity of the last term of this sum and that evaluated in the

consideration of the expansion factor of a single chain equation. The designation $()_0$ around N_{ij} indicates that this is the distribution of network vector applicable to the unstretched state.

When the network is stretched, the function N_{in} changes. The change in displacement vectors drawn from a common origin is shown in Figure 7.3. The three changes that occur are:

a) Vectors rotate toward the stretching direction.

b) Vector components oriented parallel to the stretching direction increase in length.

c) Vector components oriented perpendicular to the stretching direction decrease in length.

7.3. Affine Transformation

To quantitatively describe the change in N_{ij} upon stretching, Kuhn and Mark [3,4] assumed (and that may be partially verified) that the affine transformation fit. This affine assumption states that the components of the displacement vectors in the bulk sample change in the same ratio as do the external dimensions of the rubber, that is,

$$\alpha_x = \frac{L_x}{L_{0x}} = \frac{R_x}{R_{0x}} \quad (7.26)$$

and

$$\alpha_z = \frac{L_z}{L_{0z}} = \frac{R_z}{R_{0z}} \quad (7.27)$$

The Kuhn/Mark assumption undoubtedly overemphasizes this limitation on mobility as it presumes that the crosslink lacks mobility. The only part of the network not free to move are those on the constrained external surfaces of the sample, and a more exact treatment, covered by Guth and James, would sum over all conformations of the network, only subjected to those constraints on the external dimensions. This treatment gives special significance to the crosslinking points in that their average positions move in the same way as the external dimension of the rubber, but the intervening parts of the chain can adopt any configuration consistent with these constraints (referred to as the

“phantom network”). The only restriction on the crosslinking points is that several chains must meet at these locations. This means that they are not as free to move, as are other parts of the chain, that motion of the crosslinking points is possible subject to these constraints. The constrained external surface of the sample is the only part of the network not free to move. While the Kuhn/Mark theory does not allow spatial fluctuation of the mean position of the crosslink about its mean position, the Guth-James theory permits such fluctuation albeit independent of elongation. Because of this fluctuation, the entropy reduction upon stretching is less and the predicted modulus is 1/2 of that predicted by Kuhn/Mark. Both theories neglect the entropy reduction arising from entanglements. One attempt to include these is to consider such entanglements as physical crosslinks [5].

Flory [1] has pointed out that this device of defining microscopic variables (the fixed junction locations) by use of macroscopic constraints cannot be defended on statistical mechanical grounds. However, the same results can be obtained from statistical mechanics using a different procedure. The applicability of the affine transformation has been discussed [2,6,7] and equations of state have been derived that do not require the assumption of an affine deformation [1,2]. The derivation is based on the phantom network construct, mentioned previously, in which chains (and junction points) are permitted to move through locations occupied by neighboring chains and junctions. In real networks, steric hindrance restricts chains from a close approach to neighboring chains. Essentially, then, the phantom network model, being more exact and rigorous because it entails fewer assumptions, suggests the basic correctness of the affine deformation. Recently, Flory [8] has derived a model for the non-Gaussian behavior of electrometric networks on tensile deformation by combining elements of the affine and phantom network models. An outline of the Flory derivation is presented later in this chapter.

Benoit and coworkers [9] have furnished experimental support for the affine deformation of rubber networks. They carried out neutron scattering experiments on polystyrene/deuterated polystyrene polymers. Their analysis of the neutron scattering data showed that network structures do deform affinely. More recently, Han, Yu and coworkers

[10] measured the small angle neutron scattering (SANS) from polybutadiene networks. They concluded that their preliminary data supported the affine rather than the phantom network model. Although the precision was too low to make a firm decision on the choice between these alternatives certain, Flory [11] has suggested the need for an additional consideration in the theory. In the derivation, the number of chains, $(N_{ij})_0$, having a displacement vector, \mathbf{R}_{0i} , with coordinates $(\mathbf{R}_{0xi}$ \mathbf{R}_{0yi} $\mathbf{R}_{0zi})$ associated with a chain having j segments is given by

$$(N_{ij}) = N_j \frac{\beta_j^3}{\pi^{3/2}} \exp\left\{-\beta_j^2 [R_{0xi}^2 + R_{0yi}^2 + R_{0zi}^2]\right\} \quad (7.28)$$

realizing that

$$R_{0i}^2 = [R_{0xi}^2 + R_{0yi}^2 + R_{0zi}^2] \quad (7.29)$$

Now introducing transformations (7.26) and (7.27) (and the analogous one for R_z)

$$(N_{ij}) = N_j \frac{\beta_j^3}{(\alpha_x \alpha_y \alpha_z) \pi^{3/2}} \exp\left\{-\beta_i^2 \left[\frac{R_{0xi}^2}{\alpha_x^2} + \frac{R_{0yi}^2}{\alpha_y^2} + \frac{R_{0zi}^2}{\alpha_z^2} \right]\right\} \quad (7.30)$$

The $(\alpha_x \alpha_y \alpha_z)$ term in the denominator is necessary for normalization, so that equation 7.24 is still obeyed in the stretched state.

The entropy arising from the conformational disorder of the chain in the stretched state is given by analogy to equation 7. 25

$$S = k \left[\ln C + N_i \ln N_i + \sum_{ij} N_{ij} \ln \left(\frac{W_{ij}}{N_{ij}} \right) \right]$$

Upon evaluation (see Appendix 7A)

$$S = k \left[\ln C + N_c \ln N_c - \sum_j N_j \ln N_j - \frac{1}{2} N_c (\alpha_x^2 + \alpha_y^2 + \alpha_z^2 - 3) + N_c \ln(\alpha_x \alpha_y \alpha_z) \right] \quad (7.31)$$

S_0 is obtained from these expression when $\alpha_x = \alpha_y = \alpha_z = 1$

$$S_0 = k \left[\ln C + N_c \ln N_c - \sum_j N_j \ln N_j - \frac{3}{2} N_c \right] \quad (7.32)$$

The change in entropy on stretching is then

$$\Delta S_{\text{ELAST}} = S - S_0 = k N_c \left[-\frac{1}{2} (\alpha_x^2 + \alpha_y^2 + \alpha_z^2) + \ln(\alpha_x \alpha_y \alpha_z) \right] \quad (7.33)$$

If the uncrosslinked, undeformed network is taken as the reference state, a second contribution to the entropy (called ΔS_{net}) must be included that is the reduction in entropy arising from the restriction of network chain ends to crosslinking points. To form a crosslink, a chain end must be in a small volume element (V). The decrease in entropy caused by such a constraint on the chain end is

$$S = k \ln \left(\frac{\Delta V}{V} \right) \quad (7.34)$$

where V is the total volume of the sample

$$V = (\alpha_x \alpha_y \alpha_z) V_0$$

This is equivalent to the ideal gas case in which all the gas molecules are located in a volume, V . The smaller the ratio of the volume available to the gas molecules to the total system volume, the less probable this state becomes. ΔV will depend upon the extent of fluctuation in the crosslink point that is assumed constant, independent of M_c and of elongation. For crosslinking points, in analogous fashion, the probability of forming crosslinks approaches zero at the limit of $\Delta V = V_0 - V = 0$ where V_0 is the volume of the network in the unstretched state.

For ν crosslinking points per cm^3

$$\begin{aligned} \Delta S'_{\text{net}} &= k \nu \ln \left[\frac{\Delta V}{(\alpha_x \alpha_y \alpha_z) V_0} \right] = k \nu \ln \left[\frac{\Delta V}{V_0} \right] - k \nu \ln(\alpha_x \alpha_y \alpha_z) \\ &= \Delta S_{\text{net}}^0 - \frac{k N_c}{2} \ln(\alpha_x \alpha_y \alpha_z) \end{aligned} \quad (7.35)$$

For a tetrafunctional network where $\nu = N_0/2$, the change in S_{net} , on stretching is

$$\Delta S = \Delta S'_{net} - \Delta S^0_{net}(\alpha = 1) = -\frac{kN_c}{2} \ln(\alpha_x \alpha_y \alpha_z); \quad (\alpha = 1) \quad (7.36)$$

The total entropy of the network is then

$$\Delta S = \Delta S_{Elast} - \Delta S_{net} = kN_c \left\{ -\frac{1}{2}(\alpha_x^2 + \alpha_y^2 + \alpha_z^2 - 3) + \frac{1}{2} \ln(\alpha_x \alpha_y \alpha_z) \right\} \quad (7.37)$$

The ΔS_{net} term is zero if there is no volume change on stretching so that

$$\alpha_x \alpha_y \alpha_z = 1 \quad (7.38)$$

It should be noted that there is some controversy regarding the quantitative nature of this term. Yu and Mark [12] and Neuburger and Eichinger [13] have reported work on swelling networks prepared with differing values of V_0 and measuring the resultant elastic tension. Their results suggest the existence of a $\ln(\alpha_x \alpha_y \alpha_z)$ effect, but the magnitude is uncertain because of experimental problems. It is apparent that the contribution from this term depends on the nature of constancy of ΔV , which in turn depends upon the junction fluctuation. We have previously indicated that junction fluctuation may depend on chain entanglements that we have not specifically considered in the theory.

For an ideal rubber,

$$\Delta H = 0$$

and

$$\Delta A_{Elast} = -T\Delta S = kN_c \left\{ \frac{1}{2}(\alpha_x^2 + \alpha_y^2 + \alpha_z^2 - 3) - \frac{1}{2} \ln(\alpha_x \alpha_y \alpha_z) \right\} \quad (7.39)$$

This equation represents the answer to the problem posed at the beginning of this section of deriving the stored energy function (A_{el}) for a deformed rubber network. Note that this equation contains only the extension ratio (α) terms for characterizing the network structure. Special cases of equation 7.39 are considered in the following sections.

Equation 7.39 has proved successful in relating network structure to mechanical properties. However, a more general form of equation 7.39 that attempts to allow for the approximation used in the derivation of equation 7.39 is often taken as the starting point for network structure property studies. This is given by

$$\Delta A_{Elast} = g \frac{\nu k N_c}{2} (\alpha_x^2 + \alpha_y^2 + \alpha_z^2 - 3) - B \nu k T (\alpha_x \alpha_y \alpha_z) \quad (7.40)$$

where g and B are constants whose values depend on the network model (Table 7.1).

Table 7.1 Values of g and B for Various Rubber Network Models

Model	g	B	Reference
Affine Junction	1	1/2	3-5, 7
Chain			9
Phantom Network, James-Guth	1/2	0	2, 13
Graessley			16

The constant g is also called the front factor and is introduced to correct for several approximations associated with rubber elasticity theory. Reliable values of g and B are desired to estimate the number of elastically effective chains (ν) that contribute to network mechanical properties. Crosslinks are one source of these. Trapped entanglements in which both chains forming the entanglement have their two ends linked to other chains in the gel (Figure 7.4) are another. The earlier models for deriving the stored energy function made the plausible assumption that the chain conformations between crosslinks had the same conformations as the free chains before crosslinking [3,4,6]. James and Guth [2] critically examined this assumption by postulating a phantom network model in which the effect on the shear modulus was estimated. They found, as a result, that the front factor (g) was 1/2 compared to a value of unity for the affine theories [3,6]. Edwards and Freed [14] later obtained the same result as James and Guth without assuming any details on the crosslinking process. Edwards and Freed [14] have pointed out that a trapped entanglement is not equivalent to a crosslink in that the chain can slip at such a location. Also, the slipping of such an entanglement and its effect as an additional crosslink depends upon elongation, so that the dependence of stress upon α maybe affected. Such an entanglement will

reduce the conformational entropy but not as much as a chemical crosslink. Also, the effectiveness in reducing the entropy will depend on elongation, so a different elongational dependence of stress will arise. This cannot be adequately described by equation 7.40, and requires the introduction of terms with a different elongational dependence as in the “Mooney-Rivlin” formulation, to be discussed

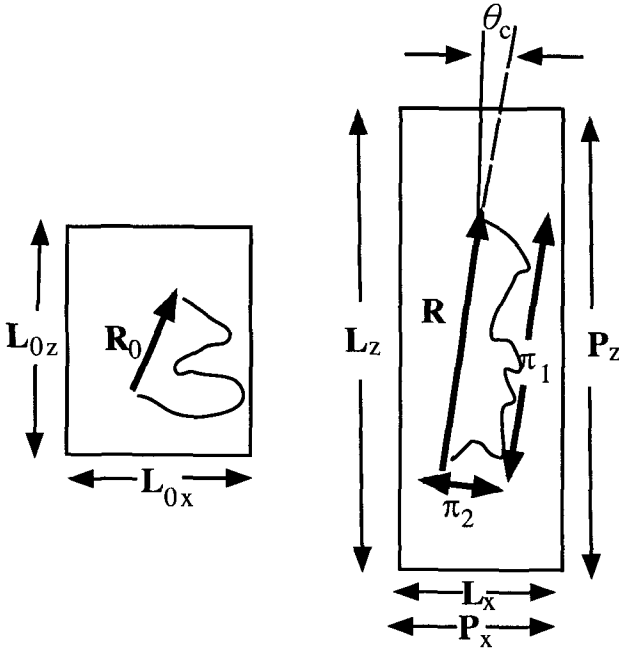


Figure 7.4 Illustration of a two dimensional affine transformation.

Edwards and Freed have introduced the “slip-ring” model as an approximate treatment of the effect of such trapped entanglements with some degree of success.

Langley [15] has derived the contribution of trapped entanglements to ν for gelled rubbers

$$\nu = \frac{q\rho}{M_0} W_g T_c^{1/2} + 2eT_e \quad (7.41)$$

where ρ = the sample density,

M_0 = the molecular weight of the polymer repeat unit,

q = the fraction of polymer repeat units that are joined by a random tetrafunctional crosslink.

W_g = the gel fraction.

The contribution of entanglements to ν is included in the $2e T_e$ term where T_e is the probability that all four strands emanating from a randomly located entanglement are bonded at the ends to the gel.

The validity of equation 7.10 was evaluated by Langley and Polmanteer [16] for polydimethylsilicone networks. They found excellent agreement and estimated that trapped entanglements contributed more than crosslink junctions did to the measured elastic modulus.

Graessley [17,18] has developed a statistical mechanical calculating device based on small network regions, the micronet, for estimating the change in chain conformation as a consequence of crosslinking. He found that the front factor depended only on the functionality (f) and not on the details of network topology, formation or crosslink distribution. His final equation is

$$\Delta A_{Elast} = \left(\frac{f-2}{f} \right)^\nu kT (\alpha_x^2 + \alpha_y^2 + \alpha_z^2 - 3) \quad (7.42)$$

For a tetrafunctional ($f = 4$) random crosslink, $g = 1/2$ – the James-Guth and Edwards-Freed result. In the limit of high f values, g approaches one, the value for the affine transformation theories. Flory (1), using cycle rank theory, has obtained the same result as Graessley. Mark [19] gives an introduction to cycle rank theory. Table 7.1 lists the various models and values of g obtained from each.

7.4. Uniaxial Stretching at Constant Volume

At constant volume, equation 7.38 applies. For uniaxial stretching in the z direction (Figure 7.1)

$$\alpha_x = \alpha_y; \quad \alpha_x^2 \alpha_z = 1; \quad \alpha_x = \alpha_z^{-1/2} \quad (7.43)$$

Thus, from equation 7.39

$$\Delta A = kTN_c \left[\frac{1}{2} \alpha_z^2 + \frac{1}{\alpha_z} \right] \quad (7.44)$$

Differentiating equation 7.44

$$f_z = \left(\frac{\partial A}{\partial L_z} \right)_{v,T} = \left(\frac{\partial A}{\partial \alpha_z} \right)_{v,T} \left(\frac{\partial \alpha}{\partial L_z} \right)_{v,T} \quad (7.45)$$

Since
$$\alpha_z = (L_z/L_{z0}) \quad (7.46)$$

$$\left(\frac{\partial \alpha_z}{\partial L_z} \right) = (1/L_{z0}) \quad (7.47)$$

Also

$$\left(\frac{\partial \Delta A}{\partial \alpha_z} \right)_{v,T} = kTN_c \left[\alpha_z - \frac{1}{\alpha_z^2} \right] \quad (7.48)$$

Thus the stress based on the original cross sectional area (or engineering stress) from equations 7.46 to 7.48 and equation 7.45 is

$$\sigma_0 = \frac{f_z}{L_{0x}L_{0y}} = \frac{kTN_c}{L_{0x}L_{0y}L_{0z}} \left[\alpha_z - \frac{1}{\alpha_z^2} \right] = kT \left(\frac{N_c}{V} \right) \left[\alpha_z - \frac{1}{\alpha_z^2} \right] \quad (7.49)$$

The stress based on the true cross sectional area is

$$\sigma = \frac{f_z}{L_xL_y} = \frac{f_z}{(\alpha_xL_{0x})(\alpha_yL_{0y})} = \frac{\sigma_0}{\alpha_x\alpha_y} = \sigma_0\alpha_z = kT \left(\frac{N_c}{V} \right) \left[\alpha_z - \frac{1}{\alpha_z^2} \right] \quad (7.50)$$

The stress may be expressed in terms of the elastic (E) and shear (G) moduli by the following. Since the tensile strain (ϵ) is given by

$$\epsilon = \frac{l-l_0}{l_0} = \alpha - 1 \quad (7.51)$$

The slope of the stress-strain curve based on the original cross sectional area is simply the elastic modulus

$$E = \left(\frac{\partial \sigma}{\partial \epsilon} \right) = \left(\frac{\partial \sigma}{\partial \alpha} \right) \left(\frac{\partial \alpha}{\partial \epsilon} \right) = kT \left(\frac{N_c}{V} \right) \left[\alpha_z - \frac{1}{\alpha_z^2} \right] \quad (7.52)$$

From the binomial series

THE RUBBERY STATE

$$\frac{1}{\alpha^2} = \frac{1}{(1+\varepsilon)^2} = 1 - 2\varepsilon + \dots \quad (7.53)$$

For very small strains, the higher order terms can be neglected. Substituting equations 7.51 and 7.53 into equation 7.52 and taking the initial modulus E_0 (or, the limit as $l \rightarrow l_0$),

$$E_0 = 3kT \left(\frac{N_c}{V} \right) \quad (7.54)$$

For crosslinked incompressible rubbers, Poisson's ratio is nearly equal to 0.5, so that (20)

$$E = 3G \quad (7.55)$$

or, substituting into equation 7.53

$$G_0 = kT \left(\frac{N_c}{V} \right) \quad (7.56)$$

These moduli equations are similar to equation 3.20 for an isolated chain in that the modulus (or force) is directly proportional to the absolute temperature. However, for a network structure, the modulus also depends on the number of crosslink junctions: the greater the number of junctions the higher the modulus and the stiffer the network.

7.5. Biaxial Stretching at Constant Volume

Consider stretching in the x and y directions so that

$$\alpha_z = \frac{1}{\alpha_x \alpha_y} \quad (7.57)$$

Thus, using equation 7.39

$$\Delta A = kTN_c \left[\frac{1}{2} \left(\alpha_x^2 + \alpha_y^2 + \frac{1}{\alpha_x^2 \alpha_y^2} - 3 \right) \right] \quad (7.58)$$

Then differentiating

$$f_x = \left(\frac{\partial A}{\partial L_x} \right)_{V,T} = \left(\frac{\partial \alpha_x}{\partial L_x} \right)_{V,T} \left(\frac{\partial A}{\partial \alpha_x} \right)_{V,T} = \frac{kTN_c}{L_{0x}} \left[\alpha_x - \frac{1}{\alpha_x^3 \alpha_y^2} \right] \quad (7.59)$$

Thus

$$\sigma_x = \left(\frac{f_x \alpha_x}{L_{0y} L_{0z}} \right)_{V,T} = kT \left(\frac{N_c}{V} \right) \left[\alpha_x^2 - \frac{1}{\alpha_x^2 \alpha_y^2} \right] \quad (7.60)$$

Similarly

$$\sigma_y = kT \left(\frac{N_c}{V} \right) \left[\alpha_y^2 - \frac{1}{\alpha_x^2 \alpha_y^2} \right] \quad (7.61)$$

Thus

$$\sigma_x - \sigma_y = kT \left(\frac{N_c}{V} \right) \left[\alpha_x^2 - \alpha_y^2 \right] \quad (7.62)$$

so that the difference between the principal stresses is proportional to the difference between the squares of the principal strains. For “balanced” biaxial stress

$$\alpha_x = \alpha_y = \alpha \quad (7.63)$$

so

$$\sigma_z = \sigma_y = kT \left(\frac{N_c}{V} \right) \left[\alpha^2 - \frac{1}{\alpha^4} \right] \quad (7.64)$$

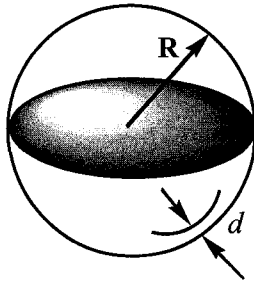


Figure 7.5 Diagram illustrating the model used in deriving equation 7.69.

7.6. Application to the Inflation of a Balloon

A “balanced” biaxial tensile stress is equivalent to uniaxial compression. Inflation of a rubber balloon is a specific example of this type of stress. The pressure required to inflate a balloon passes through a maximum. This is intuitively obvious to anyone who has ever tried to inflate a balloon using only lungpower. One’s lungs are usually strained almost to the bursting point before the balloon starts to expand. The mathematics for this situation can be given in a few steps.

Consider the force (f) pushing the two hemispheres apart (Figure 7.5)

$$f = P \times \text{Area} = \pi R^2 P \quad (7.65)$$

The stress on the rubber is then

$$\sigma = \frac{\pi R^2 P}{2\pi R d} = \frac{PR}{2d} = kT \left(\frac{N_c}{V} \right) \left[\alpha^2 - \frac{1}{\alpha^4} \right] \quad (7.66)$$

Now

$$R = \alpha R_0 \quad (7.67)$$

and since the volume of the balloon is constant

$$4\pi R^2 d = 4\pi R_0^2 d_0 \quad (7.68)$$

so that

$$d = d_0 \frac{R_0^2}{R^2} = \frac{d_0}{\alpha^2} \quad (7.69)$$

and

$$P = kT \left(\frac{N_c}{V} \right) \left(\frac{2d}{R} \right) \left[\alpha^2 - \frac{1}{\alpha^4} \right] = kT \left(\frac{N_c}{V} \right) \left(\frac{2d_0}{R_0} \right) \left[\frac{1}{\alpha} - \frac{1}{\alpha^7} \right] \quad (7.70)$$

This gives the variation of P that passes through a maximum that occurs when $\alpha = 7^{1/6}$. Such a curve (Figure 7.6) is verified experimentally [21]. Inflation of balloons is only one example of elastic instability. This phenomenon also occurs in the generation of bubbles in foam production and the development of aneurysms in arteries in the human body.

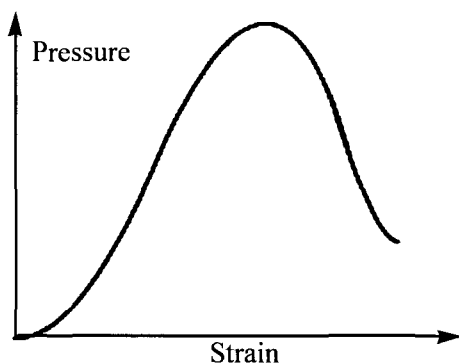


Figure 7.6 Variation of balloon inflation pressure with strain.

7.7. Network Defects -The Relationship between N_C and ν

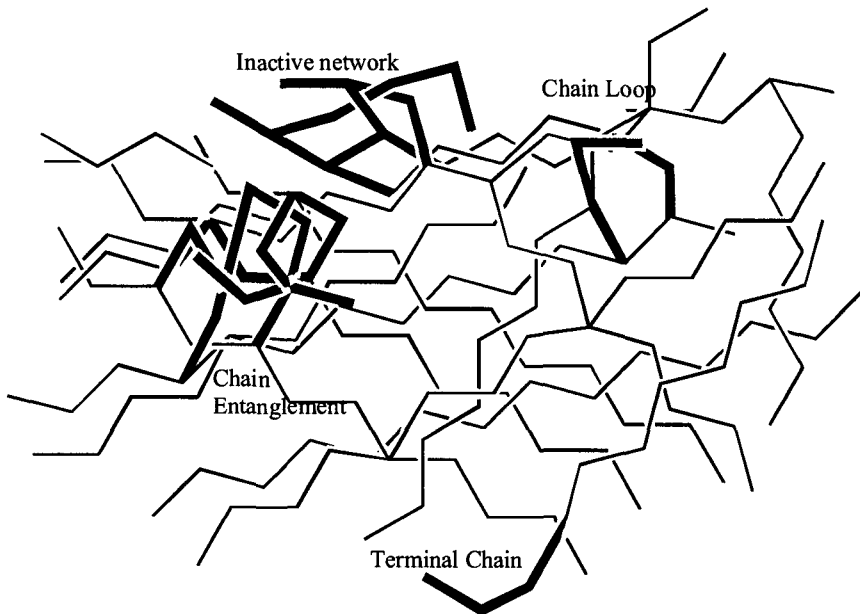


Figure 7.7. Types of network defects.

The derivation in the previous section assumes that all network junction points are effective in bearing an applied stress. However, a fraction of

THE RUBBERY STATE

these junctions will be rendered ineffective because of the network topology. Typical examples of network defects are illustrated in Figure 7.7. Various schemes have been proposed to allow for some of these defects. Thus, it was assumed that (equation 7.14) that

$$\frac{N_c}{V} = \frac{fv}{2} \quad (7.71)$$

or in words that the fraction of junction points ($fv/2$) is proportional to the number of chains between crosslinks (N_c) per unit volume. This neglects the portion of the chain adjacent to the end of the original molecule will not be an active network chain (Figure 7.7). If N_0 is the number of original molecules, each original molecule will contribute two inactive chains, thus

$$\frac{N_c}{V} = \frac{fv}{2} = \frac{2N_0}{V} \quad (7.72)$$

If M_0 is the molecular weight

$$\frac{N_0}{V} = \frac{\rho}{M_0} N_A \quad (7.73)$$

where ρ is the density and $N_A = \text{Avogadro's number } (6.02 \times 10^{23})$ and if M_c is the molecular weight between crosslinks, the total number of network chains per cm^3 (including the inactive ones) is

$$\frac{(N_0)_{total}}{V} = \frac{\rho}{M_c} N_A \quad (7.74)$$

Thus the number of active chains is

$$\frac{N_c}{V} = \frac{\rho}{M_0} \left(\frac{1}{M_c} - \frac{2}{M_0} \right) = \frac{\rho N_A}{M_c} \left(1 - \frac{2M_c}{M_0} \right) \quad (7.75)$$

The modulus is proportional to the term, N_c/V , (from equation 7.56). Thus from a plot of modulus against $1/M_0$, one extracts a value of M_c from the ratio of the slope to the intercept. Figure 7.8 illustrates the procedure. The following section describes an alternative procedure based on swelling considerations for estimating values of M_c

Model networks have been prepared by end-linking groups. First, a linear chain with reactive side chains such as propylene oxide is synthesized. Then the side groups are reacted to form a known number of crosslinks and purposely introducing defects of known types [22].

7.8. Effect of Swelling on an Isotropic Network

Rubber networks will imbibe solvent liquids until the elastic retractive force of the network crosslinks counterbalances the swelling force exerted by the liquid. If no crosslinks are present, the rubber dissolves completely on immersion in an excess of solvent. The degree of swelling is thus a function of crosslink density. As crosslink density increases, the degree of swelling decreases and vice versa. The average crosslink between junction points can be related to swelling measurements from potential considerations, as shown below.

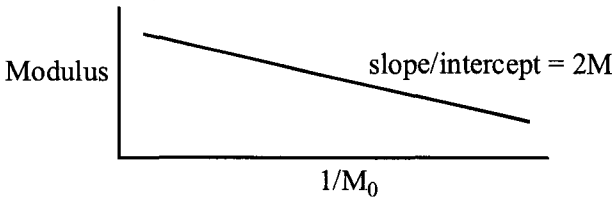


Figure 7.8. Plot of modulus against 1/M₀.

At the equilibrium degree of swelling

$$(\mu_1 - \mu_{10})_{total} = (\mu_1 - \mu_{10})_{elastic} + (\mu_1 - \mu_{10})_{mixing} \quad (7.76)$$

This equation presumes additivity of the free energy of mixing and of elasticity. Eichinger [23] has questioned and tested this assumption. The mixing term can be evaluated using the Flory-Huggins theory (equation 3.83)

$$(\mu_1 - \mu_{10})_{mixing} = RT \left[\ln(1 - \phi_2) + \phi_2 + \chi_1 \phi_2^2 \right] \quad (7.77)$$

where ϕ_2 is the volume fraction of solute.

This equation holds for a network in which the molecule is infinitely large ($x \rightarrow \infty$) and the swelling is isotropic. Thus, for filled rubbers where the rubber is locally bound to the filler particles, the extent of

swelling is reduced because of the filler-rubber bond. Again, rubbers do not swell isotropically when a rubber film bound to surfaces where dimensional changes in different directions are different. Because the bound rubber near the filler surface is constrained by the filler particle, the swelling of the rubber near the filler surface is reduced.

The elastic term in equation 7.77 is evaluated by combining equations 7.39 and 7.77 to obtain

$$\Delta A_{Elast} = \frac{\rho RT}{2M_c} \left[(\alpha_x^2 + \alpha_y^2 + \alpha_z^2 - 3) - \ln(\alpha_x \alpha_y \alpha_z) \right] \quad (7.78)$$

For swelling of an isotropic network

$$\alpha_x = \alpha_y = \alpha_z = \left(\frac{V}{V_0} \right)^{1/3} = \phi_2^{-1/3} \quad (7.79)$$

so that

$$\Delta A_{Elast} = \frac{\rho RT}{2M_c} \left[3\phi_2^{-2/3} - 3 - \phi_2^{-1} \right] \quad (7.80)$$

Then

$$(\mu_1 - \mu_{10})_{elastic} = \left(\frac{\partial \Delta A_{Elast}}{\partial n_1} \right)_{N_1, T, V} = \left(\frac{\partial \Delta \phi_{el}}{\partial n_1} \right)_{N_1, T, V} \left(\frac{\partial \Delta A_{el}}{\partial \phi_2} \right)_{N_1, T, V} \quad (7.81)$$

The above expression for ΔA_{Elast} is that of 1 cm³ of polymer (dry). If n_i moles of solvent are added to 1 cm³ of polymer, then the volume fraction of solute (ϕ_2) is given by

$$\phi_2 = \frac{1}{1 + n_1 V_1} \quad (7.82)$$

where V_1 is the molar volume of the solvent.

Then

$$\left(\frac{\partial \phi_2}{\partial n_1} \right) = \frac{V_1}{(1 + n_1 V_1)^2} = -V_1 \phi_2^2 \quad (7.83)$$

Also

$$\left(\frac{\partial \Delta A_{\text{Elast}}}{\partial \phi_2} \right) = \frac{\rho RT}{2M_c} \left[-2\phi_2^{-5/3} + \frac{1}{\phi_2} \right] \quad (7.84)$$

so that

$$(\mu_1 - \mu_{10})_{\text{Elast}} = \frac{\rho RT}{2M_c} V_1 [2\phi_2^{1/3} - \phi_2] \quad (7.85)$$

Thus, on combining equations 7.77 and 7.85

$$(\mu_1 - \mu_0)_{\text{total}} = 0 = RT \left\{ \ln(1 - \phi_2) + \phi_2 + \chi_1 \phi_2^2 + \frac{\rho RT}{2M_c} [2\phi_2^{1/3} - \phi_2] \right\} \quad (7.86)$$

The value of ϕ_2 at the equilibrium degree of swelling is the solution of this equation. The following approximations simplify finding a solution. At high degrees of swelling for which ϕ_2 is small, using a binomial series expansion

$$\ln(1 - \phi_2) \cong -\phi_2 - \phi_2^2 \quad (7.87)$$

Substituting into equation 7.86

$$-\frac{\phi_2^2}{2} + \chi_1 \phi_2^2 + \frac{\rho V_1}{2M_c} (2\phi_2^{1/3} - \phi_2) = 0 \quad (7.88)$$

as compared with $\phi_2^{1/3}$ when $\phi_2 \ll 1$

While it is best to use this equation in this more exact form, it is useful to consider an approximation valid at high degrees of swelling (low degree of crosslinking). Neglecting the ϕ_2 term because of its small magnitude as compared with $\phi_2^{1/3}$ when $\phi_2 \ll 1$ and rearranging terms

$$\frac{\rho V_1}{M_c} \phi_2^{1/3} = \left(\frac{1}{2} - \chi_1 \right) \phi_2^2 \quad (7.89)$$

or recasting

$$\phi_2^{5/3} = \frac{\rho V_1}{M_c \left(\frac{1}{2} - \chi_1 \right)} \quad (7.90)$$

Therefore, use of this equation is a good way to determine M_c . It is noted that swelling is high (ϕ_2 small) at high M_c (low degree of crosslinking). Normally, one needs to know χ_1 that can be obtained for example from osmotic pressure measurements on solutions of the uncrosslinked polymer. However, despite its constancy presumed in the Flory-Huggins theory, its value is often found to depend on concentration and degree of crosslinking. ϕ_2 is a maximum when $\chi_1 = 0$ (see Section 3.2) so that the value of M_c may be calculated from the minimum ϕ_2 value observed in a plot of ϕ_2 against the solubility parameter (δ_1) (Figure 7.9). This Flory-Rehner theory of swelling involves the affine assumption in which it is presumed that the projections of the displacement vector increase in the same ratio as the external dimensions of the sample. Various attempts to verify this by neutron scattering [24] have suggested that the chain expansion is less than the affine prediction. A "chain-unfolding" mechanism [25] has been postulated to account for this.

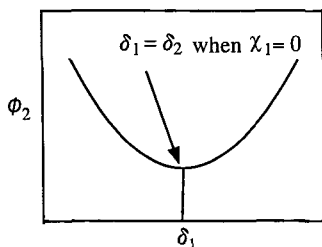


Figure 7.9 Determination of δ^2 using equation 7.90.

Despite this problem, the swelling measurement has proved to be one of the best means of measuring M_c .

7.9. Elastic Properties of Swollen Rubber

Swelling of network rubbers by solvent liquids represents an isotropic deformation. Stretching a swollen rubber network superimposes an anisotropic deformation. The two deformations may be combined as described below to obtain an estimate of the force (or modulus) required to deform a swollen rubber compared to that for unswollen rubber. The

derivation given below is based on entropy considerations. This is equivalent to the strain energy function for the case of an ideal rubber ($\Delta H = 0$).

Let $\Delta S'$ be the change in entropy in going from the unstretched, unswollen state to the stretched swollen state, from equation 7.38

$$\Delta S' = -\frac{1}{2}kN_c \left\{ \left[\alpha_x^2 + \alpha_y^2 + \alpha_z^2 - 3 \right] - \ln(\alpha'_x + \alpha'_y + \alpha'_z) \right\} \quad (7.91)$$

where

$$\alpha'_x = \frac{L_x(\text{stretched,swollen})}{L_x(\text{unstretched,unswollen})} \quad (7.92)$$

ΔS_{sw} is the entropy change on swelling the unstretched network (from equation 7.81)

$$\Delta S_{sw} = -\frac{1}{2} \left\{ kN_c \left[3\phi_2^{-2/3} - 3 \right] - \ln \phi_2^{-1} \right\} \quad (7.93)$$

Then ΔS is defined as the entropy of stretching a swollen network, or

$$\Delta S \equiv \Delta S' - \Delta S_{sw} = -\frac{1}{2} \left\{ kN_c \left[\alpha_x^2 + \alpha_y^2 + \alpha_z^2 - 3\phi_2^{-2/3} \right] \right\} \quad (7.94)$$

(assuming no volume change upon stretching). From equation 7.79

$$\alpha'_x = \frac{L_x(\text{stretched,swollen})L_x(\text{unstretched,swollen})}{L_x(\text{unstretched,swollen})L_x(\text{unstretched,unswollen})} \quad (7.95)$$

so that

$$\Delta S = -\frac{1}{2}kN_c \phi_2^{-2/3} \left[\alpha_x^2 + \alpha_y^2 + \alpha_z^2 - 3 \right] \quad (7.96)$$

Then, differentiating with respect to length

$$f_z = -T \left(\frac{\partial S}{\partial L_z} \right) = -T \left(\frac{\partial S}{\partial \alpha_z} \right) \left(\frac{\partial \alpha_z}{\partial L_z} \right) \quad (7.97)$$

where

$$\left(\frac{\partial \alpha_z}{\partial L_z} \right) = \frac{1}{L_z} \quad (7.98)$$

and

$$\alpha_z = \frac{L_z(\text{stretched,swollen})}{L_z(\text{unstretched,swollen})} \quad (7.99)$$

Thus, from equation 7.95 (and equations 7.40 to 7.43)

$$f_z = \frac{kN_c T \phi_2^{-2/3}}{L_z} \left(\alpha_z - \frac{1}{\alpha_z^2} \right) \quad (7.100)$$

and

$$\sigma_z = \frac{f_z}{L_x L_y} = \frac{kN_c T \phi_2^{-2/3}}{L_x L_y L_z} \left(\alpha_z - \frac{1}{\alpha_z^2} \right) \quad (7.101)$$

$(L_x L_y L_z)$ is the volume V_s in the swollen state, which is

$$V_s = V_0 / \phi_2 \quad (7.102)$$

$$\sigma_z = \frac{N_0}{V} kT \phi_2^{1/3} \left(\alpha_z - \frac{1}{\alpha_z^2} \right) \quad (7.103)$$

The stress may be converted to modulus by following the sequence given in equations 7.51 to 7.56

$$G_{\text{swollen}} = G_{\text{unswollen}} \phi_2^{1/3} \quad (7.104)$$

where G is the shear modulus that is equal to (kTN_c/V) or $\rho RT/M_c$ (see equation 7.75). The modulus is less for stretching a swollen sample when compared to an unswollen sample with the same cross sectional area, because the $\phi_2^{1/3}$ term will always be less than one.

7.10. Elasticity of a Sample That is Swollen When Crosslinked.

The topology of a network rubber that is crosslinked in the swollen state differs from that crosslinked in an unswollen state. The initial boundary conditions describing the chain conformation used in deriving the strain-energy function can be modified to allow for these differences. The resulting equations have been used to elucidate possible reasons for the deviations of stress-strain data from statistical theory.

The distribution function used previously, equation 7.28

$$(N_{ij})_s = \frac{N_c \beta_j^3}{\pi^{3/2}} \exp\left[-\beta_j^2(x_{0i}^2 + y_{0i}^2 + z_{0i}^2)\right] \quad (7.105)$$

is replaced for a swollen network, by

$$(N_{ij})_s = \frac{N_c \beta_j^3}{\pi^{3/2}} \exp\left[-\beta_j^2\left(\frac{x_{si}^2}{\alpha_s^2} + \frac{y_{si}^2}{\alpha_s^2} + \frac{z_{si}^2}{\alpha_s^2}\right)\right] \quad (7.106)$$

where the subscript s refers to the swollen state and o to the unswollen state.

On stretching, the dimensions for the swollen, crosslinked sample are given by

$$\alpha_x = \frac{x'_i}{x_{si}}; \quad \alpha_y = \frac{y_i}{y_{si}}; \quad \alpha_z = \frac{z_i}{z_{si}}; \quad (7.107-109)$$

Recasting equation 7.106

$$(N_{ij})'_s = \frac{N_c \beta_j^3}{\pi^{3/2} \alpha_s^3 \alpha_x \alpha_y \alpha_z} \exp\left[-\beta_j^3\left(\frac{x_{si}^2}{\alpha_s^2 \alpha_x^2} + \frac{y_{si}^2}{\alpha_s^2 \alpha_y^2} + \frac{z_{si}^2}{\alpha_s^2 \alpha_z^2}\right)\right] \quad (7.110)$$

Then, following the analogous procedure used in evaluating equation 7.37,

$$S = S_0 - kN_c \left\{ \left[\frac{\alpha_s^2 (\alpha_x^2 + \alpha_y^2 + \alpha_z^2)}{2} - 3 \right] - \frac{1}{2} \ln(\alpha_s^3 \alpha_x \alpha_y \alpha_z) \right\} \quad (7.111)$$

The strain energy function (equation 7.39) follows directly from equation 7.111 assuming $\Delta H = 0$ as in the ideal rubber case. The function for a swollen sample will be modified by the inclusion of the α_s term. This term that is essentially a scaling factor relating the unswollen dimensions to the swollen dimensions for a stretched sample, is given by

$$\alpha_s^2 = \frac{\langle r^2 \rangle}{\langle r_0^2 \rangle} \quad (7.112)$$

where $\langle r^2 \rangle$ and $\langle r_0^2 \rangle$ are the mean squared end-to-end chain lengths in the swollen and the unswollen states respectively.

For the case of uniaxial stretching at constant volume, the stress (see equations 7.40 to 7.48) modified for swelling is given by

$$\sigma_0 = \frac{N_c}{V} kT \frac{\langle r^2 \rangle}{\langle r_0^2 \rangle} \left(\alpha - \frac{1}{\alpha^2} \right) \quad (7.113)$$

For an ideal rubber, in the absence of solvent, the relation $\langle r^2 \rangle = \langle r_0^2 \rangle$ should hold. However, Tobolsky and Goebel [26] contend that even without solvent, $\langle r^2 \rangle = \langle r_0^2 \rangle$ because of steric effects. Chains are postulated to deviate from their most probable (or random) conformations because of steric hindrance between chain segments. This order is locked in during crosslinking even in dry rubber.

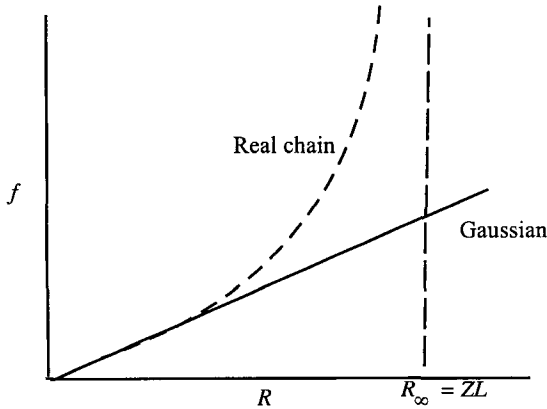


Figure 7.10. Sketch of force against end-to-end distance (R_x) showing the non-linear increase.

7.11. Elasticity of Rubbers at Small Extensions

The force-extension relation derived previously from statistical considerations does not agree well with experimental data at small extensions. As an example, a plot of uniaxial force-elongation data for natural rubber falls below the curve calculated from the theoretical equation (equation 7.48) in the region between 1.1 to 2.0 elongation

(Figure 7.10). This occurs only because the two curves are superimposed at low strains. The modulus of real networks is higher than theoretical because of entanglement effects. Use of non-Gaussian statistics only lessens the discrepancy between the calculated and the experimental curves; but the reasons for this discrepancy are not understood.

In practice, the discrepancy is minimized for uniaxial extension by using a two parameter equation that Mooney [27] first proposed on empirical grounds and later Rivlin and coworkers [28,29] developed from non-molecular, phenomenological arguments based on classical elasticity theory. As in the statistical theories, the central problem is the derivation of a stored energy function (W). In the present context, the stored energy function is obtained from the symmetry conditions associated with the deformation of an elastic body. Since the body is assumed to be a continuum, no assumptions regarding its molecular constitution are required. The requisite symmetry conditions for the extension of an elastic body at constant volume are given by three invariants [27, 28]

$$I_1 = \alpha_1^2 + \alpha_2^2 + \alpha_3^2 \quad (7.114)$$

$$I_2 = \alpha_1^2 \alpha_2^2 + \alpha_2^2 \alpha_3^2 + \alpha_3^2 \alpha_1^2 \quad (7.115)$$

$$I_3 = \alpha_1 \alpha_2 \alpha_3 \quad (7.116)$$

that do not change with deformation.

Only the first two deformations are independent since $I_3 = 1$ (based on the assumption of incompressibility). The simplest strain energy function that meets the criteria is

$$W = C_1(I_1 - 3) - C_2(I_2 - 3) \quad (7.117)$$

where C_1 and C_2 are constants. Substituting from equations 7.115 to 7.117, the strain energy functions in terms of the extension ratios

$$W = C_1(\alpha_1^2 + \alpha_2^2 + \alpha_3^2) - C_2\left(\frac{1}{\alpha_1^2} + \frac{1}{\alpha_2^2} + \frac{1}{\alpha_3^2} - 3\right) \quad (7.118)$$

This can be expressed for uniaxial extension by the Mooney-Rivlin equation

$$\frac{dW}{d\alpha} = \frac{\sigma_0}{\left(\alpha - \frac{1}{\alpha^2}\right)} = 2C_1 + \frac{C_2}{\alpha} \quad (7.119)$$

where σ_1 is the retractive force (f) per unit initial cross sectional area. Treloar [4] has pointed out that the empirical two-parameter equation that results from $dW/d\alpha$ does not concur over all strain ranges with the invariant formulation of Rivlin and coworkers that use $dW/d\alpha$. Additional details regarding the phenomenological theory may be found in Treloar's monograph [4].

The constant C_1 can be readily identified by inspection with the $N_c kT/V$ term in the force-elongation equation derived from the statistical treatment. The interpretation of the C_2 term, on the other hand, has been the subject of much debate. Mark [30] has published an extensive compilation of C_2 values under a variety of experimental conditions. Values of C_2 depend on the overall conditions of network formation and subsequent treatment. The general features of the manner that the values of C_2 shift with experimental conditions can be summarized as follows: a.) C_2 changes with time and temperature indicating a non-equilibrium nature [31,32]. However, other results suggest that some portion of the C_2 term is at equilibrium [33, 34]. b.) C_2 decreases with swelling [35, 36] and reaches a value of zero at a polymer fraction of roughly 0.23 [36]. c.) C_2 increases for unswollen rubber with increasing crosslink density [37]. However, the value is usually small for networks crosslinked in the swollen state and then dried [38]. d.) C_2 is similar in magnitude to C_1 for simple elongation measurements (Networks crosslinked in the swollen state and then dried.), but in simple uniaxial compression, C_2 has a very low or zero value [39].

It should be emphasized that the Mooney-Rivlin equation is empirical and is based on phenomenological principles; it does not involve molecular concepts and is not an explanation for the deviations from molecular theories.

Several theories based on molecular considerations have been advanced in order to interpret these and similar data. These theories have examined: a.) the role of local regions of ordered chain segments or bundles locked into the rubber during network formation [40,41]. b.)

intramolecular energetic effects originating from the barriers to internal rotation along the chain backbone [42]. A more extended calculation later indicated that this effect is minor [43]. c.) Volume exclusion for the isolated chain and found the effect to be minor [44]. Several workers [45-48] have investigated the volume exclusion properties of networks.

None of these models has proven satisfactory in assigning a molecular interpretation to the C_2 term in equation 7.117. Additional difficulties with these models are that none can predict the change in slope that occurs when an initially compressed rubber network is elongated and the sample goes from compression to elongation [49] Also, theories do not treat the large increase in stress associated with high elongations (Figure 7.10).

An approach based on statistical theory has recently been proposed [49-51] that is capable of showing a smooth transition from compression to extension as well as good agreement in the region of moderate elongation. It is based of the observation that, in the phantom network theory of James and Guth [2], the force required to elongate a network is smaller than in the affine model. As mentioned previously, both models show the same functional relationships and differ only by a numerical factor whose value is dependent on the chain functionality. For a tetrafunctional network, the force required to deform a phantom network is one half that for an affine one. Both models also assume that the strain does vary with reduced force [$f/(\alpha-1/\alpha^2)$]. According to this approach, a real network is assumed to obey an affine model at low extensions and the phantom network at high extensions. Both limits are assumed to have constant reduced force values with changes in strain. However, the force changes with strain on transition between the two limits. The physical model assumes that the junction points are impeded in their movement to accommodate an applied stress by neighboring entanglements. This restriction in mobility is approximated by a well with the width of the well determining the degree of restriction. The final equations can be fitted to compression-extension data on polydimethylsilicone with reasonable agreement [50], using only one adjustable parameter.

7.12. Guth-Smallwood Equations

Filler particles such as talc or carbon black are routinely incorporated in rubber compounds to improve mechanical properties. Guth [51] related this reinforcement effect to the Einstein viscosity law for colloidal emulsions

$$\eta^* = \eta[1 + 2.5\phi] \quad (7.120)$$

where η^* = the viscosity of the emulsion

η = the viscosity of the solvent

ϕ = the volume fraction of the dispersed phase

In Guth's model, the filler particles assumed to be spheres at low concentrations act as energy concentrating centers thereby increasing the elastic modulus. At low concentrations, up to 30% by volume, equation 7.120 is expanded in series to

$$E^* = E[1 + 2.5\phi + 14.1\phi^2] \quad (7.121)$$

where E is the elastic modulus. The factor 2.5 is valid for spherical inclusions, and different values would apply for other shapes, generally depending on the aspect ratio of the particle. Good agreement with experiment has been found using this equation.

A further refinement is the inclusion of a correction term, f , into equation 7.120. Thus,

$$E^* = E[1 + 2.5\phi + 14.1f^2\phi^2] \quad (7.122)$$

Inclusion of the f term in the Guth-Gold equation improved the agreement.

From a practical point of view, carbon black is commonly used as filler. Its role is not well understood but the reinforcement varies greatly depending the kind of carbon black. Carbon black particles are fibrous and interact to apparently form some sort of network structure. There is often hysteresis in the stress-strain curves, possibly indicating breaking of the filler-rubber bond during stretching.

References

1. P.J. Flory, *Proc. R. Soc. Lund*. **1976**, *A351*, 351
2. H.M. James and E. Guth, *J. Chem. Phys.* **1943**, *11*, 455
3. W. Kuhn, *Colloid Z.* **1936**, *76*, 258
4. L.R.G. Treloar, *The Physics of Rubber Elasticity*, 3rd Ed.; Clarence: Oxford University, **1975**
5. B. Erman, L. Connery, *Macromolecules*. **1989**, *22*, 3342
6. K. Dusek, W. Prins, *Adv. Polym. Sci.* **1969**, *6*, 1
7. P.J. Flory, J. Rehner, Jr., *J. Chem. Phys.* **1943**, *11*, 512, 521
8. P.J. Flory, *J. Chem. Phys.* **1977**, *66*, 5720
9. H. Benoit, D. Decker, R. Duplessix, C. Picot, J.P. Cotton, B. Farnoux, G. Jarnick, R. Ober, *J. Polymer Sci.:Polymer Phys Ed* **1976**, *14*, 2119
10. J.A. Hinkley, C.C. Han, B. Mozer, H. Yu, *Macromolecules* **1978**, *11*, 836
11. P.J. Flory, *Brit. Polym. J.*, **1985**, *17*, 96
12. C.U. Yu, J.E. Mark, *Polymer J* **1975**, *7*, 101
13. N.A. Neuburger, B. E. Eichinger, *Macromolecules*. **1988**, *21*, 3060
14. S.F. Edward, K.F. Freed, *J. Phys.* **1970**, *C3*, 739, 750, 760
15. N.R. Langley, *Macromolecules* **1968**, *1*, 348
16. N.R. Langley, K.E. Polmanteer, *J. Polymer Phys.:Polymer Phys. Ed.*, **1974**, *12*, 1023
17. W.W. Graessley, *Macromolecules* **1975**, *8*, 186, 865
18. D.S. Pearson, W.W. Graessley, *Macromolecules* **1978**, *11*, 528
19. J.E. Mark; B. Erman, *Rubberlike Elasticity A Molecular Primer*; John Wiley: New York, **1988**
20. J.J. Aklonis, W.J. MacKnight, *Introduction to Polymer Viscoelasticity*, 2nd Ed; Wiley-Interscience: New York, **1983**
21. R.S. Stein, *J. Chem. Educ.* **1958**, *35*, 203
22. J.E. Mark, *Acc. Chem. Rev.* **1985**, *18*, 202
23. B.E. Eichinger, *Ann. Rev. Phys. Chem.*, **1983**, *34*, 359
24. S.B. Clough, A. Maconnachie and G. Allen, *Macromolecules*, **1980**, *13*, 774
25. S.N. Magonov, N.A. Yerina, G. Ungar, D.H. Reneker, D.A. Ivanov, *Macromolecules*, **2003**, *36*, 5637
26. A.V. Tobolsky, J.C. Goebel, *Macromolecules* **1970**, *3*, 556
27. M. Mooney, *J. Appl. Phys.* **1940**, *11*, 582
28. R.S. Rivlin, *Phil. Trans. Roy. Soc. London* **1948**, *A241*, 379
29. R.S. Rivlin, D.W. Saunders, *Phil. Trans. Roy. Soc. London* **1951**, *A243*, 251
30. J.E. Mark, *Rubber Chem. and Tech.* **1975**, *48*, 495
31. A. Ciferri, P.J. Flory, *J. Appl. Phys.* **1959**, *30*, 1498
32. A. Ciferri, J.J. Hermans, *J. Polymer. Sci.* **1964**, *B2*, 1089
33. E. Guth, P.E. Wack, R.L. Anthony, *J. Appl. Phys.* **1946**, *1*, 374
34. P. Thirion, *Chim. Ind. Gemis Chim.* **1967**, *97*, 917
35. G. Allen, M.J. Kirkham, J. Padget, C. Price, *Trans. Faraday Soc.* **1971**, *67*, 1278

THE RUBBERY STATE

36. S.M. Grumbell, L. Mullens, R.S. Rivlin, *Trans. Faraday Soc.* **1953**, 49, 1495
37. W.R. Krigbaum, R.-J. Roe, *Rubber Chem. Technol.* **1965**, 38, 1039
38. J.E. Mark, P.J. Flory, *J. Appl. Phys.* **1966**, 37, 4635
39. C.U. Yu, J.E. Mark, *Macromolecules* **1975**, 7, 229
40. R. Blokland, *Elasticity and Structure of Polyurethane Networks*;
Rotterdam University; **1968**
41. M.V. Volkenstein, Y. Gotlib, O.B. Ptitsyn, *Vysokomol. Soedin.* **1959**, 1, 1056
42. W.R. Krigbaum and M. Kanebo, *J. Chem. Phys.* **1962**, 36, 99
43. K.J. Smith, Jr., *J. Polymer Sci.* A2 **1971**, 9, 2119
44. G. Gee, *Polymer* **1966**, 7, 373
45. E.A. DiMarzio, *J. Chem. Phys.* **1962**, 36, 1563
46. J.L. Jackson, M. Shen and D.A. McQuarrie, *J. Chem. Phys.* **1966**, 44, 2388
47. J.L. Jackson, *J. Chem. Phys.* **1972**, 57, 5124
48. G. Dobson and M. Gordon, *Trans. Inst. Rubber Ind.* **1964**, 40, T262
49. B. Erman, P.J. Flory, *J. Polymer Sci. Polym. Phys. Ed.* **1978**, 16(6), 1115
J. Chem. Phys. **1978**
50. E. Guth, *J. Appl. Phys.* **1945**, 16, 20
51. S. Wolff, J. -B. Donnet, *Rubber Chem. Technol.* **1990**, 63, 32

Appendix 7A – Evaluation of Equation 7.30

$$\begin{aligned}
 S &= k \left\{ \ln C + N_c \ln N_c + \sum N_{ij} \ln \left(\frac{W_{ij}}{N_{ij}} \right) \right\} \\
 S &= k \left\{ \ln C + N_c \ln N_c + \sum N_j \ln \left(\frac{\beta_j^3}{\pi^{3/2} \alpha_x \alpha_y \alpha_z} \right) \int_{\mathbf{R}_j} \beta_j^3 \left(\frac{R_x^2}{\alpha_x^2} + \frac{R_y^2}{\alpha_y^2} + \frac{R_z^2}{\alpha_z^2} \right) \right. \\
 &\quad \left. \ln \left[\frac{R_{0x_i}^2 + R_{0y_i}^2 + R_{0z_i}^2}{\beta_j^3 \left(\frac{R_x^2}{\alpha_x^2} + \frac{R_y^2}{\alpha_y^2} + \frac{R_z^2}{\alpha_z^2} \right)} \right] d\mathbf{R} \right\} \\
 S &= k \left\{ \ln C + N_c \ln N_c + \sum N_j \ln \left(\frac{\beta_j^3}{\pi^{3/2} \alpha_x \alpha_y \alpha_z} \right) \right. \\
 &\quad \left. \int_{R_x=-\infty}^{\infty} \int_{R_y=-\infty}^{\infty} \int_{R_z=-\infty}^{\infty} \left(\beta_j^3 \left[\left(\frac{1}{\alpha_x^2} - 1 \right) \frac{R_x^2}{\alpha_x^2} + \left(\frac{1}{\alpha_y^2} - 1 \right) \frac{R_y^2}{\alpha_y^2} + \left(\frac{1}{\alpha_z^2} - 1 \right) \frac{R_z^2}{\alpha_z^2} \right] \right. \right. \\
 &\quad \left. \left. - \ln \frac{N_j}{\alpha_x \alpha_y \alpha_z} \right) \exp \left[\beta_j^2 \left(\frac{R_{0x_i}^2}{\alpha_x^2} + \frac{R_{0y_i}^2}{\alpha_y^2} + \frac{R_{0z_i}^2}{\alpha_z^2} \right) \right] dR_x dR_y dR_z \right\} \\
 S &= k \left\{ \ln C + N_c \ln N_c + \sum N_j \ln N_j + N_c (\alpha_x \alpha_y \alpha_z) + \sum N_j \frac{\beta_j^5}{\pi^{3/2} \alpha_x \alpha_y \alpha_z} \right. \\
 &\quad + \left(\frac{1}{\alpha_x^2} - 1 \right) \int_{R_x} \int_{R_y} \int_{R_z} R_x^2 \exp \left[-\beta_j^2 \left(\frac{R_{0x_i}^2}{\alpha_x^2} + \frac{R_{0y_i}^2}{\alpha_y^2} + \frac{R_{0z_i}^2}{\alpha_z^2} \right) \right] dR_x dR_y dR_z \\
 &\quad \left. + \left(\frac{1}{\alpha_y^2} - 1 \right) \int_{R_x} \int_{R_y} \int_{R_z} R_y^2 \exp \left[-\beta_j^2 \left(\frac{R_{0x_i}^2}{\alpha_x^2} + \frac{R_{0y_i}^2}{\alpha_y^2} + \frac{R_{0z_i}^2}{\alpha_z^2} \right) \right] dR_x dR_y dR_z \right\}
 \end{aligned}$$

$$+ \left(\frac{1}{\alpha_z^2} - 1 \right) \int_{R_x}^{\infty} \int_{R_y}^{\infty} \int_{R_z}^{\infty} R_z^2 \exp \left[-\beta_j^2 \left(\frac{R_{ox}^2}{\alpha_x^2} + \frac{R_{oy}^2}{\alpha_y^2} + \frac{R_{oz}^2}{\alpha_z^2} \right) \right] dR_x dR_y dR_z$$

The first integral of this equation can be evaluated as

$$\begin{aligned} & \int_{R_x}^{\infty} \int_{R_y}^{\infty} \int_{R_z}^{\infty} R_x^2 \exp \left[-\beta_j^2 \left(\frac{R_{ox}^2}{\alpha_x^2} + \frac{R_{oy}^2}{\alpha_y^2} + \frac{R_{oz}^2}{\alpha_z^2} \right) \right] dR_x dR_y dR_z \\ &= \int_{R_x}^{\infty} R_x^2 \exp \left[-\beta_j^2 \left(\frac{R_{ox}^2}{\alpha_x^2} \right) \right] dR_x \int_{R_y}^{\infty} R_y^2 \exp \left[-\beta_j^2 \left(\frac{R_{oy}^2}{\alpha_y^2} \right) \right] dR_y \int_{R_z}^{\infty} R_z^2 \exp \left[-\beta_j^2 \left(\frac{R_{oz}^2}{\alpha_z^2} \right) \right] dR_z \\ &= \frac{\pi^{3/2} \alpha_x \alpha_y \alpha_z}{2\beta^5} \end{aligned}$$

CHAPTER 8

THE CRYSTALLINE STATE

8.1. Introduction

The crystalline state in polymers illustrates an important rule of thumb used in polymer science: viz, polymers have properties similar to low molecular weight organic compounds, but the long chain structure in polymers modifies these properties. In this instance, many thermoplastic polymers do possess crystalline structures analogous to those exhibited by low molecular weight paraffins and other organic crystals. The presence of a slow, kinetically determined nucleation and growth rate however reduces the amount of crystallinity and produces greater disorder. A few polymers such as polytetrafluoroethylene [1] or polyoxymethylene [2] are essentially completely crystalline in the polymerized state. An irreversible loss in the degree of crystallinity however is observed if these polymers are melted and cooled. As with other materials, the basic crystal unit cells in polymers are arranged in larger structures that become apparent as the scale of measurement increases. Thus, electron microscopy shows polymer single crystals with well-defined faces and characteristic growth habits [3] grown from dilute polymer solution. At still larger sizes, optical microscopy shows that these small crystals branch and splay, forming sheath-like structures which evolve toward spherical polycrystalline aggregates (or spherulites).

X-ray diffraction can study the ordered, crystal structures at the molecular level. Crystallographers were at first reluctant to accept that these large molecules could form crystals which were smaller than the molecules. They eventually became convinced and realized that parts of

molecules could reside within the crystals, but could emerge, enter the amorphous phase where they might end, or else reenter the crystal as a fold or connect to another crystal as a tie chain. Mark and Meyer [4], in the early days of x-ray diffraction investigations, obtained x-ray diffraction patterns from natural polymers (silk and cellulose). Subsequent work by many investigators on other polymers revealed that different polymers in common with other material classes exhibit different unit cells, crystal dimensions and can even undergo polymorphic transitions [5]. The unit cell for a specific polymer depends on packing considerations such as relative atomic sizes and interactions in the atoms comprising the chain structure. X-ray diffraction has also been used to estimate crystal orientation, the degree of crystallinity, and crystal size and perfection.

Optical microscopy has elucidated the morphology of larger structures in crystalline polymers. A detailed knowledge of spherulitic and other structural aggregates and of nucleation and growth rates during the crystalline transitions of many polymers has emerged from light microscopical studies. At a more fundamental structural level, electron microscopy has enabled polymer single crystals to be analyzed [3]. The folded chain models of polymer structure developed when these analyses were applied to bulk crystallized polymers. These techniques and others (infrared, thermal analysis, NMR) used in studying crystalline polymers have demonstrated that, by suitable thermal and mechanical treatments, the degree of crystallinity and morphology of many semi crystalline polymers can be varied over a wide range. Because of the strong influence that crystallinity exerts on polymer physical and optical properties, polymers with different properties can be produced by suitable control of crystallization during fabrication and processing. This conclusion has obvious implications in the production, for example, of polymer fibers and films.

This chapter discusses the topics of crystallinity detection and measurement, the morphology of polymer crystalline aggregates at different levels of size and the kinetics of melt-crystal phase transformation. Chapter 3 presents thermodynamic aspects of crystallinity in polymers. The treatment is intended to provide a broad

but necessarily brief introduction to a very active and lively area of polymer physics.

A bibliography at the end of the chapter provides material for study in greater depth of any particular topic.

8.2. Evidence for Crystallinity

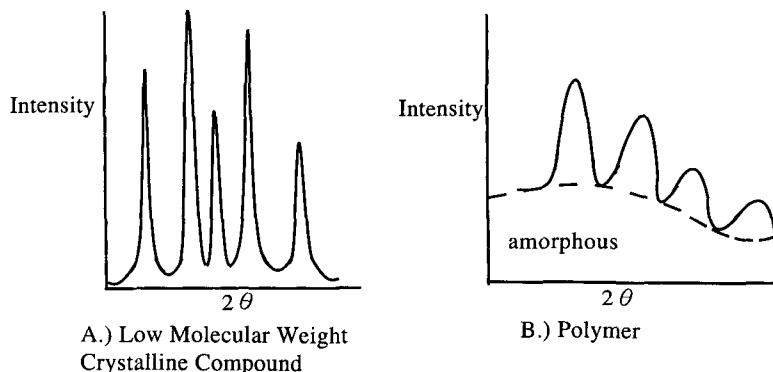


Figure 8.1. Comparison of x-ray diffraction patterns.

8.2.1. X-Ray Diffraction

The x-ray diffraction pattern of a typical inorganic crystal (Figure 8.1A) shows the sharp peaks at discrete diffraction angles characteristic of large well-formed crystals. There is also usually little background scattering present. By contrast, the pattern for a typical crystalline polymer (Figure 8.1B) has broader peaks and the entire diffraction pattern is superimposed on a diffuse background. These features have been interpreted as arising from a two-phase system – a mixture of a crystalline and an amorphous phase where the broader peaks arise from the small size and imperfection of the crystals. The greater background scattering mostly comes from the diffuse scattering of the amorphous phase. A second interpretation holds that there is a one-phase structure in which a second amorphous phase is not required. The diffuse scattering and broadened diffraction peaks can be explained based on imperfections or defects in polymer crystals. The two-phase or fringed micelle model

was the earlier model favored for interpreting x-ray diffraction data. However, more recent work on polymer single crystals and on polymers with high degrees of crystallinity has supported the model of a defective crystal structure. The model of a two phase structure also is supported by its conforming to the thermodynamics of phase changes for such systems.

The molecular structure determination of any crystal is based on the Bragg equation:

$$n\lambda = 2d \sin \theta_b \quad (8.1)$$

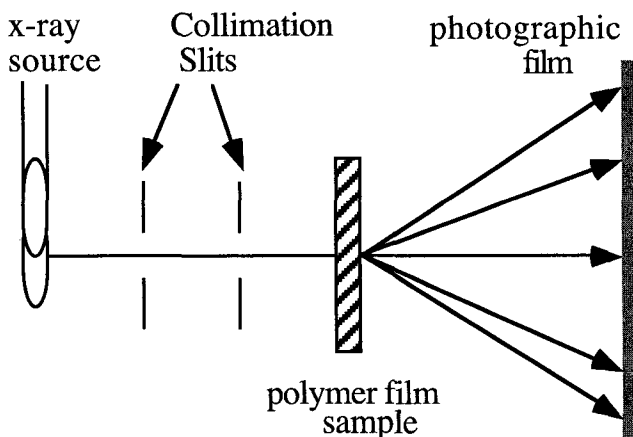


Figure 8.2. X-ray diffraction experimental arrangement.

where d is the interplanar spacing, n the order of the reflection, λ the wave length of the x-ray radiation and θ_b the diffraction angle.

Figure 8.2 depicts the geometrical arrangement. The crystal structure may be determined by fitting the observed diffraction spacings and intensities. The procedure can be illustrated using polyethylene as an example.

The x-ray reflections of the polyethylene d spacings can be calculated from the equation for an orthorhombic unit cell [6,7]

$$d = \frac{1}{\sqrt{\frac{h^2}{a^2} + \frac{k^2}{b^2} + \frac{l^2}{c^2}}} \quad (8.2)$$

where a , b , and c are the unit cell dimensions and h , k , and l are integers, the Miller indices, that describe the location of the crystal plane with respect to the unit cell axis. Thus, the Bragg equation predicts diffraction maxima at discrete values of θ_b corresponding to each set of h , k , and l . The task then is to determine the crystal unit cell and unit cell dimensions. A procedure termed indexing is used. Maxima calculated from equation 8.2 are compared with the measured maxima until a suitable match is obtained. The crystal density (ρ) is given by

$$\rho = \frac{nM_m/N_A}{V_u} \quad (8.3)$$

where n = the number of monomer units of molecular weight M_m

N_A = Avogadro's number

V_u = the unit cell volume (abc for an orthorhombic unit cell)

The kind, number and location of the atoms comprising the unit cell determine the diffracted intensity. The fitting of calculated with measured intensities is the basis for the art of structure determination. The intensity of the diffracted x-rays is

$$I = KFF^* \quad (8.4)$$

where K is a proportionality constant, F the "structure factor" given by

$$F = \sum_i f_i \exp[2\pi i(hx_i + ky_i + lz_i)] \quad (8.5)$$

and F^* the complex conjugate of F . The sum is over all atoms in the unit cell. f_i is the atomic form factor for the i^{th} atom and is a measure of its scattering ability at a given angle. x_j , y_j and z_j are the coordinates of the j^{th} atom expressed in units of fractions of the a , b and c spacings. Since n must be an integer, approximate measures of a , b and c together with an experimental density serves to define n . A problem with polymers is that one cannot obtain them in a hundred percent crystalline form. An approximate value is usually obtained by extrapolation. It is more

common to use this equation with experimental values of a , b and c to calculate an accurate value for the crystal density for use in crystallinity determinations. The intensity calculations lead to predictions of characteristic extinctions that depend on crystal symmetry. The intensities calculated for a proposed structure are compared with experimental data. Alternatively, an electron density map may be constructed by Fourier inversion [6,7]. A problem with this is that the Fourier inversion requires a knowledge of F^* obtained from $(I)^{1/2}$. The ambiguity in the "phase problem" lies in establishing the sign and resolution of F^* into its real and imaginary parts.

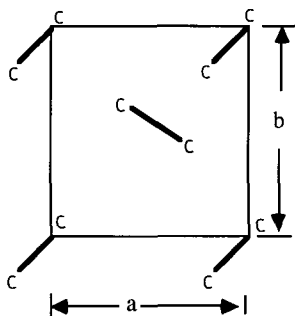


Figure 8.3. Section through the ab plane in the orthorhombic polyethylene unit cell. a and b are the unit cell dimensions.

The unit cell dimensions calculated by these procedures for polyethylene are $a = 0.740$ nm, $b = 0.493$ nm and $c = 0.254$ nm and the density is (8.6 kg/m^3) . Figure 8.3 shows the ab plane. The c -axis is parallel to the chain axis and its length of 0.254 nm is equal to the distance between alternate carbon atoms. This structure for polyethylene is identical with that determined for crystals of pure n -paraffins such as $\text{C}_{32}\text{H}_{66}$ – low molecular analogs of polyethylene. X-ray structures have been determined for many crystalline polymers. Miller [5] has published an extensive compilation of polymer unit cell data.

For large perfect crystals, sharp diffraction peaks with several orders of the same reflection are commonly observed. For smaller crystals with imperfections or defects, the peaks broaden and the intensities of the higher order reflections decrease. The effects of size may sometimes be

distinguished from that of defects by use of the paracrystalline lattice statistics proposed by Hosemann [8]. An effective crystal size (neglecting the effect of crystal defect on peak broadening) may be estimated from the Scherrer equation [6]

$$d = \frac{B\lambda}{W \cos \theta_b} \quad (8.6)$$

where W is the peak width at half the peak intensity and B is a constant near unity that is dependent on the peak shape.

8.2.2. Electron Microscopical Observations

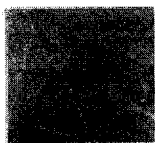


Figure 8.4. Polyethylene crystal grown from dilute solution.

Single crystals of many polymers have been grown from dilute solution [3]. For polyethylene, these are identical in appearance with single crystals of the *n*-paraffins. Polymer single crystals typically form lozenge or diamond shaped thin platelets (Figure 8.4). Electron microscopes or low-angle x-ray scattering can measure single crystal thickness. For *n*-paraffins, the thickness increases at first with increasing molecular weight and the molecules lie perpendicular to the crystal face. By carrying out such measurements for diffraction from different crystal planes, one may deduce crystal dimensions in different directions. Such measurements are in approximate agreement with those observed by electron microscopy and those deduced from small angle x-ray diffraction measurements. Keller has shown that, as molecular weight increases above about 100 carbon atoms, chain folding commences. For polymers, the thickness approaches an asymptotic value independent of the molecular weight, but dependent upon the crystallization temperature (Figure 8.5).

THE CRYSTALLINE STATE

Since the chain length for high polymers is at least several times the crystal thickness, it is postulated that, for polymers, the chains are folded back and forth through the crystals. Three models have been proposed (Figure 8.6). The regularity of this chain folding has been discussed extensively and is dependent upon crystallization conditions (see Section 8.4).

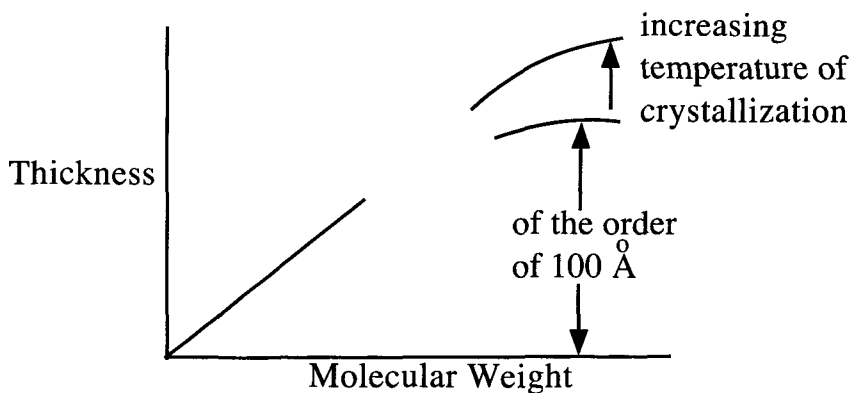


Figure 8.5. Lamellar thickness variation with molecular weight.

8.2.3. Optical Microscopy

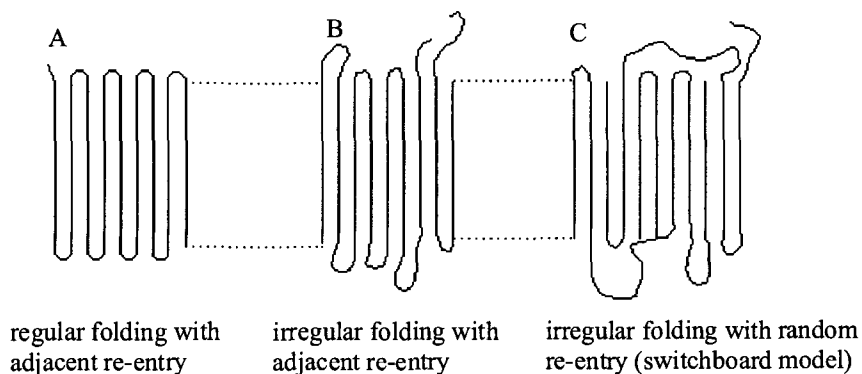


Figure 8.6. Three models of the folded chain surfaces in polymer single crystals.

The optical microscope shows the presence of crystalline structures representing a higher level of organization than the lamellar. As discussed later, crystals particularly in bulk often grow from heterogeneous nuclei (foreign particles). Crystals grow radially outward from these nuclei leading to expanding spheres termed spherulites of partially crystallized material. The spherulites originate from nuclei, usually heterogeneous, at their centers. The number of these nuclei increases with higher degrees of super cooling, so that more and smaller spherulites result from crystallization at lower temperatures. Small amounts of added materials such as sodium benzoate can serve as nucleating agents and can produce polymers having smaller spherulites, greater clarity and modified mechanical properties.

8.2.4. Thermodynamic Transitions

Chiang and Flory [9] demonstrated by dilatometric measurements that the melting process in polyethylene met the requirement of a first order phase or melt to crystal transition. Semi-crystalline polymers usually melt over a range of several degrees in contrast to the narrow melting range displayed by most pure inorganic crystals as they evolve a latent heat of crystallization. The greater range of melting temperatures observed for polymers arises from the distribution on their crystal size and perfection.

Chiang and Flory used three conditions to demonstrate the presence of a latent heat in polyethylene. They cleaned the sample of possible impurities to eliminate adventitious sites for heterogeneous nucleation and annealed the sample before melting commenced to ensure that the highest possible crystallization was achieved. Finally, Flory and Chiang heated the polyethylene sample slowly (over the period of a week before each increase in temperature) to allow the sample to equilibrate.

Enthalpy changes with temperature on solid semi crystalline polymers show similar sharp transitions buttressing the argument that semi crystalline polymers possess a phase that meets all the requirements of a thermodynamic crystal.

8.3. Determination of Degree of Crystalline

8.3.1. Density Measurements

Volume dilatometry measures changes in the specific volume, the reciprocal of density. The degree of crystallinity is calculated using the assumptions that:

i) The crystalline specific volume, \bar{V}_c , and the amorphous specific volume, \bar{V}_a , weighted by the respective volume fractions (X) are additive, or

$$\bar{V}_s = X_c \bar{V}_c + X_a \bar{V}_a \quad (8.7)$$

where, \bar{V}_s , is the sample specific volume, X_c , the volume fraction of the crystalline phase and X_a the volume fraction of the amorphous phase.

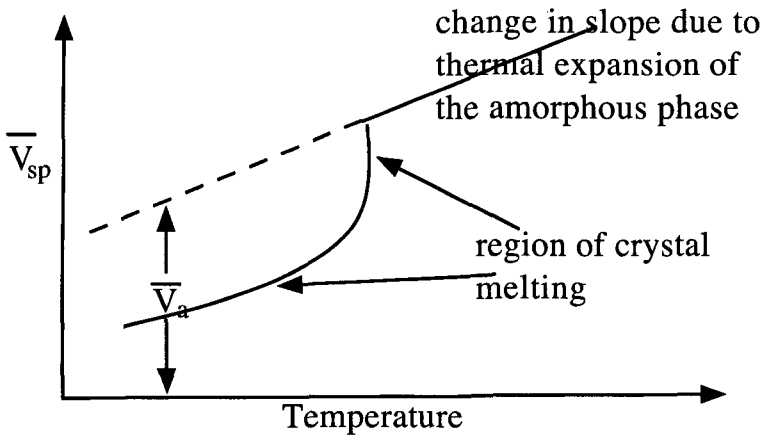


Figure 8.7. Specific volume against temperature plot for polyethylene illustrating the extrapolation of \bar{V}_a to lower temperature.

ii) For a two-phase system, the volumes are additive. Using the additivity assumption, and rearranging equation 8.7 yields

$$X_c = \frac{\bar{V}_a - \bar{V}_s}{\bar{V}_a - \bar{V}_c} \quad (8.8)$$

\bar{V}_s at any temperature is determined from extrapolation of a specific volume-temperature plot (Figure 8.7). \bar{V}_c is determined from x-ray density

$$\bar{V}_c = \frac{1}{\rho_{calc}} \quad (8.9)$$

where ρ_{calc} is the crystal unit cell density obtained from equation 8.3 or its equivalent. The specific volume of the amorphous phase is obtained by assuming that its value is the same as that of the completely amorphous polymer. This may not be true, since the amorphous density may be affected by the constraints imposed by the crystals. This has shown to be so, for example, for poly(ethylene terephthalate), where independent measures of the amorphous density were made from quantitative analysis of small angle x-ray scattering data. Figure 8.8 shows the temperature dependence of X_c , based on ρ_{calc} , for polyethylene.

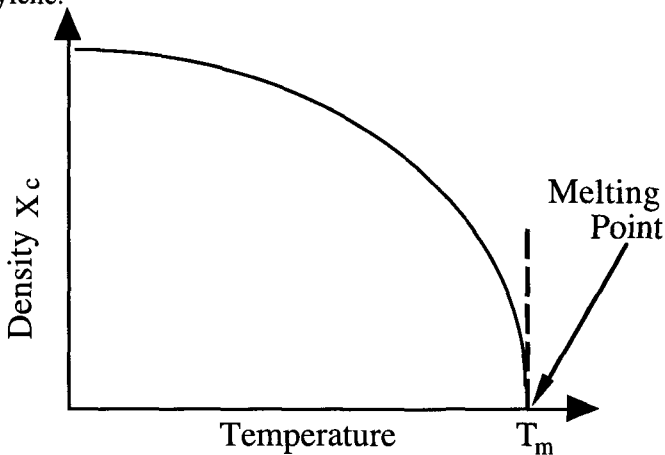


Figure 8.8. The temperature dependence of the crystal unit cell density of polyethylene.

From density data obtained on many semi-crystalline polymers, the following qualitative observations may be summarized:

- i) Most polymers are not completely crystalline.
- ii) Annealing polymers may increase the degree of crystallinity.

iii) Most polymers melt over a range of temperature, and not at a discrete temperature.

iv) The maximum melting point T_m and melting point range depend upon the crystallization temperature (T_c). T_m approaches the true (thermodynamic) melting temperature T_m^0 as crystallization is carried out at increasingly higher temperatures (or the equivalent, longer times). Figure 8.9 illustrates the graphical technique for estimating T_m^0 based on this observation.

v) The equilibrium melting point assumes that the crystals are in equilibrium with the isotropic amorphous phase. The amorphous phase in the vicinity of the crystals may not be isotropic because of the constraints of the crystals and because some chains are anchored to the crystals as loops and tie chains. When the crystals melt, the melting point may be dependent on the rate of heating.

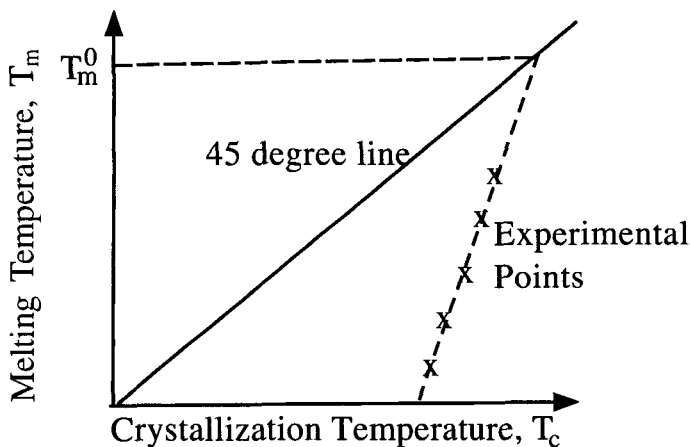


Figure 8.9. Estimation of the equilibrium melting point (T_m^0) by extrapolation of crystallization temperature-melting point data.

Several explanations have been advanced to account for the observation that the measured T_m is lower than the equilibrium melting point. Among these are:

i.) Crystals have finite size and their melting points decrease because of surface energy considerations. At lower crystallization temperatures,

the crystals are smaller and melt a lower temperature. An equation based on this hypothesis is derived in Chapter 3.8.1.

ii) Crystals are imperfect. At lower temperatures, crystallization occurs more rapidly, the number of imperfections is greater thereby reducing the melting point.

iii) Amorphous tie chains trapped between crystals become taut as crystallization proceeds. This has the effect of increasing crystal surface energy and lowering the melt temperature. (This effect is greater with higher molecular weight chains.) At lower crystallization temperatures, the faster crystallization rate results in a greater probability of tie chain entrapment. Also, tie taut chains, in addition to the effect on surface energy, influence the melting point through their influence on the entropy of the amorphous phase.

The broadening of T_m or the range of melting temperature may arise from the contributions of the three effects.

8.3.2. X-Ray Diffraction

Because polycrystalline polymers exhibit a two-component diffraction pattern, the degree of crystallinity may be obtained from the relative areas [3]. Thus,

$$X_c = \frac{K \int_0^\infty I_{cr}(S) S^2 dS}{\int_0^\infty I(S) S^2 dS} \quad (8.10)$$

where S equals $(2/\lambda)\sin \theta_b$, $I_{cr}(S)$ is the intensity of the crystalline component of the diffraction observed at S and $I(S)$ is the total intensity (Figure 8.10). This technique involves the assumption that the contribution per unit mass of the crystals does not depend upon order. Ruland [10] has examined this assumption and shown that a correction should involve allowing the constant, K , to depend upon crystal order. In principle, this dependence could be evaluated, where possible, by examining various orders of the diffraction peak. This is difficult to do and is seldom done. K is a constant, with a magnitude of roughly unity, dependent upon the amount of disorder. I_{cr} can sometimes be determined from model compound studies (e.g., *n*-paraffin crystals for polyethylene).

Another technique [11] takes the ratio of the amorphous area for a semi crystalline polymer to that of a completely amorphous polymer (measured, for example, by melting a polymer sample). The areas are obtained by integration, then

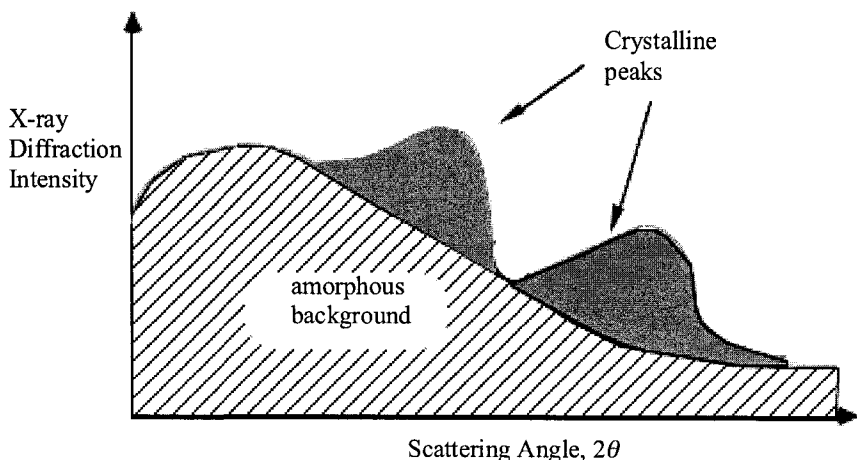


Figure 8.10. Diagram showing the ration of crystalline area to amorphous area in an x-ray diffraction pattern.

$$1 - X_c = \frac{K \int_0^{\infty} I_{am}(S) S^2 dS}{\int_0^{\infty} I_{am}(S) S^2 dS} \quad (8.11)$$

8.3.3. Infrared (IR) and Raman

It should be mentioned that for most IR bands, absorption is sufficiently strong that samples must be thin. Alternatively, IR can be studied by reflectivity using attenuated total reflectance (ATM) techniques, but such measurements provide information about portions of the sample close to the surface which may not be the same as within bulk samples.

One caution in evaluating crystallinity from the intensity of crystallization temperature is that the intensity is affected by the orientation of the transition moment of the band relative to the polarization direction of the radiation. Thus, if the polymer is oriented, this dependence should be considered.

Infrared spectra for crystalline polymers differ from those of amorphous polymers for at least two reasons:

i) Infrared bands are often sensitive to conformation. Polymer molecules in crystals are often restricted to a particular conformation. Thus, for polyethylene, the infrared data may be used to resolve the amorphous bands into gauche and trans contributions [12].

ii) Coupling of vibrations between different molecules in a unit cell may lead to the splitting of bands. For example, the 720 cm^{-1} CH_2 rocking mode in a polyethylene crystal splits into bands at 720 cm^{-1} and 729 cm^{-1} corresponding to the out-of-phase vibrations for the two chains in the polyethylene unit cell (Figure 8.3). Many crystalline polymers show a mixture of crystalline and amorphous absorption bands. Thus, polyethylene has crystalline bands at 1894 , 1176 and 1050 cm^{-1} , while amorphous bands are observed at 1368 , 1352 and 1303 cm^{-1} [13]. The ratio of absorbance for a crystalline band to that for an amorphous correlates well with density and x-ray diffraction. Thus, Cobbs and Burton [14] used the $972/975\text{ cm}^{-1}$ ratio for the infrared spectrum of poly(ethylene terephthalate) and observed a linear correlation measurements.

For Raman spectra, on the other hand, an experimental advantage is that samples can be thicker compared to those needed for infrared. Also, fiber optics techniques may be employed for measurements in local regions using Raman spectra. A disadvantage is that Raman measurements give problems in samples that are turbid as a consequence of Rayleigh scattering by inclusions.

8.3.4. Wide Line Nuclear Magnetic Resonance

The width of NMR bands is dependent upon the heterogeneity of the average magnetic field (\mathbf{H}) about an absorbing nucleus [15]. Thus,

$$E = \hbar\nu = c(\mathbf{H} \cdot \mathbf{u}) \quad (8.12)$$

where ν = the absorption frequency

c = a constant

\mathbf{u} = the magnetic moment of the absorbing nucleus and

$$\mathbf{H} = \mathbf{H}_0 - \mathbf{H}^* \quad (8.13)$$

where H_0 = the applied magnetic field

H^* = the local field about a given nucleus due to neighbor interactions.

For molecules in dilute solution in which mobility is high, field heterogeneities average out and absorption bands are narrow. Such averaging does not occur with a glassy or a crystalline polymer because the molecules are too rigid. Broad bands usually characterize NMR absorption in the solid state. For molecules in a rigid environment, H^* , depends on the local state of the nucleus with different bonding (e.g., the change in chemical environment between the protons in a methyl and a methylene group). Thus, there is present a distribution of frequencies that form a wide band. In addition, in a solid, the local magnetic field is anisotropic so that the width depends upon the angle between the crystal and the magnetic field (Figure 6.8).

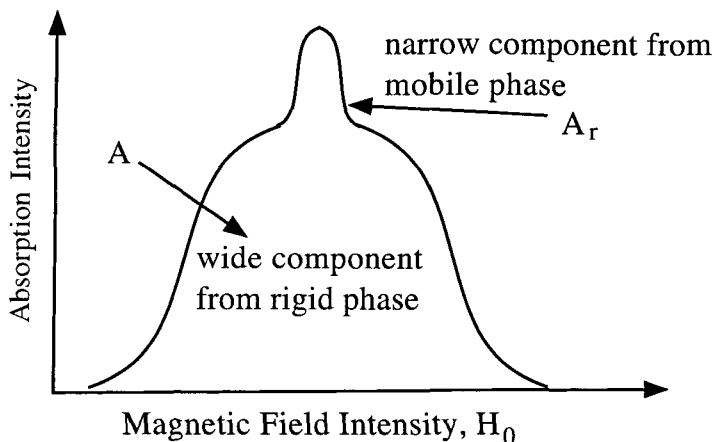


Figure 8.11. Sketch showing resolution of NMR spectrum into mobile and rigid phases.

For a polycrystalline polymer, the absorption band possesses a broad component from the crystalline phase (if it is above its T_g) (Figure 8.11). The degree of crystallinity (X_c) may be calculated from the ratio

$$X_c = \frac{A_r}{A} \quad (8.14)$$

where A is the area under the broad components and A_r the area under the narrow component. Nmr results do not always correlate with those obtained from other methods. The difficulty is that nmr measures mobility rather than crystallinity. Thus, below its T_g , a rigid amorphous phase behaves like a crystal in response to nmr magnetic fields.

8.3.5. Thermal Measurements

This determination is based on measurement of enthalpy, a fundamental thermodynamic quantity. The basic equation is given by

$$X_c = \frac{\Delta H}{\Delta H_c} \quad (8.15)$$

where ΔH = the enthalpy of fusion of the sample

ΔH_u = the enthalpy of the completely crystalline polymer.

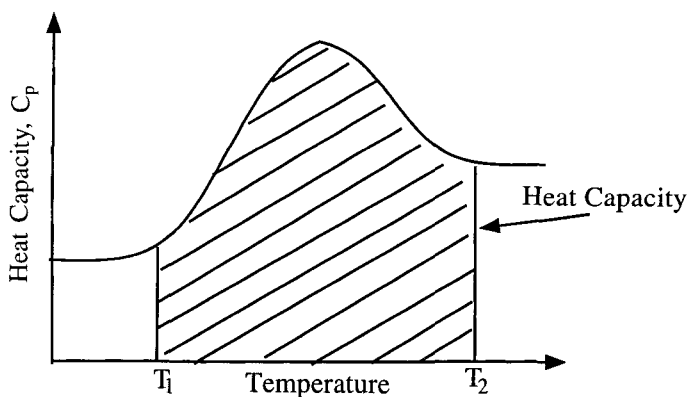


Figure 8.12. Plot of C_p against temperature for the graphical integration of equation 8.21.

Thus

$$\Delta H = H_a - H \quad (8.16)$$

$$\Delta H_c = H_a - H_c \quad (8.17)$$

where H_a , H_c and H are the enthalpies of the completely amorphous, the completely crystalline and the polymer sample respectively. ΔH between any two states can be obtained from the heat capacity at constant pressure (C_p) by integration, or

$$\Delta H = \int_{T_i}^{T_f} C_p dT \quad (8.18)$$

This expression may be evaluated by computer (Figure 8.12) by plotting C_p data obtained from calorimetric, DSC or (indirectly) from DTA measurements [16]. One finds that enthalpy varies with temperature in a manner similar to that of specific volume (see, Figure 8.18).

Section 6.6 discusses other aspects of nuclear magnetic resonance.

8.4. Morphology

8.4.1. Electron Microscope

As discussed above (Section 8.2.2), crystal lamellae are composed of folded chains. No means however exist for direct observation of these folds so that the detailed morphology of the fold surface must be inferred from indirect evidence. Three models for folded surface morphology have been proposed (Figure 8.6).

For very low degrees of super cooling, model A is postulated to predominate. The evidence for regular folding with adjacent reentry is:

i) The observed pyramidal structure.

The single crystals are not planar, but instead form hollow pyramids. Four sectors may be distinguished based on their differing orientation on microscopic observation. The tilt of the sectors is due to the fold packing. The tilt angle α may be calculated from crystallographic considerations as

$$\tan \alpha = \frac{\ell}{d} \quad (8.19)$$

where d is the distance between chains in the crystal and $\lambda = nc$ where n is an integer and ℓ is the monomer repeat distance. The fold surface lies

along the 110 crystal plane but the four sectors differ in the orientation of the folds (Figure 8.13).

It should be mentioned that pyramidal crystals are only seen if they do not collapse as occurs when they are dried on a surface. When they do collapse on drying, cracks develop.

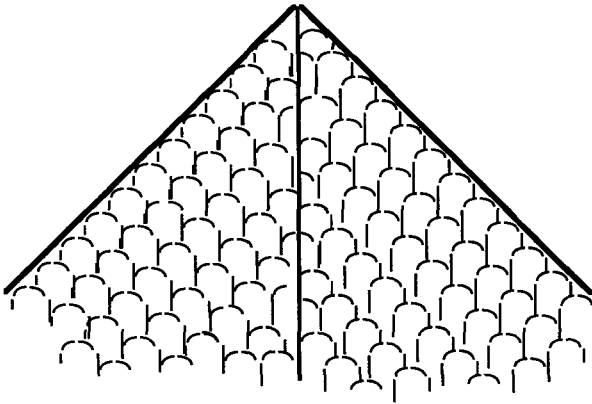


Figure 8.13 Diagrammatic sketch showing relation between the crystal plane and fold surface in a polymer single crystal.

ii) Moiré Patterns

In more concentrated solutions, crystals stack in layers. Adjacent layers give interference patterns with each other analogous to the effect observed when window screens lie on top of one another. These “moiré patterns” show that the layers are in crystallographic register with each other and are best interpreted in terms of packing of regular folds on the single crystal surface.

At higher degrees of super cooling, the fold surface, proposed in model B (Figure 8.14), is more likely. The evidence for irregular folding with adjacent re-entry is based on:

i.) Density

THE CRYSTALLINE STATE

The experimental density of the crystal is lower than the density calculated from crystallographic data (11), or

$$\rho_{calc} = \frac{\text{weight}}{\text{volume}} = \frac{M_m n_m / A}{abc} \quad (8.20)$$

The lower density however has been hypothesized as originating from disordered material deposited on the fold surfaces. crystallized polymer samples.

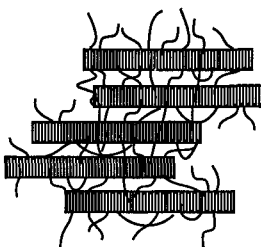


Figure 8.14. Tie molecules between crystal lamellae.

ii) nmr

Nuclear magnetic resonance (nmr) studies indicate the presence of a mobile compound even for solution grown crystals.

iii) X-ray diffraction

X-ray diffraction from single crystal preparations proves the presence of disordered material [3].

iv) Kinetics

Theoretical kinetic predictions are consistent with irregular surface folding. For bulk crystallized polymer samples, etched surface and fracture sections [17] show lamella structure. The thicknesses of the lamellae in bulk polymers are comparable with those of solution grown single crystals. These structures are interpreted as originating from chain folded layers. It is probable, based on kinetic arguments of crystallization in bulk polymers, that folding in these lamellae is not regular and that

there are tie chains between lamellae (Figure 8.14), as shown by Keith and Padden [18]. These tie chains are responsible, in part, for the mechanical strength of bulk crystallized polymer samples.

The evidence cited in support of the model B structure also supports the model C fold surface structure. In addition, Flory and Yoon [19] have argued that the steric hindrance to forming a sharp bend over a few chain atoms precludes the prevalence of adjacent reentry.

The relative amount of random reentry to adjacent reentry will vary with polymer chain structure. The energy required for a chain to form a bend determines the extent to which adjacent reentry is favored. The lower the energy expended to form a tight bend, the more adjacent reentry loops will occupy a fold surface [20].

8.4.2. Optical Microscopy

Spherulitic structures are often large enough to be visible by the optical microscope. Crystalline lamellae form the radii of these spherulites with one crystalline axis (the *b* axis in polyethylene) tending to lie in the radial direction. The lamellae often twist and form branches. The branching is necessary to fill the spherulitic volume [21] Since one axis is radial, the spherulite is usually optically anisotropic the radial and tangential refractive indices having different values. If the spherulite is viewed between crossed Polaroids™, this optical anisotropy has the appearance of a Maltese cross (Figure 8.15). The transmission (*T*) of an anisotropic crystal located between two polarizers is

$$T = \sin^2\left(\frac{\delta}{2}\right)\sin 2\theta \quad (8.21)$$

where δ is the optical retardation of the crystal and θ is the angle between the sample optic axis and the polarizers. The transmission is zero when $\theta = 0^\circ$ or 90° and is a maximum when $\theta = 45^\circ$.

This consideration assumes that the optic axis lies either parallel or perpendicular to the lamellae which would be the case, for example, if the chains were oriented perpendicular to the lamellae. There are cases where the chains are tilted with respect to the lamellae in which case, the optic axis may be tilted at some angle with respect to the lamellar axis.

For an angle of 45° , for example, the dark arms of the Maltese cross will lie at 45° to the axes of the crossed polars rather than along the polarization directions.

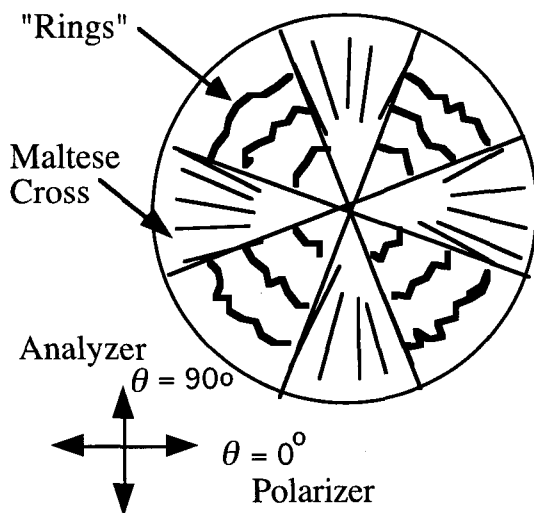


Figure 8.15. Polyethylene spherulite between crossed polars showing Maltese cross and ringed structure.

The ringed appearance (Figure 8.15) arises from twisted lamellae. The continuity of the rings through a 360° rotation suggests that the lamellae twist in phase. Spherulites contain amorphous material situated between and on the surface of lamellae. This is often polymer with low tacticity or branched polymer that does not readily crystallize and is therefore excluded from the growing crystal during the crystallization process.

8.4.3. Liquid Crystals

Liquid crystals, as the name implies, are fluid materials that show x-ray (and other diffraction) peaks with the narrow widths characteristic of crystal like order. Polymers as well as low molecular weight compounds are capable of forming liquid crystalline phases for certain conditions of temperature, shear rate, chain stiffness and electrical fields. Phase

diagrams are used to summarize the temperature-pressure regime over which liquid crystals are stable. Liquid crystal polymer chains commonly

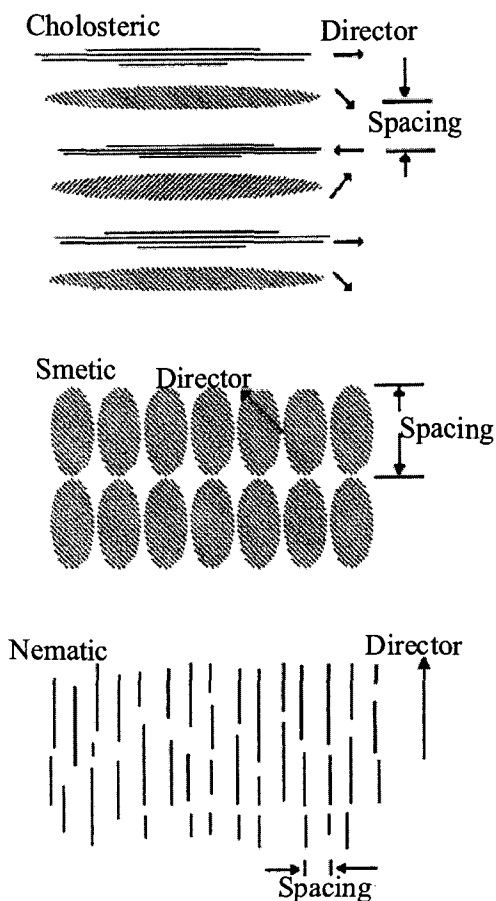


Figure 8.16. Liquid crystalline structures.

comprise anisotropic structural units (mesogenic groups) either as chain backbone groups, as branches or both. The three main types are depicted in Figure 8.16. The common denominator is chain packing or the placement of stiff rods in a confined volume. The least ordered is the nematic which consists of the packing of long rods or order along the chain axis. Next is the smectic that has the packing for the spacing of

nematic planes. The final type is the cholesteric in which the spacing results from the helical packing of nematic rods. A director (a vector perpendicular to the axis or plane of the liquid crystal) is commonly used to specify the average orientation of a liquid crystal domain. Typically, birefringence and scattering techniques are used to measure director orientation. Correlation functions could also be used for the same purpose and, in addition, would furnish additional information on orientations at longer ranges. These could be determined at several characteristic distances by the use of visible, neutron and x-ray radiations. The resultant data could then be coordinated to provide a more complete description of the liquid crystal orientation.

Kevlar™ fibers [22] were the first application of liquid crystals in polymers. A special technique had to be developed spin fibers because they were too stiff to be processed by the known fiber spinning methods. The straight stiff nature of these chains however confers exceptional strength on the final Kevlar fiber.

Several fibers based on liquid crystal precursors have been subsequently produced. Keller [23] postulates the existence of a liquid crystalline phase during the melt-crystalline transition in polyethylene (and other polymers).

8.5 Mechanisms of Crystallization

8.5.1. Nucleation and Growth

J. Willard Gibbs in the 1880s [24] first presented the basic premises for this mechanism. The stable phase in a crystal/melt system varies with temperature. Above the melt temperature, the liquid melt is the stable phase below the melt temperature; the crystal is the stable phase. At just below the melt or first order transition temperature, fluctuations in the size of the crystal phase occur. Most are too small and return to the melt phase. However, a few fluctuations are large enough to become stable. They therefore provide a surface for other molecules in the melt to transfer over to the crystal phase. The crystal phase then grows from these homogeneous nuclei at the expense of the melt phase. Dirt and other adventitious contaminants of the right size range can furnish a

surface on which a crystal phase can grow. This latter type of nucleation (heterogeneous) is common in polymers due to the presence of residual catalysts and polymer additives. Ross and Frolen [25] distinguished between the two types of nucleation mechanisms by applying a technique first used in cloud seeding experiments to polyethylene. The technique relies on the statistical principle that, if a sample is divided into many fine droplets, some droplets will not contain contaminants and therefore will nucleate by a homogeneous mechanism. The cleaned polymer samples were divided into small droplets, heated to above the melting point for several minutes to insure that all the chains had melted and then slowly cooled. An optical microscope was used to find the number of particles that crystallized. Two maxima in the temperature range were noted. The maximum at the higher temperature is due to heterogeneous nucleation while that at the lower temperature is due to homogeneous nucleation. This is discussed in more detail in Section 8.6 below.

Growth occurs by a secondary nucleation mechanism in which crystals form on the surface of the primary nucleus. The assumed growth model is that of a sphere. The barrier to nucleation is lower for growth so that the number of crystals formed during this stage is determined by the undercooling. At small undercoolings in which the phase transition occurs close to the melting point, few heterogeneous nuclei are present so that the transition proceeds mainly by a growth mechanism. This results in a few large crystalline structures. Conversely, for large undercoolings, many homogeneous nuclei form and growth proceeds from many centers resulting in many small crystalline structures.

8.6. Kinetics of Crystallization

8.6.1. Temperature Dependence of the Nucleation Rate

The temperature dependence of the nucleation rate is described by the rate constant (k_n) in the Avrami equation. This dependence is assumed to originate from a balance between diffusion of chain segments to the nucleus and the free energy barrier for incorporation of the segments into the nucleus. Thus,

$$k_n = A \exp[-E_d/kT] \exp[-\Delta G^*/kT] \quad (8.22)$$

where A = a pre exponential front factor.

E_d = the activation energy for viscous flow.

ΔG^* = the free energy required to form a stable nucleus.

ΔG^* is estimated by minimizing the sum of the two free energies: the volume free energy decrease characteristic of a crystal volume increase and the surface free energy increase associated with the formation of fresh crystal surface. Mathematically, for an assumed spherical nucleus,

$$\Delta G = 4\pi r^2 \sigma_s - \frac{4}{3} \pi r^3 \Delta g \quad (8.23)$$

where Δg is the free energy difference per unit volume between the melt and an infinite crystal and σ_s , the surface free energy per unit surface area, or

$$\Delta G = 4\pi \left[r^2 \sigma_s - \frac{r^3 \Delta g}{3} \right] \quad (8.23A)$$

The free energy is minimized when

$$\frac{\partial \Delta G}{\partial r} = 0 = 4\pi(2r\sigma_s - r^2\Delta g) \quad (8.24)$$

Solving equation 8.24 for r yields

$$r^* = \frac{2\sigma_s}{\Delta g} \quad (8.25)$$

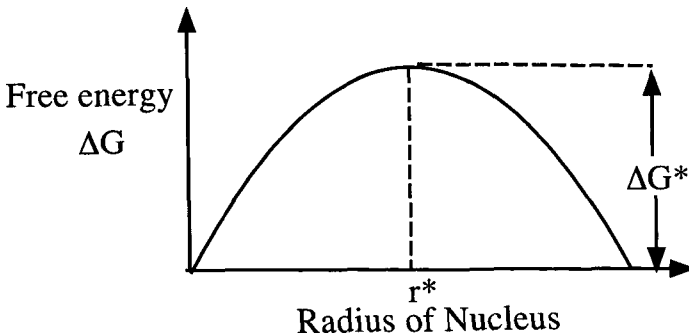


Figure 8.17 Free energy barrier to attainment of a critical sized nucleus.

where r^* is the critical nucleus size that must be formed to attain a stable entity (Figure 8.17). Nuclei smaller than r^* will not be stable because of their high surface energy. As r increases, the surface area to volume ratio decreases so stability increases. At $r > r^*$, growth of the nuclei leads to a decrease in free energy.

Classical nucleation theory assumes that the surface energy density, σ , is independent of the size of the nucleus. This is probably not true when the nucleus is very small and consists of just a few molecules. Also, the theory assumes that the interface between the nucleus and the amorphous phase is sharp. On a microscopic scale, the interface is probably diffuse with a width that could be comparable with the nucleus size at high supercooling.

It is further assumed in classical nucleation theory that ΔG reaches ΔG^* by random thermal fluctuations and thereby is able to surmount the barrier to growth. Once r equals r^* , then the nuclei will continue to grow spontaneously. ΔG^* may be obtained by substituting equation 8.25 in equation 8.24

$$G^* = \frac{16}{3} \pi \frac{\sigma_s^3}{\Delta g^2} \quad (8.26)$$

To evaluate g , the definition

$$\Delta g \equiv \Delta h - T\Delta s \quad (8.27)$$

is used where Δh and Δs are the entropy and enthalpy differences per unit volume between the melt and the infinite crystal. At the equilibrium melting point, $\Delta G_m = 0$ and

$$\frac{\Delta h_m}{\Delta s_m} = T_m \quad (8.28)$$

Assume as before, that in the temperature interval between T and T_m , $(\Delta h/\Delta s)$, is independent of temperature, so that

$$\frac{\Delta h}{\Delta s} = \frac{\Delta h_m}{\Delta s_m} = T_m \quad (8.29)$$

Then, from equations 8.26 and 8.28,

$$\Delta g = \Delta h \left(1 - \frac{T\Delta s}{\Delta h} \right) = \Delta h \left(1 - \frac{T}{T_m} \right) = \Delta h \left(\frac{\Delta T}{T_m} \right) \quad (8.30)$$

where ΔT is the “undercooling”. Then substituting the expression for Δg in equation 8.29 into equation 8.27

$$\Delta g = \Delta G^* = \frac{16}{3} \pi \frac{\sigma_s^3}{\Delta h^2} \left(\frac{T}{T_m} \right)^2 \quad (8.31)$$

or into equation 8.24

$$r^* = \frac{2\sigma_s T_m}{\Delta h \Delta T} \quad (8.32)$$

Thus, the larger the under cooling, the smaller the value of ΔG^* (and the more rapid the nucleation) and the value of r^* (the smaller the size of the critical nucleus) required to initiate crystallization. Other models for the nucleus give similar equations. For example, for disc shaped nuclei

$$\Delta g = \Delta G^* = 8\pi \frac{\sigma_s^2 \sigma_e}{\Delta h} \left(\frac{T_m}{\Delta T} \right)^2 \quad (8.33)$$

where σ_s and σ_e are the side and the end free energies per unit surface area respectively. Thus, from equation 8.43

$$\Delta g = k_n = A \exp \left[\frac{-E_d}{kT} \right] \exp \left[\frac{-16\pi}{3} \frac{\sigma_s^3}{\Delta h^2} \left(\frac{T_m}{\Delta T} \right)^2 \left(\frac{1}{T} \right) \right] \quad (8.34)$$

From these equations, it is evident that smaller nuclei form at higher ΔT (or lower crystallization temperature). The size of the growing crystal relative to the size of its nucleus decreases, so that smaller crystals arise from low temperature crystallization. As discussed previously, these will melt at a lower temperature, giving rise to the important observation that crystals formed at a low temperature melt at a low temperature.

8.6.2. Nucleation and Growth

Nucleation of the embryonic crystals in the liquid phase followed by growth or accretion of the solid phase onto the nucleus in the mechanism usually used to describe polymer crystallization kinetics as with metals,

ceramics and low molecular weight materials. The rate of polymer crystallization shows a strong temperature dependence (Figure 8.18).

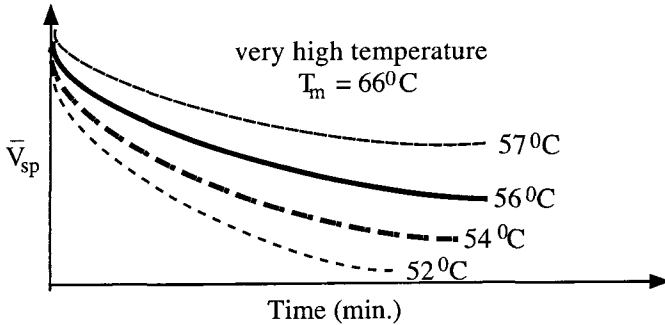


Figure 8.18. Temperature dependence of polymer crystalline rate.

Also, most systems do not crystallize at reasonable rates until the temperature is at least several degrees below the melting point so that a measurable undercooling ($\Delta T = T_m - T$) is required. The crystallization curves measured at several temperatures can be superimposed along the time axis when plotted in terms of $1 - X_c$ against $\ln t$ (Figure 8.19). The nuclei may be classified into two types: heterogeneous nuclei present in the melt that may comprise residual catalyst, dirt particles and other adventitious impurities, and homogeneous nuclei formed from polymer chains as result of thermal fluctuations.

The crystalline phase typically grows as spherical aggregates called spherulites. However, other geometries such as disks or rods may be found with, as shown below, a consequent modification of the rate equation. M. Avrami [26] first derived these rate equations in the form used for polymer kinetics for the solidification of metals. The weight of the crystalline phase is calculated as a function of time at constant temperature. As will be described below, the temperature dependence of crystallization can be derived from classical nucleation theory.

Three growth regimes occur in polymer crystals. Regime 1 completes a surface layer of crystalline lamellae before starting another layer. Regime 3 starts new layers before the underlying layers are complete.

This gives rise to a rough surface. Regime 2 represents an intermediate stage between Regimes 1 and 3. Changes in the slopes of rate versus temperature plots distinguish the different growth regimes [27]. These ideas can be applied to solid polymers.

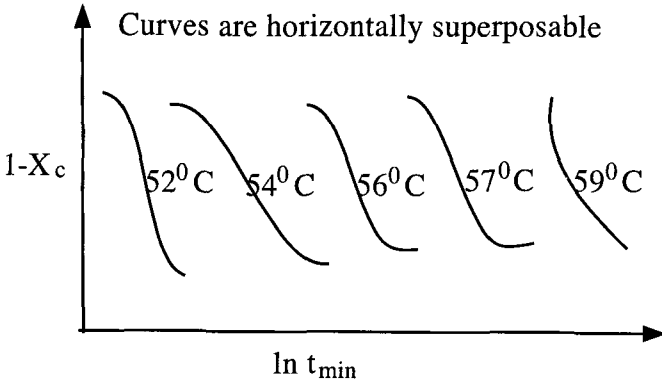


Figure 8.19. Plots of $1-X_c$ against the logarithm of time at different temperatures.

The Avrami equation is obtained as follows. For spherical growth from heterogeneous nuclei, for which all are assumed to start growing simultaneously, the number of nuclei per unit volume (ν) is assumed constant. The growth rate (G) is given by

$$G = \frac{dr}{dt} \quad (8.35)$$

where r is the radius of the sphere growing from the nucleus. The growth rate may be observed microscopically and is usually constant. The significance of a constant G may be seen as follows.

$$V_s(t) = \frac{4}{3}\pi r(t)^3$$

$$\frac{dV}{dt} = 4\pi r^2 \frac{dR}{dt} = A \frac{dR}{dt} = GA \quad (8.36)$$

If G is constant, then the rate of volume increase is proportional to the surface area of the growing sphere, a reasonable conclusion since growth occurs at this developing surface. This assumption requires that the radial lamellae branch at a rate sufficient to maintain density and that the degree of crystallinity is constant throughout the spherulite. This infers

that there is no secondary crystallization, since if there were, crystallization would continue behind the growth front, so that the degree of crystallinity would vary with radius.

The volume of spherulites $V_s(t)$ at time (t) is

$$V_s(t) = \frac{4}{3} \pi r(t)^3 \quad (8.37)$$

The weight of spherulites $W_s(t)$ at this time is

$$W_s(t) = \rho_s V_s(t) \quad (8.38)$$

where ρ_s is the spherulitic density. The weight of crystals $w_c(t)$ is

$$W_c(t) = X_{cs} W_s(t) \quad (8.39)$$

where X_{cs} is the degree of crystallinity of the spherulite which is assumed constant. The degree of crystallinity of the polymer is then

$$X_c = \frac{W_c(t)}{\rho} \quad (8.40)$$

where ρ is the density of the polymer (which will vary slightly during the crystallization process). Thus, on combining equations 8.23 through 8.26

$$X_c = \frac{X_{cs} \rho_s}{\rho} v\left(\frac{4}{3}\right) \pi r(t)^3 \quad (8.41)$$

If all nuclei start growing simultaneously at time = 0 (the case of heterogeneous nuclei),

$$r(t) = Gt \quad (8.42)$$

and

$$X_c(t) = \frac{X_{cs} \rho_s}{\rho} v\left(\frac{4}{3}\right) \pi G^3 t^3 \quad (8.43)$$

Equation 8.43 is the Avrami equation for heterogeneous nucleation followed by three-dimensional growth. This equation neglects the impingement of the growing spherulites on one another and assumes that the spherulites can grow in regions already crystallized

This equation predicts that the degree of crystallinity increase as t^3 . This is initially true, but obviously cannot continue since it would lead to $X_c > 1$. The difficulty arises because the supply of amorphous material becomes exhausted and the rate of crystallization decreases toward zero as the amorphous material is nearly all consumed. This decrease appears in the theory because growing spherulites impinge so that their volume is then

$$A = 4\pi r^2 f(t) \quad (8.44)$$

where $f(t)$ is the fraction of the area lost by impingement. A model of random location of nuclei leads to

$$f(t) = 1 - \phi_c \quad (8.45)$$

where ϕ_c is the volume fraction of spherulites. Thus $f(t)=1$ at the beginning of crystallization, but approaches zero as ϕ_c approaches unity. In this case

$$\frac{d\phi_c}{dt} = \nu GA(1 - \phi_c) \quad (8.46)$$

On substituting 8.40 in 8.41 and integrating, the Avrami equation becomes

$$\frac{\phi_c}{1 - \phi_c} = \nu G 4\pi r^2 = \nu G^3 4\pi t^2 \quad (8.47)$$

$$-\ln(1 - \phi_c) = 4\pi G^3 \frac{t^3}{3} \quad (8.48)$$

For two dimensional growth of discs,

$$V_s = 1 - \exp[-2\pi\nu dG^2 t^2] \quad (8.49)$$

For the case of heterogeneous nucleation, the exponent n of the Avrami equation is equal to the dimensionality of growth.

For homogeneous nucleation in which the nuclei may form during the crystallization process, the exponent n is

$$n = \text{dimensionality of growth} + 1 \quad (8.50)$$

Table 8.1 shows the dependence of K and n on the mechanism of nucleation and growth. Measurements of n have shown that it decreases as crystallization proceeds. Mandelkern [28]) has considered the case of sporadic nucleation on predetermined nuclei that cause a decrease in n as crystallization proceeds. However, n may also decrease when X_{cs} is not constant but varies with time. A comparison of degree of crystallinity measurements with spherulitic growth rate measurements on the same polymer [29] shows this. The polymer continues to crystallize after the volume fills with spherulites. The value of n for this secondary crystallization is usually less than for the primary crystallization process. This difference gives rise to a change of n with time. Reference 30 treats this problem theoretically as do Hilliar [31] and Price [32].

Table 8.1 Correlation between Types of Nucleation and
the Avrami Exponent n

Nucleation Type	n	Growth Geometry
Heterogeneous	2	Disc (or spherulite with severe impingement problems)
Homogenous	2.5	Sphere
Heterogeneous	3	Sphere
Homogenous	3	Sphere

8.6.3. Experimental Determination of n and k

i. Slope-Intercept Method

According to the Avrami equation,

$$1 - X_c = X_c = \exp[-kt^n] \tag{8.51}$$

where X_a is the weight fraction of polymer in the amorphous phase and taking logarithms on both sides

$$\ln(-\ln X_A) = \ln k + n \ln t \quad (8.52)$$

Thus, a log-log plot of X_A against time (Figure 8.20) yields n from the slope and $\ln k_s$ from the intercept.

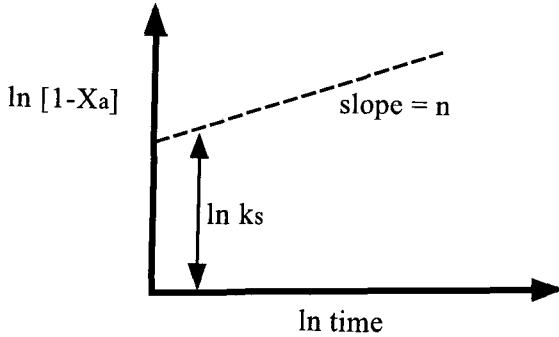


Figure 8.20. Log-log plot of X_a against time showing technique for estimating values of Avrami parameters n and k_s .

ii. Half-life Method

At the crystalline half-life ($t_{1/2}$), $X_A = 1/2$, so equation 8.39 becomes on substitution

$$-\ln(1/2) = \ln 2 = 0.69 = k_s t_{1/2}^n \quad (8.53)$$

or, rearranging

$$k_s = \frac{0.69}{t_{1/2}^n} \quad (8.54)$$

The value of n may be determined from the slope (S) of the crystallization isotherm in the vicinity of $t_{1/2}$

$$S = \frac{\partial X_a}{\partial \ln t} = \frac{\partial X_a}{\partial t} \frac{\partial t}{\partial \ln t} = t \frac{\partial X_a}{\partial t} = t(-nkt^{n-1}) \exp[-kt^n] \quad (8.55)$$

At $t = t_{1/2}$

$$\frac{\partial X_a}{\partial \ln t} = -n(\ln 2) \frac{1}{2} = -0.35n \quad (8.56)$$

Thus, the slope depends only upon n and is independent of k_s . Also, the isotherms should be horizontally super-imposable. If they are not, this means that n is changing with time.

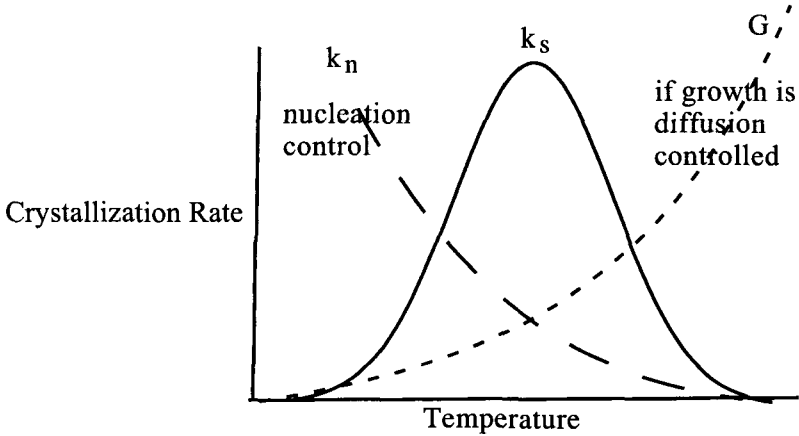


Figure 8.21. Diagram showing the maximum in crystallization rate due to the competing nucleation and growth controlled processes.

8.6.4. Temperature Dependence of the Rate of Homogeneous Crystallization

As shown below (Section 7.4d), the rate of homogeneous nuclei formation increases as the under cooling ($T_m - T$) increases. The converse behavior is associated with the rate of crystal growth. At high temperatures just below the melt temperature, nucleation is slow, but chain segmental diffusion is rapid so that crystallization will occur starting from a few centers giving rise to large structures. At low temperature, the nucleation rate is high but the growth rate controlled by segmental diffusion is slow. Thus, crystallization initiates at many centers giving rise to small structures (such structures will have a depressed melting point giving rise to the previously mentioned observation that crystals formed at a low temperature, and high undercooling, melt at a lower temperature). Often, spherulitic growth is

nucleation controlled so that a maximum in the growth rate-temperature plot (Figure 8.21) is observed as a consequence as discussed in Section 8.6.1.

Nucleation is a general phenomenon for phase changes such as condensation of a vapor (to form fog and rain), boiling of liquids and amorphous polymers-amorphous polymer phase separations (with a competing mechanism of spinodal decomposition). Nucleation requires an activation energy to surmount the free energy needed to form a stable nucleus (Figure 8.17). Spinodal requires no activation energy, but needs a very stable temperature control in order to remain within its stability region (Figure 3.7). In many cases, the temperature cannot be maintained and the spinodal structure switches to a nucleation and growth regime. The activation energy requirement does not hold for the case of heterogeneous nucleation because the heterogeneity (dirt, residual catalyst, etc.) serves as a pre-formed nucleus.

References

1. Y.P. Khanna, *J. Mater. Sci. Letters*. **1988**, 7, 817
2. R. S. Manley, *J. Polymer Sci.* **1960**, 47, 509
3. P. Geil, *Polymer Single Crystals*; Interscience Wiley: New York, **1963**
4. K.H. Meyer, H. Mark, *BER*. **1928**, 61, 1939
5. R.L. Miller, in *Polymer Handbook*, 2nd Ed;
J. Brandrup, E.H. Immergut, eds., Academic: New York, **1975**
6. L.E. Alexander,
X-Ray Diffraction Methods in Polymer Science; Krieger: Huntington, NY, 1979
7. M.L. Miller, *The Structure of Polymers*; Reinhold: New York, 1966,
8. R. Hosemann, R.N. Baghchi, *Paracrystallinity*, Interscience: New York, **1959**
9. R. Chiang and P.J. Flory, *J. Amer. Chem. Soc.* **1961**, 83, 2057
10. W. Ruland, *Coll. Polym. Sci.*, **1977**, 255, 417-427
11. S. Krimm, *J. Chem. Phys.* **1954**, 22, 567
12. R.S. Stein, G.B.B.M. Sutherland, *J. Chem. Phys.* **1954**, 22, 1993
13. S. Krimm, *Adv. Polym. Sci.* **1960**, 2, 51
14. W.H. Cobbs, Jr., R.L. Burton, *J. Polymer Soc.* **1953**, 10, 275
15. W.P. Slichter, D.W. McCall, *J. Polymer Sci.* **1957**, 26, 171
16. D.J. Blundell, D.R. Beckett, P.H. Willcocks, *Polymer*, **1983**, 22, 704
17. M.M. Winram, D.T. Grubb, S. Keller, *J. Mater. Sci.* 1978, 13, 791
18. H.D. Keith, F.J. Padden, Jr., *J. Appl. Phys.* **1959**, 30, 1479
19. P.J. Flory, D.Y. Yoon, *Nature* **1978**, 272, 226
20. W. Mattice, *Macromolecules*. **1990**, 23, 000

TOPICS in POLYMER PHYSICS

21. T.S. Chung, *Polym. Eng. Sci.* **1989**, 26(13), 901
22. S. L. Kwolek and P.W. Morgan, *J. Chem. Educ.* **1959**, 36, 182-184
23. A. Keller and Z.D. Cheng, *Polymer*, **1998**, 39(19), 4461-4487
24. J.W. Gibbs, *Collected Works, Vol 1*; Dover: New York, **1961**
25. G.S. Ross, L.J. Frolen, *J. Res NBS A*, **1975**, 79A, 701
26. M. Avrami, *J. Chem. Phys.* **1939**, 7, 1103; *ibid*, **1940**, 8, 212
27. J.D. Hoffman, J.I. Lauritzen, Jr., *J. Appl. Phys.*, **1973**, 44, 4340
28. L. Mandelkern, *Crystallization of Polymers*, McGraw-Hill, New York, **1964**
29. S. Hoshino, E. Meinecke, J. Powers, R.S. Stein. S. Newman,
J. Polymer Sci. **1965**, A3, 3041
30. R.S. Stein and J. Powers, *J. Polymer Sci.* **1962**, 56, 59
31. I.H. Hillier, *J. Polymer Sci.* **1962**, A3, 3067
32. F.P. Price, *J. Amer. Chem. Soc.* **1952**, 74, 34

Glossary of Symbols Arranged by Chapters

Chapter 1

W_n = the weight of material with degree of polymerization n

n = the degree of polymerization

N_n = the number of molecules with degree of polymerization n
whose weight is Mn

$\langle M_n \rangle$ = the number average molecular weight

$\langle M_w \rangle$ = the weight average molecular weight

$\langle M_z \rangle$ = the Z average molecular weight

P = the polydispersity index

p = the probability of propagation of a monomer unit

n = the number of monomers

P_n = the probability of forming a chain containing n number of monomers

C = a proportionality constant

M_0 = the molecular weight of a monomer unit.

M_n = the molecular weight of the chain of degree of polymerization, n .

Chapter 2

ϕ = the rotational angle or the angle between non bonded atoms

μ = the dipole moment for the C-Cl bond in units of debyes

x = the direction along the chain axis

y = the direction perpendicular to the chain axis

$P(\phi)$ = the probability of a given value of ϕ

$U(\phi)$ = a calculated potential energy function

U^{3n} = Fourier coefficient terms

U_0 = the single parameter, defining the height of the rotational barrier

$U(\phi)$ is described relative to an arbitrary reference value of zero at $\theta = 0$.

r_{ij} = the interaction potential between the i^{th} and the j^{th} atoms separated by the distance r

$\langle \mathbf{R} \rangle$ = the straight line vector distance between the ends of the molecule

ϕ_{i+2} = the ϕ coordinate of \mathbf{a}_{i+2} in the coordinate system defined by \mathbf{s}_i and \mathbf{s}_{i+1} .

η = an average coos ϕ value

l = bond length

ϕ_{i+2} = the ϕ coordinate of \mathbf{a}_{i+2} in the coordinate system defined by \mathbf{s}_i and \mathbf{s}_{i+1} .

θ_1 and θ_2 = two different bond angles

Z = the number of stiff segments in a Kuhn-Grun model chain

\mathbf{a}_i = a unit vector along a Kuhn segment,

α = the dihedral angle

L = the statistical segment length

Q , = the partition function,

U_1 , = the potential energy of the trans state,

ϵ_n = the statistical weight assigned to the gauche conformer

$\sigma = e^{\sigma/RT}$ = the statistical weight of the gauche conformer

Ω_l = reference bond angle

$|\mathbf{A}|$ = Transformation matrix

$\langle R^2 \rangle$ = the root mean square chain distance

ω = the statistical weight for the steric overlap of g^+g^- pairs

ψ = the statistical weight for g^-g^- or g^+g^+ pairs

τ = the statistical weight for a gauche conformation.

$P(R_x)$ = the probability of obtaining a given value end to end chain distance

N_1 = the number of segments lying in the $+X$ direction

N_2 = the number of segments lying in the $-X$ direction

C = a normalization constant

α = arbitrary constant used in Lagrange's method of undetermined multipliers

β = arbitrary constant used in Lagrange's method of undetermined multipliers

$\mathcal{L}(x)$ = the Langevin function of x

$\mathcal{L}(x)^{-1}$ = the inverse Langevin function of x

N = the number of ways of distributing n distinguishable molecules over R states

n = the number of distinguishable molecules

R = the number of states

P = the probability of a given distribution

GLOSSARY

C = a constant of proportionality subject to the conditions of a constant number of molecules and of constant energy

k = Boltzmann's constant = $R/N_a = 1.38 \times 10^{-23}$ J/K

T = temperature (in units of degrees Kelvin)

E = enthalpy

S = entropy

A = free energy

R = the gas constant = 0.0821 atmos- $m^3/kmol^0K$

N^A = Avogadro's constant = 6.02×10^{23} per gram mole the number of molecules in one mole of a substance.

C_v = the specific heat at constant volume

w_0 = probability in equation 2A.43

\mathbf{P} = a vector in a two coordinate axis system

S = the polymer chain matrix

$|I|$ = the identity matrix

D = the determinant of $|M|$

$|\hat{M}|$ = the adjoint of matrix $|M|$

$|M|$ = matrix for restricted rotation with a symmetrical barrier

$|M|^{-1}$ = the reciprocal of $|M|$

$\eta = \cos \phi$

$U_n \eta$ = the statistical weight of a conformation with $E'_{zn'}$. and z refers to the rotational state of bond $i-1$ and n to that of bond i .

Ω_ϕ = the statistical weight of the entire chain.

Z = the conformational partition function

$|U_i|$ = statistical weight matrices

λ_1 = the value of the largest eigenvalue

\mathbf{J}^* = the row specifying the first bond = $\begin{vmatrix} 1 & 0 & 0 \end{vmatrix}$

\mathbf{J} = the column specifying the n^{th} bond = $\begin{vmatrix} 1 \\ 1 \\ 1 \end{vmatrix}$

\mathbf{R} = the total end to end vector distance

\mathbf{R}^T = the transpose of \mathbf{R}

\mathbf{l}_i = a column vector

- \mathbf{l}_i^T = the transpose or row form of \mathbf{l}
 C_x^s = the number of ways of obtaining x more heads than tails
 S = the number of occurrences of an event

Chapter 3

- H = the heat content or enthalpy
 E = the internal energy of the system
 G = the Gibbs free energy (constant pressure and volume)
 $-dW_e$ = all types of work, other than pressure-volume work, done by the system,
 P = the pressure
 V = the volume
 S = the entropy
 T = the temperature
 A = Helmholtz free energy (constant volume and temperature)
 dW_e = the elastic work
 f = the force required to stretch an elastic material
 f_e = force related to the internal energy
 f_s = a force associated with entropy
 K = proportionality constant in force-temperature measurements
 $\mathcal{L}(x)^{-1}$ = the inverse Langevin function
 θ = the angle between a chain segment and the displacement vector (\mathbf{R})
 \mathbf{R} = the displacement vector
 $V(\theta)$ = the potential energy of a chain segment oriented at an angle θ
 $W(\theta)$ = the probability of a segment having an orientation angle θ
 W = the statistical weights of the conformational matrices, trans and gauche
 ΔH_m = the enthalpy of mixing
 ΔS_m = the entropy of mixing
 ΔG_m = the Gibbs free energy of mixing
 P = the probability or number of ways of placing N_1 solvent and N_2 solute molecules into a total of N spaces
 N_1 = the number of solvent molecules
 N_2 = the number of solute molecules
 N = the total number of spaces

GLOSSARY

x_1 = mole fraction solvent

N_1 = number of solvent molecules = number of solvent cells

xN_2 = number of solute segments = number of solute cells

x = the ratio of the polymer volume to the solvent volume

N = the total number of lattice cells

P = the total probability for all polymer molecules

P_1 = the number of ways of putting the first molecule in the lattice

P_2 = the number of ways of putting in the second molecule in the lattice

$\phi_1 = \frac{N_1}{N_1 + xN_2}$ = the volume fraction of solvent

$\phi_2 = \frac{xN_2}{N_1 + xN_2}$ = the volume fraction of polymer

ΔV_m = the volume of mixing

χ_1 = the polymer/solvent interaction parameter

$(\Delta S_m)_1$ = the partial molal entropy of mixing

$(\Delta H_m)_1$ = the partial molal enthalpy of mixing

$(\Delta G_m)_1$ = the partial molal Gibbs Free Energy of mixing

$\mu_1^0 = \left(\frac{\partial G}{\partial n_1} \right)^0$ = the chemical potential of the solvent in pure solvent

$\mu_1 = \left(\frac{\partial G}{\partial n_1} \right)$ = the chemical potential of the solvent in solution

π = the osmotic pressure

A_2 = the second virial coefficient

V_1 = the molal volume

ρ_2 = the solution density

$\psi(1-\theta/T)$ = enthalpy term used in solubility determinations

$m_1 = V_1/V_2$ = degree of polymerization

V_1 = molal volume of polymer 1

V_2 = molal volume of polymer 2

V_0 = molal volume of an idealized polymer molecule

$I(q, t)$ = the scattering intensity at time t and scattering angle q

$R(q)$ = the growth rate at angle q

$q = (\sin \theta)/2$ = the reduced scattering angle

S_m = the scattering intensity corrected for electronic density

ϵ_s = quench depth,

D_c = the diffusion constant for coarsening

dQ = the amount of heat transferred in or out of a system.

dT = the temperature change accompanying the transfer process.

V = the specific volume

α = the coefficient of the (cubic) thermal expansion

β = the (isothermal) compressibility

ϵ_0 = the zero point vibrational energy

ϵ_{vib} = the vibrational energy

ϵ_0 = the crystal energy plus the electronic energy (Joules/mole) of the crystal in its ground state

Q = the partition function

n_i = the number of normal modes of vibration with frequency ν_i

h = Planck's constant

dv/dn = the density of normal modes

$\Delta G_m = G_{\text{cryst}} - G_{\text{amorph}}$ = the difference in the Gibbs free energy

μ_u^c = the chemical potential (the free energy per mole) of the crystalline phase

μ_u = the chemical potential (the free energy per mole) of the liquid phase

μ_u^0 = the chemical potential of the standard state assumed to be that of the pure liquid at the same temperature and pressure.

n = the number of moles of the chain repeat unit

V_u = the molar volume of the repeat unit

ϕ_1 = the volume fraction of the diluent

χ_1 = the polymer/solvent interaction parameter = equation 3.B-21

T_m^0 = the undiluted melting point

n = the number of moles

X_2 = the mole fraction of solute

X_E = the mole fraction of chain ends.

V_m = the molar volume

α = the elongation ratio

n = the number of statistical segments per cc

N_c = the number of chains per unit volume (V)

N = the number of statistical segments per chain

GLOSSARY

X_c = the degree of crystallinity

G = the Gibbs Function (constant pressure and temperature)

H = the enthalpy or heat content at constant pressure and temperature

T = the temperature expressed in units of degrees Kelvin

S = the entropy

E = the internal energy at constant temperature and volume

Q = the heat absorbed by the system

W = work done by the system

$\left(\frac{\partial G_A}{\partial n_{1A}}\right) \equiv \mu_{1A}$ = the chemical potential of component 1 in phase A

n_{1A} = the number of moles of component 1 in phase A

N_{11} = the number of solvent-solvent contacts per cm^3

N_{11} = the number of solvent-solvent contacts per cm^3

N_{12} = the number of solvent-solute contacts per cm^3

N_{22} = the number of solute-solute contacts per cm^3

ϵ_{11} = the potential energy of a solvent-solvent contact

ϵ_{12} = the potential energy of a solvent-solute contact

ϵ_{22} = the potential energy of a solute-solute contact

N_1 = the number of solvent molecules per cm^3

z = the coordination number of the lattice

P_{11} is the probability that a lattice site about the central site is occupied
by a solvent molecule

ϕ_1 = the volume fraction of solvent

x = the number of lattice sites occupied by a solute molecule

P_{12} = the probability that a solvent molecule occupies a lattice site

n_i = the number of moles of i

N_a = Avogadro's number = 6.02×10^{23}

$\Delta\mu_1$ = the increase in μ_1 , because of the applied pressure.

$$x = \frac{\text{volume mole fraction}}{\text{weight mole polymer}}$$

A_2 = the second virial coefficient

Chapter 4

c = the velocity of electromagnetic wave propagation

λ = the wave length

ν = the frequency or the number of waves per unit time

v_m = the wave velocity in a material,

η = the refractive index

λ_0 = the wave length in vacuum

λ = the wave length in the medium

θ_1 = the incident angle

θ_r = the refraction angle

P = the polarizability per unit volume

$(\alpha_m)_i$ = the molecular polarizability of the i^{th} molecule

$\langle \eta \rangle$ = the averaged value of η_1 and η_2

$\Delta \eta$ = the birefringence or the difference between η_1 and η_2

E_0 = the amplitude of the incident field

ω = the angular frequency ($2\pi\nu$)

α = the polarizability of the atom in an isotropic force field

m = the dipole moment

r = the distance of the observer from the scatterer.

y = the angle between the plane of the polarization seen by the observer and the dipole moment.

ϕ = the phase angle which takes into account that the wave must travel a distance, d , to reach the observer

d = the distance a wave must travel from its source to reach an observer

q = the electronic charge

m_0 = the electronic mass = 0.511 Mev

Z = the atomic number of an element

K_j = a constant proportional to the scattering power of the j^{th} scatterer

N = the number of identical randomly oriented molecules

R = the Rayleigh Ratio

V_s = the scattering volume

$P(\theta)$ = interference factor

$(R - R_0)$ = the Reduced Rayleigh ratio neglecting intramolecular effects

$\mathbf{s} = \mathbf{s}_0 - \mathbf{s}$ = the propagation or scattering vector

\mathbf{s}_0 = the unit vector in the incident ray direction

\mathbf{s}_1 = the unit vector in the scattered ray direction

\mathbf{r}_j = the vector to the j^{th} scattering element

GLOSSARY

F = the structure or form factor for the object which is a characteristic of its geometry

$\rho(\mathbf{r})d\mathbf{r}$ = the amplitude scattered by a three dimensional element with a volume $d^3\mathbf{r}$

u = the angle between \mathbf{r} and \mathbf{s} .

V_{sp} = the sphere volume

$\Phi(U)$ = the sphere scattering function = $\frac{3}{U^3}[\sin U - U \cos U]$ eqn 4.57

U = a parameter that is a measure of the scattering angle and depends upon the ratio of R to λ .

n , the multiplicity factor, is an integer commonly termed the order of the diffracted ray

N = the number of spheres in a linear array

α , β and γ = the direction cosines of the vector \mathbf{s}

\mathbf{s} = the vector

\mathbf{H} = the reciprocal lattice vector

h_1 , h_2 , and h_3 = the Miller indices

\hbar = Planck's constant = 6.626×10^{-34} J/Hz

E_1 and E_2 = the energies of the lower and the higher states in the system

ν = the photon frequency.

ϵ , = the extinction coefficient of a material with thickness, l ,

l , = the thickness of a material

I_t = the transmitted beam intensity

I_0 = the incident beam intensity

a_i , = absorbance

$d(hkl)$ = the spacing of the reciprocal lattice

θ_i = the angle between the transition moment axis and the polarization direction of radiation

ν_a = the vibrational frequency

ν_c = the emitted frequency.

\mathbf{P} = the unit vector polarized in the direction of the absorbed radiation

\mathbf{A} = the unit vector of the emitted radiation

I = the intensity of the emitted light

\mathbf{M}_a = the unit vector along the absorption transition direction

\mathbf{M}_e = the unit vector along the emission transition moment direction

K = a proportionality constant.

θ_m = the angle between the common transition moment direction and the polarization direction.

SOC = the stress-optical coefficient

b_1 = the polarizability of bond 1

b_2 = the polarizability of bond 2

$(b_1 - b_2)_S$ = the statistical segment anisotropy

$(b_1 - b_2)_m$ = the anisotropy of the monomer unit

Z_0 = the number of monomer units in the statistical segment

$(b_1)_j$ and $(b_2)_j$ = the principal polarizabilities of the j th bond that lie at an angle θ_{ij} with respect to the i^{th} axis

\mathbf{r}^T = the transpose (i.e., the row form) of the end-to-end vector \mathbf{r}

a_i = the traceless tensor representing the anisotropy of the polarizability associated with the group i of the chain

\mathbf{a}_i = the polarizability tensor

a_i = the average scalar polarizability

$|\mathbf{E}|$ = the identity matrix

Z = the conformational partition function

$|\mathbf{Q}_i|$ = the generator matrix

Γ_{pm} = the effective anisotropy of the methylene group

α = the linear term for the first order contribution to the polarizability

β = the nonlinear term or hyperpolarizability optical coefficient for a second order contribution to the polarizability

γ = the nonlinear term for a third order contribution to the polarizability

Chapter 5

$q_1 = q_2 = 1$ electrostatic unit (ESU) of charge in vacuum

ϵ = the dielectric constant of a material

r = the distance of the repulsive force (F) between like charges

F = the repulsive force between like charges

\mathbf{E} = the force on 1 ESU of charge

\mathbf{D} = electromagnetic displacement is the value of \mathbf{E} in a vacuum

V = the voltage in electrostatic units

C = the capacitance of a body

η = the refractive index

A = the cross sectional surface area

GLOSSARY

σ = the polarization charge density

L = the separation of the centers of charge

N = the number of atoms per cm^2

P = polarization per cm^3

α = the atomic polarizability

β = the atomic polarizability higher order term

N = the number density of atoms

M = the molecular weight

ρ = the density

N_A = Avogadro's number = 6.02×10^{23} /mole

$D(t)$ = the time dependent electric displacement

$E(t)$ = corresponding electric field

t = dielectric relaxation time.

ω = the angular frequency

δ = the dielectric loss angle analogous to the mechanical loss angle

ϵ^* = the complex dielectric constant

ϵ_0 = the static or low frequency value of the dielectric constant,

ϵ_∞ = the limiting value at high or optical frequencies

τ = the relaxation time or the time required for the stress to relax to 1/e of its initial value

ϵ' = the in phase or energy storage component

ϵ'' = the out of phase or energy dissipating component of the energy absorbed by the dielectric at different frequencies.

$\tan \delta$ = the dielectric loss tangent

ν = the frequency

$\phi(\tau) d \ln \tau$ = the fraction of the change in dielectric constant originating from mechanisms having relaxation times between $\ln \tau$ and $\ln \tau + d(\ln \tau)$.

β = a parameter with limits $0 < \beta < 1$

σ = the conductivity

n = the number of charge carriers

u = the mobility of a charge carrier

e = the charge of the carrier

I = the current flow

E = the voltage

ρ = the resistivity

d = the piezoelectric strain constant
 G = the piezoelectric stress constant
 x = the stress level of a dielectric constant
 ΔT = the temperature difference
 p_x = the piezoelectric coefficient.

Chapter 6

\hbar = Planck's constant
 c = the velocity of light
 λ = the wave length.
 E_1 = a lower electronic or molecular energy level
 E_2 = a higher electronic or molecular energy level
 ν = frequency of a photon
 ϵ = the extinction coefficient for a material with thickness
 l = material thickness
 I_0 = the incident beam intensity
 I_t = the transmitted beam intensity
 a_i = the absorbance along the associated transition moment
 θ_1 = the angle between the transition moment axis and the direction of polarization of the radiation of the i^{th} absorption band
 f = a force constant or constant of proportionality
 F = the applied force
 x = the associated bond deformation.
 E = the total energy of a system
 V potential energy
 K = the kinetic energy
 m_i = the atomic mass
 ν_i = the vibration for the i^{th} atom
 B_i = the i^{th} normal coordinate
 N = the number of atoms for a chain in the equations of motion
 $|\mathbf{x}|$ = the column vector of the Cartesian coordinates
 f_{ij} = an element in a square 3×3 matrix
 $|\mathbf{x}|$ = the transpose or row vector of $|\mathbf{x}|$
 $|\dot{\mathbf{x}}|$ = the column vector of the velocities, \dot{x} , expressed in Cartesian coordinates
 $\mathbf{M}|$ = the 3×3 diagonal matrix (Appendix VI-B) of the atomic masses

GLOSSARY

- $|\mathbf{x}|$ = the transpose or row vector of $|\dot{\mathbf{x}}|$
 k = termed the wave vector whose modulus is equal to $2\pi/\lambda$,
 t = the time
 $\omega(k)$ = frequency distribution
 ν_a = the incident radiation is absorbed at one frequency
 ν_e (Anti Stokes line) scattered at a lower frequency to a higher frequency
(Stokes line)
 E_0 = incident electric field with a frequency ν_0
 E = the electronic field induced in a diatomic molecule
 α = the polarizability
 s = the amplitude of the normal coordinate
 q = a particular vibration
 ε = the phase of the vibration
 ν_{\max} = the frequency at which the band has a maximum
 ε_{\max} = the intensity of the absorption
 \mathbf{H}_0 = the applied magnetic field
 g = the spectroscopic splitting factor
 r = the distance between protons
 β = the angle between a line joining the protons and \mathbf{H}_0
 S_2 = the mean-square deviation of the field from the center of the line \mathbf{H}_0
 M_n = the mass of a neutron particle
 λ = the wave length of a neutron beam
 v = the particle velocity
 $\Delta (= x_2 - x_1)$ = changing path distance
 r = is the reflection coefficient
 T = the transmission coefficient of the beam splitter
 $A(\nu)$ = the frequency distribution
 $I(D)$ and $B(n)$ = orthogonal functions
 $F(\nu)$ = the frequency distribution
 N = number of points in a Fourier Transform
 q = a set of normal coordinates
 λ = the root, characteristic value or eigenvalue for an equation of motion
 $\omega = 2\pi\nu$ (ν is the frequency) = the circular frequency
A and B represent the species group symmetric and non-symmetric respectively to an axis of symmetry at constant amplitude

The subscript g (German gerade-even) denotes a species symmetric with respect to a center of symmetry or an inversion operation; while the subscript u (German ungerade-odd) refers to a species non-symmetric to a center of symmetry.

Chapter 7

f = the force on a single chain

R = the distance between chain ends

k = the gas constant

T = temperature

f = the force on a single chain

L_0 = Length in the unstretched state

$L_x L_y L_z$ = Lengths in the stretched state along the x, y and z axes

N = the total number of chains with contractile force (f_z) of the chains in the N_z direction

f_z = the applied force in the z direction

P = a hydrostatic force

α = the extension ratio,

ν = the crosslinking points per cm^3

f = the functionality of each crosslinking point

\mathbf{R}_{ij} = a network displacement vector that connects two adjacent crosslinking points

j = the number of statistical segments for the network chain associated with the i^{th} vector

N_{ij} = the number of displacement vectors of type \mathbf{R}_{ij} (in the unstretched state)

N_j = the number of network chains per cm^3 having j statistical segments

P_{ij} = the probability that a chain of j segments will have a vector distance, \mathbf{R}_i , between its ends

L = the statistical segment length.

q = the probability that a segment is not crosslinked

Ω = the number of conformations of a network

W_{ij} = the number of conformations of a chain of j segments with distance R_i between its ends

V = the total volume of the sample

GLOSSARY

ΔA_{Elast} = the stored energy function for a deformed rubber network

ρ = the sample density,

M_0 = the molecular weight of the polymer repeat unit,

q = the fraction of polymer repeat units that are joined by a random tetrafunctional crosslink.

W_g = the gel fraction.

M_c = the molecular weight between crosslinks

Φ_2 = the volume fraction of solute

$\Delta S'$ = the change in entropy in going from the unstretched state, unswollen state to the stretched, swollen state

I_1, I_2, I_3 = the three invariants that do not change with deformation. These constants are used for the case of the extension of an elastic body at constant volume

η^* = the viscosity of an emulsion

η = the solvent viscosity

ϕ = the volume fraction of the dispersed phase

Chapter 8

d = the interplanar spacing

n = the order of the x-ray reflection

λ = the wave length of the x-ray reflection

θ_b = the diffraction angle

a, b and c = the unit cell dimensions

h, k and l = the Miller indices that describe the location of the crystal plane with respect to the unit cell axis.

n = the number of monomer units of molecular weight M_m

N_a = Avagadro's number

V_n = the unit cell volume (abc for an orthorhombic unit cell)

K = a proportionality constant

F = the structure factor

F^* = the complex conjugate of F

f_j = the atomic form factor or the sum over all atoms in the unit cell, and is a measure of its scattering intensity at a given angle.

x, y and z = the coordinates of the j^{th} atom expressed in terms of

V_s = the sample specific volume

V_c = the crystalline specific volume

V_a = the amorphous specific volume

X_c = the volume fraction of the crystalline phase

X_a = the volume fraction of the amorphous phase

ρ_{calc} = the crystal unit cell density

T_m = the maximum melting point

T_c = the crystalline melting point

$(T_m)^0$ = the thermodynamic melting point

S = the intensity of the crystalline component of the diffraction at S

I_{cr} = the total intensity

X_c = the degree of crystallinity

K = a proportionality constant with a value near unity.

\mathbf{H} = the average magnetic field about an absorbing nucleus

ν = the absorption frequency

c = a constant

u = the magnetic moment of the absorbing nucleus

\mathbf{H}_0 = the applied magnetic field

\mathbf{H}^* = the local field about a given nucleus due to neighbor interactions.

A = the area under the broad band component

A_r = the area under the narrow band component

T_g = the glass temperature

ΔH = the enthalpy of fusion of the sample

ΔH_u = the enthalpy of the completely crystalline polymer

ΔH_a = the enthalpy of the completely amorphous phase

ΔH_c = the enthalpy of the completely crystalline phase

ΔH = the enthalpy of the polymer sample

C_p = the heat capacity at constant pressure

α = the tilt angle between the sectors in polymer single crystals

d = the distance between chains in the crystals

l = the monomer repeat distance

ρ_{calc} = the experimental crystal density

T = the transmission of an anisotropic crystals located between two polarizers.

δ = the optical retardation of the crystal

θ = the angle between the sample optic axis and the polarizers

ν = the number of nuclei per unit volume

GLOSSARY

- G = the growth rate of crystalline phase nuclei
 r = the radius of the sphere growing from the crystalline nuclei
 $V_s(t)$ = the volume of spherulites at time (t)
 $W_s(t)$ = the weight of spherulites at time (t)
 ρ_s = the spherulitic density
 $W_c(t)$ = the weight of the crystals
 X_{cs} = the degree of crystallinity of the spherulites
 X_c = the degree of crystallinity of the polymer
 ρ = the polymer density
 ϕ_c = the volume fraction of spherulites
 n = an exponent in the Avrami equation dependent on nucleation and growth mechanisms
 M = the mass of a fractal structure
 R = a measure of the fractal structure size
 D = the fractal dimension used as an exponent in the fractal equation
 A = a pre exponential front factor
 E_d = the activation energy for viscous flow
 ΔG^* = the free energy required to form a stable nucleus
 Δg = the free energy difference per unit volume between the melt and an infinite crystal
 σ_s = the surface free energy per unit surface area
 r^* = the critical nucleus size that must be attained before a stable nucleus is formed
 ΔT = the “under cooling” between the melt temperature and the actual lower temperature

This page is intentionally left blank

Index

- .Scalar Product 98
absolute..... 25
absorbance.....310, 329
absorption308, 309, 310, 311,
313, 317, 319, 320, 323, 325,
329
addition polymers..... 11, 14, 32
affine assumption348, 366
Alternating copolymers..... 34
amorphous phase380, 382, 389,
390, 391, 392, 397, 407, 415
amplitude of the incident field
..... 211
angular frequency.....211
Anti Stokes line 319
Argand diagram..... 294
A-stage resin (or Resol)..... 26
Asymmetric Barriers 66
asymmetric groups 18
Atactic 16, 17
attenuated total reflectance ... 394
Avrami equation406, 410, 412,
413, 414
Baekeland 12, 26, 39
Banbury mixer..... 29
biaxial stress 359
binodal 160
binomial series 357, 365
birefringence205, 211, 213, 238,
239, 240, 253, 254
block copolymer..... 31, 33
block copolymer morphology
..... 159
bond anisotropy 242
Bond polarizability 240
Bovey 39
Bragg diffraction angle..... 229
Bragg equation: 383
branched polyethylene 14
Brillion lines..... 206
Brillouin zone..... 315
Brownian motion 139, 140
Bulk polymerization 19
butadiene-styrene (SBR)..... 32
Cahn-Hillard-Cook equation 162
capacitance286, 288, 290, 297
Carbon black 37, 331
Carothers 10, 11, 39
Cartesian coordinates312, 313,
333, 336
cellulose acetate 12
centrifugation techniques..... 21
ceramers 38
Chain End-to-End Distribution
Functions 71
chain folding 386, 387
characteristic ratio..... 68, 69
chemical potential171, 172,
173, 185, 196, 197, 200, 201
Chirality fluctuations 244
circularly polarized light..... 205
cis 1,4 polybutadiene 60
classical nucleation theory407,
410
classical thermodynamic state
functions 89
Classical thermodynamics 184

- Clausius-Mosotti equation 291,
307
- coefficient of the (cubic)
thermal expansion..... 167
- Cole-Cole plot 295
- colligative properties..... 21
- Comb polymers 35
- Composites 37, 39
- condensation polymers 11, 26
- condenser..... 289, 290, 297
- condition for constructive
interference 233
- conductivity 285, 286
- conformation 45, 49, 60, 61, 62,
63, 66, 67, 78, 116, 117
- conformational entropy of a
chain..... 139, 140
- Conformational Partition
Function 117, 242
- Conjugated systems 324
- Cooley-Tukey algorithm..... 331
- copolymer..... 18, 25, 33, 34, 35
- correlation function 246, 247,
249, 268, 269
- crosslinked fractions (gel)..... 27
- crosslinking 341, 345, 347, 349,
351, 352, 354, 356, 366, 371
- crosslinks 12, 27, 29, 33, 341,
345, 346, 349, 352, 354, 362,
363
- crystal lamellae 398
- crystal unit cell density 390
- crystallization in natural rubber
..... 181
- crystallization temperature 386,
391, 392, 394, 409
- Curie brothers..... 296
- cycle rank theory..... 356
- deBroglie equation..... 326
- deBroglie waves..... 204
- Debye-Bueche equation 246,
247, 248
- degree of crystallinity 380, 381,
389, 391, 393, 396, 411, 412,
414
- degree of polymerization 20, 21,
40
- dendrimers..... 35
- Density fluctuations 244
- Depolarization of Scattering. 257
- deuterium labeling 69
- dichroism..... 236, 238
- dielectric constant 286, 287, 288,
293, 294, 295, 297, 298, 307
- diene polymers 17
- diffraction 205, 206, 226, 229,
231, 232, 234, 235
- dipole moment 309, 311, 315,
321, 337
- dipole moments..... 207
- direction cosines 233, 235
- disc shaped nuclei 408
- dispersion curve 314
- dispersive technique..... 329, 331
- Doppler effect 326
- effective field 291
- eigenvalue 334
- Einstein viscosity law 374
- elastic instability 360
- elastic scattering..... 326
- elastic work 135
- Elastomers 12, 340, 346

INDEX

- electric displacement.....292, 298
electrical field strength288, 298,
301
electromagnetic displacement
.....288
electron microscopy380, 381,
386
Electrostatic Potential (Voltage
.....302
Emulsion polymerization..20, 32
end group analysis.....21
engineering stress.....357
entanglements346, 349, 353,
354, 355, 356, 374
Enthalpy.....388
entropy340, 344, 347, 349, 351,
352, 354, 367, 368
entropy of mixing147, 148, 149,
152, 154, 158, 194
epoxy37
equation of motion311, 312,
314, 334
equations of motion311, 313,
333
equilibrium centrifugation21
ethylene propylene rubber31
extension ratio343, 353, 372
extinction coefficient236, 310,
323
first law of thermodynamics.185
Flory-Huggins Theory147, 364,
366
Flory-Rehner theory of swelling
.....366
fluorescence.....205, 206, 238
folded chains398
force constants314, 315, 316,
333
force-extension relation 344, 371
form factor.....221, 223, 243
Fourier inversion.....385
Fourier transform infrared329
Fourier transformation.....330
fractional precipitation.....23
free energy of mixing147, 154,
158
frequency204, 206, 207, 211,
212, 213, 215, 216, 235, 237,
238, 249, 251, 252
fringed micelle model.....382
front factor.....354, 356
FTIR309, 329, 331
gauche conformation ..51, 60, 71
Gaussian approximation141,
145
Gaussian function73, 83
gel permeation chromatographic
.....24, 25
gel point.....27, 32
Gibbs free energy..134, 169, 186
glass temperature12, 28
Goodyear13, 39
GPC technique24
Graft copolymers34, 159
Guth and James.....349
Guth-Gold equation375
gutta percha.....30, 31
Heat capacity.....166
heat content or enthalpy135,
184
heat of mixing191, 193, 194

- Helmholtz free energy 136, 137, 187, 344
- heterogeneous nuclei 388, 405, 409, 410, 412
- heterotactic 17
- high performance liquid chromatography 22
- homogeneous nuclei 405, 406, 409, 416
- Hookian springs 314, 333
- hydrogen 213
- hydrogen bonds 136, 169
- ideal rubber... 139, 142, 144, 145
- Inelastic scattering 326
- Inflation of a rubber balloon. 359
- infrared 308, 309, 311, 315, 317, 321, 323, 327, 329, 337, 394, 395
- infrared spectra 45
- infrared spectrum 395
- Initiation 18, 19
- insulators 285, 286
- interaction parameter 154, 155, 156, 173, 174, 194
- interference conditions 329
- interference factor 218, 223
- interference problem 214
- internal energy 341
- internal field 210, 240, 243, 291, 305, 306
- Interpenetrating polymer networks 36
- ionic initiator 33
- IPN 36
- Isotactic 16
- Kerr Effect 71, 250, 254
- Kevlar 403
- Kevlar™ 37
- Kronecker delta 228, 235
- Kuhn/Mark assumption 349
- lamellae 401, 402, 410
- Langevin 296
- Langevin function 81, 83, 142, 144
- light absorbance 205
- Light scattering 25, 162, 211
- Linear polyethylene 14, 65
- liquid crystals 160, 403
- Living polymerization 35
- Lorenz field 210, 240
- Lorenz-Lorentz equation 209, 262, 291
- low angle light scattering 182
- Lower Critical Solution Temperature 161
- magic spinning angle 325
- MALDI (matrix assisted Laser desorption/ionization), 25
- Mark and Meyer 380
- mass spectrometric technique. 25
- Maxwell equations 187
- mean square end to end distance 55
- melting point 168, 169, 170, 171, 173, 174, 175, 176, 177, 178, 180
- melting point depression of solid polymers 175
- melting temperature 167, 170
- method of determinants 335
- method of steepest descents... 87
- Michelson interferometer 329

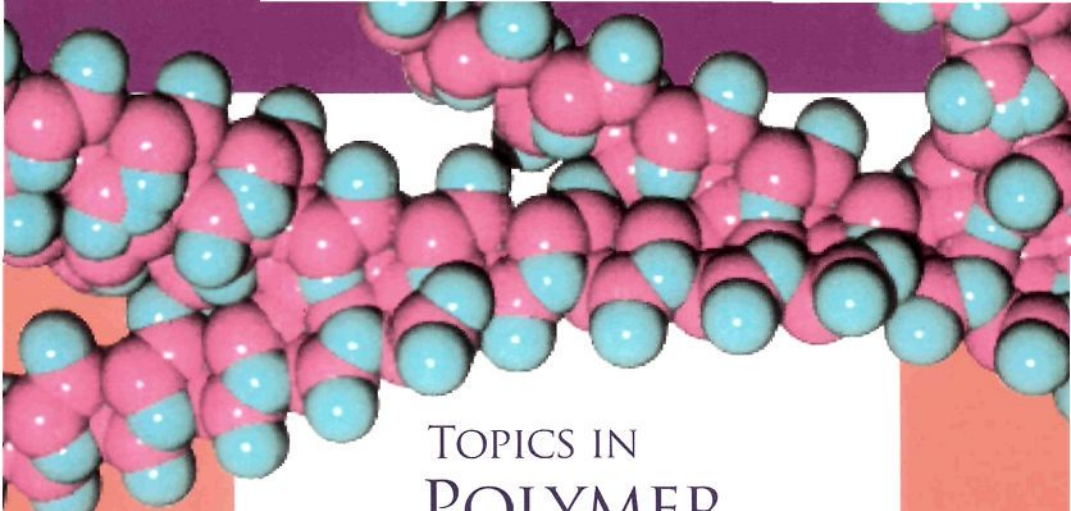
- micronet..... 356
- Mie scattering..... 212
- Miller Indices 227, 264, 383
- moiré patterns..... 399
- molecular contour length 52
- molecular weights 20, 21
- Mooney-Rivlin equation 372,
373
- morphology 167, 180
- most probable distribution 23, 42
- Natta 15, 39
- natural rubber 10, 13, 27, 29, 30,
31, 32
- network defects 361
- Neutron radiation 209
- neutron scattering 69, 162, 211,
249, 250, 326
- neutron scattering experiments
..... 350
- nmr..... 16, 325, 326
- non-Gaussian case..... 144
- non-Gaussian statistics..... 371
- non-linear optics..... 210, 251
- normal coordinates 312, 333,
334
- normal modes 321, 336, 337
- novalac resin..... 27
- Nuclear magnetic resonance... 14
- Nucleation 404, 406, 409, 413,
416
- nucleation and growth 160, 162,
164
- number average molecular
weight..... 21, 23, 41
- nylon 66..... 11
- Oligomers..... 20
- optical microscope 388, 401, 405
- Optical microscopy 380
- or enthalpy 135, 157, 166, 169,
177, 184
- Orientation fluctuations 244
- orientation function..... 237
- orthorhombic crystal..... 231
- Osmotic pressure 21, 154, 156,
174, 196, 198, 200, 202
- partial molal entropy of mixing
..... 154
- Particulate fillers 37
- pentane interaction..... 61
- phantom network 349, 350, 354,
374
- phase angle..... 212
- Phase diagrams..... 403
- phase problem 385
- phenol-formaldehyde polymers
..... 12
- pi electron conjugation 285
- pi orbital overlap..... 285
- piezoelectric 285, 295, 296, 297,
298, 299
- Piezo-electric..... 254
- piezoelectric coefficient..... 298
- piezo-electric detectors 298
- piezoelectric strain constant 296,
297
- piezoelectric stress coefficient
..... 296, 297
- plane polarized light 205, 215
- PMMA..... 299
- polarizability 207, 209, 210, 211,
213, 218, 239, 240, 241, 251,
253, 257, 258, 262

polarization charge density ...	290
Polaroid™	216
poling operation	298
polybutylene terphthalate	36
polycaprolactone	36
polydimethylsilicone networks	356
polydispersity index	23
Polyetherimide (PEI™)	37
Polyethylene 29, 242, 309, 316, 323, 383, 385, 386, 388, 390, 393, 395, 401, 404, 405	
polyethylene terephthalate 390, 395	
polyimide resins	37
polymer miscibility	154, 158
polymer molecular weight 19, 20, 21	
polymer single crystals 380, 381, 382	
polymethyl methacrylate ..	12, 28
polyoxymethylene 10, 11, 58, 380	
polypropylene.....	14, 15, 17, 35
polystyrene,	10, 12
polystyrene/polybutadiene.....	37
polystyrene/polyphenylene oxide.....	36
polysulfone	37
polytetrafluoroethylene.....	380
polyvinyl chloride 14, 36, 311, 331	
polyvinylidene fluoride 254, 285, 296, 298, 299	
potential.....	303
Propagation.....	18
proton resonance	325
Pyroelectricity	296
quasi-elastic light scattering .	249
radius of gyration 53, 84, 100, 104	
Raman 308, 309, 317, 319, 321, 323, 327, 328, 337	
Raman spectra	395
random copolymer	176
Random Walk	55, 122, 125
Random Walk of Gaussian Chains	122
rate of polymer crystallization	409
Rayleigh Ratio	217, 218, 262
Rayleigh-Gans approximation	212, 245
Rayleigh-Gans-Debye approximation.....	224
reciprocal lattice 226, 227, 234, 264	
refraction	205, 206, 207, 209
refraction angle	209
refractive index 207, 209, 210, 211, 213, 243, 250, 253, 262, 263	
Roedel.....	14, 39
root mean square distance	52
rotational isomeric approximation.....	49
Rotational Isomeric State (RIS) Approximation.....	61, 116
rotational isomeric state model	146
rotational isomeric state models	241

INDEX

- rotational isomers..... 44
- rubber elasticity.....341, 344, 354
- rubber network342, 344, 350, 353, 367, 374
- rubbers12, 29, 32, 33, 340, 342, 371
- scalar product226, 227, 266
- scattering by gas molecules ..216
- Scattering from a Collection of Molecules.....261
- scattering from a fluctuating medium245
- scattering phenomena ...205, 213
- Scherrer equation 386
- second law of thermodynamics 185
- second virial coefficient199, 203
- secondary nucleation mechanism..... 405
- Shear modulus.....354, 369
- silicone polymer..... 58, 60
- small angle x-ray diffraction. 386
- soluble factions (sol)..... 27
- solution polymerization 19
- Solution Thermodynamics.... 147
- specific volume389, 390, 398
- speed of light.....214
- sphere scattering function..... 225
- spherulites380, 388, 401, 409, 411, 412, 413, 414
- spinodal decomposition160, 161, 162, 164
- spinodal temperature..... 162, 163
- State functions..... 184
- Statistical Mechanics 85
- Statistical Mechanics71, 86, 93, 121
- statistical segment239, 240, 241, 345, 346
- statistical segment length.. 54, 55
- statistical segment model53, 55, 61, 70, 72, 179
- statistical thermodynamics140, 184
- statistical weight matrix62, 65, 67, 117, 118
- statistical weight matrix for polyethylene 117
- statistics of the random walk .. 72
- Staudinger 10, 39
- Step growth 19
- stereoregularity 15, 17
- stereo-specific catalysts 35
- Stokes line 319
- stored energy function353, 354, 372
- strain optical coefficient 63
- strain-energy function..... 369
- stress-optical coefficient239, 242
- stress-temperature coefficients 71
- structure factor 223, 384
- styrene butadiene rubber..... 33
- surface energy 176, 177
- surface energy density 407
- suspension polymerization 19
- Syndiotactic..... 16, 17
- synthetic rubbers 12, 27
- tacticity 15, 16, 17
- Taylor power series..... 124

Telomers.....	20	ultra-high molecular weight	
temperature jump	161	polyethylene	170
Termination.....	18	ultraviolet	308, 309, 323, 324
tetrahedral bonding with free		uniaxial orientation	236, 237,
rotation.....	70		259
the Boltzmann equation	148	unit cell.....	380, 383, 384, 395
the internal energy	135, 136,	unit cell dimensions	383, 385
137, 138, 139, 167, 185, 193		unpolarized light	205, 217
The Magnitude of the		Upper Critical Solution	
Reciprocal Vector H.....	266	Temperature.....	161
The Nature of the Reciprocal		van der Waals forces.....	136
Vector H.....	264	Vector Addition	97
thermal neutrons.....	327	Vector Bragg Equation .	228, 229
thermodynamic phase	168	vibrational mode ...	315, 316, 321
Thermodynamics of Elasticity		Vulcanization	31
.....	134	wave equation	309, 334
thermoplastic rubbers.....	33	wavelength	204, 206, 207, 211,
thermoplastics	12, 28	215, 218, 219, 232, 244, 250	
thermosets.....	12	wave-vector Bragg.....	226
theta conditions	147	weight average molecular	
theta solvent	69	weight	21, 23, 40, 41
Thomson scattering.....	212, 213	Wide Line Nuclear Magnetic	
three dimensional lattice	153	Resonance.....	395
three-dimensional partition		x-ray diffraction	10, 380, 382,
function	94		395
Torlon™	37	X-ray diffraction patterns	168
trans 1,4 polybutadiene.....	60	x-ray scattering	211, 212, 213,
trans conformation	45, 47, 49,	243	
60, 115		Yau	25, 39
two-phase system	382, 389	Z average molecular weight ...	22



TOPICS IN POLYMER PHYSICS

This book can serve as an introduction to students interested in learning the techniques used in developing mathematical models of physical phenomenon in polymers; or it can furnish the background information to the experienced professional desiring to broaden his/her knowledge of polymers. The senior author presented material in this book to students interested in learning the fundamental mathematics underlying many areas of polymer physics and in lectures to audiences with varying backgrounds in polymer physics. Too many times, the basic equations are presented in final form from either lack of space or the assumption that the derivation is widely disseminated and does not require repetition. A wide variety of topics are covered, from the statistical physics and thermodynamics of polymers, to the optical and electrical behavior of polymers, as well as spectroscopy techniques for polymers.

Imperial College Press

www.icpress.co.uk

P302 hc

ISBN 1-86094-411-6



9 781860 944116